



UNIVERSIDAD
DE MÁLAGA

bionand
Centro Andaluz de
Nanomedicina & Biotecnología

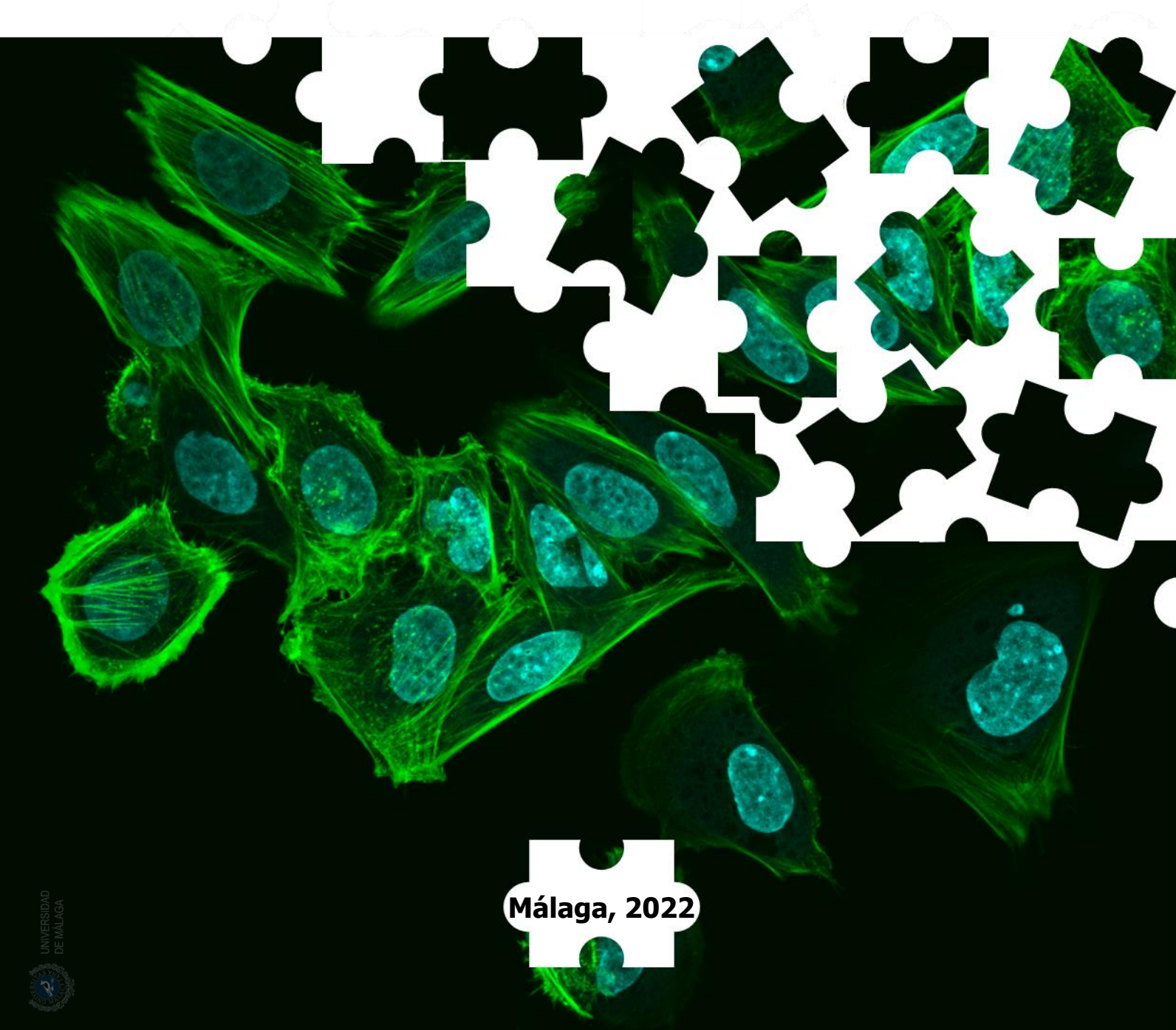


UNIÓN EUROPEA
Fondo Europeo de Desarrollo Regional

Novel approaches for osteosarcoma treatment: drug combination, nanotechnology and cell therapy

Doctoral thesis

Liliya Kazantseva



Málaga, 2022



Universidad de Málaga

Facultad de Ciencias
(Programa de Doctorado de Biotecnología Avanzada)



UNIVERSIDAD
DE MÁLAGA



TESIS DOCTORAL

Novel approaches for osteosarcoma treatment: drug combination, nanotechnology and cell therapy

Autora:

Liliya Kazantseva

Directores:

José Becerra Ratia
Leonor Santos Ruiz


Málaga, 2022





UNIVERSIDAD
DE MÁLAGA

AUTOR: Liliya Kazantseva

 <https://orcid.org/0000-0003-0966-472X>

EDITA: Publicaciones y Divulgación Científica. Universidad de Málaga



Esta obra está bajo una licencia de Creative Commons Reconocimiento-NoComercial-SinObraDerivada 4.0 Internacional:

<http://creativecommons.org/licenses/by-nc-nd/4.0/legalcode>

Cualquier parte de esta obra se puede reproducir sin autorización pero con el reconocimiento y atribución de los autores.

No se puede hacer uso comercial de la obra y no se puede alterar, transformar o hacer obras derivadas.

Esta Tesis Doctoral está depositada en el Repositorio Institucional de la Universidad de Málaga (RIUMA): riuma.uma.es



UNIVERSIDAD
DE MÁLAGA



Escuela de Doctorado

DECLARACIÓN DE AUTORÍA Y ORIGINALIDAD DE LA TESIS PRESENTADA PARA OBTENER EL TÍTULO DE DOCTOR

Dña. Liliya Kazantseva

Estudiante del programa de doctorado Biotecnología Avanzada de la Universidad de Málaga, autora de la tesis, presentada para la obtención del título de doctor por la Universidad de Málaga, titulada “*Novel approaches for osteosarcoma treatment: drug combination, nanotechnology and cell therapy*”

Realizada bajo la tutorización de Leonor Santos Ruiz y dirección de José Becerra Ratia y Leonor Santos Ruiz

DECLARO QUE:

La tesis presentada es una obra original que no infringe los derechos de propiedad intelectual ni los derechos de propiedad industrial u otros, conforme al ordenamiento jurídico vigente (Real Decreto Legislativo 1/1996, de 12 de abril, por el que se aprueba el texto refundido de la Ley de Propiedad Intelectual, regularizando, aclarando y armonizando las disposiciones legales vigentes sobre la materia), modificado por la Ley 2/2019, de 1 de marzo.

Igualmente asumo, ante a la Universidad de Málaga y ante cualquier otra instancia, la responsabilidad que pudiera derivarse en caso de plagio de contenidos en la tesis presentada, conforme al ordenamiento jurídico vigente.

En Málaga, a 18 de noviembre de 2022

| | |
|--|------------------------------------|
| Fdo.: Liliya Kazantseva Doctoranda | Fdo.: Leonor Santos Ruiz Tutora |
| Fdo.: José Becerra Ratia y Leonor Santos Ruiz Directores de tesis | |



EFQM AENOR



Edificio Pabellón de Gobierno. Campus El Ejido.
29071

Tel.: 952 13 10 28 / 952 13 14 61 / 952 13 71 10
E-mail: doctorado@uma.es



UNIÓN EUROPEA
Fondo Europeo de Desarrollo Regional

This project has received funding from the European Union's Horizon 2020 research and innovation programme under the Marie Skłodowska-Curie, grant agreement No 7131721

Acknowledgements

The completion of the present work would not be possible without the contribution of different people. First of all, I am extremely grateful to Pepe for giving me the opportunity to carry out this thesis in his laboratory. Thank you for your engagement and enthusiasm for solving different obstacles that were on my way so I could finish the work accordingly.

Very especial thanks to Leonor for taking me as your student and believing in me through these years. I value immensely your knowledge, constant guidance, patience and all the opportunities that you have been given to me so I could grow professionally.

Being surrounded by amazing people from the lab who transmitted the good vibes and were ready to help with any question I had made it everything so easy. Even though working in a little bit different topic from my lab mates, I was still able to learn something new from all of you during the numerous discussions through the coffee breaks and lunch time. I am really lucky to call my lab mates not just colleagues but friends. Rick, thank you for sharing your knowledge, the will to offer a help and cheer me up when the things seemed to go wrong. Gustavo, for your guidance especially in the first year when I was new in the lab and not able to localize reactive or glassware. Thank you for your patience, help and showing another way of working on the experiments. Marta, who could think that a Czech and a Russian would be friends, but it was possible. Thank you for your friendship, support and belief in me especially in the moments of distress. For always having time to help and teach me in the lab, for taking care not only of my cells but my plants as well when I was on conference or vacations. Sara, for being a good friend, available to help and teach me tricks to solve Chemistry-related calculations. Miguel, for your support and availability to listen to me. Fabi and Ivan, for your moral support in the last year of my thesis. Sandra and Jose Miguel, for your conversations that made the final pace of this work easier. Cristina, Ana and MariCarmen, thank you for being available to help me with my experiments when I had to go to the Faculty.

There are several people from different groups that helped me a lot. Clara, my desk neighbour, thank you for showing me how to process the data from the confocal microscope in ImageJ and giving me tips on how to improve the images of my experiments. Along with Ernesto, for suggesting the right program to analyse lab data and pictures. Saretta, another desk neighbour, for your friendship, encouragement and teaching a little bit of Italian. Juan, for being available to talk about a wide range of topics and always give a good advice. Verena, for being a great friend, your constant support and for helping me through the difficult times by taking me out to disconnect. Maria Cristina, for your friendship, optimism and help.

The Cell Culture Unit was a place of work full of confessions, laughs, motivation and conversations about science. I want to thank my cell culture buddies Lidia, Jose, Carlos and Alicia

for your support and encouragement. COFUNDs, Claudia, Ana, Vladimir, Amene, Precious, Ashish and Jonas, for all types of conversations, going outs and help.

The completion of this thesis would not be possible without the kind technical assistance of the technicians such as John, Luisa, Juan Felix, Eva, Reyes, Alex, Reme, Mari and Monica. Thanks for your patience, will to help and always finding a gap to answer my questions regarding a particular process. A special gratitude to Ainhoa, for making the first year of incorporation to BIONAND so much easier, for being there to solve different issues and to remind all the administrative procedure that should be done. Almudena and Irene, for continuing the work of Ainhoa and be available to help.

To my friends especially Laura, Alba, Bea and Noe for your friendship, endless support and always be proud of my achievements throughout all these years.

Last but not least, I am so thankful for my parents. It would be not possible without your sacrifices and unconditional support that gave me the strength to overcome every obstacle.

Abstract

Osteosarcoma is one of the most common malignant tumours of bone, primarily affecting children and adolescents. The implementation of chemotherapy, combined with advancement in surgery and radiotherapy, has substantially improved cancer therapy in patients with localized disease. However, it is almost inefficient for patients with metastasis, as at this point the malignant cells are typically resistant to the standard drug combination. The presence of a plethora of unwanted side effects, associated to chemotherapeutic agent toxicity, is also common. To guarantee a better drug delivery with less adverse effects, different approaches were evaluated.

Combination therapy is commonly used to enhance drug effects. The first strategy of this thesis evaluated the potential of oridonin, a natural product from the medicinal herb *Rabdosia rubescens*, to act in combination with doxorubicin for osteosarcoma treatment. The results show that oridonin and doxorubicin have a synergistic effect, increasing osteosarcoma cells death through increased levels of reactive oxygen species (ROS), alteration of mitochondria membrane potential and a higher rate of apoptosis. A pilot *in vivo* experiment could not prove this effect, due to dosing problems, but it showed a protective liver effect of oridonin against doxorubicin-induced hepatotoxicity.

The second strategy attempted a more complex approach, where drug repositioning, nanoencapsulation and cell therapy are combined. Drug repositioning, which is based on “recycling” an already known drug from one disease to another, is a rapid and cost-efficient approach to the development of new therapies. Paclitaxel is commonly used for treating breast and lung cancer, but there are few studies on its efficiency against osteosarcoma. Combination of nanotechnology and cell therapy gives chance to generating a “nano-engineered” mesenchymal stem cell that would be able to both actively target the tumour site and protect the paclitaxel-loaded nanoparticle against the components of the body. Thus, the aim was to evaluate the efficiency of paclitaxel alone and incorporated inside a thermo-responsive polymer for osteosarcoma treatment. Moreover, study the effects of different chemotherapeutic drug approaches on mesenchymal stem cells before preparing a “nano-engineered” cell vehicle.

Different concentrations of free and nanoencapsulated paclitaxel were evaluated against osteosarcoma cells by using both traditional 2D cultures and 3D culture systems. Finally, the effects of different presentations of paclitaxel on both viability and proliferation of mesenchymal stem cells were assessed, as well as the ability of these cells to uptake the drug-loaded nanoparticles and later release the cargo. The results showed that paclitaxel, alone and loaded inside a thermo-sensitive nanoparticle, was able to reduce the viability of different osteosarcoma cell lines in 2D cultures, presenting different cells lines a dissimilar-sensitivity to the treatment. The empty nanoparticle demonstrated to be biocompatible, as no cytotoxic effects were detected in neither 2D nor 3D osteosarcoma cultures, nor in MSC cultures. In a microtissue model (3D

cultures) paclitaxel-loaded nanoparticles presented a better outcome against osteosarcoma, as compared to the free, non-encapsulated drug. Finally, mesenchymal stem cells stayed viable after exposure to both presentations of paclitaxel. However, the treatment was able to affect the morphology and reduce proliferation of these cells. According to the findings, paclitaxel loaded nanoparticle is a good candidate for osteosarcoma therapy and its incorporation inside a cell vehicle is a promising approach, although additional studies are still required to implement the technology.

Keywords: osteosarcoma, doxorubicin, oridonin, paclitaxel, mesenchymal stem cells, nanoparticles, combination therapy, cell therapy, drug repositioning

Abstract in Spanish: Resumen

El osteosarcoma es un tumor maligno que afecta a los huesos. La enfermedad empieza con la transformación neoplásica de los osteoblastos, células de origen mesenquimal propias del tejido óseo, encargadas de producir la matriz extracelular característica del hueso. Los osteoblastos transformados adquieren una capacidad de división descontrolada acompañada de una producción de matriz ósea poco eficiente, en donde el hueso que se forma es inmaduro, y suele denominarse como tejido osteoide. Éste se caracteriza por presentar una matriz extracelular orgánica no mineralizada constituida principalmente por colágenos tipo I y V, y en menor medida por colágeno tipo III. A diferencia de ésta, la matriz ósea sana está compuesta mayoritariamente de colágeno tipo I. Las modificaciones postraduccionales de este tipo de colágeno son las que determinan su especificidad en cada tejido. En el osteosarcoma a diferencia del hueso sano, los residuos de lisina del colágeno tipo I están hidroxilados. Como consecuencia, las propiedades mecánicas se ven afectadas y esta característica es muy relevante en el comportamiento de osteoblastos. La rigidez ósea es necesaria para que las células madres mesenquimales puedan posteriormente diferenciarse en el linaje osteoblastico y permitir la formación de un nuevo hueso.

El osteosarcoma es un tipo de cáncer que afecta particularmente a los niños y adolescentes. Representa un 3-5% de los cánceres infantiles, con una incidencia anual de 5,6 casos por millón de pacientes pediátricos. El osteosarcoma se presenta principalmente entre los 10 a 14 años y es más común en los niños que en las niñas. Este tipo de cáncer se desarrolla preferentemente en la porción ancha de los huesos largos, conocida como metáfisis, que crece durante la infancia. Los más afectados son tibia, fémur y húmero. Los síntomas que presentan los pacientes son dolores alrededor de la rodilla, que son de carácter intermitente, pero que pueden empeorar durante la noche. Esta aflicción hace que algunos niños empiecen a cojear. La visita al médico no siempre termina con un diagnóstico correcto, ya que los síntomas a veces se confunden con una tendinitis. Además, el dolor se puede atribuir al dolor de crecimiento. Las fracturas patológicas no son comunes en las primeras etapas del desarrollo del osteosarcoma y tienen una incidencia de entre el 5% y el 12%. Sin embargo, es muy frecuente que se observen en etapas avanzadas del cáncer del hueso. Por último, síntomas como fiebre o pérdida de peso se aprecian en tumores malignos, pero no en condiciones benignas.

Aunque el osteosarcoma es típico en los niños, existe un segundo pico de incidencia en pacientes mayores de 60 años. En este grupo el cáncer de hueso es considerado raro y representa menos del 1% de todos los tipos de cáncer. En personas mayores, el osteosarcoma es considerado un tumor secundario, consecuencia de una exposición previa a la radiación para tratar otro tipo de cáncer en la juventud, o por la enfermedad ósea de Paget, un trastorno que se caracteriza por una descomposición y formación ósea anormal que causa deformidades en el hueso. A diferencia de los pacientes pediátricos, donde el tumor suele formarse en los huesos largos, en personas mayores se da en mandíbula o la pelvis.

Actualmente, el tratamiento del osteosarcoma consiste en quimioterapia preoperatoria, seguida de cirugía de remoción y quimioterapia posoperatoria. La cirugía es un proceso fundamental de la terapia que consiste en la extirpación completa del tumor y el tejido que lo rodea. El cáncer de hueso tiene varios subtipos que varían en agresividad, y que son establecidos por un patólogo a partir de los estudios histológicos de la biopsia del paciente. A día de hoy no existen marcadores moleculares que permitan la detección o pronosis del osteosarcoma en muestras de suero o tejido, ni marcadores celulares que permitan detectar de forma específica las células tumorales en sus fases tempranas de transformación, lo que impone el análisis histológico del tumor como herramienta única para determinar el tipo de tumor y su posible evolución. Así, a partir de las características histológicas, se determina si existe la necesidad de combinar la cirugía con la quimioterapia. Para osteosarcoma poco agresivo, que no suele invadir tejidos y órganos cercanos, el tratamiento quirúrgico suele considerarse suficiente. En tumores agresivos, con alto riesgo de producir metástasis, es necesario emplear quimioterapia junto con la extirpación del tejido canceroso. En este caso, la cirugía va revelar el efecto de la quimioterapia y permitirá tener una idea de la supervivencia del paciente. Se considera una buena respuesta cuando se observa más del 90% de necrosis en el sarcoma, siendo lo contrario predictivo de mal pronóstico.

Antiguamente, la cirugía era el único tratamiento para el osteosarcoma con un bajo índice pronóstico. Esto se debía a que las células cancerígenas habían escapado del tumor y se habían diseminado por todo el cuerpo. La implementación de la quimioterapia, en los años setenta del pasado siglo, aumentó sustancialmente la tasa de supervivencia de los pacientes, alcanzando un 65% en los primeros 5 años después de la terapia del cáncer. Hoy en día, la quimioterapia se administra generalmente antes y después de la cirugía. La preoperatoria tiene como objetivo reducir y delimitar el tumor, haciéndolo visible con respecto al tejido circundante, facilitando así la eliminación de las células cancerosas durante la resección quirúrgica. Si este procedimiento se hace de manera correcta y el tumor había respondido a quimioterapia, la probabilidad de que el cáncer vuelva a aparecer será baja. Otra ventaja de la quimioterapia preoperatoria es ganar tiempo para planificar cómo se va proceder en la cirugía para que sea lo más leve posible sin tener que comprometer la funcionalidad de la extremidad afectada por el cáncer. Este proceso dura entre 8 y 10 semanas.

La quimioterapia posoperatoria se administra dos semanas después de que las heridas de la operación hayan cicatrizado. Los pacientes lo reciben durante 20 semanas. El propósito de quimioterapia posoperatoria es eliminar las células cancerosas que puedan quedar en el cuerpo, ya que su presencia, por más mínima que sea, puede ser la causa de la recurrencia del cáncer en el futuro.

Actualmente la combinación estándar de fármacos empelada en la quimioterapia del osteosarcoma comprende dosis altas de metotrexato, cisplatino y doxorubicina. Éste puede ser considerado como el tratamiento estándar que se administra a los pacientes pediátricos, y no ha podido ser mejorado en las últimas décadas. Se ha visto que la administración de uno o dos agentes quimioterapéuticos no ha mejorado el pronóstico, mientras que la combinación de tres o más fármacos ha aumentado las tasas de supervivencia. Al utilizar diferentes fármacos con distintos mecanismos de acción, el tumor tiene menos posibilidades de mutar y adaptarse a nuevas condiciones. Los pacientes que hayan respondido favorablemente a quimioterapia preoperatoria siguen recibiendo la misma combinación de medicamentos en la quimioterapia posoperatoria. Hoy en día, la tasa de supervivencia de los pacientes tratados con cirugía y quimioterapia es de 65% después de 5 años. Sin embargo, cuando el osteosarcoma forma metástasis, generalmente en los pulmones, esta tasa de supervivencia se reduce al 20%. Este valor no ha cambiado en los últimos 30 años. Una de las razones es la falta de biomarcadores fiables y validados para el diagnóstico de osteosarcoma. Otra es la resistencia de las células cancerígenas a los agentes quimioterapéuticos a través de mecanismos que incluyen desregulación de las vías de señalización, autofagia y presencia de células madre cancerosas poco proliferativas. Los agentes quimioterapéuticos presentan numerosos efectos secundarios, representando un enorme obstáculo en el enfoque multifarmacológico. Muchos de estos efectos, tales como la alopecia, las náuseas y los vómitos, son temporales y dejan de manifestarse al terminar la quimioterapia. Pero otros efectos adversos pueden ser permanentes y potencialmente mortales. Entre ellos, el más destacable es la cardiotoxicidad causada por la administración de doxorubicina. Este efecto es acumulativo, y puede conducir a una insuficiencia cardíaca irreversible. La miopatía es una de las principales causas de muerte en los sobrevivientes de osteosarcoma pediátrico.

Capítulo I. Tratamiento combinatorio de doxorubicina y oridonina.

La baja tasa de supervivencia de los pacientes de osteosarcoma con metástasis, y la presencia de efectos secundarios causados por los distintos agentes quimioterapéuticos, indican que se deben plantear nuevas vías terapéuticas que permitan una vehiculización segura de los fármacos hacia el tumor. Con miras a lograr esto, en el presente trabajo se han evaluado diferentes estrategias. Una es la terapia combinada, que consiste en la coadministración de doxorubicina con un nuevo fármaco prometedor, la oridonina. Este último es un diterpeno aislado de *Rabdosia rubescens*, una hierba medicinal popular en los países asiáticos. La oridonina es un producto natural que ha mostrado efectos citotóxicos en distintos tipos de células cancerosas cuando se administra sólo o en conjunto con otros agentes quimioterapéuticos. Hasta la fecha, no hay estudios de la combinación compuesta de doxorubicina y oridonina en el osteosarcoma.

Para poder evaluar las estrategias propuestas en este trabajo (capítulo I y capítulo II), se han seleccionado tres líneas de osteosarcoma, MG63, Saos-2 y U2OS, que difieren en la funcionalidad de la proteína supresoras de tumores, p53. U2OS presenta la versión normal del gen *p53*, mientras que MG63 contiene varias mutaciones en *p53* y en el gen que codifica CDKN2A (*cyclin-dependent kinase inhibitor 2A*). Por su parte, Saos-2 posee mutaciones nulas que conllevan la falta de funcionalidad en la proteína p53. Estas características van a ser determinantes en la respuesta a los distintos tratamientos que presenten las células, y con ello van a ser representativas de distintos tipos de osteosarcoma, o de distintas poblaciones celulares dentro de un tumor. Esto es importante debido a que el tumor no es una masa homogénea, sino una estructura compuesta de muchas células que tienen diferentes tipos de mutaciones y morfologías.

La eficacia de combinar un agente quimioterapéutico conocido como es la doxorrubicina (DOX) junto con un producto natural novedoso, oridonina (ORI), fue evaluada en Saos-2 y U2OS. Primero se estudió el efecto citotóxico de cada fármaco para determinar la concentración que produce el 50% de muerte celular (CD_{50}). A partir de este dato se prosiguió a combinar las distintas concentraciones de DOX (CD_{50} , $CD_{50}/2$ and $CD_{50}/10$) junto con varias de ORI (CD_{50} , $CD_{50}/2$ and $CD_{50}/10$). Después el índice de combinación (IC) fue calculado para cada pareja de fármacos en *CompuSyn*, un programa que cuantifica la interacción entre fármacos mediante el método de Chou-Talalay. En base a los resultados obtenidos, se eligió la mejor combinación de fármacos para ser estudiada en Saos-2 y U2OS. Para establecer si la presencia de ORI facilita la acumulación intracelular de DOX, se midió la fluorescencia intrínseca (roja) de DOX en el citómetro 2 horas después de que las células fueron sometidas al tratamiento a cada uno de los fármacos de manera separada y conjunta. Posteriormente para entender cómo los medicamentos inducían la citotoxicidad, se analizaron el potencial de membrana mitocondrial, la apoptosis y la inducción de las especies reactivas de oxígeno mediante citometría de flujo. Por último, la expresión de diferentes proteínas anti-apoptóticas de la familia Bcl-2 se determinó mediante *Western Blot*.

Después de evaluar las combinaciones de DOX y ORI *in vitro* en dos líneas de osteosarcoma diferentes, se prosiguió a confirmar su eficacia en un modelo *in vivo*, mediante un estudio piloto. Para ello se puso a punto un modelo de xenotrasplante de las líneas tumorales humanas en ratones inmunodeficientes (nu/nu CD1), y posteriormente se evaluó el tratamiento combinado de DOX+ORI, usando como controles DOX y ORI administrados individualmente, o ningún tratamiento. El tratamiento con DOX y ORI fue administrado durante 10 días. A lo largo del proceso tanto el peso como el tamaño del tumor fueron monitorizados periódicamente. Al terminar el tratamiento, los ratones fueron sacrificados y los tumores extraídos, medidos y fijados para su conservación. Se evaluaron también los cambios en el tamaño y peso del corazón y el hígado. Tanto los tumores como los órganos fueron sometidos a análisis histológico mediante

técnicas histoquímicas (Hematoxilina-Eosina y Tricromico de Masson-Goldner). En el caso del corazón, en donde se quería evaluar la presencia de fibrosis, se empleó también rojo sirio.

Los resultados obtenidos muestran que la administración individual de DOX y ORI redujo la viabilidad de Saos-2 y U2OS de manera dosis-dependiente después de 48 horas de exposición. DOX fue más tóxico en comparación con ORI, ya que las concentraciones bajas eran capaces reducir la viabilidad de las células de osteosarcoma al 50%. El valor de CD_{50} en Saos-2 fue 5 μM para DOX y 20 μM para ORI, mientras que en U2OS los valores fueron 1 μM y 12 μM , respectivamente. Estos resultados pueden correlacionarse con la función de p53. La proteína funcional en U2OS induce la apoptosis en respuesta al daño producido por los agentes quimioterapéuticos a dosis relativamente bajas, mientras que la p53 mutada de Saos-2 no es tan eficaz y, por esta razón, requirió una mayor concentración de los fármacos para lograr reducir al 50% su viabilidad celular.

El tratamiento combinatorio de DOX y ORI resultó ser más citotóxico que las drogas usadas por separado. En base al IC calculado, se encontró sinergismo en casi todas las combinaciones de ambos fármacos en Saos-2, mientras que en U2OS la mayoría produjo efectos aditivo o antagonico. Las combinaciones con mayor tasa de mortalidad consistieron en compuestos de concentraciones de DOX y ORI más bajas que sus respectivos CD_{50} . Basándonos en los valores de IC se seleccionaron las siguientes combinaciones para proseguir los estudios: 2.5 μM DOX + 10 μM ORI para Saos-2 y 1 μM DOX + 10 μM ORI para U2OS.

Con el fin de comprender el mecanismo responsable de la apoptosis observada en ambas líneas de osteosarcoma, se evaluó la acumulación intracelular de DOX y la inducción de especies reactivas de oxígeno (ROS). En U2OS el tratamiento simultáneo con DOX y ORI tuvo efectos similares a uno de los fármacos aplicados de manera separada. No hubo diferencia en la inducción de ROS y apoptosis entre DOX y DOX+ORI, lo que sugiere que los efectos anticancerígenos son causados principalmente por el agente quimioterapéutico y ORI no ha contribuido a la citotoxicidad de DOX. En cambio, en Saos-2, se observó una mayor acumulación de DOX en presencia de ORI. También los niveles de apoptosis y la inducción de ROS fueron mayores en células tratadas con ambos fármacos. En conjunto, los datos sugieren que los efectos sinérgicos observados entre DOX y ORI pueden actuar a través de ORI induciendo una mayor acumulación de DOX dentro de Saos-2. En consecuencia, la inducción de ROS podría ser responsable del daño mitocondrial y la activación de la cascada de señalización que termina con la apoptosis. El análisis por *Western Blot* reveló una alteración en la expresión de diferentes proteínas antiapoptóticas de la familia *Bcl-2* en Saos-2.

El hecho de que los resultados obtenidos hayan mostrado que diferentes líneas tumorales presentan distinta respuesta a la terapia con DOX+ORI, confirmaría la heterogeneidad del cáncer,

que apoya la idea actual de pasar de la quimioterapia convencional a una quimioterapia personalizada, que usaría diferentes fármacos, o combinaciones de ellos, en función de las características del tumor. La combinación de DOX y ORI representa un enfoque prometedor para aquellos tumores que presentan características similares a Saos-2, mientras que sería menos eficientes contra células como U2OS. En general, los datos del presente trabajo han mostrado que, en tumores sensibles a la combinación, la adición de ORI permite reducir las dosis de DOX y, por ende, se esperaría poder reducir sus efectos adversos, como la cardiotoxicidad.

Dados los prometedores resultados obtenidos en los estudios *in vitro* con Saos-2, se prosiguió a evaluar la combinación de DOX+ORI en un estudio piloto con ratones inmunodeficientes. Por ser un estudio preliminar, las concentraciones administradas se eligieron en base a la literatura disponible. Después de administrar los fármacos durante 10 días por vía intraperitoneal, algunos ratones del grupo de DOX fueron hallados muertos. Por otra parte, la dosis de ORI se tuvo que reajustar porque los animales mostraron signos de dolor. Esto sugiere que las dosis estudiadas eran altas y se necesitaría probar un rango amplio de dosis de DOX y ORI, tanto por separado como en combinación, en un futuro examen *in vivo*. Con las condiciones probadas no se encontraron cambios significativos en el volumen del tumor al terminar el tratamiento. Tampoco se observó efecto cardioprotector de ORI. Sin embargo, se pudieron detectar efectos hepatoprotectores en presencia del producto natural.

Capítulo II. Reposicionamiento de paclitaxel encapsulado en PNIPAM, y vehiculizado en MSC.

En este capítulo se abordó una estrategia más compleja en comparación con el capítulo I, en donde se ha probado reposicionamiento de un agente quimioterapéutico, se encapsulación dentro de una nanopartícula termosensible, y su vehiculización en células madre mesenquimales (MSC).

El reposicionamiento de medicamentos se basa en el reciclaje de fármacos comúnmente aprobados para otro tipo de enfermedad, u otro tipo de cáncer. Este enfoque es rápido y rentable para el desarrollo de nuevas terapias, ya que los fármacos no son diseñados *de novo*. Los agentes quimioterapéuticos reciclados ya están aprobados, lo que significa que no hay que realizar estudios preclínicos de seguridad. Con ello, el tiempo y el costo de las Fases I y II de los nuevos ensayos clínicos pueden reducirse considerablemente.

Los agentes quimioterapéuticos que se administran a un paciente con osteosarcoma en general actúan sobre el material genético de las células malignas. Paclitaxel es un fármaco que se emplea para tratar pacientes con cáncer de mama y de pulmón. Su mecanismo de acción es a través de una estabilización los microtubulos produciendo una detención del ciclo celular en fase G2/M que conduce a la inducción de apoptosis. Hasta la fecha existen pocos estudios sobre la eficacia del paclitaxel en el tratamiento del osteosarcoma.

Los agentes quimioterapéuticos carecen de especificidad, ya que cuando se administran se distribuyen por todo el cuerpo, donde pueden dirigirse tanto a células sanas como cancerígenas. Esto hace que la cantidad de fármaco que llega al tumor sea menor, comprometiendo el éxito de la terapia. El encapsulamiento de los agentes quimioterapéuticos dentro de las nanopartículas es una estrategia en investigación para lograr que los fármacos estén protegidos durante su recorrido por el cuerpo (vehiculización), o que incluso se acumulen o sean atrapados en el tumor (vectorización). Además, diversas modificaciones pueden hacer que las nanopartículas liberen el fármaco que portan, específicamente, dentro de, o junto a, las células cancerígenas (liberación controlada). Así, por ejemplo, se han desarrollado nanopartículas biocompatibles que incorporan moléculas que hacen que reconozcan de forma específica el tumor (vectorización) y liberen el fármaco bajo un estímulo específico, como cambio de temperatura o pH (liberación controlada). La nanotecnología es, por tanto, una estrategia muy prometedora en el tratamiento del cáncer. Esta tecnología permitiría reducir tanto las dosis como los efectos adversos de los agentes quimioterapéuticos. Por estos motivos, en el presente trabajo se evaluó la incorporación de paclitaxel dentro de una nanopartícula PNIPAM termosensible, que experimenta un cambio cuando la temperatura es superior a 32 °C, siendo entonces capaz de liberar el fármaco.

Debido a que, hasta la fecha, no se han encontrado marcadores específicos en la superficie de las células de osteosarcoma, es complicado dirigir las nanopartículas de PNIPAM hacia las células cancerígenas. Por ende, la siguiente estrategia fue evaluar las células madre mesenquimales como vehículo de las nanopartículas cargadas con paclitaxel. En los últimos tiempos existe un interés creciente en esta estrategia debido a las características favorables de las células mesenquimales, que incluyen hipoinmunogenicidad y alta capacidad para migrar hacia regiones donde existe inflamación o hipoxia, ambas características propias del ambiente tumoral. En el presente trabajo, el uso de las células mesenquimales tiene un doble propósito. Por un lado, proteger las nanopartículas de la eliminación por parte de los macrófagos; y por otra, depositar el nanoconjugado en el tumor gracias a la capacidad migratoria de las células mesenquimales. La combinación de la nanotecnología con la terapia celular representa una terapia novedosa para el cáncer del hueso.

Para determinar la aplicabilidad de paclitaxel (PTX) en el tratamiento del osteosarcoma, sus efectos fueron evaluados como fármaco libre y encapsulado dentro de la nanopartícula termosensible PNIPAM. Se usó Rojo Nilo (NiR) como marcador fluorescente de la nanopartícula para facilitar su detección dentro de las células en los estudios de microscopía. En todos los experimentos, NiR@PNIPAM, la nanopartícula sin el fármaco, se empleó como control para asegurar que los efectos producidos por PTX+NiR@PNIPAM fueran realmente causados por PTX y no por la propia nanopartícula, o la presencia de impurezas producidas durante su síntesis.

Las nanopartículas fueron caracterizadas con la ayuda del microscopio electrónico de transmisión. Con las imágenes obtenidas se visualizó la morfología y se determinó su tamaño.

Los efectos de PTX, libre y encapsulado, en la viabilidad celular fueron estudiados en tres líneas de osteosarcoma: MG63, Saos-2 y U2OS, tanto en cultivos planos (2D), como en cultivos 3D (esferoides celulares y de colágeno). La internalización de las nanopartículas NiR@PNIPAM por parte de células de osteosarcoma se visualizó mediante microscopía confocal gracias al marcaje fluorescente con Rojo Nilo.

Para mejorar aun el tratamiento de osteosarcoma, se hizo un pequeño experimento en donde se evaluó ORI en combinación con PTX libre y encapsulado. Tal como se había hecho con DOX+ORI, se estudiaron distintas concentraciones de PTX/PTX+NiR@PNIPAM (CD_{50} , $CD_{50}/2$ and $CD_{50}/10$) junto con varias de ORI (CD_{50} , $CD_{50}/2$ and $CD_{50}/10$) para luego calcular el índice de combinación, IC, en *CompuSyn*.

Tras evaluar la aplicabilidad de PTX, libre o encapsulado, contra las diferentes líneas de osteosarcoma, se decidió implementar el tratamiento mediante el uso de terapia celular. Se usaron células madre mesenquimales (MSC) de dos orígenes diferentes, tejido adiposo (AD-MSC) y médula ósea (BM-MSC). Para que estas células puedan cumplir su rol tienen que ser capaces de tolerar el fármaco antes de llegar al tumor y liberarlo en el mismo. Por lo cual, tanto las AD-MSC como las BM-MSC fueron sometidas al tratamiento de PTX, PTX+NiR@PNIPAM y NiR@PNIPAM, y se estudió el efecto del mismo sobre las propiedades celulares. Para que las MSC puedan ser utilizadas como vehículo de las nanopartículas deben incorporarlas al interior celular, cosa que se comprobó mediante microscopía confocal y microscopía electrónica de transmisión. Se confirmó también la capacidad migratoria de las células que habían incorporado la nanopartícula mediante ensayos *scratch*. Por último, el medio condicionado por MSC expuestas a PTX y PTX+NiR@PNIPAM fue recogido en varios tiempos muestrales tras la exposición (24, 48, 72 y 96 horas), y se usó sobre las células de osteosarcoma. De esta forma se comprobó si las MSC eran capaces de liberar PTX, metabolitos de PTX o la nanopartícula cargada con el fármaco. Para ello, se evaluó la viabilidad de las tres líneas de osteosarcoma tras ser sometidas a los medios condicionados.

La nanopartícula PNIPAM evaluada en el presente trabajo presentó una estructura esférica sin formar agregaciones, dato obtenido a partir de las imágenes del microscopio electrónico de transmisión. PTX+NiR@PNIPAM presentó un tamaño superior a NiR@PNIPAM, lo que indicaría que la diferencia se debe a la presencia del agente quimioterapéutico. También se confirmó la capacidad de las nanopartículas para responder a los cambios en la temperatura: cuando ésta era superior a 32 °C el tamaño de las nanopartículas se hacía menor.

Los estudios de citotoxicidad de NiR@PNIPAM, PTX+NiR@PNIPAM y PTX libre, en tres líneas de osteosarcoma (MG63, Saos-2 y U2OS) mostraron que la nanopartícula sin el agente quimioterapéutico es inocua para las células, lo que indicaría que los efectos citotóxicos de PTX+NiR@PNIPAM se deben a la presencia de PTX. Por tanto, PNIPAM parece ser un vehículo seguro para ser empleado en la terapia del cáncer.

Para determinar la sensibilidad del osteosarcoma al PTX, y si ésta se ve afectada al ser el fármaco encapsulado dentro de PNIPAM, las diferentes líneas del cáncer de hueso (MG63, Saos-2 y U2OS) fueron sometidas al tratamiento con distintas concentraciones de PTX y PTX+NiR@PNIPAM. Los resultados confirmaron que las tres líneas de osteosarcoma evaluadas eran sensibles al agente quimioterapéutico en sus dos versiones, libre y encapsulada, aunque cada una mostró una sensibilidad diferente, siendo Saos-2 la más afectada, y U2OS la más resistente. No se encontraron diferencias de citotoxicidad entre PTX y PTX+NiR@PNIPAM.

Normalmente la eficacia de un fármaco se evalúa en células cultivadas en monocapa (2D). Actualmente existen discrepancias en la correlación de los resultados obtenidos en los sistemas de cultivo 2D y el escenario *in vivo*, debido a las diferencias en la morfología, expresión genética y capacidad migratoria y proliferativa de las células en ambos tipos de cultivo. El sistema de cultivo en esferoides (3D) se considera mucho más representativo de la situación *in vivo*, en donde la arquitectura de esferoides simula un tumor avascular. Por esta razón, se decidió confirmar los efectos de PTX+NiR@PNIPAM y PTX en un sistema de cultivo celular 3D. Tras probar distintos métodos de formación de esferoides, se comprobó que sólo la línea MG63, de fenotipo fibroblástico, poseía la capacidad de formar esferoides en cultivo, en tanto que las líneas epitelioideas U2OS y Saos-2 no se organizan en este tipo de estructura. Al igual que en células cultivadas en monocapa, los esferoides multicelulares de MG63 resultaron ser sensibles a PTX libre y encapsulado. En este caso, la nanopartícula cargada con el fármaco tuvo mejor rendimiento que PTX sin encapsular, resultado que difería de los resultados obtenidos en los cultivos 2D. Es posible que los esferoides respondan al daño inducido por PTX con una densificación, lo que bloquea o dificulta la penetración del fármaco hacia las capas internas estructura. Este mecanismo “de escape” podría ser eludido por la nanopartícula, que presenta otro mecanismo de entrada en las células.

La ausencia de la matriz extracelular en los esferoides multicelulares representa una desventaja en este modelo, ya que es una parte fundamental en los tumores, en particular de los tumores óseos. La presencia de matriz extracelular tiene un rol importante en la proliferación, migración e invasión de las células cancerígenas. Por esta razón, se consideró necesario evaluar los efectos de PTX y PTX+NiR@PNIPAM en esferoides de colágeno. Para ello, MG63, Saos-2 y U2OS fueron mezcladas con la matriz y dejadas crecer en unas placas “*ultra-low attachment*”,

hechas con un tipo de plástico que no favorece la adhesión celular. Los resultados del experimento mostraron que la viabilidad celular era mínimamente afectada, sin detectarse diferencias entre los tratamientos. Esto podría indicar que la matriz extracelular actúa como barrera para ambas presentaciones de PTX, dificultando su movilidad, o que la presencia de la matriz ejerce en las células un efecto citoprotector, a través de la señalización ejercida por las moléculas de adhesión células-matriz.

Se conoce que la sobrevivencia y capacidad de invasión a tejidos cercanos por parte de las células cancerígenas depende de la degradación de la matriz extracelular, que se logra mediante la secreción de proteasas. Existen estudios en donde se indica que PTX, aparte de estabilizar los microtúbulos, inhibe la síntesis de colagenasa, comprometiendo la viabilidad y migración de las células cancerígenas. Para evaluar este efecto del agente quimioterapéutico en osteosarcoma, se sembraron esferoides de colágeno de MG63 en una placa Petri, y se estudiaron a lo largo de varios días mediante tinción diferencial de células vivas y muertas (tinción *LIVE/DEAD*). Los controles, y los esferoides sometidos a la concentración más baja de ambas presentaciones de PTX, mostraron una reducción de tamaño, y migración celular hacia la placa. Por otro lado, la exposición a concentraciones crecientes de PTX y PTX+NiR@PNIPAM redujo la viabilidad de MG63 dentro del esferoide de colágeno. Es razonable suponer que el agente quimioterapéutico afectó la liberación de proteasas, comprometiendo así la invasibilidad de las células cancerosas.

Tras confirmar la capacidad de ambas presentaciones de PTX en inhibir la migración de células de osteosarcoma (es decir, su capacidad invasiva o metastática), se repitió el experimento en MG63 y U2OS para poder cuantificar la distancia de migración desde el esferoide de colágeno en una placa de 96 pocillos. Sin embargo, no fue posible ya que las células cubrieron completamente la superficie del pocillo. Al igual que en el experimento anterior las concentraciones crecientes de PTX y PTX+NiR@PNIPAM afectaron la migración fuera del esferoide de colágeno. Además, por observar una estructura no compactada del gel se podría sugerir, también en estos casos, una reducida liberación de colagenasa.

Los resultados expuestos apoyan la posibilidad de reciclar PTX para el tratamiento del osteosarcoma, y que la nanoencapsulación no afecta negativamente a la capacidad del fármaco para inducir muerte celular tumoral. Para indagar más en el destino intracelular de la nanopartícula usada en este trabajo, se estudió la localización intracelular de NiR@PNIPAM en tres líneas celulares de osteosarcoma mediante microscopio confocal. En las tres líneas celulares, la nanopartícula se localizó acumulada en la región perinuclear. En algunos casos pudo observarse que los acúmulos de NiR@PNIPAM estaban localizados en el interior de una vesícula. La velocidad de incorporación y acumulación intracelular de NiR@PNIPAM fue diferente entre las líneas celulares.

Una característica importante de las nanopartículas es que no son específicas, y su capacidad de llegar al tumor depende principalmente de la fenestración anormal en las paredes de los vasos que rodean al mismo. Para dirigir el fármaco hacia el tumor, se evaluó la estrategia de emplear células madre mesenquimales (MSC) como vehículo de los nanoconjugados. Se evaluaron tanto MSC de tejido adiposo (AD-MSC), como MSC de médula ósea (BM-MSC). La capacidad de estas células para incorporar NiR@PNIPAM y PTX+NiR@PNIPAM se confirmó mediante microscopía confocal y microscopía electrónica de transmisión. Para garantizar una entrega dirigida del fármaco sin afectar las propiedades del vehículo celular, los efectos de ambas presentaciones de PTX sobre las células mesenquimales fueron evaluados en un período de 24 horas. Se confirmó nuevamente la inocuidad de NiR@PNIPAM, como había ocurrido en los experimentos con las líneas de osteosarcoma. La viabilidad de células mesenquimales de origen adiposo y médula ósea fue poco afectada al ser expuestas a un amplio rango de concentraciones de PTX y PTX+NiR@PNIPAM. Sin embargo, ambas presentaciones del agente quimioterapéutico disminuyeron tanto la capacidad de proliferación como la de migración de estas células. Los efectos producidos por PTX y PTX+NiR@PNIPAM fueron similares y no duraderos, ya que al terminar de aplicar el tratamiento, las células mesenquimales recuperaron su capacidad proliferativa.

El siguiente paso fue evaluar la capacidad de incorporar y liberar ambas presentaciones de PTX por parte de células mesenquimales. Para esto, se recolectó el medio condicionado en diferentes tiempos y se administró en las tres líneas de osteosarcoma. La viabilidad de las células cancerígenas no fue afectada, lo que sugiere que las células mesenquimales deberían exponerse a concentraciones mucho más altas de las empleadas para garantizar una liberación suficiente de nanopartícula en células de osteosarcoma. En su estado actual, la nanopartícula usada no permite esa posibilidad porque, al liberar parcialmente el fármaco a temperatura fisiológica, afecta al vehículo (la célula), reduciendo su capacidad migratoria. No obstante, una reformulación que eleve su LCST ligeramente por encima de los 37 °C sería adecuada para este fin.

Finalmente, se evaluó el tratamiento combinado de PTX y PTX+NiR@PNIPAM con ORI, como una posible estrategia para incrementar la eficacia antitumoral de PTX. En todos los casos se encontraron combinaciones sinérgicas. Los resultados de ORI+PTX fueron mejores que los de ORI+PTX encapsulado. Esta diferencia podría ser atribuida al mecanismo de incorporación dentro de la célula, en donde PTX entra por difusión pasiva, mientras que la nanopartícula lo hace por endocitosis. Este breve ensayo, que es, hasta la fecha, el primer estudio que evalúa la combinación ORI y PTX en osteosarcoma, sugiere que el tratamiento combinado de ORI y PTX debería recibir más atención en el futuro y podría representar una alternativa a los fármacos comúnmente administrados para tratar algunos tipos de osteosarcoma.

En resumen, los resultados del presente trabajo muestran que la terapia combinada de DOX y PTX con ORI, permitió incrementar la eficacia antitumoral de estos fármacos, lo que podría reducir las concentraciones de los mismos empleadas en quimioterapia, reduciendo así sus efectos secundarios. La nanopartícula PNIPAM fue biocompatible, no habiendo dañado ni a las células cancerígenas, ni a las mesenquimales. Además, la encapsulación de PTX dentro de PNIPAM demostró tener efectos similares o mejores al fármaco libre. Estos datos proponen a esta nanopartícula como una buena candidata para la encapsulación de fármacos, después de modificarla para elevar su LCST. Por último, se ha visto la capacidad de las MSC para incorporar y tolerar la nanopartícula cargada con el fármaco.

Index

| | |
|---|-----------|
| Abbreviations..... | 1 |
| Figures index..... | 7 |
| Tables index | 11 |
| I. Introduction | 17 |
| 1. General overview of osteosarcoma | 19 |
| 2. Bone | 21 |
| 2.1. Bone cells..... | 22 |
| 2.1.1. Osteoblasts | 22 |
| 2.1.2. Osteocytes | 23 |
| 2.1.3. Osteoclasts..... | 23 |
| 2.1.4. Osteoprogenitor cells..... | 23 |
| 2.2. Bone development..... | 24 |
| 2.2.1. Intramembranous ossification | 25 |
| 2.2.2. Endochondral ossification | 25 |
| 2.2.2.1. Bone growth in length and diameter | 25 |
| 3. Clinical presentation of osteosarcoma..... | 27 |
| 3.1. Localization..... | 27 |
| 3.2. Grading..... | 27 |
| 3.3. Histological classification | 28 |
| 3.3.1. Conventional osteosarcoma..... | 28 |
| 3.3.2. Telangiectatic osteosarcoma..... | 28 |
| 3.3.3. Small cell osteosarcoma | 29 |
| 3.3.4. Epithelioid osteosarcoma | 29 |
| 3.3.5. Giant cell-rich osteosarcoma | 29 |
| 3.3.6. Low-grade central osteosarcoma..... | 29 |
| 3.3.7. High-grade surface osteosarcoma | 30 |
| 3.3.8. Periosteal osteosarcoma | 30 |
| 3.3.9. Parosteal osteosarcoma | 30 |
| 4. Risk factors..... | 31 |
| 4.1. Inherited syndromes | 31 |
| 4.1.1. Retinoblastoma..... | 31 |
| 4.1.2. Li-Fraumeni..... | 31 |
| 4.1.3. Rothmund-Thompson, Werner and Bloom..... | 32 |
| 4.2. Paget's disease..... | 32 |
| 4.3. Ionizing radiation | 33 |

| | |
|--|-----------|
| 5. Symptoms of osteosarcoma..... | 33 |
| 6. Diagnosis..... | 34 |
| 7. Staging..... | 35 |
| 8. Osteosarcoma treatment..... | 36 |
| 8.1. Chemotherapy..... | 37 |
| 8.1.1. Methotrexate..... | 38 |
| 8.1.2. Doxorubicin..... | 39 |
| 8.1.3. Cisplatin..... | 40 |
| 8.1.4. Ifosfamide..... | 41 |
| 8.2. Surgery..... | 41 |
| 8.3. Radiation therapy..... | 43 |
| 9. Novel therapeutic options..... | 43 |
| 9.1. Drug repositioning..... | 43 |
| 9.1.1. Paclitaxel..... | 44 |
| 9.2. Oridonin..... | 45 |
| 9.3. Nanoparticles..... | 46 |
| 9.4. Cells as drugs vehicles..... | 51 |
| II. Hypothesis and objectives..... | 53 |
| General Hypothesis..... | 55 |
| General Objective..... | 55 |
| Strategy I..... | 56 |
| Hypothesis..... | 56 |
| Objectives..... | 56 |
| Strategy II..... | 57 |
| Hypotheses..... | 57 |
| Objectives..... | 57 |
| III. Materials and methods..... | 59 |
| 1. Cell lines..... | 61 |
| 1.1. Osteosarcoma..... | 61 |
| 1.1.1. MG63..... | 61 |
| 1.1.2. U2OS..... | 61 |
| 1.1.3. Saos-2..... | 61 |
| 1.2. Human adipose and human bone marrow tissue-derived mesenchymal stem cells (huAD-MSC and huBM-MSC)..... | 62 |
| 2. Antibiotics..... | 62 |

| | |
|---|-----------|
| 3. FBS heat inactivation | 62 |
| 4. Cell passage..... | 62 |
| 4.1. Cell counting using Neubauer chamber | 63 |
| 5. Doubling time..... | 64 |
| 6. Resazurin assay | 65 |
| 6.1. Calibration curve | 66 |
| 7. Cell fixation..... | 66 |
| 8. Cell freezing..... | 67 |
| 8.1. Osteosarcoma cell lines | 67 |
| 8.2. MSC | 67 |
| 9. Cell thawing | 67 |
| 10. Drugs | 68 |
| 10.1. Doxorubicin (DOX) | 68 |
| 10.2. Oridonin (ORI)..... | 68 |
| 10.3. Paclitaxel (PTX)..... | 68 |
| 11. Nanoparticles..... | 69 |
| 11.1. Nanoparticle's characterization | 69 |
| 12. Statistical analysis | 69 |
| Strategy I: Doxorubicin and oridonin combination..... | 71 |
| 1. Effects of DOX and ORI on cell viability | 73 |
| 2. Effects of DOX and ORI combination | 73 |
| 3. Cell uptake of DOX..... | 73 |
| 4. Mitochondrial membrane potential | 74 |
| 5. Apoptosis assay | 74 |
| 6. Reactive oxygen species assay | 75 |
| 7. Western blot | 76 |
| 8. Pilot osteosarcoma xenograft model in nude mice..... | 76 |
| 9. Histological analysis | 77 |
| 9.1. Hematoxylin-Eosin (HE) staining..... | 77 |
| 9.2. Masson-Goldner Trichrome staining..... | 78 |
| 9.3. Picrosirius Red staining..... | 79 |
| Strategy II: Paclitaxel, MSC and combination treatment..... | 81 |
| Part I: Osteosarcoma | 81 |
| 1. 2D cell culture | 83 |
| 1.1. Effects of PTX, PTX+NiR@PNIPAM and NiR@PNIPAM on cell viability | 83 |
| 1.2. Concentration determination of PTX and PTX+NiR@PNIPAM that is able to reduce cell viability to 50% at day 2 | 83 |

| | |
|---|------------|
| 2. 3D cell culture | 84 |
| 2.1. Cellular spheroids in a 96 Ultra Low Attachment (ULA) conical well plate | 84 |
| 2.1.1. LIVE/DEAD assay | 84 |
| 2.2. Hanging drop | 85 |
| 2.3. Collagen spheroids | 86 |
| 2.3.1. Collagen spheroids in a 96 ULA well plate | 86 |
| 2.3.2. Collagen spheroids on a Petri dish | 86 |
| 2.3.2.1. LIVE/DEAD assay | 87 |
| 2.3.3. Osteosarcoma cell migration from collagen spheroids | 87 |
| 3. Cell uptake of NiR@PNIPAM | 87 |
| Strategy II: Paclitaxel, MSC and combination treatment | 89 |
| Part II: Mesenchymal stem cells | 89 |
| 1. Effects of PTX, PTX+NiR@PNIPAM and NiR@PNIPAM on cell viability | 91 |
| 2. Cell uptake | 91 |
| 2.1. Transmission electron microscopy of NiR@PNIPAM | 91 |
| 2.2. Confocal scanning laser microscopy of NiR@PNIPAM and PTX+NiR@PNIPAM within huAD-MSC | 92 |
| 3. Proliferation-migration assay | 92 |
| 3.1. Scratch assay | 92 |
| 3.2. 2-well insert assay | 93 |
| 4. Conditioned medium | 93 |
| 5. Time-lapse | 94 |
| Strategy II: Paclitaxel, MSC and combination treatment | 95 |
| Part III: Paclitaxel/Paclitaxel+NiR@PNIPAM and oridonin combination | 95 |
| 1. Effects of PTX+NiR@PNIPAM/PTX and ORI combination | 97 |
| IV. Results and discussion | 99 |
| Strategy I: Doxorubicin and oridonin combination | 101 |
| Results | 105 |
| 1. Cell culture treatment | 105 |
| 2. Combination treatment | 106 |
| 3. Effects of combination treatment on osteosarcoma cells morphology | 108 |
| 4. Cell uptake of DOX | 109 |
| 5. Mitochondrial membrane potential | 110 |
| 6. Apoptosis induction | 112 |
| 7. Induction of reactive oxygen species | 113 |
| 8. Western blot | 114 |

| | |
|---|------------|
| 9. Effects of ORI on human osteoblasts | 115 |
| 10. Pilot osteosarcoma xenograft model in nude mice..... | 116 |
| Discussion..... | 122 |
| Future perspectives | 128 |
| Strategy II: Paclitaxel, MSC and combination treatment..... | 129 |
| Results | 133 |
| Part I: Osteosarcoma | 133 |
| 1. Nanoparticles..... | 133 |
| 1.1. Characterization of NiR@PNIPAM and PTX+NiR@PNIPAM..... | 133 |
| 2. 2D cell culture | 134 |
| 2.1. Effects of PTX, PTX+NiR@PNIPAM and NiR@PNIPAM on cell viability | 134 |
| 2.2. Concentration that achieves 50% of cell death after 2 days of treatment..... | 136 |
| 3. 3D cell culture | 137 |
| 4. Collagen spheroids | 141 |
| 5. Cell uptake of NiR@PNIPAM..... | 146 |
| Part II: Mesenchymal stem cells | 148 |
| 1. Effect of free and encapsulated PTX on MSC | 148 |
| 2. Cell uptake | 149 |
| 3. Migration of MSC carrying drug-loaded nanoparticles | 151 |
| 4. Conditioned medium..... | 154 |
| 5. Time-lapse..... | 155 |
| Part III: Osteosarcoma: combination treatment..... | 156 |
| Discussion..... | 160 |
| Future perspectives | 168 |
| V. General discussion..... | 169 |
| VI. Conclusions..... | 175 |
| VII. Bibliography | 181 |
| VIII. Appendix: Supplementary material..... | 207 |
| IX. Publications..... | 215 |

Abbreviations

A

AJCC: American joint committee for cancer

ALP: Alkaline phosphatase

AM: Acetoxymethyl

B

BMP: Bone morphogenic protein

BSP: Bone sialoprotein

C

CD₅₀: Concentration that achieves 50% of cell death

CI: Combination index

CM: Conditioned medium

CSC: Cancer stem cells

CT: Computed tomography

D

DHFR: Dihydrofolate reductase

DMEM-hg: Dulbecco's modified eagle's medium-high glucose

DMP1: Dentine matrix protein 1

DMSO: Dimethyl sulfoxide

DOX: Doxorubicin

DOXol: Doxorubicinol

E

ECACC: European collection of authenticated cell cultures

ECM: Extracellular matrix

EPR: Enhanced permeation and retention effect

EthD-1: Ethidium homodimer-1

F

FBS: Fetal bovine serum

FDA: Food and drug administration

¹⁸F-FDG: ¹⁸F-fluorodeoxyglucose

H

huAD-MSc: Human adipose tissue-derived mesenchymal stem cells

huBM-MSc: Human bone marrow tissue-derived mesenchymal stem cells

J

JNK: c-Jun N-terminal kinase

L

LCST: Lower critical solution temperature

LDH: Lactate dehydrogenase

LFS: Li-Fraumeni syndrome

LFL: Li-Fraumeni like syndrome

LV: Leucovorin

M

MAP: High-dose methotrexate, doxorubicin and cisplatin

α MEM: Minimum essential medium eagle, α modification

MHC: Major histocompatibility complex

MMP: Mitochondrial membrane potential

MRI: Magnetic resonance imaging

MSC: Mesenchymal stem cells

MTX: Methotrexate

N

NADPH: Nicotinamide adenine dinucleotide phosphate

NaOH: Sodium hydroxide

NF- κ B: Nuclear factor- κ B

NiR: Nile red

NK: Natural killer

O

OCN: Osteocalcin

ORI: Oridonin

P

PBS: Phosphate buffer saline

PEG: Polyethylene glycol

PET: Positron emission tomography

PLGA: Poly(lactic-co-glycolic acid)

PNIPAM: Poly(N-isopropylacrylamide)

pRB: Retinoblastoma protein

PS: Phosphatidylserine

PTX: Paclitaxel

R

RES: Reticuloendothelial system

ROS: Reactive oxygen species

T

TEM: Transmission electron microscopy

U

ULA: Ultra low attachment

W

Wnt: Wingless and Int-1

Figures index

| | |
|---|-----|
| Figure 1. World rates of osteosarcoma incidence | 20 |
| Figure 2. Evidence of osteosarcoma found in ancient bone | 21 |
| Figure 3. Zones of the long bones | 22 |
| Figure 4. Bone cells..... | 24 |
| Figure 5. Components of epiphyseal growth plate | 26 |
| Figure 6. Effects of PTX microtubule targeting..... | 44 |
| Figure 7. Representation of EPR effect..... | 48 |
| Figure 8. Schematic representation of a liposome..... | 49 |
| Figure 9. Schematic representation of a nanocrystal..... | 49 |
| Figure 10. Structural changes in the thermoresponsive nanoparticle | 50 |
| Figure 11. Neubauer chamber for cell counting..... | 64 |
| Figure 12. Schematic representation of a 12-well plate for doubling time estimation..... | 65 |
| Figure 13. Schematic representation of cell dilution in a 96-well plate | 66 |
| Figure 14. General overview of the materials and methods used in strategy I..... | 71 |
| Figure 15. General overview of the materials and methods used in part I of strategy II | 81 |
| Figure 16. Schematic representation of hanging drop in a 60 mm culture tissue dish | 85 |
| Figure 17. General overview of the materials and methods used in part II of strategy II | 89 |
| Figure 18. Schematic representation of huAD MSC seeded in a transwell of a 24-well plate..... | 91 |
| Figure 19. Schematic representation of scratch procedure in a well of a 24-well plate | 93 |
| Figure 20. Schematic representation of 2 well culture-insert and its removal in a well of 24-well plate..... | 93 |
| Figure 21. Toxicity evaluation of DOX and ORI..... | 105 |
| Figure 22. Toxicity evaluation of DOX and ORI combination..... | 106 |
| Figure 23. Combination index..... | 107 |
| Figure 24. Effects of ORI, DOX and combination of both on osteosarcoma cells | 108 |
| Figure 25. Cellular uptake of DOX in Saos-2 | 109 |
| Figure 26. Cellular uptake of DOX in U2OS | 110 |
| Figure 27. Effects of ORI, DOX and combination of both on osteosarcoma cells mitochondrial membrane potential..... | 111 |
| Figure 28. Effects of ORI, DOX and combination of both on osteosarcoma cells apoptosis .. | 112 |
| Figure 29. Intracellular levels of ROS caused by ORI, DOX and combination of both in osteosarcoma cells..... | 113 |
| Figure 30. Effects of ORI, DOX and the combination of both on the expression of apoptosis-related proteins in Saos-2..... | 114 |
| Figure 31. Effects of ORI on NH OST..... | 115 |
| Figure 32. Radiographs of mice tumours | 116 |

| | |
|---|-----|
| Figure 33. Histological characteristics of Saos-2 tumours in athymic nude mice..... | 117 |
| Figure 34. Effects of DOX and ORI treatment on osteosarcoma tumour growth | 118 |
| Figure 35. Saos-2 tumours..... | 119 |
| Figure 36. Livers from control and treated mice..... | 120 |
| Figure 37. Liver weight from control and treated mice..... | 120 |
| Figure 38. Collagen content in the hearts of athymic nude mice | 121 |
| Figure 39. TEM images of the nanoparticles | 133 |
| Figure 40. <i>In vitro</i> toxicity evaluation of PTX+NiR@PNIPAM, NiR@PNIPAM and PTX... | 135 |
| Figure 41. <i>In vitro</i> toxicity evaluation of PTX+NiR@PNIPAM and PTX after 2 days of treatment..... | 137 |
| Figure 42. Spheroid formation | 138 |
| Figure 43. Hanging drop spheroid formation in Saos-2 and U2OS | 138 |
| Figure 44. Proliferation index of MG63 spheroids | 140 |
| Figure 45. Two colour fluorescent staining of MG63 spheroids..... | 141 |
| Figure 46. <i>In vitro</i> toxicity evaluation of osteosarcoma cells grown on collagen spheroids.... | 142 |
| Figure 47. MG63 collagen spheroids treated with PTX..... | 143 |
| Figure 48. MG63 collagen spheroids treated with PTX+NiR@PNIPAM | 144 |
| Figure 49. Control MG63 and U2OS collagen spheroids | 145 |
| Figure 50. MG63 and U2OS collagen spheroids treated with PTX+NiR@PNIPAM and PTX | 145 |
| Figure 51. U2OS and MG63 uptake of NiR@PNIPAM | 146 |
| Figure 52. Saos-2 uptake of NiR@PNIPAM | 147 |
| Figure 53. <i>In vitro</i> toxicity evaluation of PTX+NiR@PNIPAM, NiR@PNIPAM and PTX in MSC | 149 |
| Figure 54. huAD-MSC and huBM-MSC uptake of nanoparticles | 149 |
| Figure 55. TEM images of huAD-MSC incorporation of NiR@PNIPAM..... | 150 |
| Figure 56. Scratch assay in huBM-MSC..... | 152 |
| Figure 57. 2-well insert assay in huBM-MSC..... | 153 |
| Figure 58. huAD and huBM-MSC anti-proliferative activity against osteosarcoma cell lines | 154 |
| Figure 59. Representative images from time-lapse | 156 |
| Figure 60. Toxicity evaluation of PTX+NiR@PNIPAM/PTX and ORI combination..... | 157 |
| Figure 61. CI of Saos-2 | 158 |
| Figure 62. Toxicity evaluation of PTX+NiR@PNIPAM and ORI combination | 158 |
| Figure 63. CI of U2OS | 159 |
| Figure 64. Toxicity evaluation of PTX+NiR@PNIPAM and ORI combination | 159 |
| Figure 65. CI of MG63..... | 160 |

Tables index

| | |
|--|-----|
| Table 1. Enneking system for staging of malignant musculoskeletal tumours | 36 |
| Table 2. AJCC staging system..... | 36 |
| Table 3. Composition of NiR@PNIPAM and PTX+NiR@PNIPAM..... | 69 |
| Table 4. Drug concentrations used for DOX + ORI combination therapy in osteosarcoma cell lines | 73 |
| Table 5. Determination of appropriate conditions for inoculation process <i>in vivo</i> | 76 |
| Table 6. Process of tissue dehydration during paraffin embedding..... | 77 |
| Table 7. Hematoxylin-Eosin staining procedure | 78 |
| Table 8. Masson-Goldner staining procedure..... | 78 |
| Table 9. Picrosirius Red staining procedure | 79 |
| Table 10. DOX+ORI treatment <i>in vitro</i> and <i>in vivo</i> | 118 |
| Table 11. Characterization of nanoparticles | 134 |

“I was taught that the way of progress was neither swift nor easy”.

Marie Curie

I. Introduction

“I want to walk into a room, be it a hospice for the dying or a hospital for sick children, and feel that I am needed. I want to do, not just to be”.

Princess Diana

1. General overview of osteosarcoma

Everybody in their life has a friend or a family member who is suffering or has suffered from cancer. This should not be a surprise: 1.93 millions of people died from cancer in Europe in 2018 (Ferlay et al., 2018). The disease affects differently to youngsters and adults. The most common cancer types in adults are lung, colorectal, breast and pancreatic cancer (Ferlay et al., 2018). In children and teenagers, on the other side, lymphoma, brain cancer and osteosarcoma are most frequently seen.

Osteosarcoma is one of the most common malignant tumours of bone. It is composed from transformed osteoblast, cells of mesenchymal origin, that produce immature bone or osteoid tissue (Durfee, Mohammed, & Luu, 2016; Kansara, Teng, Smyth, & Thomas, 2014). It is characterized by an organic unmineralized extracellular matrix consisting mainly of collagens type I and V, and to a lesser extent of collagen type III (Fernandes, Harkey, Weis, Askew, & Eyre, 2007; Shapiro & Eyre, 1982). This is in contrast to the normal, healthy bone matrix, which is mainly composed of collagen type I. In healthy tissues, post-translational modifications of this type of collagen are responsible of tissue-dependent differences (Shapiro & Eyre, 1982). In osteosarcoma, the lysine residues of collagen type I present more hydroxylation compared to the healthy bone. This difference in mechanical properties can be a determinant point in osteoblasts behaviour, as bone stiffness is important for mesenchymal stem cells differentiation into the osteoblastic lineage and, hence, new bone formation (Baumann & Hennet, 2016; Fernandes et al., 2007; Shapiro & Eyre, 1982).

Osteosarcoma represents a 3-5% of childhood cancers, with an annual incidence of 5.6 cases per million of paediatric patients (Mirabello, Troisi, & Savage, 2009). It occurs mainly between the ages of 10 to 14 (Durfee et al., 2016). For this group of patients there are similar geographical rates, which means there is no specific region that with predominant prevalence. In most countries osteosarcoma is more common in boys than in girls. The general incidence rate is 3-5 per million in males and 2-4 million in females. Although the initial onset of the disease is predominant in girls, it increases in puberty for boys, suggesting a possible influence of hormonal change in the pathogenesis (**Figure 1**) (Mirabello et al., 2009). Cancer develops preferentially in the wide portion of the long bones known as metaphysis that grows during the childhood. The most affected are tibia, femur and humerus (Kansara et al., 2014).

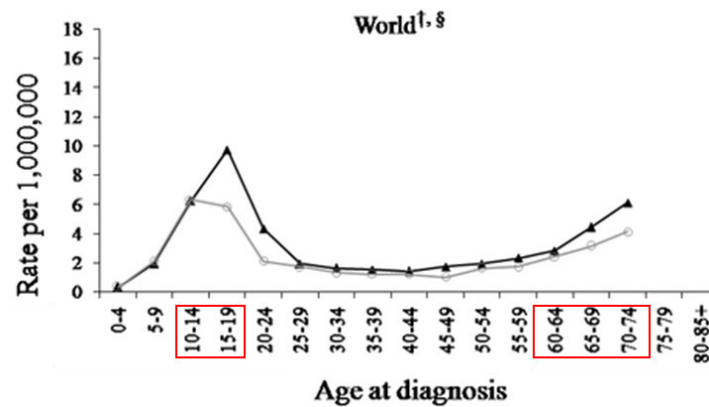


Figure 1. World rates of osteosarcoma incidence. The black line with triangles represents male rates and the grey line with circles are female rates. The red boxes highlight the two main peaks of osteosarcoma incidence. Adapted and modified from (Mirabello et al., 2009).

There is a second peak of incidence in patients over the age of 60, where osteosarcoma is a rare type that accounts for less than 1% of cancers (**Figure 1**). In elders, osteosarcoma is considered to be a secondary tumour caused by previous exposure to irradiation during the treatment of another type of cancer, or by sarcomatous transformation of Paget's disease of bone. In general, the incidence rate is 2.5-5 cases per million in males and 1.5-4 in females, which makes a worldwide ratio of 1.01:1 (M:F). Unlike with paediatric patients, there is a considerable geographical variation in osteosarcoma incidence in the elders, being the higher rates observed in Australia, Canada and UK (Mirabello et al., 2009). Another significant difference concerns the location where the tumor occurs: while in paediatric patients the tumor appears predominantly in the long bones, in the elderly it usually appears in the jaw or pelvis (Durfee et al., 2016; Kansara et al., 2014).

Interestingly, bone cancer has accompanied human beings, as well as other vertebrates, throughout history. The earliest documented case of osteosarcoma in a human ancestor belongs to a hominin unearthed in Swartkrans cave (South Africa), who died between 1.6 and 1.8 million years ago (**Figure 2**). The disease, located in the foot bone, was unveiled with 3D imaging methods. Neoplastic evidence in human fossils is rare. This could be influenced by the short life expectancy of people in those days, as compared to nowadays. Modern advances have given rise to an increased life expectancy that, paradoxically, gives better chance for cancer development. Cancer is commonly seen in patients over the age of 60 (Odes et al., 2016).

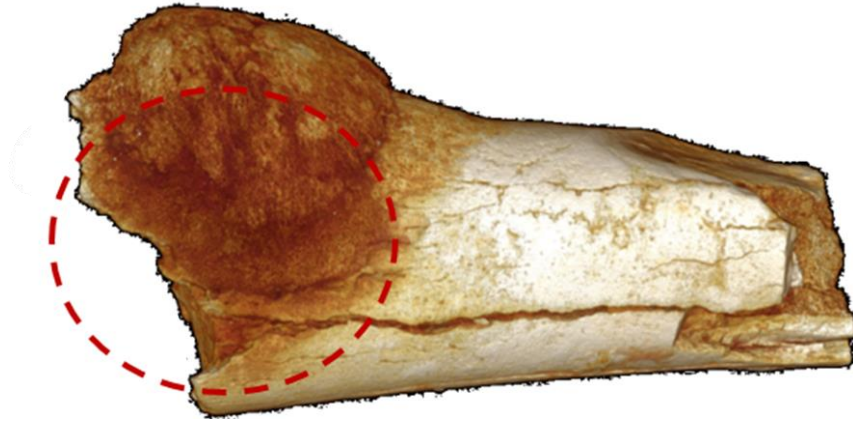


Figure 2. Evidence of osteosarcoma found in ancient bone. Micro-CT longitudinal rendered view of a hominin left 5th metatarsal bone found in Swartkrans cave (South Africa). An osteosarcoma is visible as a hemi-spherical mass that protrudes the cortex (encircled by the red line). Adapted from (Odes et al., 2016).

2. Bone

Bone is a specialized connective tissue, whose mineralized matrix make it unique from the rest of the connective tissues (Boskey & Robey, 2013; Kansara et al., 2014). It has a remarkable regenerative capacity after structural or tissue damage (Boskey & Robey, 2013; Zreiqat, Dunstan, & Rosen, 2015). It is composed mainly of (Boskey & Robey, 2013; Zreiqat et al., 2015):

- Mineral phase: whose principal component is hydroxyapatite.
- Organic phase: collagen type I, considered to be the building block representing 90% of the organic bone matrix, followed by 5% of non-collagenous proteins and 2% of lipids.
- Water.

The rigid morphology enables bone to perform several key functions. One of them is the protection of vital organs, such as lung and heart. Another one is muscle support, necessary for proper body structure and movement. Also, it provides a microenvironment for haematopoiesis, responsible for blood cells formation, and participates in calcium and phosphate storage, necessary for the maintenance of homeostasis (Cowan & Kahai, 2018; Czerniak, 2015; Kansara et al., 2014).

Based on their morphological features, bones can be classified in two categories: flat and tubular bones. Flat bones include skull, pelvis, scapula, clavicle and sternum, characterized by thin and curved features. They give support for muscles attachment and protection to the internal organs. Tubular bones are subdivided into short and long bones. Short bones comprise metacarpals and phalanges, bones of variable shapes whose main function is to provide support and stability. Finally, long bones are femur, tibia and humerus, which are important in leverage and are composed of the following zones:

- Diaphysis, the central part located between the proximal and distal ends of the bones. It contains the medulla and bone marrow.
- Epiphysis, the wide section at both ends of the bone.
- Metaphysis the regions where each epiphysis meets the diaphysis. This narrow part contains an epiphyseal plate, also known as growth plate, composed of cartilage in a growing bone. After reaching between 18 and 21 years of life, the human bones stop to grow. In this case the cartilage is replaced by bone and the growth plate becomes an epiphyseal line (**Figure 3**) (Biga et al.; Cowan & Kahai, 2018; Czerniak, 2015).

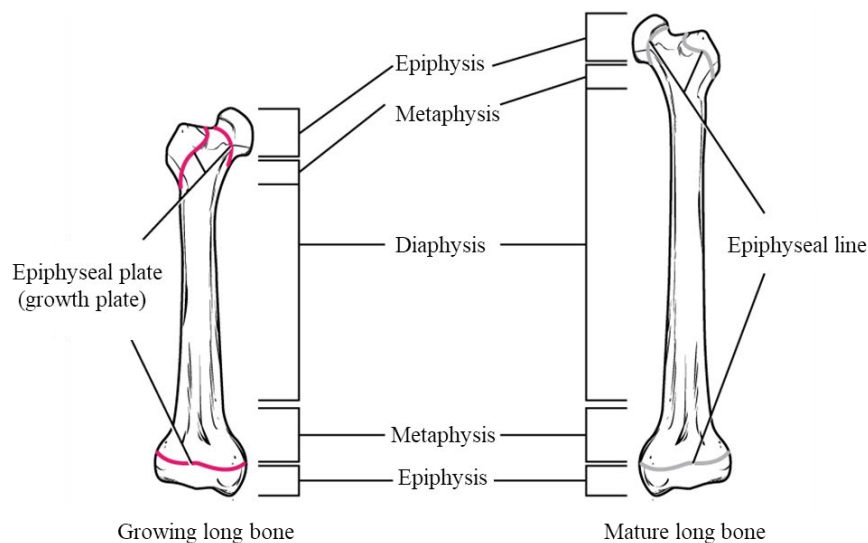


Figure 3. Zones of the long bones. Schematic representation of different regions of the growing femur of adolescents (left), and the mature femur of adults (right). Adapted from (Biga et al.).

2.1. Bone cells

2.1.1. Osteoblasts

Osteoblasts are cuboidal cells lining the bone surface that are specialized in bone matrix formation (**Figure 4**). Their active participation in mineralization is possible due to their abundance in Golgi apparatus, rough endoplasmic reticulum and several secretory vesicles (Czerniak, 2015; Florencio-Silva, Sasso, Sasso-Cerri, Simões, & Cerri, 2015). Osteoblast arise from mesenchymal stem cells (MSC), whose differentiation into preosteoblastic lineage is a controlled process that involves the expression of specific genes (*Runx2* is the most important, as lack of osteoblasts was observed in mice bearing *Runx2* null mutation), protein synthesis (bone morphogenic proteins -BMP-, and members of Wiggless -Wnt-, pathways) and deposition of collagenous extracellular matrix (mainly collagen type I). During this process the activity of alkaline phosphatase can be detected. The final step in osteoblast differentiation is the mineralization of the extracellular matrix (ECM) and the expression of several bone markers that

include osteocalcin (OCN), bone sialoprotein (BSP) I/II and collagen type I (Florencio-Silva et al., 2015; Hanna, Mir, & Andre, 2018).

2.1.2. Osteocytes

Osteocytes are the most numerous bone cells and are responsible of bone mineral maintenance. They present a dendritic morphology and a life span of 25 years (**Figure 4**) (Biga et al.; Czerniak, 2015; Florencio-Silva et al., 2015). They arise from a subpopulation of osteoblasts entrapped in a mineralized extracellular matrix. During the transformation of osteoblasts into osteocytes, many intracellular changes occur. One of such is characterized by the reduction of Golgi apparatus and rough endoplasmic reticulum, leading to a decrease in protein synthesis and secretion. Moreover, there is a decrease in the expression of the osteoblastic markers, such as osteocalcin and collagen type I. On the contrary, dentine matrix protein 1 (DMP1) and sclerostin start to be expressed (Florencio-Silva et al., 2015). The only feature that osteocytes preserve from osteoblasts is the lack of mitotic activity ('Bone Formation and Development - Anatomy and Physiology - OpenStax', n.d.). These cells communicate with the neighbour osteocytes and vascular system for nutrient and oxygen supply through tiny tunnels within the bone matrix known as canaliculi (Biga et al.; Florencio-Silva et al., 2015).

2.1.3. Osteoclasts

Osteoclasts are terminally differentiated, multinucleated cells found on the bone surface (**Figure 4**). Unlike osteoblasts and osteocytes, which derive from mesenchymal cells that commit to an osteogenic lineage, osteoclasts originate from mononuclear cells that belong to hematopoietic stem cell lineage. These cells are responsible of bone resorption, which is the removal of old bone. Bone resorption by the osteoclasts is in equilibrium with new bone formation by osteoblasts. In general, the mentioned balance is part of bone remodelling. To be able to perform their functions, osteoclasts have many mitochondria, and acidic vacuoles bearing lysosomal enzymes (Biga et al.; Czerniak, 2015; Florencio-Silva et al., 2015; Stenbeck, 2002). As osteocytes, osteoclasts lack an abundant rough endoplasmic reticulum and Golgi apparatus, indicating their limited ability to synthesize and secrete proteins. During the resorption phase, osteoclasts need to suffer structural changes to ensure a tight attachment to the bone matrix. For this, the actin cytoskeleton rearranges and the cell acquires a ruffled border, where the membrane contains a vacuolar-type H⁺-ATPase (V-ATPase), necessary for the acidification and dissolution of the rigid mineralized bone matrix (Florencio-Silva et al., 2015; Stenbeck, 2002).

2.1.4. Osteoprogenitor cells

Osteoprogenitor cells are cells with high mitotic potential, and a certain commitment towards the osteogenic lineage. Their function is to differentiate and restore the osteoblastic population

during physiological renewal or bone healing (**Figure 4**). These cells are localized in the bone marrow, the periosteum, a membrane that covers the bone surface except in the joints of long bones; and the endosteum, a vascular membrane that extends in the inner part of the bone. They also line the inner surface of the Haversian canals. Osteoprogenitor cells derive from non-hematopoietic MSC, which are located in the bone marrow stroma. Although there are no unique identifying markers for MSC, the International Society for Cellular Therapy established the following criteria in 2006:

- Adhesion to plastic substrate when cultured *in vitro*.
- Expression of specific surface markers such as CD73, CD90 and CD105, but not of CD11b, CD14, CD34 or CD45; CD19 or CD79 α ; and HLA-DR.
- Ability to differentiate into osteoblasts, adipocytes or chondrocytes.

Currently, there is a growing interest in MSC as cellular vehicle for drugs, as these cells don't trigger the immune response and have the capacity to migrate specifically into injury or tumour sites, an ability known as homing (Bernardo et al., 2007; Biga et al.; Le et al., 2017; Lin et al., 2019).

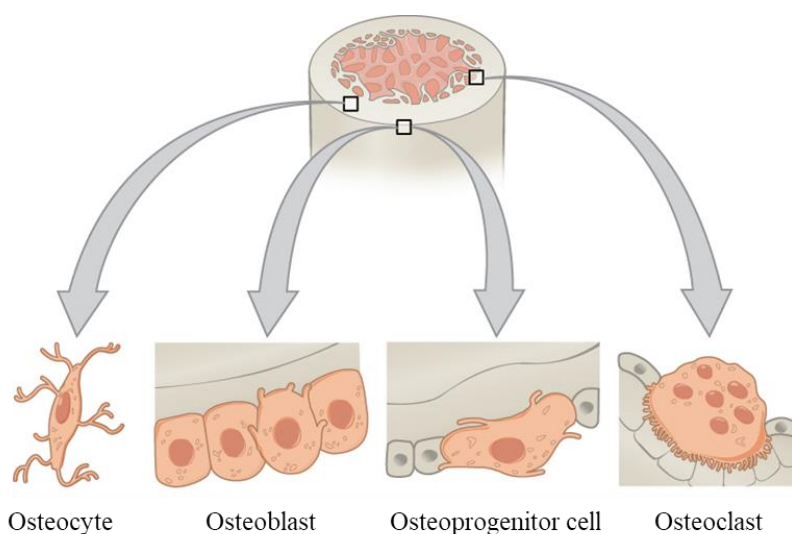


Figure 4. Bone cells. Morphology and localization of the characteristic cells of bone tissue. Adapted from (Biga et al.).

2.2. Bone development

Bone formation in vertebrates is not exclusive of embryonic development, but it can occur after birth, when bone healing is necessary after suffering from fracture, or during ectopic bone generation (H. Zreiqat et al., 2015). Two main processes are implicated:

2.2.1. Intramembranous ossification

Intramembranous ossification is a process that starts during foetal development and lasts until the end of adolescence. It is responsible of flat bone formation (Biga et al.; H. Zreiqat et al., 2015). During the embryonic development of the skeleton, MSC migrate to the site of the future bone, proliferate and condense into circular structures known as nodules. Some of these cells will differentiate into capillaries, while others will become osteoblasts. The last will secrete an unmineralized matrix, composed mainly of collagen, known as osteoid that, over time, will be calcified by the deposition of mineral salts. During this process, some of the osteoblasts will be entrapped in their own secreted matrix, becoming osteocytes (**Figure 5**). Finally, MSC on bone surface will form the periosteum, while the osteoblasts from the inner part will deposit osteoid matrix around the capillaries, enabling layer formation. Deposition of new bone will be done in parallel to the already-calcified bone (Berendsen & Olsen, 2015; Biga et al.; Marie & Cohen-Solal, 2018).

2.2.2. Endochondral ossification

Similar to intramembranous ossification, endochondral ossification starts during embryonic development and continues after birth. It is implicated in the formation of long bones and bones forming the base of the skull. During embryonic development, some of the MSC will differentiate into chondrocytes, cartilage forming cells that will proliferate and produce cartilaginous matrix. Later these cells will transform into hypertrophic chondrocytes, non-proliferative cells with an increased volume. The calcification of the cartilaginous matrix limits the nutrient supply, leading to the apoptosis of the hypertrophic chondrocytes. During this stage there is invasion of blood vessels, hematopoietic cells, osteoblasts and osteoclasts, that will eventually establish the bone marrow, resorb the hypertrophic cartilage and replace it with bone matrix produced by osteoblasts, forming the primary ossification centre that can be seen during foetal development. Unlike intramembranous ossification, where there is a direct calcification of the matrix, in endochondral ossification cartilaginous matrix serves as a template for the following bone formation. After birth, the same process repeats in the epiphyseal regions known as secondary ossification centres (Berendsen & Olsen, 2015; Biga et al.; Boskey & Coleman, 2010; Gilbert, 2000).

2.2.2.1. Bone growth in length and diameter

Bone elongation in mammals would be not possible if bone completely replaced the cartilaginous tissue before birth. During postnatal development the bones extend in both directions from diaphysis. The ossification front meets with the epiphyseal growth plate composed of chondrocytes, and located at each end of the bone (**Figure 3**). The epiphyseal growth plate consists of the following zones (**Figure 5**):

- Reserve or resting zone: it is located at the end of the epiphyseal growth plate and contains a small number of inactive chondroblasts. They act as the reserve of the chondrocyte precursors. Together with the proliferative zone, this area is responsible for bone elongation.
- Proliferative zone: it consists of a high number of chondrocytes that undergo mitosis and keep the growth plate active, being responsible for growth plate elongation.
- Zone of maturation and hypertrophy: where chondrocytes stop dividing and terminally differentiate, while producing a cartilaginous matrix that undergoes a calcification process.
- Zone of calcified matrix: it is connected to the diaphysis and is composed of apoptotic chondrocytes that have become completely surrounded by calcified matrix. This area is invaded by blood vessels and osteoblasts that will transform the calcified cartilaginous matrix in a proper osseous tissue.

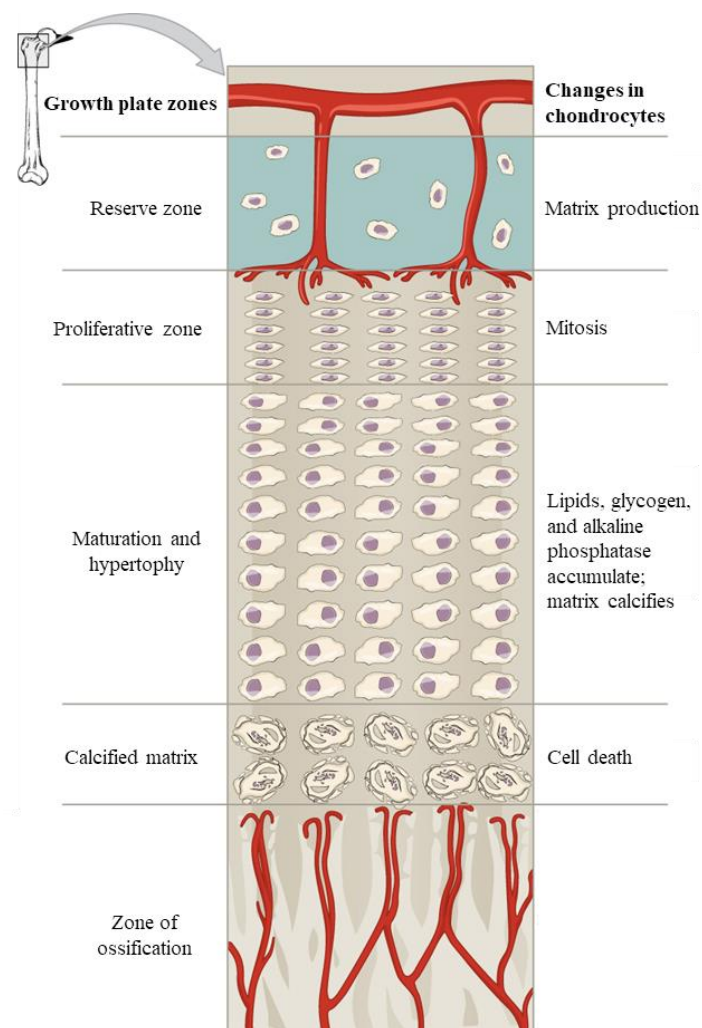


Figure 5. Components of epiphyseal growth plate. Adapted from (Biga et al.).

The bone stops elongation when there are no more chondrocytes and all the cartilage is replaced by bone in the epiphyseal plate, which remains as a thin epiphyseal line (Biga et al.; Douglas, 2011; Gilbert, 2000).

For proper skeletal stability, bone grow in length is not enough. Width bone growth occurs along with bone elongation, and it will last even when bone elongation is over. This process is characterized by bone deposition directly underneath the periosteum (Biga et al.; Rauch, 2005).

3. Clinical presentation of osteosarcoma

3.1. Localization

Osteosarcoma can be localized to bones or spread to different locations of the body. This will determine the treatment options and the possible outcome. It can be classified in the following three main groups:

- Localised osteosarcoma: tumour presence at a specific site or nearby tissue where it originated. For these patients there is a good prognosis as they can expect a 5-year survival rate of 60 to 70% of the patients.
- Metastatic osteosarcoma: cancer cells spread from the initial origin site in the bone to other parts of the body. Lungs are the most common place involved in osteosarcoma metastasis and are associated with a poor prognosis, with a 5-years survival rate of 20% of the cases.
- Recurrent osteosarcoma: cancer reappears after the treatment. In 30% of patients with localized disease, local or distant recurrence can be observed in the first 3 years after treatment. This number is much bigger in metastatic osteosarcoma, affecting 80% of patients. Unfavourable treatment increases the probability of future recurrence and goes along with poor prognosis, similar to that of patients with metastasis (Bacci et al., 2002; Durfee et al., 2016; Picci, 2007).

3.2. Grading

Cancers can be subdivided in three different groups based on the state of differentiation and mitotic activity of its cells:

- Low-grade: cancer cells are localized on the bone surface and have a normal fibroblastic differentiated morphology. They grow slowly and have a low metastatic potential. However, over time these cancer cells can invade deeper structures. Low-grade cancer cells account for 6% of osteosarcomas. For this type there is a good prognosis with a 5-year survival of more than 80% of the patients (Durfee et al., 2016; Lindsey, Markel, & Kleinerman, 2017; Toki et al., 2019).

- Intermediate-grade: deeper structures are slightly invaded by cancer cells, whose mitotic activity is higher than those of low-grade (Limaiem & Sticco, 2019; Lindsey et al., 2017).
- High-grade: malignant cells with undifferentiated morphology characterized by high mitotic activity and local invasion ability. This type of cells represent the most aggressive cancer type. They are also the most commonly seen in all osteosarcomas. The prognosis of high-grade cancers depends on the localization explained above (Durfee et al., 2016; Lindsey et al., 2017; Toki et al., 2019).

3.3. Histological classification

3.3.1. Conventional osteosarcoma

Conventional or classic osteosarcoma is one of the most common and deadly types of osteosarcomas, and accounts for 80% of cases. It is not typical in patients under 6 or over 60 years, which would mean its predominance to be in the second and third decades of life. In 90% of cases it occurs in the metaphysis of long bones, but it also can arise in the diaphysis and, in lower extent, in the epiphysis (Durfee et al., 2016; Fox & Trotta, 2013; Kansara et al., 2014; Kimura et al., 2017; Misaghi, Goldin, Awad, & Kulidjian, 2018; Prater & McKeon, 2019). This type of osteosarcoma is composed of high-grade, genetically unstable, malignant mesenchymal cells that produce an osteoid tissue, which is a histological hallmark in the diagnosis. Conventional osteosarcoma can be divided in three histological subtypes:

- Osteoblastic: mainly composed from osteoblasts and osteoid matrix.
- Chondroblastic: predominance of chondrocytes and cartilaginous matrix.
- Fibroblastic: prevalence of fibroblastic spindle cells.

The denomination will depend on the predominance of the specific subtype. However, presence of three subtypes in a varying degree is usually observed, with the presence of osteoid matrix as a common feature is (Kansara et al., 2014; Lin & Patel, 2013; Misaghi et al., 2018; Prater & McKeon, 2019).

3.3.2. Telangiectatic osteosarcoma

Telangiectatic osteosarcoma is a rare high-grade osteosarcoma that represents 7% of all the osteosarcoma subtypes, and affects patients in their second decade of life (Fox & Trotta, 2013; Misaghi et al., 2018). It is localized in the metaphysis of the long bones, most times in the femur, followed by the tibia and humerus. Telangiectatic osteosarcoma is highly vascularized. Histologically, it can be observed as blood-filled cavities surrounded by malignant osteoblasts (Fox & Trotta, 2013; Kansara et al., 2014; Misaghi et al., 2018). Due to this characteristics it is commonly confused with aneurysmal bone cyst (Prater & McKeon, 2019). Another important feature of this subtype of osteosarcoma is the presence of pathological fractures, which are not

correlated with poor outcome. There are many discrepancies related to the prognosis, as some reports believe in a worse or similar life expectancy to that of patients with conventional osteosarcoma. High vascularization is considered to be the reason of good treatment response in others (Fox & Trotta, 2013; Lin & Patel, 2013; Misaghi et al., 2018).

3.3.3. Small cell osteosarcoma

Small cell osteosarcoma is a rare high-grade type that accounts for 1% of osteosarcoma cases, usually observed in patients in their third or fourth decade of life. It can be localized in the pelvis, femur or proximal humerus. Histologically, it is composed of small, not-uniform, rounded cells, resembling Ewing's sarcoma. However, they can be distinguished by osteoid production, which is absent in Ewing's sarcoma (Fox & Trotta, 2013; Kansara et al., 2014; P. P. Lin & Patel, 2013; Misaghi et al., 2018; Prater & McKeon, 2019).

3.3.4. Epithelioid osteosarcoma

Epithelioid osteosarcoma is another rare high-grade type of osteosarcoma that predominantly affects people over the age of 40. It is localized in the metaphysis of long bones, followed by mandible and, to some extent, maxilla. This type of tumour consists of poorly differentiated osteoblasts with epithelioid features organized in several structures such as cords, sheets or rosettes. Histologically, epithelioid osteosarcoma resembles many tumours with epithelioid characteristics. This is why its diagnosis poses a challenge and it can be easily confused with carcinoma. Patients with this aggressive subtype of osteosarcoma have a poor prognosis (Alqahtani, Alsheddi, & Al-Sadhan, 2015; Lin & Patel, 2013; Okada, Hasegawa, & Yokoyama, 2001; Prater & McKeon, 2019).

3.3.5. Giant cell-rich osteosarcoma

Giant cell-rich osteosarcoma is a rare high-grade osteosarcoma that constitutes 3% of all osteosarcomas, affecting patients in their second decade of life. This subtype occurs in femur and tibia, and is characterized by the presence of osteoclast-like giant cells, and the absence of osteoid matrix. The diagnosis is challenging as the mentioned features resemble a benign giant cell bone tumour, a disease normally observed in old patients (Cahayadi, Antoro, & Swandika, 2019; Chow, 2016; Fox & Trotta, 2013; Prater & McKeon, 2019).

3.3.6. Low-grade central osteosarcoma

Low-grade central osteosarcoma is a rare low-grade tumour that accounts for 1% of all osteosarcomas. It affects people from the second to the fourth decades of life. This cancer occurs mostly in femur and tibia. Histologically, it is composed of both a fibrous stroma and a variable amount of osteoid matrix. Low-grade central osteosarcoma is hard to diagnose because of its low-

grade nature, and because it presents some similar features to fibrous dysplasia and desmoplastic fibroma. Unlike the previously mentioned subtypes, this cancer is less aggressive. This is why patients have better prognosis compared to the individuals with conventional osteosarcoma. However, when it is not diagnosed in time or the treatment is not properly done, low-grade central osteosarcoma can recur as a high-grade with poor prognosis (Fox & Trotta, 2013; Malhas et al., 2012; Misaghi et al., 2018; Prater & McKeon, 2019).

3.3.7. High-grade surface osteosarcoma

High-grade surface osteosarcoma is another rare high-grade tumour that originates at the bone surface and constitutes less than 1% of all osteosarcomas. It affects individuals at their second or third decades of life. The tumour in its majority is located in the diaphysis and then in the metaphysis of the femur, followed by the tibia. Histologically, it is identical to conventional osteosarcoma, where 80% of the subtype is osteoblastic and 20% is chondroblastic. High-grade surface osteosarcoma can recur if inadequate treatment is employed. The prognosis is considered to be similar to the conventional osteosarcoma. Nevertheless, there is a report from a small group with a 5-year survival rate of 82% (Fox & Trotta, 2013; Prater & McKeon, 2019; Kumar, Barwar, & Khan, 2014; Staals, Bacchini, & Bertoni, 2008).

3.3.8. Periosteal osteosarcoma

Periosteal osteosarcoma is a rare intermediate-grade surface variant of the tumour that represents 2% of all osteosarcomas. It is typical in patients in their second and third decades of life and is localized mostly in the diaphysis of tibia, femur and humerus. The sarcoma originates in the inner layer of periosteum, leading to its elevation. Histologically, it shows an abundant cartilaginous matrix with a small amount of osteoid (Fox & Trotta, 2013; Grimer et al., 2005; Kansara et al., 2014; Misaghi et al., 2018; Prater & McKeon, 2019; Kumar et al., 2014).

3.3.9. Parosteal osteosarcoma

Parosteal osteosarcoma is a low-grade surface variant that accounts for 5% of all osteosarcomas and, unlike the previously mentioned subtypes, it is prevalent in females, where it occurs in the metaphysis of the femur. Histologically, parosteal osteosarcoma is localized in the outer surface of the periosteum forming cartilaginous matrix with a small amount of osteoid tissue. Its differentiated morphology and low-grade nature are determinants of good prognosis, with a 5-year survival rate of 80% of affected patients. However, when the diagnosis is not done on time, this subtype can dedifferentiate into a high-grade conventional osteosarcoma with poor prognosis. Recurrence is observed when inadequate treatment is performed and metastasis probability in this case is low (Fox & Trotta, 2013; Kansara et al., 2014; Misaghi et al., 2018; Prater & McKeon, 2019; Kumar et al., 2014).

4. Risk factors

Different factors can increase the probability of developing osteosarcoma in children or adults. Needless to say, neither the presence of risk factors necessarily leads to cancer progression, nor their absence means to be free from disease in the future. The following risk factors have been observed to be associated to osteosarcoma development.

4.1. Inherited syndromes

4.1.1. Retinoblastoma

Hereditary retinoblastoma is a rare paediatric type of ocular cancer, whose mutation in the *RB1* tumour suppressor gene is responsible of 80-90% of the observed cases of eye tumours (Kleinerman, Schonfeld, & Tucker, 2012). This gene encodes for retinoblastoma protein (pRB), which is involved in several important cellular processes like: control of cell differentiation in both embryonic and adult tissues; regulation of the cell cycle, restricting the progression from G1 to S phase when there is a considerable DNA damage; control of apoptosis (Hickman, Moroni, & Helin, 2002; Kleinerman et al., 2012). All these cell functions are deregulated when the *RB1* gene presents mutations. Germline mutation in *RB1* gene is responsible for hereditary retinoblastoma that affects both eyes, and is normally diagnosed before 12 months of age. On the contrary, somatic mutation of the gene causes a non-hereditary form of the disease affecting only one eye, and can be diagnosed between the first 2 to 5 years of life. Patients with hereditary retinoblastoma present high risk of developing other primary types of cancers, where osteosarcoma, which is diagnosed between 10 and 20 years of age, accounts for 30% of all the cases. Brain cancer and melanoma can also occur, but to a less extent (Kleinerman et al., 2012). The risk of osteosarcoma is further increased when patients undergo the high-dose radiation therapy (superior to 5 Gy) that is normally used to treat retinoblastoma (Kleinerman et al., 2012; Wong et al., 1997). In this case bone cancer usually appears within the exposed zone, *i.e.* the skull, but in 40% of patients osteosarcoma can be detected in distal parts such as limbs. In addition to radiotherapy, patients can receive cumulative doses of chemotherapy as another treatment option. Combination of both has been reported to increase even more the risk of bone cancer development, compared to the individual treatment. Patients with somatic mutations in the *RB1* gene have low probability to experience osteosarcoma, similar to the general population (Kleinerman et al., 2012).

4.1.2. Li-Fraumeni

Li-Fraumeni is another rare disorder that predispose children and young adults to develop different types of cancer that include soft tissue sarcoma, breast cancer and brain cancer, among others. It is classified into classic Li-Fraumeni syndrome (LFS) and Li-Fraumeni-like syndrome (LFL), which shares some of the characteristics of LFS (Yoshida et al., 2012). *TP53* is a tumour suppressor gene that encodes for p53 protein, responsible of a wide range of functions. control of

cell cycle arrest, apoptosis, senescence and DNA repair. This protein is also known as “guardian of the genome” as it prevents mutations to be propagated to the daughter cells during cell division. It has been observed that 70% of LFS patients have a germline mutation in *TP53*, whose alterations are common in cancer. The frequency of paediatric osteosarcoma is higher than expected in these patients and is diagnosed in 12% of LFS individuals (Correa, 2016; Martin, Squire, & Zielenska, 2012; Mirabello et al., 2015). It is suggested that germline mutations of *TP53* screening should be taken into account in the early diagnosis of osteosarcoma. The confirmation of both TP53 alterations and a family history of cancer are indicative of a possible risk of tumour development and should be complemented with additional tests, such as whole body magnetic resonance imaging (MRI) screening (Hameed & Mandelker, 2018; Mirabello et al., 2015).

4.1.3. Rothmund-Thompson, Werner and Bloom

Rothmund-Thompson, Werner and Bloom are different syndromes that predispose to osteosarcoma. Their common characteristics are mutations in proteins of the RecQ family, which are DNA helicases responsible of the DNA double strand unwinding and repair during replication (Calvert et al., 2012; Martin et al., 2012). From these syndromes, Rothmund-Thompson, characterized by mutations in *RecQL4* gene, is strongly associated with osteosarcoma development (Hameed & Mandelker, 2018; Wang et al., 2003). In a clinical study of a cohort of 33 young patients between 1 and 30 years, 11 presented osteosarcoma, and all of them carried deleterious mutations in the *RecQL4* gene, responsible of loss of helicase function (Wang et al., 2003). In another study, focused on an international cohort, bone cancer was detected in 13 out of 41 Rothmund-Thompson patients (Wang et al., 2001). On the contrary, Werner and Bloom syndromes have an elevated incidence of several types of cancer, besides osteosarcoma (Hameed & Mandelker, 2018; Wang et al., 2001). The Werner condition is common among Japanese, probably due to a founder effect. In this population bone cancer usually occurs at a later age, between 35 and 57 years, and tumour localization is outside the common sites, as it can occur in ankle or foot (Calvert et al., 2012; Hameed & Mandelker, 2018). Similar to Werner syndrome, Bloom condition is caused by a founder effect observed in Ashkenazi Jews. The osteosarcoma incidence is rare among this population, but it is elevated as compared to the general population (Calvert et al., 2012).

4.2. Paget’s disease

This is bone disorder that normally affects elderly people over the age of 55 years, and is characterized by a disruption in bone remodelling. At the initial stages of the disease, an abnormal increase in osteoclast activity is observed. This is followed by elevated activity of both osteoblasts and osteoclasts, leading to accelerated bone remodelling. Finally, as the disorder progresses, bone formation exceeds bone resorption, resulting in bone overgrowth and deformity. It is not well

understood how, but osteosarcoma is a rare complication of Paget's disease, being the sarcoma normally located in the pelvis, femur or humerus (Deyrup et al., 2007; Hansen, Seton, & Merchant, 2007). In these cases there is a 5-year survival rate of 10% of the patients, a poor prognosis when compared to paediatric osteosarcoma, whose survival rate, for a localized disease, is 65% (Deyrup et al., 2007; Durfee et al., 2016; Hansen et al., 2007). The low survival in elderly patients is believed to be caused by the aggressiveness of the given chemotherapy (Deyrup et al., 2007).

4.3. Ionizing radiation

Ionizing radiation is the main environmental factor to be implicated in 2% of osteosarcomas (Picci, 2007). Normally, bone tissue is resistant to the adverse effects that may arise after the exposure to radiation. However, administration of high doses, superior to the therapeutic amounts used to treat other cancer (which, in turn, can be over 1.000 cGy), increase the risk of bone cancer formation. Low doses used to treat other types of benign cancer can pose a risk factor as well. In case of inherited syndromes, such as retinoblastoma, where radiation is one of the treatment options, there is an increase in the probability of a secondary osteosarcoma that can arise up to 12 to 16 years after the primary irradiation (Ferris I Tortajada et al., 2005; Mirabello et al., 2009; Picci, 2007; Stiller, Bielack, Jundt, & Steliarova-Foucher, 2006).

5. Symptoms of osteosarcoma

The first sign of the malignancy is bone pain in the affected zone, normally around the knee. These pains are intermittent at rest and can get worst during the night. The pain can lead to limping. The medical visit with such symptoms is not always successful, as confusion with tendinitis is common. Also, the bone pain can be attributed to growth pain and in some cases the doctor is uncertain to give a proper diagnosis.

Bone pain can go along with or without a palpable mass that will depend on tumour size and location. In benign cancer it can be observed over the bone and produce no complications. On the contrary, in malignant tumours the swelling grows faster and, in advanced stages, can produce changes in the skin, such as striation, ulceration or hyperthermia.

Pathological fractures are not common in early stages of osteosarcoma. They have an incidence between 5% and 12%. However, they are typically observed in advanced stages or in telangiectatic subtypes.

Symptoms such as fever or weight loss are normally observed in malignant tumours, but not in benign conditions (Chung et al., 2016; Durfee et al., 2016; Fletcher, Unni, & Mertens, 2002; Widhe & Widhe, 2000).

6. Diagnosis

A starting point to evaluate a suspected osteosarcoma, when there is presence of long-term bone pain with or without palpable mass, is X-ray imaging, which includes the acquisition of several views of the whole bone and adjacent joints. Radiography will show the rate of tumour's growth, dimension of osteoid mineralization and bone destruction. The most common features are the presence of sun-burst appearance, elevation of the periosteum that will form a Codman's triangle, and heterogeneity in matrix mineralization with areas of bone destruction and soft tissue (Durfee et al., 2016; Eftekhari, 2009; Misaghi et al., 2018; Prater & McKeon, 2019).

Detection of the suspected lesions should be further confirmed, as radiography in some cases is not clear and doesn't show features such as skip metastasis, which is a small secondary focus of osteosarcoma proximal to the primary tumour in the same bone, and can be observed in 2% of high-grade cancers (Eftekhari, 2009; Enneking & Kagan, 1975; Leavey, Day, Booth, & Maale, 2003). MRI is considered to be a gold standard method in osteosarcoma diagnosis for its multiplanar capacity, soft tissue contrast, and no usage of ionizing radiation. It allows the delimitation of the tumour extension both inside and outside the bone (Deeab, Dick, Sergot, Sundblon, & Gedroyc, 2011; Eftekhari, 2009; Prater & McKeon, 2019). It is an accurate technique that generates the image based on intrinsic magnetic properties of the body unlike other imaging procedures that depend on one specific tissue characteristic (Berger, 2002; Ibrahim & Dublin, 2018). Because of this, it can clearly show tumour invasion, the presence and degree of soft tissue, skip metastasis and proximity to the neurovascular system. In order to examine as much area as possible, and obtain the maximum information of the lesions, MRI scanning is normally done on the entire bone, including the joints above and below the tumour (Durfee et al., 2016; Misaghi et al., 2018; Prater & McKeon, 2019).

The information obtained from radiography and MRI can be complemented by laboratory analysis. To date, there are no specific biochemical markers to diagnose osteosarcoma. However, elevated levels of alkaline phosphatase (ALP) due to increased osteoblastic activity, and lactate dehydrogenase (LDH), whose role in bone tumour is not clear, are considered as prognostic factors. High serum levels of both biomarkers are regarded as poor predictors (Bacci et al., 1994; Fu, Lan, Cai, Lu, & Yu, 2018; Misaghi et al., 2018; Prater & McKeon, 2019).

Based on the radiography, MRI, or the combination of both, a biopsy will be required as the last and definitive assay to confirm the diagnosis. This can be performed using two different approaches: open biopsy or core needle biopsy. Open biopsy is done under general anaesthesia, where a bone sample is obtained through small incision. Previously it was considered as a gold standard for its high accuracy, until a considerable number of complications were reported that included increased risk of infections, wound healing problems and contamination of local soft

healthy tissues with tumour cells. Core biopsy is an alternative that replaced the traditional open approach. It is done with local anaesthesia, where an incision is made to surgically place a trocar. Then, a Jamshidi needle, cylindrical in shape with a conical cutting end, will be introduced through the trocar and get a tapered sample of the tumour when withdrawn. This process can be repeated several times until enough sample is harvested. Core biopsy is as accurate as open biopsy, but reduces considerably the risk of local contamination, lowers the recovery time and is more cost-effective (Kundu, 2014; Misaghi et al., 2018; Prater & McKeon, 2019; Taupin, Decouvelaere, Vaz, & Thiesse, 2016). The diagnosis is confirmed when the biopsy samples are analysed in fresh or frozen format by the pathologist. The histologic findings will reveal the grade and subtype of osteosarcoma (Durfee et al., 2016; Prater & McKeon, 2019).

When the definitive diagnosis is established, patients usually undergo computed tomography (CT) scan and X-ray of the chest, as lungs are the most common location of metastasis. CT is the preferred method as it implies no exposure to high levels of radiation, but is sensitive enough to detect very small tumor nodules (up to 3 mm) (Durfee et al., 2016; Eftekhari, 2009; Misaghi et al., 2018; Paioli et al., 2017; Prater & McKeon, 2019). Another recommended method for this assessment is 18F-fluorodeoxyglucose (¹⁸F-FDG) positron emission tomography (PET) combined with CT. It provides whole-body information, ¹⁸F-FDG is a metabolic activity marker. When injected in the patient, it provides whole-body information of the glycolytic activity of the tissues. As glycolysis is known to be increased in tumour cells, ¹⁸F-FDG PET/CT can detect subtle lesions, skip metastasis, lung nodules and distant high-grade cancers in other bones (Brenner, Bohuslavizki, & Eary, 2003; Eftekhari, 2009; Kundu, 2014; Misaghi et al., 2018; Zhang & Guan, 2018).

7. Staging

Staging is a process that determines the localization of the tumour, whether or not it has spread to other parts of the body. This information is useful to plan the appropriate treatment and establish the prognosis (Durfee et al., 2016). There are two popular staging systems:

- Enneking system for staging of malignant musculoskeletal tumours: it is based on the histological grade, the presence or absence of metastasis, and the extension of the tumor, which is classified as intracompartmental, if it is restricted within the bone, or extracompartmental, if it is outside the bone (**Table 1**). This staging system is commonly used by orthopaedic surgeons (Jawad & Scully, 2010; Kundu, 2014; Prater & McKeon, 2019).

Table 1. Enneking system for staging of malignant musculoskeletal tumours.

| Stage | Grade | Site | Metastasis |
|-------|-----------|-------------------------|-------------------------------------|
| IA | Low (G1) | Intracompartmental (T1) | No metastasis (M0) |
| IB | Low (G1) | Extracompartmental (T2) | No metastasis (M0) |
| IIA | High (G2) | Intracompartmental (T1) | No metastasis (M0) |
| IIB | High (G2) | Extracompartmental (T2) | No metastasis (M0) |
| III | Any (G) | Any (T) | Regional or distant metastasis (M1) |

The table was adapted from (Jawad & Scully, 2010).

- Staging system by the American Joint Committee for Cancer (AJCC): it is based on histological grade, involvement of lymph nodes and whether or not there is metastasis. Instead of localization, a tumour size (T) is considered in this system (**Table 2**). AJCC is popular among oncologists as it takes into account features that help defining the appropriate treatment option. For example, large tumours tend to form metastasis and for this reason patients receive chemotherapy.

Table 2. AJCC staging system.

| Stage | Grade | Size | Lymph node | Metastasis |
|-------|-----------|---------------------|---|--------------------------|
| IA | Low (G1) | Less than 8 cm (T1) | None (N0) | No metastasis (M0) |
| IB | Low (G1) | More than 8 cm (T2) | None (N0) | No metastasis (M0) |
| IIA | High (G2) | Less than 8 cm (T1) | None (N0) | No metastasis (M0) |
| IIB | High (G2) | More than 8 cm (T2) | None (N0) | No metastasis (M0) |
| III | Any (G) | Any (T) | Skip metastasis | Skip metastasis |
| IVA | Any (G) | Any (T) | None (N0) | Lung metastasis (M1) |
| IVB | Any (G) | Any (T) | Lymph node metastasis (N1) or none (N0) | Non-lung metastasis (M1) |

The table was adapted from (Durfee et al., 2016).

8. Osteosarcoma treatment

The current treatment options consist of pre-operative or neoadjuvant chemotherapy, followed by surgery and post-operative or adjuvant chemotherapy. Surgery consist on the complete removal of the tumour, and it is always used (Durfee et al., 2016; Kansara et al., 2014; Misaghi et al., 2018; Zhang et al., 2015). The characteristics of osteosarcoma will determine if there is a need to combine surgery with chemotherapy (Gulia, Puri, Pruthi, & Desai, 2014; Tiwari et al., 2014). Surgery is enough to treat low and intermediate-grade subtypes (Chen, Xu, Xu, & Yu, 2017; Grimer et al., 2005; Gulia et al., 2014; Misaghi et al., 2018). However, some discrepancies exist as to whether or not chemotherapy should be incorporated with surgery when treating intermediate-grade osteosarcomas (Grimer et al., 2005; Gulia et al., 2014). Many studies conclude that there is no significant difference in survival between those patients who received

chemotherapy and those who didn't (Okada et al., 1994; Wold, Unni, Beabout, Sim, & Dahlin, 1984). In some cases, such as parosteal osteosarcoma, where there is a risk of dedifferentiation and metastasis, adjuvant chemotherapy should be considered (Okada et al., 1994). High-grade osteosarcoma treatment consist of neoadjuvant chemotherapy, surgery and adjuvant chemotherapy. In this case, surgery is fundamental as it will reveal the outcome of the chemotherapy. A good response is considered when more than 90% of necrosis is observed in the sarcoma, while the opposite is predictive of a poor prognosis (Carrle & Bielack, 2006; Durfee et al., 2016; Misaghi et al., 2018).

8.1. Chemotherapy

For a long time, surgery was the only treatment against osteosarcoma. The vast majority of patients were not able to survive the cancer, would it be localized or metastatic disease. The implementation of chemotherapy in 1970 substantially increased the survival rate of osteosarcoma, reaching a 65% in the first 5 years after cancer therapy. Nowadays the chemotherapy is generally given before and after surgery. Neoadjuvant chemotherapy is pre-operative treatment, being its main goals:

- To reduce and delimitate the tumour, making it visible against the surrounding tissue, thus facilitatng the removal of cancer cells during surgical resection. When the process is successful, the rates of local recurrence are low.
- Providing time to plan the limb-salvage surgery, while the neoadjuvant chemotherapy is administered.
- To determine the effects of chemotherapy on cancer cells. The amount of remaining tumour cells after neoadjuvant chemotherapy will reveal the prognosis and establish the posterior chemotherapeutic regime.

The total process of neoadjuvant chemotherapy induction takes between 8 and 10 weeks. Then osteosarcoma patients undergo surgical resection of the tumor, followed by adjuvant chemotherapy, which is given two weeks later, when the wounds from the operation are healed (Carrle & Bielack, 2006; Chou & Gorlick, 2006; Durfee et al., 2016; Kansara et al., 2014; Misaghi et al., 2018). The purpose of this chemotherapy is to remove the cancer cells that might be left in the body and have the ability to restart the disease. Patients receive adjuvant chemotherapy for 20 weeks (Carrle & Bielack, 2006; Chou & Gorlick, 2006).

Nowadays the standard drug combination used in osteosarcoma chemotherapy comprises high-dose methotrexate, cisplatin and doxorubicin, a drug combination commonly known as MAP. Treatment with one or two drugs have not improved prognosis, but the combination of three or more drugs has increased survival rates. On using different drugs with distinct

mechanisms of action, the tumour has less chance to mutate and relapse. Patients with good response after neoadjuvant chemotherapy continue receiving the same combination of drugs in adjuvant chemotherapy, while those with poor response are switched to another combination or get additional drugs, such as ifosfamide and etoposide. However, poor response is associated with low survival rate. It was found that addition of ifosfamide and etoposide along with MAP in this group of patients during the adjuvant chemotherapy showed lack of improvement in the overall survival, but increased side effects (Carrle & Bielack, 2006; Chou & Gorlick, 2006; Durfee et al., 2016; Marina et al., 2016; Misaghi et al., 2018).

The administration of high doses of chemotherapy is better tolerated in children as compared to older patients, as more deaths are observed to be caused by therapy toxicity in elder patients (Anninga et al., 2011). One important feature of osteosarcoma is drug resistance, which is prominent during metastasis. While the majority of patients with localized disease show long-term, recurrence-free, survival rates, only 20% of patients with metastasis reach a 5-year survival rate. This number has remained unchanged for the last 30 years. Recurrence is another obstacle related to poor prognosis, for which there is no standard drug combination. It can be caused by remaining cells after tumour resection, poor response to neoadjuvant chemotherapy and intrinsic or acquired drug resistance of malignant cells. Other complications related to the administration of chemotherapy are side effects and infections associated with mucositis and myelosuppression (Carrle & Bielack, 2006; Chou & Gorlick, 2006; Durfee et al., 2016; Kansara et al., 2014).

The drugs most commonly used in osteosarcoma chemotherapy are presented below.

8.1.1. Methotrexate

With the development of chemotherapy in 1970, methotrexate (MTX), along with doxorubicin (DOX) was the first broad-spectrum drug to be used for cancer treatment. It acts by inhibiting dihydrofolate reductase (DHFR), whose main function is to produce tetrahydrofolate from dehydrofolate reduction. This compound is a folic acid derivative and is essential in *de novo* synthesis of purines and pyrimidines, necessary for DNA elongation. This cascade of events leads to a blockage in DNA synthesis, cell cycle arrest in S phase, and cell death through apoptosis (Chan & Cronstein, 2013; Chou & Gorlick, 2006; Friedman & Cronstein, 2019; Xie et al., 2016). Currently the applicability of MTX as part of a combination treatment is questioned. It was found that this drug increased the levels of cancer stem cells (CSC) markers, undifferentiated and chemotherapy resistant cells. Administration of a combination of cisplatin and DOX successfully inhibit osteosarcoma growth. However, when MTX is incorporated, proliferation of malignant cells is not affected. This suggest that MTX maintains an undifferentiated state in CSC that could explain the poor response to the chemotherapy (Cavalcanti et al., 2017).

Acute kidney injury is one of the common side effects caused by crystal precipitation of MTX and its metabolites within renal tubules. With time, it leads to renal dysfunction, where the drug is not eliminated from the body. High MTX plasma concentrations can further end up in hepatic, skin, lung and bone marrow toxicities. To attenuate the adverse effects of MTX, leucovorin (LV) is given. Plasma concentration of MTX is constantly monitored as it will be an indicator of the clearance of the chemotherapeutic agent and will determine if precaution should be taken. Normally, the crystal precipitates are not detected in the urine, because the alkaline pH solubilizes the acidic MTX. For this reason, the treatment should always include regular hydration regimes and adjustment of LV doses (Holmboe, Andersen, Mørkrid, Slørdal, & Hall, 2012; Howard, McCormick, Pui, Buddington, & Harvey, 2016).

8.1.2. Doxorubicin

DOX is an anthracycline isolated from the bacteria *Streptomyces peucetius*. Nowadays it is widely used for osteosarcoma treatment, alone or in combination with MAP. DOX is an important chemotherapeutic agent for its broad-spectrum mode of action (González-Fernández et al., 2017; Yang, Teves, Kemp, & Henikoff, 2014) :

- Intercalation between DNA strands, forming adducts with guanine and blocking DNA replication and transcription, thus leading to cell death.
- Stabilization of Topoisomerase II complex during replication and transcription when double strand breaks are done to release DNA torsion. Thus, the activity of the enzyme is inhibited and the broken DNA strand is not linked back, which leads to apoptosis.
- Induction of oxidative stress. DOX is a chelator that, when complexed with iron, is implicated in the production of hydroxyl radicals from hydrogen peroxide. As a result, cell death is caused by DNA damage (Thorn et al., 2011; Yang et al., 2014).

There is no leading mechanism of action, as in the total DOX administration small fractions are responsible of each one of the mentioned effects that, altogether, induce apoptosis of malignant cells (Yang et al., 2014). Patients receive DOX by intravenous injection, which rapidly distributes the drug within the body. *In vivo*, it has a plasma clearance half-life between 30 and 48 hours. DOX is metabolized in the liver to form the following metabolites: doxorubicinol (DOXol), DOXol aglycone, DOX deoxyaglycone, DOX hydroxyaglycone and DOX-semiquinone. However, half of the DOX is eliminated from the body in its original state mostly through biliary excretion, with some amount detectable in urine (Gerson, Caimi, William, & Creger, 2018; Johnson-Arbor & Dubey, 2021; Wang et al., 2019).

The efficiency and therapeutic usage of DOX are limited by its dosage-cumulative effects, which cause numerous side effects, being the most dangerous its considerable cardiotoxicity. Heart failure caused by DOX-induced cardiotoxicity is an irreversible side effect of this drug.

DOXol is the only active metabolite, from the five produced by the degradation of DOX in liver, that has been proved to be implicated in cardiopathy. Cardiotoxicity can be prevented by giving a regime administration of low-doses of DOX. Also, it is common to receive a cardioprotectant medicine, dexrazoxane, whose mechanism of action is believed to be the reduction of cell oxidative stress. As an iron chelator, dexrazoxane reduces the amount of DOX-iron complexes. (Dessypris, Brenner, Baer, & Hande, 1988; Johnson-Arbor & Dubey, 2021; Thorn et al., 2011).

Interestingly, there are insights that cardiotoxicity is a result of an independent mechanism that is completely different from the process implicated in apoptosis induction. It is not well understood how exactly cardiopathy is originated, but some possible explanations have been proposed:

- Formation of DOX-iron complexes alter iron homeostasis, as the metal starts to cycle between Fe^{2+} and Fe^{3+} forms, with considerable ROS production. The hypothesis is questionable, because unlike dexrazoxane, other iron chelators such as deferasirox failed to prevent cardiac dysfunction triggered by DOX administration.
- Disruption of the electron-transport chain caused by the high affinity of DOX for cardiolipin, a phospholipid of the mitochondrial internal membrane. A subsequent accumulation of the drug increases ROS generation. Also DOX activates NADPH oxidase and endothelial nitric synthase, leading to further oxidative stress (Cappetta et al., 2017; Gorini et al., 2018; Ichikawa et al., 2014; Thorn et al., 2011).

8.1.3. Cisplatin

Cisplatin is platinum-based metal-containing compound that gets activated within the cell. It targets DNA forming adducts with, or binding covalently to, purine bases. As intra and inter-strand crosslinks are formed, DNA replication and repair machinery are no longer able to perform their function, leading to cell apoptosis. Given its mechanism of action, it has been suggested that cisplatin is effective against malignant cells with high proliferation rate, while its effect is reduced in cancer cells with slow growth.

Nephrotoxicity is a common adverse side-effect of cisplatin, and it is caused by renal accumulation of the drug. Patients undergo an appropriate hydration regime before and during the treatment, and are then constantly monitored, and their doses adjusted, based on renal function. Cisplatin can act on bone marrow leading to myelosuppression. In this case patients are vulnerable to infections due to reduction of the white blood cells. For this reason, complete blood counts are performed before and during the treatment. Neurotoxicity can be another cause to stop cisplatin administration. However, sometimes neuropathy can develop later in life, with irreversible effects after the treatment. Other side-effects include hepatotoxicity, cardiotoxicity, ocular toxicity and ototoxicity (Dasari & Tchounwou, 2014; Gold & Raja, 2019).

8.1.4. Ifosfamide

Ifosfamide is an alkylating agent, which needs to be activated in the liver. The active form acts on DNA forming intra and inter-strand crosslinks that cease replication and end up in cell apoptosis. Normally, ifosfamide is given in combination with other chemotherapeutic drugs, which can be etoposide or MAP.

Nephrotoxicity is one of the serious complications observed in children, as damage produced in glomerulus and proximal tubules are irreversible. If it occurs, paediatric patients receive vitamin D and phosphate supplements. Neurotoxicity is a complication observed when ifosfamide is given orally, which happens less with intravenous administration. Myelosuppression can be detected when high doses of the chemotherapeutic agent are given, but this side effect can be reduced when by administered the drug concentration is fractioned doses (Fan, Cai, Zhu, & Ding, 2015; Furlanut & Franceschi, 2003; Gangireddy & Nookala, 2020).

8.2. Surgery

Historically, amputation was the method of choice to treat osteosarcoma. Since 1970 the development of novel surgical strategies and chemotherapy enabled limb salvage to be the preferred procedure in bone cancer treatment. The surgery involves tumour resection and limb reconstruction. In general, during limb salvage the functionality and appearance of the affected limb are conserved, while the tumour is removed. Tumour excision is done leaving wide margins, to prevent future recurrence, whose emergence is influenced by tumour grade and surgeon's experience in resection procedures. Even though limb salvage has nowadays become the method of choice, patients can still undergo amputation. However, the removal of the extremity is reserved for special cases where the functionality of the limb can't be conserved during the surgery. No matter the chosen procedure, there are similar overall survival rates, recurrence and metastasis between limb salvage and amputation groups (Brigman, Kumagai, & McGuire, 2003; Durfee et al., 2016; Gradl et al., 2015; Jauregui et al., 2018; Misaghi et al., 2018; Prater & McKeon, 2019).

During limb salvage the surgeon can face many complications caused by the localization and size of the tumour. One of such includes the resection of the tumour, an abnormal mass of tissue, when it is localized in the growth plate. In this case either the tumour or its resection damage the metaphysis, resulting in interferences in bone elongation that can considerably affect growth, given the skeletal immaturity of children. Another complicated case is that where joints are surrounded by the tumorous mass tissue, a circumstance often observed due to cancer propensity to develop around the knee. In these cases, the leg must be amputated above the knee. However, sometimes the leg can be partly salvaged by rotationplasty. This surgical technique is indicated for patients with tumours localized in the knee or the distal part of the femur. In rotationplasty,

the knee and distal femur are resected, along with the tumour, and the lower leg is re-joined, with a 180°-rotation, so that the ankle replaces the knee, and the foot serves as anlage point to a prosthesis. This procedure restores the functionality of the leg, but has several limitations, including the psychological impact caused by a stand-out cosmetic appearance of the limb.

Despite the complications associated to the surgery, limb salvage is a safe and efficient method. The reconstructive surgery after tumour removal has the goal of restoring the natural process of bone growth and functionality of the limb. At present, there are different available options:

- Non biological reconstruction, consisting of metallic prostheses. The first prostheses used to be customised to the requirements of the patients, but with time these were replaced by “off the shelf” options, consisting of non-expensive components for immediate implantation. The most common site of insertion is the distal part of femur. In paediatric patients during the resection it is common to have the growth plate compromised. The solution is to use expandable prostheses, which can be elongated between 1 and 2 cm per surgical intervention, so that the length of the affected limb is correlated with the healthy one. Prostheses enable patients to return to everyday functional activities in a short time. However, over time mechanical failure and infections are the most common complications. In some cases, they can lead to amputation. For this reason, patients have to undergo several revisions after the reconstruction of the affected limb (Durfee et al., 2016; Jeys et al., 2008; Misaghi et al., 2018; Prater & McKeon, 2019; Shehadeh, Malawer, & Henshaw, 2010).
- Biological replacement, consisting of allografts or autografts. Allograft reconstruction is based on replacing the excised portion of bone with a donor bone, matching in size and shape, whose source is post-mortem organ donation. One of the important advantages of this procedure is the low level of rejection, as bone composition in people is similar, making the structure relatively universal. Surgery is performed to reconstruct the affected zone and, with time, both native and implanted bones will be joined. In the case of knee reconstruction, combination of allograft and prosthesis is used for its good insertion and ability to facilitate the immediate weight bear capacity. However, the success of allograft integration can be affected by fractures, infections and non-union. The latter is increased following chemotherapy or radiotherapy (Bullens et al., 2009; Durfee et al., 2016; Misaghi et al., 2018; Prater & McKeon, 2019).

Autograft is another method for reconstruction, especially when there is no access to donor banks. There are bones, such as clavicle and fibula, whose reconstruction is not essential as they don't have to bear weight. Thus, limb salvage from these bones has no impact in the global skeletal functionality (Prater & McKeon, 2019). In other cases the

affected portion of the bone is recycled. After its excision, the autograft is irradiated or pasteurized and then reincorporated back. An alternative approach includes combination with vascularized fibula: a segment from vascularized fibula is inserted into the medullary canal of the autograft and then the structure is finally placed into the original anatomical site. This combination of acellular and vascularized bone has shown to promote a faster integration of the implant with the host bone. Similarly to allograft the most common complications of autografts are fractures and infections (Liu, Ling, Zhang, Liu, & Guo, 2019; Misaghi et al., 2018; Prater & McKeon, 2019).

8.3. Radiation therapy

The localization of some tumours makes it difficult or even impossible to perform surgical resection. This is the case when osteosarcoma occurs in the pelvis or spine, which have a complex anatomy and are surrounded by vital organs. Radiation therapy is the only available solution for these types of patients, as it can locally control the disease, relieve the pain and possibly prolong the survival. However, this treatment option is not common in osteosarcoma patients (Hegyí et al., 2011; Mahajan et al., 2008; Schwarz, Bruland, Cassoni, Schomberg, & Bielack, 2009).

9. Novel therapeutic options

9.1. Drug repositioning

De novo development of novel drugs takes a lot of time, effort and money. It involves laboratory studies and clinical trials that have as a purpose to establish pharmacodynamics, pharmacokinetics and side effects of the chemotherapeutic agents under evaluation. The average duration starting from drug discovery until its final approval can take one decade as a minimum. The vast majority of promising compounds under research do not reach the patients, as they fail in different phases of the clinical trials due to toxicity or efficacy reasons. Thus, the number of approved drugs per year by the US Food and Drug Administration (FDA), and the European Medicines Agency (EMA) has considerably decreased compared from the 90s of the past century.

Drug repositioning, also known as drug repurposing, is gaining much attention as it is based on recycling an already available drug from one disease to another. It is a relatively rapid and cost-efficient approach, as biocompatibility, drug-drug interaction and toxicity studies have already been done. Also, this approach is giving a “second chance” to those agents that failed in their original indication. One of the notable examples is thalidomide, initially given for morning sickness during pregnancy. Severe teratogenicity observed in children caused the drug to be taken off the market. However, after further studies thalidomide was shown to be effective against leprosy. Finally, the FDA approved its usage and distribution for this disease, under strict control due to its known side effects. In 2006 this drug was again repositioned and approved by the FDA for refractory multiple myeloma treatment in combination with dexamethasone (Li, Yan, & Yu,

2017; Nowak-Sliwinska, Scapozza, & Altaba, 2019; Sleire et al., 2017; Turanli et al., 2018; Umscheid, Margolis, & Grossman, 2011).

9.1.1. Paclitaxel

Paclitaxel (PTX) is a natural compound from the taxane family, originally isolated in 1964 from the bark of the Pacific yew tree, *Taxus brevifolia* Nutt, (1849). Several studies demonstrated the therapeutic effect of this compound against leukemia and ovarian cancer. PTX isolation by humans threatened *T. brevifolia* to the point that it is now included in the list of endangered species, as bark harvest kills the tree. High demand of the drug and scarcity of its source material produced a crisis in a supply. The shortage of the chemotherapeutic agent was solved out by using 10-deacetylbaccatin III or baccatin III. These precursors can be converted into taxol through a semisynthetic procedure, and they are obtained from renewable twigs of other *Taxus* species, typically the European yew, *T. baccata*. Nowadays the drug is commercialized with the brand name Taxol and the FDA has approved its use for ovarian and breast cancers, non-small cell lung carcinoma and AIDS-related Kaposi's sarcoma (Farrar & Jacobs, 2020; Kingston, 2007; Weaver, 2014).

PTX exerts its cytotoxic effect by targeting microtubules. In eukaryotic cells, microtubule length can dynamically increase and by assembling and disassembling α - and β -tubulin heterodimers. Microtubule network is essential for cell shape and cell division. PTX binds the β -tubulin subunits of the microtubules, leading to its stabilization. It does not obstruct the addition of new tubulin subunits, but it prevents microtubule disassembling. Microtubule stabilization induces cell cycle arrest in G₀/G₁ and G₂/M phases, leading to cell death (**Figure 6**) (Cooper, 2000; Šašić, 2007; Weaver, 2014; D. Zhang, Yang, Wang, & Dong, 2014).

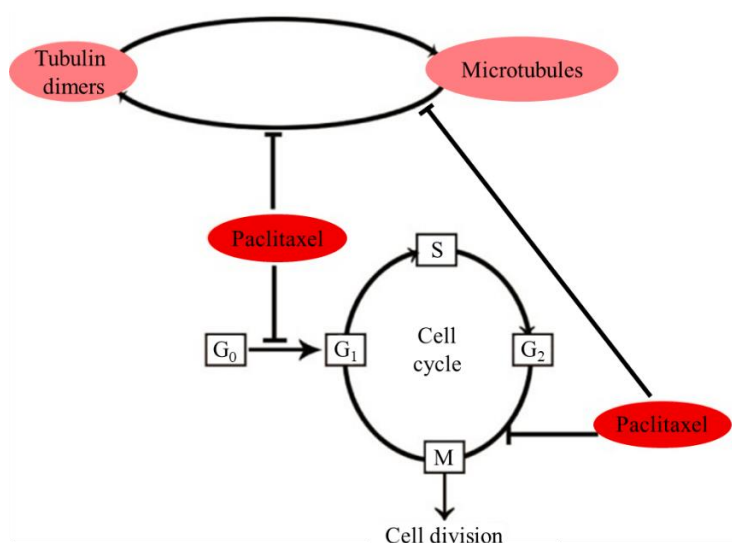


Figure 6. Effects of PTX microtubule targeting. Modified from (D. Zhang et al., 2014).

Besides this canonical mechanism of action, it has been proposed that PTX has the ability to induce apoptosis through other pathways. Huang *et al.* found that exposing PTX-sensible cells from different solid tumours to this drug increased the expression of IKK β , leading to the release of the transcriptional factor NF- κ B, whose nuclear translocation activated apoptosis-related genes (Huang, Johnson, Norris, & Fan, 2000). In ovarian cancer, PTX induced cell death through c-Jun N-terminal kinase (JNK) activation (Lee, Li, Templeton, & Ting, 1998). Alexandre *et al.* observed that, in breast cancer cells, this chemotherapeutic agent enhanced NADPH-oxidase activity, leading to increased reactive oxygen species (ROS) (Alexandre, Hu, Lu, Pelicano, & Huang, 2007).

Logically, anti-tumour efficiency of PTX is correlated with side effects. PTX is a potent irritant, and during its intravenous administration special care is usually taken to avoid drug leakage. If it still occurs, hyaluronidase is administered as an antidote (Farrar & Jacobs, 2020). During chemotherapy with PTX, the general health condition of patients is constantly monitored. Bone marrow suppression results in neutropenia and leukopenia, being these effects reversible after treatment completion. Infections and anaemia attributed to myelosuppression are common. Hypersensitivity is common and it is usually minimized by corticosteroid treatment prior PTX administration. Neurotoxicity is a dose and time-dependent adverse effect that considerably limits the clinical efficiency of PTX. Other common side effects include cardiotoxicity, alopecia, nausea and vomiting (Farrar & Jacobs, 2020; Kohler & Goldspiel, 1994; Marupudi *et al.*, 2007).

9.2. Oridonin

With its wide diversity in structural and biological characteristics, natural products are a source of novel therapeutic agents that are still being explored. Between 1999 and 2013, FDA approved 31 drugs that were based on natural products or its derivatives. One of such products is the already-mentioned PTX, which was discovered as part of a program of the United States National Cancer Institute, in partnership with the U.S. Department of Agriculture, to screen the plant kingdom for antitumoral agents. Following this movement, the interest in remedies from non-western traditional medicines, particularly those coming from Herbology, has raised over the last decade.

Another natural product with potential antitumor activity is oridonin (ORI). This is a diterpenoid isolated from the *Isodon* plant *Rabdosia rubescens*, a medicinal herb popular among Asiatic countries. It has been traditionally used by native people of Henan province, in China, to treat oesophageal cancer (Chen *et al.*, 2005; Tian, Xie, Sheng, Wan, & Zhu, 2017). Japanese and Koreans use different *Isodon* plants as a home remedy for oesophageal and liver cancer (Zhou *et al.*, 2007). Several studies have demonstrated its wide variety of mechanisms of action, which include:

- inhibition of angiogenesis, tumour growth and metastasis,
- arrest of cell cycle progression,
- induction of autophagy and apoptosis (Ding et al., 2016; Xu, Wold, Ding, Shen, & Zhou, 2018). This multifunctionality and a proposed relative safety postulate ORI as a potential candidate drug in the treatment of different types of cancer, such as liver, colorectal, breast and ovarian (Li et al., 2019; Luo et al., 2019; Tan et al., 2011; Wang & Zhu, 2019; Xia, Zhang, Li, & Guan, 2017; Yao et al., 2017).

In case of osteosarcoma, chemotherapy resistance, especially in metastatic disease, is a challenge for successful cancer therapy. This is why alternatives are needed and a natural product with proven anti-tumour activity is one of the choices. The interest in ORI effects in osteosarcoma is recent and the few available studies seem to confirm its potential as an appealing therapeutic strategy. It has been described that this natural compound induces mitochondria-mediated apoptosis through the activation of PPAR- γ and inhibition of Nrf2 pathways (Lu et al., 2018). Also, ORI could prevent osteosarcoma metastasis initiation by affecting the transition from differentiated epithelial into non-differentiated mesenchymal state (Sun et al., 2018).

9.3. Nanoparticles

The administration of chemotherapeutic agents target both malignant and healthy cells, leading to the emergence of adverse side-effects. On other hand, the application of some drugs is limited by their poor solubility and bioavailability. Nanotechnology could help solving these drawbacks, giving a new chance to these chemotherapeutic agents. Incorporating drugs into nanoparticles could overcome their insolubility properties and target them specifically to the target tissue (Alexis, Pridgen, Molnar, & Farokhzad, 2008; Dadwal, Baldi, & Kumar Narang, 2018; Rizvi & Saleh, 2018).

According to the most generally accepted definition, nanoparticles are particles spanning between 1 and 100 nm in diameter. Because nanoparticles used in drug delivery as should assure the loading of the necessary amount of cargo, the particles used in nanomedicine are normally bigger, in the range of 10 to 1000 nm. However the most preferred sizes are still those under 200 nm (De Jong & Borm, 2008; Rizvi & Saleh, 2018). The nanoparticles should have certain characteristics that determine a successful delivery of the drug to the target site. Apart from being safe and able to release the drug, these characteristics include:

- Surface properties. The nanoparticles are hydrophobic in nature, and this characteristic enables blood proteins to non-specifically adsorb on the surface of the nanocarrier while being in the circulation. This opsonization leads to a rapid clearance of the nanoparticles from the bloodstream through phagocytosis by the macrophages of the reticuloendothelial

system (RES), mostly located in the liver and spleen. On the contrary, the hydrophilic nanoparticles have less interaction with the circulating proteins, which makes them virtually undetectable by the components of the immune system. To confer hydrophilic properties to the hydrophobic nanocarriers, a coating with an inert polymer polyethylene glycol (PEG) is usually used. Also, these types of nanoparticles are known as “stealth” for their steric repulsion activity. The surface modification provides the nanoparticles a longer circulation lifetime, increasing their chances to reach the target tissue, such as tumours. It is well established that PEGylated nanoparticles present better therapeutic efficiency compared to those without PEG (Alexis et al., 2008; Rizvi & Saleh, 2018).

- Size. A wide range of nanoparticle sizes can be used for proper drug delivery, but the best ones are considered to be those smaller than 200 nm (De Jong & Borm, 2008; Rizvi & Saleh, 2018). Fang *et al.* observed that PEG-PHDCA nanoparticles of 80 nm presented only 6% of serum protein adsorbed to their surface, as compared to those of 171 and 243 nm, where the amount of protein adsorbed was 23 and 34%, respectively (Fang et al., 2006). As already mentioned, a reduced opsonization can guarantee that the nanocarrier will reach its target. Besides, there is another aspect related to the nanoparticle size that should be taken into account. The lymphatic system of the liver is responsible of filtering all the particles that are present in the blood capillaries. When it detects particles bigger than 100 nm, the lymph nodes label them as foreign and activate the macrophages for the particle clearance from the body. To be able to escape from the mononuclear phagocytic system, the nanocarriers should be less than 100 nm. Therefore, small nanoparticles get to their target tissue easier than large ones (De Jong & Borm, 2008; Rizvi & Saleh, 2018).

Nanoparticles can reach the tumours through two main mechanisms, known as passive and active targeting. When a tumour reaches a size of 2 to 3 mm, it needs its own supply of oxygen and nutrients to continue dividing. Hence, angiogenesis is activated. Unlike that of healthy tissues, the vasculature of the cancer cells is defective. It is characterized by shape irregularities, increased fenestration caused by improper alignment of the endothelial cells, and lack of the smooth muscle layer that is responsible of the dilated state of the vessels. All this leads to an enhanced permeability in the vasculature irrigating solid tumours. Moreover, the lymphatic drainage is deficient. As a result, the tumour tissue accumulates the nanoparticles that were easily incorporated due to increased permeability, without being able to eliminate them. This process is known as enhanced permeation and retention effect (EPR), and is used to refer to the passive delivery of nanoparticles to the tumours (**Figure 7**).

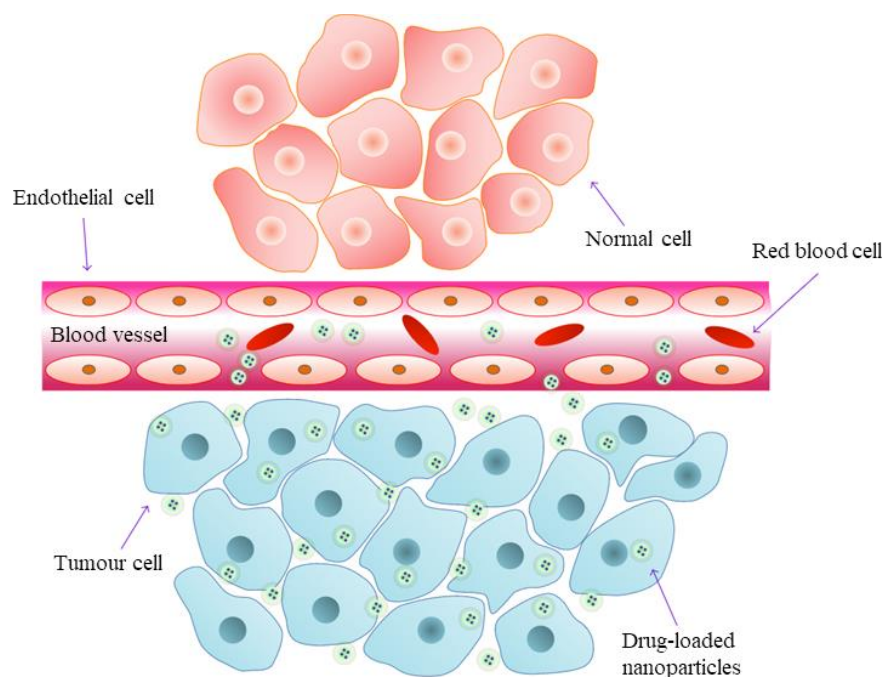


Figure 7. Representation of EPR effect. Adapted from (Yu et al., 2016).

EPR effect favours the therapeutic effect of drugs vehicle in nanoparticles, by facilitating incorporation and retention of the nanoparticles in the tumour tissue. The cut-off size of the nanocarriers for extravasation, accumulation and diffusion to the tumours is approximately 400 nm or even more. It depends on the alignment of the endothelial cells in different cancer types.

Besides EPR effect, which does not necessarily occur in all solid cancers, another strategy is employed to target nanoparticles to the tumours. Active targeting is a modification of the nanoparticle surface where the nanocarrier is coated with a ligand, such as a peptide, protein or antibody, that recognizes a receptor typically overexpressed in malignant cells (Alexis et al., 2008; Dadwal et al., 2018; Greish, 2007). One example is folic acid surface-modified titanium dioxide nanoparticles, used for osteosarcoma treatment. The expression of the folate receptor is enhanced in many tumours, including bone cancers, while it is almost undetectable in healthy cells. In this way the interaction of the folic acid with its receptor enables the intracellular incorporation of the nanocarrier, leading to a better therapeutic outcome, as compared to the nanoparticles without any surface modifications (Ai, Liu, & Liu, 2017; Kularatne & Low, 2010). It is really important for the targeted agent to selectively bind to an antigen or receptor that overexpressed in the cancer cells, but not in the healthy one (Dadwal et al., 2018).

While many nanoparticles are still under being evaluated as drug delivery agents, FDA has already approved for clinical usage several formulations. The most common types are liposomes, nanocrystals and polymeric nanocarriers. Liposomes are spherical nanoparticles with a size of 80 to 300 nm, composed of a lipid bilayer surrounding a central aqueous core (**Figure 8**). It can carry

both hydrophilic and hydrophobic drugs entrapped inside the aqueous core or lamellar lipid bilayer, respectively (Haghiralsadat et al., 2017; Ventola, 2017; Wilczewska, Niemirowicz, Markiewicz, & Car, 2012). The first liposome drug formulation, approved in 1995, was Doxil. It is a nanoparticle designed to deliver DOX, and used to treat ovarian cancer, multiple myeloma and Kaposi's sarcoma. Many other liposomes have been approved, whose usage is not restricted to cancer treatment, but can be administered as analgesics or to manage fungal infections (Ventola, 2017).

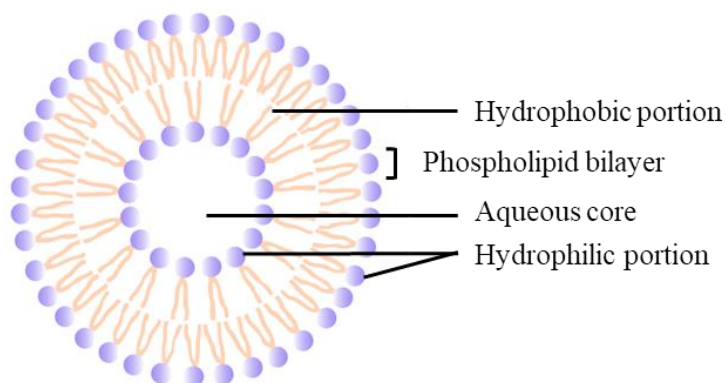


Figure 8. Schematic representation of a liposome. Adapted from (Yu et al., 2016).

Nanocrystals are particles completely composed of a drug crystal and, therefore, their theoretical cargo loading is 100% (**Figure 9**). They are designed as stable nanocarriers that increase the bioavailability of poorly soluble drugs (Lu, Li, & Wu, 2016; Ventola, 2017). Most commercially available nanocrystals are hydroxyapatite-based, designed as a bone graft substitutes. This is exploited under several trademarks that include EquivaBone™, NanOss™ and Ostim™ (Ventola, 2017).

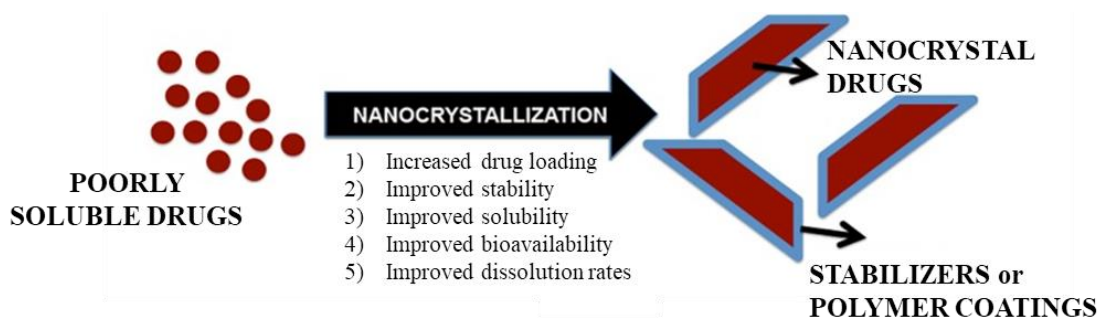


Figure 9. Schematic representation of a nanocrystal. Adapted from (Jarvis, Krishnan, & Mitragotri, 2019).

Polymeric nanoparticles are the most common type of nanocarriers for clinical research and usage. They can be obtained from natural or synthetic sources with a size range of 10 to 1000 nm.

The cargo can be entrapped inside the nanoparticle or coated in a covalent way on the surface of the nanocarrier. Biodegradable polymers are the ones getting more attention, as after releasing the drug they are metabolized and completely removed from the body (Dadwal et al., 2018; Ventola, 2012; Ventola, 2017). One of such polymeric nanoparticles is poly(lactic-co-glycolic acid) (PLGA), whose properties such as biodegradability, low toxicity and sustained cargo release gained them the FDA approval for drug delivery (Sadat Tabatabaei Mirakabad et al., 2014).

“Smart” polymers are an emerging class of drug carriers that release the entrapped cargo in response to stimuli such as temperature, pH, light, ultrasounds and magnetic forces. They were developed to increase the specificity and the efficiency of the nanoparticles, by securing the release of the drug specifically at the target site (Wells et al., 2019; Yang et al., 2016).

Recently, reversible thermoresponsive nanoparticles have been developed as “smart” nanocarriers for drug delivery. The most studied is poly(N-isopropylacrylamide) (PNIPAM), which presents a lower critical solution temperature (LCST) of 32 °C. This temperature determines the structural transition needed for drug release. When the temperature is below LCST, PNIPAM is soluble, with a swollen morphology in the aqueous media, caused by interaction between the water molecules and the polymer through formation of hydrogen bonds. This configuration enables drug entrapment. However, temperatures higher than LCST produce the collapse of the nanoparticle structure, due to predominance of the hydrophobic interactions inside PNIPAM, while hydrogen-bonding with the water molecules is reduced. In this condition, the nanocarrier is insoluble and suffers a shrinkage that leads to the release of the loaded drug (**Figure 10**) (Karimi et al., 2016; Salimi, Dilmaghani, Alizadeh, Akbarzadeh, & Davaran, 2018).

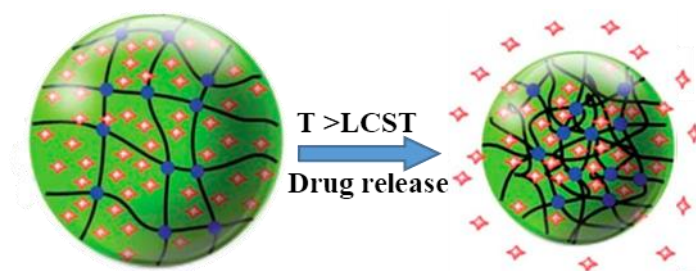


Figure 10. Structural changes in a thermoresponsive nanoparticle. Adapted from (Karimi et al., 2016).

The PNIPAM transition temperature can be modified to a desired one by performing a copolymerization synthesis with different monomers like acrylic, methacrylic, fumaric and vinylacetic acids (Hoare & Pelton, 2007). In addition to thermoresponsive capacities, further modifications can achieve response to pH changes or magnetic stimuli (Jalili, Jaiswal, Peak, Cross, & Gaharwar, 2017; Yang et al., 2016). As an example, addition of acrylamide and a magnetic nanoparticle to PNIPAM not only increases LCST to 45 °C, but provides sensibility to

both temperature and magnetic field stimuli, which can then be used to induce drug release (Jalili et al., 2017).

9.4. Cells as drugs vehicles

MSC are undifferentiated cells with a fibroblastic morphology that possess a long-term self-renewing capacity. They present multipotent properties that confer them the ability to differentiate into different mesodermal cell types such as osteocytes, chondrocytes and adipocytes. Originally they were isolated from the bone marrow stroma, where they represent a 0.001-0.01% of all cells. MSC are characterized by several unique features that make them a potential vehicle for drug delivery.

Although initially isolated from the bone marrow, multipotent stem cells can be isolated from almost all tissues, such as liver, muscle, skin and lungs, suggesting a potential role in organ homeostasis, maintenance and repair. Still, the most common sources for clinical application are bone marrow, adipose tissue and umbilical cord, as they can be readily obtained in a non-invasive way from a donor (Bernardo et al., 2007; Krampera, Franchini, Pizzolo, & Aprili, 2007; Porada & Almeida-Porada, 2010; Wei et al., 2013). The amount of MSC in the obtained heterogeneous population is very low and, for this reason, they must be expanded *in vitro*. The selection of the right cell population is performed following criteria established by the International Society for Cellular Therapy in 2006 (and previously described in 2.1.4). Currently the characterization of MSC has some obstacles as there is no unique marker that distinguishes these cells from the rest in a sample of tissue obtained from a donor, as the majority of the antigens used are shared with different cell types (Lin et al., 2019; Porada & Almeida-Porada, 2010).

The low level of expression of the major histocompatibility complex (MHC) class II is responsible of the hypoimmunogenicity of MSC. Thanks to this characteristic, the immune response, represented by CD8+ T-cells or natural killer (NK), is not evoked by MSC, making these cells safe for transplantation (even allogenic), as well as increasing their circulation time. In addition it has been observed, both *in vitro* and *in vivo*, that MSC to modulate the immune response by affecting the generation and proliferation of T cells, B cells, macrophages and NK, which leads to a reduction in inflammation (Amara, Touati, Beaune, & De Waziers, 2014; Porada & Almeida-Porada, 2010; Wei et al., 2013).

From the point of view of drug vehiculation, the most appealing characteristic of MSC is their ability to migrate to places where there is an inflammatory process. This quality is known as “homing”. The tumour microenvironment is similar to a tissue with inflammation, as during tumour growth cancer cells secrete cytokines and growth factors that act as chemoattractants to the cells of the immune system (Ghaedi et al., 2011). The homing capacities of MSC into tumour sites make them a valuable candidate to act as a vehicle for drug delivery and personalized cell

therapy. It was observed that cells administered through an intravenous injection were able to reach lung cancer after 24 hours, without getting engrafted in healthy tissues. Although MSC can persist in the malignant tissue for several weeks, most of them are cleared in the first week after administration, leaving just a small number of cells in the targeted tissue (Lin et al., 2019). Local intra-arterial injection can be used to increase the accumulation of MSC in the tumour (Wei et al., 2013). Some parameters of MSC therapy still need to be refined, like, for example, the dosage. Precaution should be taken as the administration of too many MSC can lead to embolism and death of the patient (Yao et al., 2017).

Apart from specifically migrating to the tumour site, these cells are able to localize the metastasis, which is a step forward in cancer therapy, especially for those invasive types of cancers that are not successfully eradicated with conventional treatment (Porada & Almeida-Porada, 2010; Yao et al., 2017).

MSC from different origins present slight variations on RNA and protein levels that could possibly have an influence on their homing capacities and the overall outcome of cell therapy (Porada & Almeida-Porada, 2010). Also, there are many studies on the effect that MSC exert on the tumour cells, reporting rather contradictory results: some groups found that MSC favoured the proliferation of the cancer cells, while others showed inhibitory effects on the tumour. For example, increased tumour progression caused by MSC was found in human breast and colorectal cancer. On the contrary, anti-tumour effects were observed in primary human glioma and liver cancer (Lin et al., 2019). Despite these discrepancies, engineered MSC loaded with a chemotherapeutic drug or nanoparticle, or transduced with a viral vector carrying a specific tumour suppressor, have shown promising anti-tumour effects. One of the drawbacks of this approach is the limited drug loading capacity, due to reduced intracellular space, and to the possible cytotoxic effect the drug may cause on the MSC itself (Amara et al., 2014; Wei et al., 2013; Yao et al., 2017).

II. Hypothesis and objectives

*“People will always have something to find, discover, invent,
because the very source of this knowledge is inexhaustible”.*

Ivan Goncharov

General Hypothesis

Development of combination chemotherapies with novel anti-tumour drugs, together with advanced therapies based on the application of mesenchymal stem cells and stimuli-responsive nanoparticles is a promising strategy that enhance the responsiveness of osteosarcoma cells, with reduced treatment-related side effects.

General Objective

To design and evaluate novel osteosarcoma therapies based on combination therapy with recently discovered drugs, nanoparticle encapsulation, and use of mesenchymal stem cells as vehicles to target the treatment specifically towards the tumour.

Strategy I

Hypothesis

Incorporation of oridonin along with doxorubicin for osteosarcoma treatment may both potentiate the cytotoxicity of the latter, and reduce the therapeutic doses of doxorubicin, leading to a decrease in adverse effects, like cardiotoxicity.

Objectives

Overall objective

Gain an insight on the potential of doxorubicin and oridonin combination for osteosarcoma treatment, by focusing on both *in vitro* and *in vivo* models of paediatric osteosarcoma.

Specific objectives

1. Determine the cytotoxic effect of doxorubicin and oridonin, administered individually and in combination, by using *in vitro* models of osteosarcoma (Saos-2 and U2OS cells).
2. Gain insights into the cellular mechanisms of the combined effect of doxorubicin and oridonin, by focusing on mitochondrial function, reactive oxygen species generation and apoptosis.
3. Evaluate the effects of oridonin in human osteoblasts *in vitro*.
4. Determine the anti-cancer effects of doxorubicin and oridonin combination treatment in an osteosarcoma xenograft *in vivo* model (Saos-2 cell line implanted in athymic nude mice).

Strategy II

Hypotheses

- Paclitaxel repurposing into osteosarcoma may be a suitable therapy for this disease.
- Cell therapy and nanotechnology-based drug delivery can be combined to develop a novel treatment for osteosarcoma, based on the ability of mesenchymal stem cells to migrate to tumour sites, and the potential of nanoparticles to carry chemotherapeutic drugs and deliver them in response to specific stimuli.

Objectives

Overall objectives

1. Evaluate the feasibility of paclitaxel repurposing for osteosarcoma therapy.
2. Evaluate the feasibility of paclitaxel encapsulation into thermoresponsive PNIPAM nanoparticles.
3. Evaluate the feasibility of using adult mesenchymal stem cells for drug vehiculization and specific targeting towards the tumour.
4. Evaluate the feasibility of a combination therapy for osteosarcoma consisting of paclitaxel and oridonin, being the former either free or encapsulated in PNIPAM nanoparticles.

Specific objectives

1. Characterization of the PNIPAM nanoparticles, either loaded with a Nile Red tag and paclitaxel, or just with the Nile Red tag (PTX+NiR@PNIPAM and NiR@PNIPAM, respectively).
2. Determine the effect of paclitaxel in several *in vitro* models of osteosarcoma (MG63, U2OS and Saos-2 cells), either free or encapsulated in nanoparticles.
3. Determine the effect of free and PNIPAM-encapsulated paclitaxel in mesenchymal stem cells.
4. Assess the ability of mesenchymal stem cells to incorporate PNIPAM nanoparticles.
5. Determine, *in vitro*, the ability of PNIPAM-loaded mesenchymal stem cells to migrate towards the tumour cells and interact with them.

- Determine the ability of oridonin to potentiate the effect of paclitaxel in osteosarcoma cells, *in vitro*.

III. Materials and methods

“A scientist in his laboratory is not a mere technician: he is also a child confronting natural phenomena that impress him as though they were fairy tales”.

Marie Curie

1. Cell lines

1.1. Osteosarcoma

Different commercially available osteosarcoma cell lines were chosen for the present thesis, each one representative of a different type of bone tumour.

1.1.1. MG63

MG63 human cell line derives from a 14 years old boy osteosarcoma. It has a fibroblastic morphology and is characterized by presence of mutations in *p53* gene (**Supplementary material, Figure A1**). MG63 cell line was purchased from the European Collection of Authenticated Cell Cultures (ECACC). It was incubated at 37 °C in a humidified atmosphere with 5% CO₂ (standard culture conditions). MG63 cell line was maintained in the following growth media:

- Minimum Essential Medium Eagle, α modification (α MEM) (Sigma-Aldrich).
- 10% of Fetal Bovine Serum (FBS) (Sigma-Aldrich).
- L-glutamine 2 mM (Sigma-Aldrich).
- 1X of MEM Non-Essential Amino Acids solution, containing L-alanine, L-asparagine, L-aspartic acid, L-glycine, L-serine, L-proline and L-glutamic acid (Sigma-Aldrich).

1.1.2. U2OS

U2OS human cell line derives from a 15 years old girl osteosarcoma. It has an epithelial morphology and it is characterized by carrying a wild-type version of *p53* gene (**Supplementary material, Figure A1**). U2OS cell line was purchased from the ECACC. It was incubated in standard culture conditions. U2OS cell line was maintained in the following growth media:

- McCoy's 5A Medium (Sigma-Aldrich).
- 10% of FBS (Sigma-Aldrich).
- L-glutamine 2 mM (Sigma-Aldrich).

1.1.3. Saos-2

Saos-2 human cell line derives from an 11 years old girl osteosarcoma. It has an epithelial morphology and is characterized by a null mutation in a *p53* gene (**Supplementary material, Figure A1**). Saos-2 cell line was purchased from ECACC. It was incubated in standard culture conditions. Saos-2 cell line was maintained in the following growth media:

- McCoy's 5A Medium (Sigma-Aldrich).
- 15% of FBS (Sigma-Aldrich).
- L-glutamine 2 mM (Sigma-Aldrich).

1.2. Human adipose and human bone marrow tissue-derived mesenchymal stem cells (huAD-MSC and huBM-MSC)

huAD-MSC and huBM-MSC have a fibroblastic morphology (**Supplementary material, Figure A2**). They were purchased from Merck. huAD-MSC and huBM-MSC were seeded at a density of 5,000 cells/cm², and incubated in standard culture conditions. They were maintained in the following growth media:

- Dulbecco's Modified Eagle's Medium-high glucose (DMEM-hg) with 4500 mg/L of glucose (Sigma-Aldrich).
- 10% of FBS (Sigma-Aldrich).
- L-glutamine 2 mM (Sigma-Aldrich).

2. Antibiotics

In some experiments that state so the next antibiotics were added to the complete cell culture medium reaching the final concentration of:

- Penicillin 100 U/mL (Sigma-Aldrich)
- Streptomycin 0.1 mg/mL (Sigma-Aldrich).
- Amphotericin B 0.125 µg/mL (Sigma-Aldrich).

3. FBS heat inactivation

FBS heat inactivation is necessary to inactivate the complement, which is a group of proteins of the immune system, present in the serum. This procedure is required as some cell lines can be sensitive to the complement activity. The basic protocol for FBS heat inactivation was:

1. The serum bottle was thawed at 4 °C overnight, as all stock serum bottles are stored at -20 °C.
2. The next day the water bath was warmed until 56 °C.
3. The thawed serum bottle was placed in water bath for 30 minutes to initiate the inactivation process. To promote a uniform serum heating the bottle was agitated every 10 minutes.
4. Under sterile conditions the content of the bottle was divided into 25 mL/aliquots and stored at -20 °C.

4. Cell passage

Cell passage or cell subculturing is an essential process to expand and maintain viable the cultures by transferring them from one culture vessel into a fresh one. Normally, this process is done when cells have covered 80-90% of the available surface (usually referred as 80-90%

confluence). T75 flask was the most common culture vessel used for cell growth. For all cell types used in this work the general procedure of cell passage was performed as described next:

1. The complete cell culture medium was pre-warmed in advance.
2. The medium from T75 flask was removed by aspiration and the monolayer was washed with 6 mL of phosphate buffer saline (PBS) to wash off serum from the medium, which is known to inactivate trypsin. PBS was then removed by aspiration.
3. 2 mL of TrypLE Express Enzyme (Gibco) were added and the T75 flask was placed in the incubator in standard culture conditions for 4-5 minutes. After this time the cells were examined under an inverted microscope. At this moment cells should be in suspension and appear round, which would indicate cell detachment. If there was presence of coated cells or clumps, the culture vessel was gently tapped several times on the hand and/or left in the incubator for more time.
4. 4 mL of medium was added to inactivate trypsin. The amount of medium added is proportional or higher than of trypsin.
5. Cell suspension was homogenised by pipetting to break up the clumps and detach some of the cells from the flask surface.
6. Cell counting was performed by using a Neubauer chamber. The procedure is described in 1.5.1.
7. The total volume from T75 flask was transferred into a Falcon tube.
8. The Falcon tube was centrifuged at $500 \times g$ for 5 minutes.
9. The supernatant was removed by aspiration and the pellet was resuspended in 1 mL of cell culture medium by gentle pipetting.
10. The necessary amount of cell suspension was transferred into a freshly prepared T75 flask with 10-15 mL of cell culture medium and placed in incubator in standard culture conditions.

4.1. Cell counting using Neubauer chamber

The cell counting protocol of (Kaur, Faktorová, Peña-Diaz, & Lukeš, n.d.) was followed with some modifications:

1. The Neubauer chamber was cleaned with ethanol 70% prior to cell counting.
2. To ensure the depth of the chamber the coverslip was fixed on the raised glass rails.
3. 50 μ L of cell suspension were mixed with 50 μ L of Trypan Blue solution (Trypan Blue 0,4 % aqueous solution, sterile-filtered, purchased from Sigma-Aldrich). This mix could be further diluted with PBS if needed (*i.e.*, when the suspension contained too many cells to be counted).

4. 10 μL of the mix were loaded under the coverslip placed in the Neubauer chamber. This process was repeated for the second chamber.
5. The Neubauer chamber was placed on the inverted microscope stage and focused with 10X objective.
6. Each Neubauer chamber contains a square grid, 3 mm \times 3 mm size. Cells were counted in the four large corner squares, 1 mm \times 1 mm size (**Figure 11**). At least 8 large squares were counted, and the average cell number per square calculated. Bright-looking cells were considered alive, while blue (Trypan Blue-labelled) cells were considered dead.

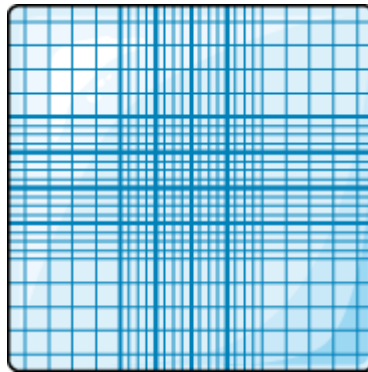


Figure 11. Neubauer chamber for cell counting.

7. The cell number per mL of cell suspension was calculated as: Mean counted cell number/square divided by the square volume (1 mm side \times 1 mm side \times 0.1 mm depth).
8. To calculate the cell number in the original suspension, the obtained cell number/mL was corrected according to dilution factor and volume of the original suspension.

$$\begin{aligned}
 \text{Total Cells/mL} &= \text{Mean value of cell number from eight squares} \times 10^4 \\
 &\quad \times \text{dilution factor of mixed sample} \\
 &\quad \times \text{total volume from which } 50 \mu\text{L was obtained}
 \end{aligned}$$

5. Doubling time

To determine the time required by MG63, U2OS and Saos-2 to double cell population, they were seeded in triplicates in 12-well plate at a density of 10^5 cells/well and let grow for 24, 48, 72 and 96 hours in standard culture conditions (**Figure 12**). Every day cell number was determined by Trypan Blue extrusion assay in each well by counting cells in a Neubauer chamber. The triplicate mean value was used for doubling time estimation calculated in an online programme Doubling Time (Roth, 2006).

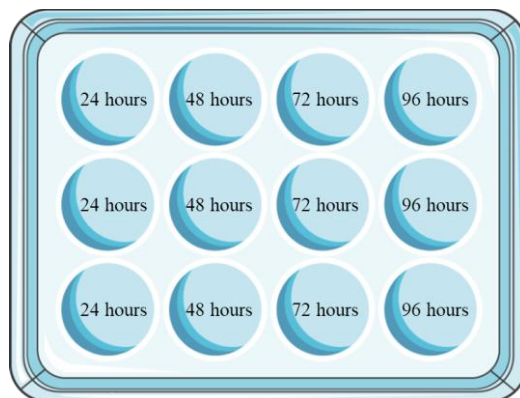


Figure 12. Schematic representation of a 12-well plate for doubling time estimation.

6. Resazurin assay

In the present work cell proliferation was estimated by resazurin assay, which is based on mitochondrial enzymatic reduction of the weakly blue fluorescent dye resazurin into fluorescent pink resorufin expelled outside the cell to the medium. The rate of reduction from blue to pink colour was quantified at excitation 530 nm and emission 590 nm wavelengths on fluorometer plate reader. The fluorescence signal is proportional to the number of cells present in a 96-well plate under specific conditions. In the last two decades, the resazurin assay has been widely used to evaluate the cytotoxicity of different drugs for being rapid and intuitive test. However, the drawback of this assay is that the metabolic activity of the cells could be affected by the treatment. For this reason, the produced fluorescent signal is not always proportional to the number of cells (Lavogina et al., 2022).

The resazurin stock solution with a final concentration of 450 μM was prepared in PBS. It was sterilized through a syringe filter with a pore size 0.2 μm . Aliquots of stock solution were stored at -20 $^{\circ}\text{C}$. The working solution with a final concentration of 90 μM was prepared by diluting the stock 5 times with complete cell culture medium.

The basic procedure of cell proliferation and viability estimation based on resazurin fluorescent dye is as follows:

1. Cell culture medium was removed from each well of 96-well plate by aspiration and rinsed with 100 μL of PBS.
2. 100 μL of resazurin working solution was added to each well.
3. The plate was incubated in standard culture condition for 3-4 hours that depended on each cell lines.
4. 70 μL of each well were transferred to a new black 96-well fluorometer microplate.
5. The fluorescence was read at excitation 530 nm and emission 590 nm wavelength on fluorometer plate reader (Perkin Elmer LS55 Fluorescence spectrometer).

6.1. Calibration curve

A calibration curve is essential to convert resazurin assay fluorescence measurements into cell number values. Given that resazurin to resorufin conversion depends on cell metabolism, a calibration curve is needed for each cell line. To establish the calibration curve, 200,000 cells of each cell line used in this work (MG63, U2OS, Saos-2, huAD-MSC and huBM-MSC) suspended in 200 μL of specific culture medium, were seeded in of the first well of a 96-well plate, while the rest 7 had 100 μL of complete cell culture medium. 100 μL out of 200 μL were sequentially transferred to the next well. This process was repeated 5 more times in a row. Blank was a well with complete medium and without cells (**Figure 13**). The plates were incubated for 2 hours in a standard culture conditions to allow cell attachment. Later, cell proliferation was measured by incubating cells in 100 μL of resazurin working solution. MG63, U2OS, huAD and huBM-MSC were incubated for 3 hours, while Saos-2 for 4 hours in a standard culture conditions. Finally, the fluorescence was measured on fluorometer plate reader.

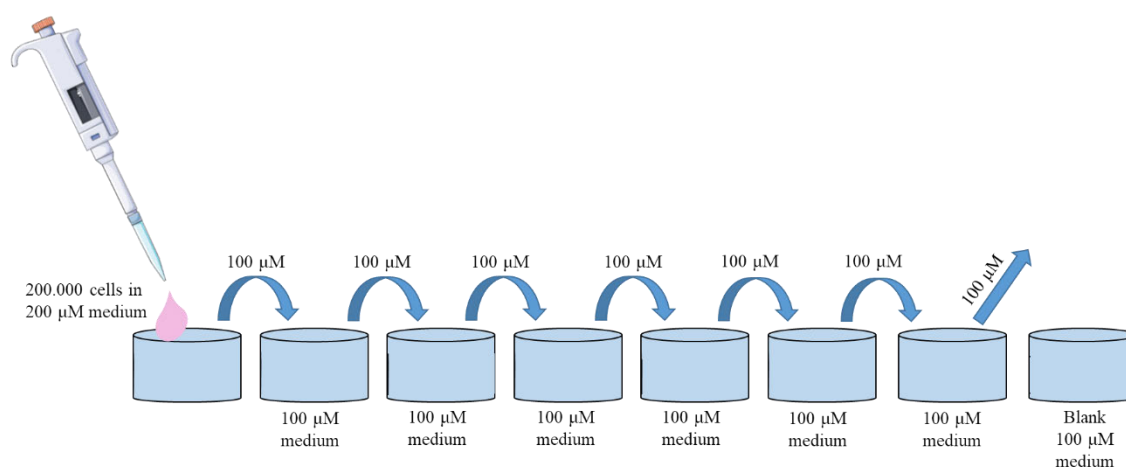


Figure 13. Schematic representation of cell dilution in a 96-well plate.

From **Supplementary material Figures A3 and A4** the number of cells was determined following the next formulas:

$$\text{MG63:} \quad y = 79.315x - 143.56$$

$$\text{Saos-2:} \quad y = 54.156x - 101.2$$

$$\text{U2OS:} \quad y = 67.893x - 107.34$$

$$\text{huAD-MSC:} \quad y = 68.954x - 120.05$$

$$\text{huBM-MSC:} \quad y = 68.493x - 121.33$$

7. Cell fixation

Fixation is a process where the structure and the intracellular composition of the cell is preserved, while the proteolytic enzyme induced autolysis and microbial contamination is

prevented. There are several fixative groups and one of them are aldehydes that interact through amine groups to cross-link proteins. The common and routinely used fixative agent is 3.7% formaldehyde stabilized with methanol to prevent formaldehyde polymerization.

The basic procedure of cell fixation was the following:

1. Cell culture medium was removed by aspiration and rinsed with PBS.
2. 3.7% formaldehyde stabilized with methanol was added in a volume enough to cover the cell-seeded well or plate surface.
3. The sample was incubated at room temperature (RT) for 30 minutes.
4. The fixative agent was removed and the sample was rinsed three times with PBS.
5. Cells were stored, if needed, in PBS at 4 °C until required. To prevent content evaporation the plate was covered in aluminium foil during storage.

8. Cell freezing

Cryopreservation is a method whereby cells are frozen, maintaining their viability, for long-term storage in liquid nitrogen tanks. The freezing procedure followed for different cell lines:

1. Cells were detached with trypsin (TrypLE, Gibco), and counted as detailed in 4.
2. Cells were pelleted and resuspended, at the desired concentration, in cell freezing medium.
3. Cells were aliquoted into sterile cryotubes, which were then placed into a CoolCell™ freezing container to ensure a cooling rate of -1 °C/min when stored at -80 °C overnight.
4. After freezing them to -80 °C, cryotubes were transferred to liquid nitrogen tanks for long-term storage.

The specific freezing media and suspension concentrations for each cell type used in this work are the following:

8.1. Osteosarcoma cell lines

Cell pellet was resuspended at a concentration of 10^6 cells/mL in a cell freezing medium consisting of 70% complete cell culture medium, 20% FBS and 10% dimethyl sulfoxide (DMSO).

8.2. MSC

huAD-MSC and huBM-MSC cell pellet was resuspended at a concentration of 0.5×10^6 cells/mL in a cell freezing media that consisted from 90% FBS and 10% DMSO. Aliquots were stored in liquid nitrogen.

9. Cell thawing

Frozen cells were thawed according to the following protocol:

1. The complete cell culture medium was pre-warmed in advance.

2. The cryovials were removed from liquid nitrogen and placed in a 37 °C water bath to thaw the sample.
3. 1 mL of cell suspension in freezing medium was transferred into a 15 mL-tube containing 9 mL of pre-warmed cell culture medium, and centrifuged at $500 \times g$ for 5 minutes.
4. The supernatant was removed by aspiration and the cell pellet was resuspended in 1 mL of cell culture medium.
5. The necessary amount of cells were seeded in a tissue-culture flask, with the appropriate volume of cell culture medium, and placed in incubator in standard culture conditions.

10. Drugs

10.1. Doxorubicin (DOX)

Doxorubicin hydrochloride, a neoplastic drug, was purchased from Sigma-Aldrich. The stock solution was prepared in DMSO at a concentration of 10 mM under sterile conditions. Aqueous solution of DOX is characterized by an orange-red colour. Aliquots were made and stored at -20 °C, protected from light. On the day of the experiment, the working solution of DOX was prepared by diluting the stock in cell culture medium.

10.2. Oridonin (ORI)

Oridonin, a compound with anti-tumour properties, was purchased from Sigma-Aldrich. Stock solution was prepared to a final concentration of 10 mM by dissolving oridonin powder in DMSO under sterile conditions. It yielded a transparent ORI solution. Aliquots were made and stored at -20 °C. On the day of the experiment, the working solution of ORI was prepared by diluting the stock in cell culture medium.

10.3. Paclitaxel (PTX)

Paclitaxel, an anti-neoplastic compound, was at first a kind gift of Dr. Juan M. López-Romero Research Group. For subsequent experiments, it was purchased from Tocris Bioscience (although the first 6 mg used in this work were a kind gift of Dr. Juan M. López-Romero Research Group). The stock solution was prepared in DMSO at a concentration of 18 mg/mL. Aliquots were made and stored at -20 °C. On the same day of the experiment, the 18 mg/mL stock solution was diluted to an intermediate PTX stock, 0.018 mg/mL (21100 nM), in cell culture medium lacking FBS and L-glutamine. From the intermediate stock, treatment concentrations were prepared by dilution in complete cell culture medium. The preliminary studies in the laboratory showed the amount of DMSO present in the treatment conditions was minimal to overshadow the effects of the chemotherapeutic agent. The solubility of PTX was detected not to be affected by

different dilutions. For this reason, the observed effects in the present work can be considered as caused by PTX itself.

11. Nanoparticles

PNIPAM nanoparticles were kindly provided by Juan M. Lopez-Romero's Research Group. To allow their detection, both PNIPAM particles were fluorescently tagged with Nile Red (NiR). Besides, PNIPAM were either loaded with paclitaxel (PTX+NiR@PNIPAM), or unloaded (NiR@PNIPAM), to be used as controls (**Table 3**).

Table 3. Composition of NiR@PNIPAM and PTX+NiR@PNIPAM.

| Composition | Nanoparticles | |
|-----------------------|---------------|----------------|
| | NiR@PNIPAM | PTX+NiR@PNIPAM |
| [PNIPAM] | 0.015 mg/mL | 0.015 mg/mL |
| NiR fluorescent probe | 0.01 mM | 0.01 mM |
| PTX | - | 0.018 mg/mL |

Aliquots of nanoparticles were made and stored at RT. Prior to the experiment the samples were homogenized in an ultrasonic bath.

11.1. Nanoparticle's characterization

The morphology and particle's size were determined in dry conditions by Transmission Electron Microscopy (TEM) imaging. PNIPAM is a thermo-responsive polymer that undergoes a reversible shrinkage, with subsequent cargo release when the temperature is superior to 32 °C, which is its lower critical solution temperature (LCST).

To observe the size changes, stock dispersions of NiR@PNIPAM and PTX+NiR@PNIPAM were homogenized by ultrasound and diluted 50 times in MiliQ water. The samples were stored at RT and at 37 °C (the temperature cells normally exposed in the incubator) for 24 hours. Afterwards, TEM images were acquired by transferring a small volume (4 µL) of nanoparticle dispersion to a copper grid. The size was calculated by measuring 100 particles in a random field with *ImageJ* free software.

12. Statistical analysis

All graphs and statistical analyses of the quantitative data were performed using *Excel 16.0* and *Prism 6.0c*. Student's t-test was applied for comparisons of unpaired two-samples. For multiple comparisons the results were analysed by a two-way analysis of variance (ANOVA) followed by Tukey's multiple comparison test. Values with $p < 0.05$ were considered statistically significant. Data are represented as mean±SD. Kruskal-Wallis test was used to study Western-blot semi-quantitative data.

Strategy I: Doxorubicin and oridonin combination

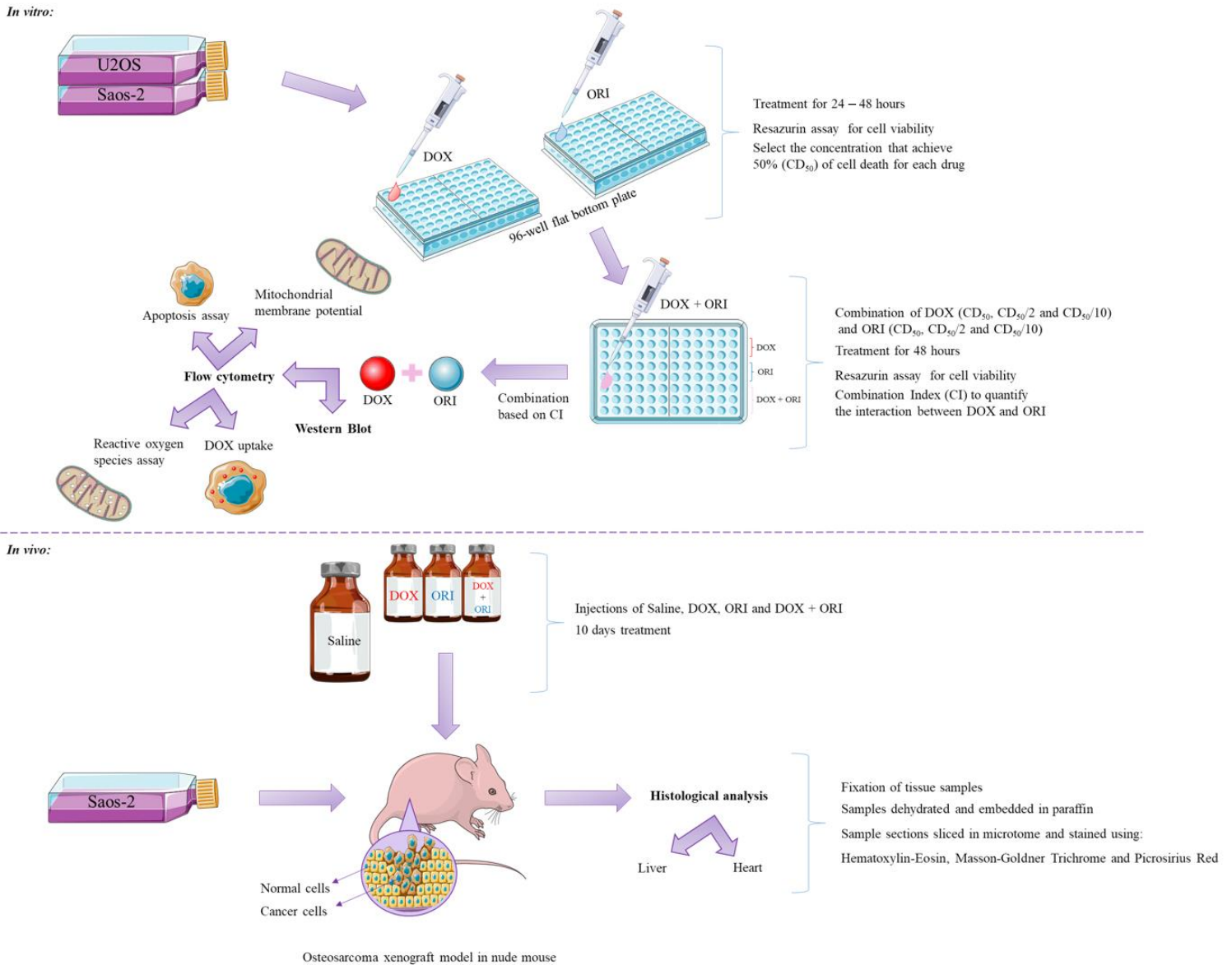


Figure 14. General overview of the materials and methods used in strategy I

1. Effects of DOX and ORI on cell viability

The effects of DOX and ORI on cell viability was assessed using resazurin assay. U2OS cells were seeded in a 96-well plate, at a density of 10^4 cells/well in 100 μ L of the corresponding medium. Saos-2 were seeded similarly, at a density of 20×10^3 cell/well. The plates were incubated in standard culture conditions for 24 hours, and then treated with different concentrations of DOX (0.1-10 μ M) or ORI (10-40 μ M) for 24 and 48 hours. Six wells were used for each condition. After the incubation, the treatment medium was removed and the cells were rinsed with PBS. U2OS were incubated for 3 hours in 20% resazurin solution 450 μ M, dissolved in culture medium. In case of Saos-2 the incubation was for 4 hours. The fluorescence of the resazurin fluorescent dye was measured on a fluorometer plate reader at excitation = 530 nm and emission = 590 nm wavelengths.

2. Effects of DOX and ORI combination

Cell viability after combined drug therapy was estimated through resazurin assay as described above. U2OS and Saos-2 were treated with different combinations of DOX (CD_{50} , $CD_{50}/2$ and $CD_{50}/10$) and ORI (CD_{50} , $CD_{50}/2$ and $CD_{50}/10$).

The interaction between DOX and ORI was analyzed by Chou-Talalay method (Chou, 2010). In brief, the effect value (Fa) was calculated for each drug or drug combination, as:

$$Fa = 1 - (\text{obtained viability after drug treatment})$$

Fa data were analyzed using *CompuSyn* software (www.combosyn.com), which calculates the combination index (CI) for the drugs studied. Combination index values below one ($CI < 1$), are indicative of synergism; $CI = 1$ indicate there is an additive effect; and $CI > 1$ are indicative of antagonism (Chou, 2010).

3. Cell uptake of DOX

DOX has an intrinsic red fluorescence that serves as a useful tool for its detection. Intracellular presence of DOX was measured in a *Gallios* flow cytometer (Beckman Coulter, Brea, California, USA). For this purpose, U2OS and Saos-2 cells were seeded at a density of 150,000 cells/well in 12-well plates and incubated for 24 hours in standard culture conditions. Then, Saos-2 were treated for 2 hours with a chosen combination of DOX and ORI, and U2OS, were treated for 2 and 4 hours (**Table 4**).

Table 4. Drug concentrations used for DOX+ORI combination therapy in osteosarcoma cell lines. The concentration was chosen for each cell line according to viability after treatment with the drugs, and the combination index calculated for DOX+ORI.

| | U2OS | Saos-2 |
|----------------|------|--------|
| DOX (μ M) | 1 | 2.5 |
| ORI (μ M) | 1.2 | 10 |

Untreated cells, and cells treated with only one of the drugs, served as controls. The treatments were done in triplicate. After incubation, cells were rinsed with PBS, collected by trypsinization and centrifuged at $500 \times g$ for 5 minutes. The supernatant was removed and the pellet resuspended in 1 mL of cold PBS with 2% of FBS. Then, the cells were transferred by filtration to round-bottom polystyrene tubes and analysed by flow cytometry. Red fluorescence, corresponding to intracellular doxorubicin, was detected in the cytometer FL3 channel. For each sample, 25,000 events were collected.

4. Mitochondrial membrane potential

The loss of mitochondrial membrane potential (MMP) is a hallmark of apoptosis. It is usually attributed to early apoptotic events followed by activation of pro-apoptotic proteins implicated in cell death. JC-1 is a membrane-permeable dye that concentrates as red fluorescent aggregates in the mitochondria of healthy cells. However, when the integrity of mitochondria is affected, their membrane potential is dissipated, and there is no JC-1 accumulation in the mitochondria. Instead, it is dispersed through the cell as green fluorescent monomers.

The changes of the mitochondrial inner membrane electrochemical potential in living cells were detected with *Mitochondrial staining kit* (Sigma-Aldrich), according to manufacturer's instructions. Briefly, U2OS and Saos-2 were seeded at a density of 150,000 cells/well in 12-well plates, and incubated in standard culture conditions. After 24 hours for U2OS and 32 hours for Saos-2, the osteosarcoma cell lines were treated with DOX, ORI and DOX+ORI at the concentrations collected in table 4. Untreated cells were used as controls. The treatments were done in triplicate. U2OS was exposed for 48 hours, while Saos-2 for 16 hours. This treatment time was maintained throughout all the experiments in strategy I. After drug exposure, drug-containing media were removed, and cells were washed with PBS, collected by trypsinization and pelleted by centrifugation at $500 \times g$ for 5 minutes. The pellet was resuspended and incubated for 20 minutes, in standard culture conditions, in 1 mL of JC-1 staining mixture ($5 \mu\text{g/mL}$ JC-1 dissolved in staining buffer, provided with the kit). Cells treated with valinomycin were used as a control of mitochondrial gradient dissipation. For this purpose, valinomycin was added at a final concentration of $0.2 \mu\text{g/mL}$ to the JC-1 staining mixture. After incubation in JC-1 staining solution, the cells were pelleted by centrifugation, the supernatant removed and pellet resuspended in ice-cold JC-1 staining buffer. The fluorescence of the stained cells was measured by flow cytometry. JC-1 monomers (green) were detected in the FL1 channel and JC-1 aggregates (red) were detected in FL2 channel. For each sample 10,000 events were collected.

5. Apoptosis assay

Drug effect on cell death was studied by Annexin-V/Hoechst labeling. Phosphatidylserine (PS) is a protein with intracellular localization in normal cells. However it is exposed on the

surface of the apoptotic cells. Annexin V has the ability to bind to PS on outer leaflet of cell membrane, making it useful in apoptosis detection. Hoechst 33258 is a fluorescent DNA dye that does not permeate cell membrane of healthy cells, but it penetrates the cell if the membrane is damaged, as is the case in necrotic cells. Then Hoechst 33258 can be used to detect cell necrosis.

U2OS and Saos-2 cells were seeded at a density of 150,000 cells/well in 12-well plates and incubated in standard culture conditions to let cell attachment and expansion. Cells were treated with DOX, ORI and DOX+ORI at the concentrations described in table 4. Cells without any treatment were used as controls. The treatments were done in triplicate. After drug exposure, U2OS and Saos-2 were rinsed with PBS, collected by trypsinization and pelleted by centrifugation. Pelleted cells were resuspended in 100 μ L Annexin V binding buffer containing 2.5 μ L Annexin V-FITC conjugate (Elabscience) and 1 μ g/mL Hoechst 33258. After a 20 minutes incubation, 400 μ L of binding buffer were added and the cells were filtered to disaggregate clumps and transferred to round-bottom polystyrene tubes, prior to flow cytometry analysis. The fluorescence of Annexin V-FITC was detected in FL1 channel, while that of Hoechst 33258 was detected in FL9. Cells in the lower left quadrant (Annexin V-FITC-/Hoechst 33258-) were considered to be live cells. Early apoptosis (Annexin V-FITC+/Hoechst 33258-) was considered for cells located in the lower right quadrant. Late apoptosis (Annexin V-FITC+/Hoechst 33258+) was considered for cells localized in the upper right quadrant. Finally, necrosis (Annexin V-FITC-/Hoechst 33258+) was considered for cells localized in the upper left quadrant.

6. Reactive oxygen species assay

Intracellular reactive oxygen species (ROS) were detected with *Fluorometric Intracellular ROS kit* (Sigma-Aldrich), in which a cell-permeable sensor reacts with intracellular ROS, resulting in a fluorometric product ($\lambda_{ex} = 540 / \lambda_{em} = 570$ nm) proportional to the amount of ROS present.

U2OS and Saos-2 were seeded at a density of 150,000 cells/well in 12 well plates and incubated in standard culture conditions for 24 and 32 hours, respectively, to let cell attachment and expansion. Then, cells were treated with the doses of DOX, ORI and DOX+ORI specified in table 4. Untreated cells were used as control. Each condition was done in triplicate. After drug exposure, cells were rinsed with PBS, collected by trypsinization and pelleted by centrifugation. The cells were resuspended in 500 μ L of assay buffer and 500X ROS detection reagent stock solution was added to each tube. The cells were incubated for 1 hour in standard culture conditions and red fluorescence intensity was measured by flow cytometry. For each sample 10,000 events were collected.

7. Western blot

Saos-2 cells were seeded at a density of 150,000 cells/well in 12-well plates and incubated in standard culture conditions to let cell attachment and expansion. Cells were treated with DOX, ORI and DOX+ORI at the concentrations described in table 4. Saos-2 without any treatment were used as controls. After 16 h of drug exposure cells were harvested with a scraper, and lysed in RIPA lysis buffer containing a mix of protease inhibitors. The total protein concentration was determined using Bradford protein assay. Proteins were separated on SDS-PAGE and transferred onto nitrocellulose membrane. Non-specific antibody binding was blocked with 5% non-fat milk. The membrane was incubated with the following primary anti-bodies: anti-Bcl-2 (1:1000), anti-Bcl-XL (1:1000), anti-Mcl-1 (1:1000), and anti- β -actin (1:2000) overnight at 4 °C. Afterwards, a horseradish peroxidase-conjugated secondary antibody (1:5000) was incubated at room temperature for 2 h. Finally, the protein bands were visualized with ECL Western Blotting Substrate and photographed with ChemiDoc XRS+ (Bio-Rad). Experiments were performed thrice. Semi-quantification of band densitometry was carried out by measuring band density with *ImageJ* software. All bands in a gel were normalized against the gel background, and then Mcl-1, Bcl-2 and Bcl-XL bands were normalized against their corresponding β -actin loading controls.

8. Pilot osteosarcoma xenograft model in nude mice

The *in vivo* experiment was authorized by Council of Agriculture, Fishing and Rural development (12/12/2019/195). Moreover, a course in animal experimentation was completed in order to properly manage mice. An osteosarcoma xenograft model was established through subcutaneous inoculation of Saos-2 cells into young adult nude mice (nu/nu CD1 strain). Several cell doses and inoculation media were tested to establish the inoculation protocol that yielded the higher success in tumor formation (**Table 5**).

Table 5. Determination of appropriate conditions for inoculation process *in vivo*.

| Cell line | Cell number | Basement membrane matrix mixed with serum-free McCoy's 5A | | Injectable volume |
|-----------|----------------------------|---|----------|-------------------|
| | | Collagen type I, Rat Tail | Matrigel | |
| Saos-2 | 10 ⁶ | 0.1 mg/mL | 4 mg/mL | 100 μ L |
| | 2 \times 10 ⁶ | | | |
| U2OS | 10 ⁶ | | | |
| | 2 \times 10 ⁶ | | | |

To *in vivo* evaluate DOX+ORI combination therapy, 8 week-old female mice were subcutaneously inoculated with 2 \times 10⁶ Saos-2 cells in 100 μ L of serum-free McCoy's 5A medium

containing 50% Matrigel (Corning). Both flanks were inoculated, so every mouse carried two tumours. One month after the inoculation, mice were separated into 5 different groups according to the treatment that was to be applied: saline (control), ORI 30 mg/kg, DOX 5 mg/kg, DOX 10 mg/kg and DOX 5 mg/kg + ORI 30 mg/kg. The size of each tumour was measured with a calliper and animal weight was monitored every other day. The administration of ORI 30 mg/kg alone and in combination with DOX produced visible pain signs. For this reason, it was decided to reduce and carry on the following injections with ORI 20 mg/kg. The treatment lasted 10 days in total. Afterwards, mice were sacrificed by CO₂ inhalation. The resected tumours were measured, fixed overnight by immersion in 3.7% formaldehyde, and stored in ethanol 70% at RT. The tumour volume was calculated according to (Li et al., 2019):

$$V = Length \times \frac{Width^2}{2}$$

Later the calcification degree of each tumour was assessed by X-ray, performed with an Albira (Bruker) *in vivo* imager.

In each specimen, the major organs. *i.e.* heart, liver, guts and spleen were dissected out and preserved by fixation in 3.7% formaldehyde. Morphological changes in the size and weight of the liver were assessed.

9. Histological analysis

Fixed tumors and organ samples were dehydrated by successive immersion in ethanol of increasing grade, and embedded in paraffin, as described in **table 6**. Paraffin-embedded samples were cut with a microtome to obtain 8 µm-thick sections that were mounted in silane-treated glass slides. Sections were stained with Hematoxylin-Eosin, Masson-Goldner Trichrome, and Picrosirius Red, as described below.

Table 6. Process of tissue dehydration during paraffin embedding.

| Treatment | Duration (min) | Number of cycles |
|--------------|----------------|------------------|
| Ethanol 70% | 60 | 2 |
| Ethanol 80% | 60 | 1 |
| Ethanol 96% | 60 | 2 |
| Ethanol 100% | 60 | 2 |
| Substance X | 30 | 3 |
| Paraffin | 120 | 2 |

9.1. Hematoxylin-Eosin (HE) staining

The HE stain is a standard test for histological examination of tissues. In a simple way it enables identify component like nuclei, cytoplasm or connective tissue (Chan, 2014). **Table 7** describes the steps performed for sections staining. Afterwards, samples were mounted with Eukitt.

Table 7. Hematoxylin-Eosin staining procedure.

| Treatment | Duration (min) | Number of cycles |
|--|------------------|------------------|
| Xylene | 10 | 2 |
| Ethanol 100% | 10 | 2 |
| Ethanol 96% | 10 | 2 |
| Ethanol 70% | 10 | 1 |
| Distilled water | 10 | 1 |
| Hematoxylin solution, Harris modified | 5 | 1 |
| Ethanol 96% + drops of acetic acid | 5 | 1 |
| Running water | 5 | 1 |
| Ethanol 96% | 5 | 1 |
| Eosin yellowish, hydroalcoholic solution | 3 | 1 |
| Ethanol 96% | Brief immersions | 3 |
| Ethanol 100% | 10 | 2 |
| Xylene | 10 | 2 |

9.2. Masson-Goldner Trichrome staining

Masson-Goldner Trichrome is a three-color staining that facilitates the distinction between bone matrix and connective tissue, whose procedure is summarized in **table 8** (Rentsch, Schneiders, Manthey, Rentsch, & Rammelt, 2014). Finally, samples were mounted with Eukitt.

Table 8. Masson-Goldner staining procedure.

| Treatment | Duration (min) | Number of cycles |
|--|-----------------|------------------|
| Xylene | 5 | 2 |
| Ethanol 100% | 2 | 2 |
| Ethanol 96% | 2 | 2 |
| Ethanol 70% | 2 | 1 |
| Distilled water | 2 | 1 |
| Weigert's Hematoxylin kit Solution A (main component: hematoxylin) + Solution B (main components: ferric chloride and hydrochloric acid) 1 (Solution A) : 1 (Solution B) | 10 | 1 |
| Distilled water | Brief immersion | 1 |
| Running water | 8 | 1 |
| Ponceau acid fuchsin solution | 4 | 1 |
| Eosin yellowish, hydroalcoholic solution | 3 | 1 |
| Acetic acid 1% | 0.5 | 1 |
| Phosphomolybdc acid-orange G solution | 30 | 1 |
| Acetic acid 1% | 0.5 | 1 |
| Light green 0.2% (Goldner III) | 6 | 1 |
| Acetic acid 1% | 2 | 1 |
| Running water | 1 | 1 |
| Ethanol 96% | 2 | 2 |
| Ethanol 100% | 2 | 2 |
| Xylene | 5 | 2 |

9.3. Picrosirius Red staining

Picrosirius Red is a collagen staining, commonly used for cardiovascular fibrosis detection (Chen et al., 2011). The overview of the procedure is represented in **table 9**. Later, the stained samples were mounted with a help of Eukitt.

Table 9. Picrosirius Red staining procedure.

| Treatment | Duration (min) | Number of cycles |
|--------------------------|------------------|------------------|
| Xylene | 10 | 2 |
| Ethanol 100% | 10 | 2 |
| Ethanol 96% | 10 | 2 |
| Ethanol 70% | 10 | 1 |
| Distilled water | 5 | 1 |
| Picrosirius red solution | 30 | 1 |
| Running water | 6 | 1 |
| Distilled water | Brief immersions | 3 |
| Ethanol 96% | 1 | 1 |
| Ethanol 100% | 1 | 1 |
| Ethanol 100% | 10 | 1 |
| Xylene | 10 | 2 |

Strategy II: Paclitaxel, MSC and combination treatment

Part I Osteosarcoma

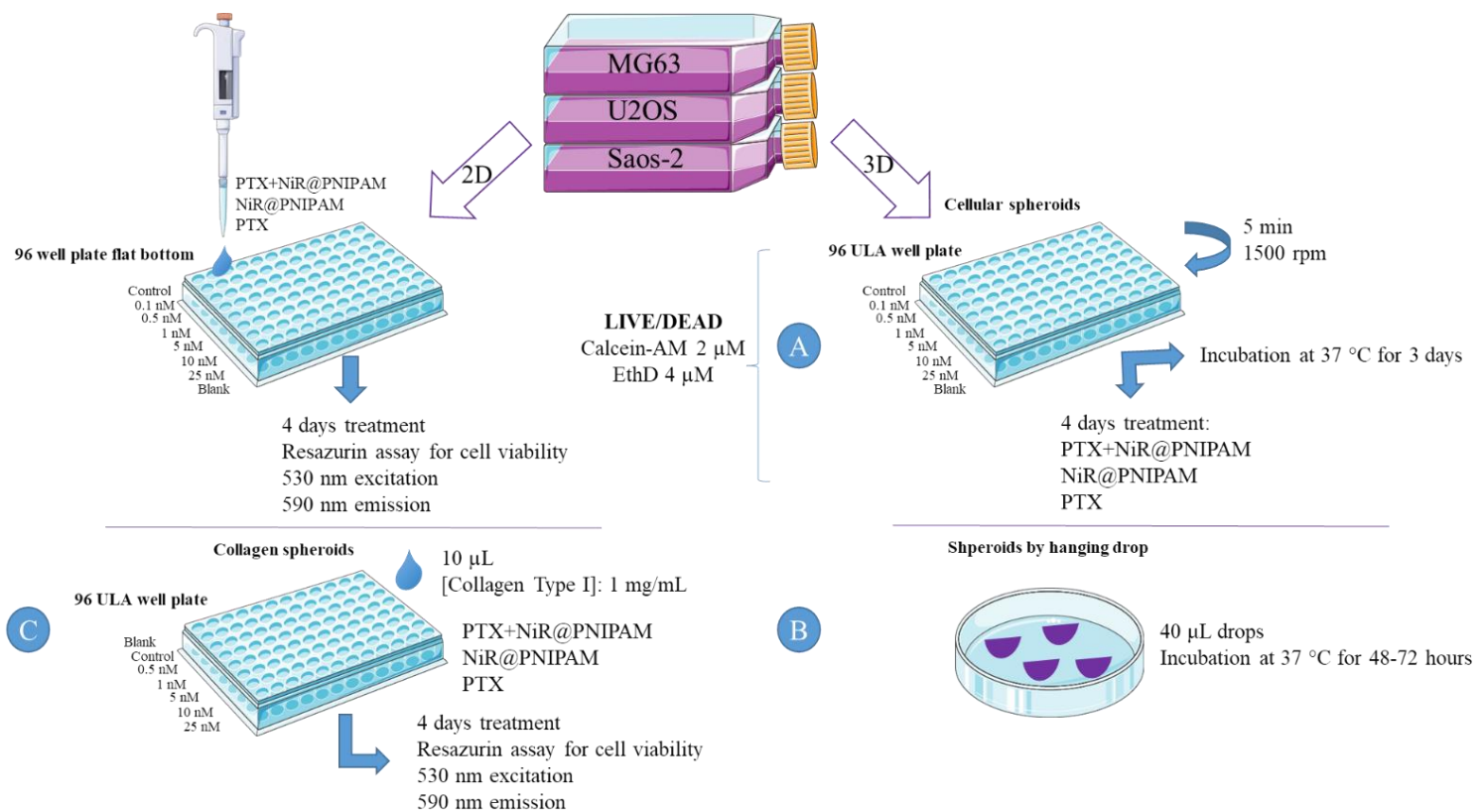


Figure 15. General overview of the materials and methods used in part I of strategy II.

1. 2D cell culture

1.1. Effects of PTX, PTX+NiR@PNIPAM and NiR@PNIPAM on cell viability

To establish the applicability of PTX in osteosarcoma treatment, its effects were evaluated in two different presentations: PTX drug dissolved in the culture medium (*free* or *nude* PTX), and PTX encapsulated in PNIPAM, a thermo-sensitive nanoparticle (PTX+NiR@PNIPAM). Together with the drug, the nanoparticles were loaded with Nile Red (NiR), as a fluorescent tag. NiR@PNIPAM nanoparticles was used as controls, and their effect was evaluated, along with that of drug-loaded nanoparticles, in all the performed experiments, to ascertain that any observed effects caused by PTX+NiR@PNIPAM were actually caused by the drug, and not by the nanoparticle itself, or the presence of impurities produced during its synthesis.

Cell viability was assessed by resazurin assay. MG63 and U2OS cells were seeded at a density of 10^4 cell/well in 100 μ L of the corresponding medium, in 96-well plates. Saos-2 cells were seeded at a density of 20×10^3 cell/well. To let cell attachment, the plates were incubated in standard culture conditions for 24 hours. After this time, the three osteosarcoma cell lines were treated with PTX, PTX+NiR@PNIPAM and NiR@PNIPAM (0-25 nM) for 4 days. Untreated cells were used as negative controls. Non-seeded wells with medium were used as blanks. Four wells were used for each condition. Because the nanoparticles had not been synthesized in sterile conditions, antibiotics were used in all the experiments while working with PTX+NiR@PNIPAM, NiR@PNIPAM and PTX, to avoid alterations in the results due to bacterial contamination. At days 2 and 4, cell proliferation was assessed with resazurin-based fluorescent dye. MG63 and U2OS were incubated for 3 hours in 20% 450 μ M resazurin solution, dissolved in culture medium. In the case of Saos-2 the incubation lasted for 4 hours. The fluorescence of the resazurin fluorescent dye was measured on a fluorometer plate reader at excitation = 530 nm and emission = 590 nm wavelengths.

1.2. Concentration determination of PTX and PTX+NiR@PNIPAM that is able to reduce cell viability to 50% at day 2

MG63, U2OS and Saos-2 were seeded in the same way explained above. After being incubated for 24 hours in standard culture conditions, cells were treated with different concentrations of PTX, PTX+NiR@PNIPAM and NiR@PNIPAM in ranging from 5 nM to 2000 nM for 2 days. Six wells were used for each condition. Cell viability was determined using resazurin assay.

2. 3D cell culture

2.1. Cellular spheroids in a 96 Ultra Low Attachment (ULA) conical well plate

MG63 was seeded at a density of 10^3 cell/well in 200 μ L of medium in a 96 ultra low attachment (ULA) conical well plate. The plates was centrifuged in a swinging bucket rotor at 290 g RCF and RT. Then, they were incubated for 72 hours in standard culture conditions to promote spheroid formation. After that, the spheroids were photographed using a stereomicroscope (M165, Leica).

The day of drug treatment, the plate was tilted, to avoid disrupting the spheroids, and 100 μ L of medium were removed from each well with a micropipette. Vacuum-aspiration was avoided, as microtissues can be easily lost due to aspiration force. 100 μ L of PTX, PTX+NiR@PNIPAM and NiR@PNIPAM treatment were added so that the final concentrations of PTX, PTX+NiR@PNIPAM and NiR@PNIPAM were 0.1, 0.5, 1, 5, 10 and 25 nM. Untreated spheroids and wells with medium were used as controls and blanks, respectively. The plates were incubated for 4 more days in standard culture conditions. At day 2, the treatment medium was replaced by a fresh one, following the caution and procedures explained before. Spheroids from each well were photographed in a stereomicroscope after 4 days of incubation. Spheroid volume was calculated according to (Virgone-Carlotta et al., 2017). For this, the acquired pictures were converted into binary images, where major (L_M) and minor (L_m) axes were measured with *ImageJ* free software. The mean diameter of each spheroid was calculated with the following formula:

$$D = \frac{L_M + L_m}{2}$$

Assuming the spherical shape of the microtissues, the volume was calculated as:

$$V = \frac{4}{3}\pi R^3$$

Finally, this data were used to calculate the proliferation index as a percentage of the controls. This corresponded to the volume of each spheroid after the treatment, divided by the volume of the control. This value was multiplied by 100 and graphically represented as a percentage.

2.1.1. LIVE/DEAD assay

The effects of the treatment with different concentrations of PTX, PTX+NiR@PNIPAM and NiR@PNIPAM on spheroid cell viability were evaluated with *LIVE/DEADTM Viability/Cytotoxicity* (for mammalian cells, ThermoFisher Scientific), a fluorescent assay based on two probes. Calcein acetoxymethyl (AM) is a nonfluorescent cell-membrane permeable dye. Within the cell AM is removed by the action of esterases, leading to calcein retention, which produces a strong green fluorescence. Ethidium homodimer-1 (EthD-1) is a membrane-impermeable dye that enters only when the cell membrane is damaged. Inside the cells, it binds

to DNA producing a bright red fluorescence. In this way Calcein AM is representative of live cells, while dead cells are marked with EthD-1.

LIVE/DEAD™ assay was done immediately after the stereomicroscope pictures of the spheroids were acquired. For this procedure aspiration was again avoided, to prevent spheroid disruption. 150 μL of medium was removed from each well with a pipette, leaving 50 μL of the treatment. The spheroids were washed two times with 150 μL of PBS to remove the esterase activity present in serum-supplemented medium, as it can lead to false overestimation of live cells. Then, 150 μL of PBS were removed from each well and 50 μL of PBS solution containing both Calcein AM (2 μM final concentration) and EthD-1 (4 μM final concentration) were added. The plate was incubated in standard culture conditions for 30 minutes. Later, 50 μL were removed and the spheroids were washed two times with the same amount of PBS. The fluorescently labeled spheroids were observed and imaged with a stereomicroscope. Finally, the images were processed in *ImageJ* free software.

2.2. Hanging drop

Hanging drop is an easy procedure which consists of lying small drops on a Petri dish lid that later will be inverted, to enable spheroid formation by cell aggregation at the bottom of the drop, due to gravitation force.

U2OS and Saos-2 were suspended to have a final cell density of 5,000, 10,000 and 20,000 cells in 40 μL drops, and 5 drops were placed in the lid of 60 mm tissue culture dishes (Ibidi), sufficiently apart from each other so as to not touch each other upon lid inversion. In parallel, 2 mL of a complete McCoy's 5A medium were added to the bottom of the dish to act as a hydration chamber (**Figure 16**). Carefully the lid was inverted onto the medium filled bottom chamber and the 60 mm tissue culture dishes were incubated in standard culture conditions for 48 hours to promote spheroid formation. Images of each drop were obtained using a stereomicroscope.

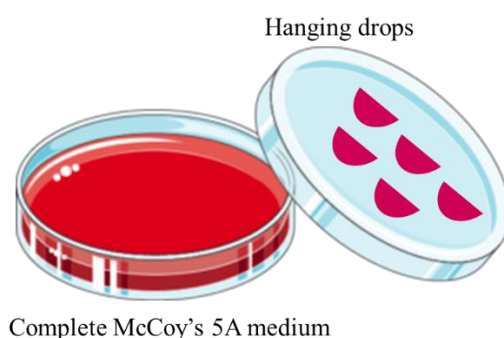


Figure 16. Schematic representation of hanging drops in a 60 mm tissue culture dish. The bottom of the dish is filled with a complete medium to act as hydration chamber. 40 μL drops are placed on the inverted lid, that later is put upside down to lock the dish.

2.3. Collagen spheroids

2.3.1. Collagen spheroids in a 96 ULA well plate

To generate spheroids containing both cells and extracellular matrix, osteosarcoma cell lines were suspended in a neutralized rat-tail collagen type I solution (1 mg/mL final concentration), at a cell density of 500/cells/ μ L, and spheroids were produced as 10 μ L-drops of this suspension. For this purpose, a commercial solution of rat-tail collagen type I (Corning), was diluted to 2 mg/mL with culture medium. As the commercial collagen solution is acidic, NaOH 1N was added to neutralize the diluted collagen. The volume of NaOH was calculated with the following formula, provided by the supplier:

$$1N \text{ NaOH volume} = 0.023 \times \text{Volume of original commercial solution used}$$

The 2 mg/mL neutralized collagen solution was mixed (1:1) with a 1,000 cells/mL suspension of osteosarcoma cells and 10 μ L-drops were seeded in ULA conical 96-well plates to generate the spheroids. All these procedures were performed while keeping the collagen tubes in ice, to prevent collagen gelation. After placing the 10 μ L drops in the plates, they were incubated between 1 and 2 hours in standard culture conditions to promote collagen gelation and spheroid formation. Then, 200 μ L of medium were added to each well to cover the spheroids, and plates were incubated for 24 hours in standard culture conditions.

The procedure followed to evaluate the effect of PTX and PNIPAM-encapsulated PTX on collagenic spheroids, was similar to that previously described for other spheroids. Briefly, medium covering the spheroids was removed and replaced by 200 μ L of 0.5, 1, 5, 10 and 25 nM PTX and PTX+NiR@PNIPAM. Untreated spheroids and wells with medium were used as controls and blanks, respectively. Six spheroids were used for each treatment condition. The plates were incubated for 4 days and at day 2 the treatment medium was replaced by a fresh one. The viability of osteosarcoma cells grown on collagen spheroids was assessed by resazurin assay. For this, the medium was carefully removed by aspiration and 100 μ L of resazurin working solution were added to each well. U2OS spheroids were incubated for 3 hours, while MG63 and Saos-2 spheroids were incubated for 4 hours. Finally, the fluorescence was read at excitation 530 nm and emission 590 nm wavelengths on a fluorescence plate reader.

2.3.2. Collagen spheroids on a Petri dish

Collagen spheroids prepared as described above were seeded as 4 drops of 10 μ L on the bottom of a small Petri dish (diameter = 30 mm). After gelation, the spheroids were covered with 1.5 mL of culture medium and incubated for 24 hours. The next day the medium was removed and replaced with a treatment medium composed of 0.5, 5, 10 and 25 nM of PTX or PTX+NiR@PNIPAM. Untreated collagen spheroids were used as controls. For each treatment condition one Petri dish was used and incubated for 4 days. At day 2 the treatment medium was

replaced for a fresh one. Spheroids were imaged after treatment with a stereomicroscope, and then subject to with live/dead assay as described below.

2.3.2.1. LIVE/DEAD assay

LIVE/DEAD™ assay was performed on the collagen spheroids immediately after stereomicroscope pictures were acquired. Spheroids were washed with 1.5 mL of PBS and covered with a PBS solution containing Calcein AM (2 μ M final concentration) and EthD-1 (4 μ M final concentration). The Petri dishes were incubated in standard culture conditions for 30 minutes. Then, the dye solution was removed and the spheroids were washed with 1.5 mL of PBS. The fluorescently-labeled spheroids were observed and photographed with a stereomicroscope. Images were processed in *ImageJ* free software.

2.3.3. Osteosarcoma cell migration from collagen spheroids

To observe cell migration of osteosarcoma cells from collagen spheroids, these were prepared as previously described, with a slight modification: 10 μ L drops were deposited on the wells of flat 96-well plates, and the plates were inverted to ensure that the cell suspension did not spread over the well surface but, instead formed a spheric structure (hanging drop method). After collagen gelation, spheroids were formed and the plates could be again inverted to recover its normal (lid-up) position. Spheroids were covered with 100 μ L of culture medium and the plates were incubated for 24 hours in standard culture conditions. Spheroids were then treated with 0.1, 0.5, 1, 5, 10 and 25 nM of PTX or PTX+NiR@PNIPAM during 4 days. Spheroids without any treatment were used as controls. At day 2 the treatment medium was replaced for a fresh one. Osteosarcoma cell migration from collagen spheroid was observed, and photographed with an inverted microscope. Cell migration was measured on the taken images with *ImageJ*.

3. Cell uptake of NiR@PNIPAM

To assess PNIPAM nanoparticle internalization by osteosarcoma cells, they were observed, by virtue of their red fluorescent tag (NiR), with a confocal microscope. Previously, cells were double-stained to label chromatin and actin microfilaments with Hoechst 33342 and Phalloidin-Atto 488, respectively. For this, MG63, U2OS and Saos-2 were seeded, in a total number of 100,000 cells, in 35 mm glass bottom dishes and let attach and expand for 24 hours. Then, cells were exposed to 100 nM NiR@PNIPAM for 12-15 hours (MG63 and Saos-2) or 24 hours (U2OS). Osteosarcoma cells not exposed to the nanoparticle were used as controls. After incubation, nanoparticle-containing medium was removed, cells were rinsed with 1 mL of PBS and fixed with 1 mL of 3.7% formaldehyde. Then, they were washed again with PBS and double-stained with Hoechst 33342 (cyan fluorescence) and Phalloidin-Atto 488 (green fluorescence), as follows: cells were covered in a PBS solution containing Hoechst 33342 (5 μ g/mL final

concentration) and Phalloidin-Atto 488 (0.5 $\mu\text{g}/\text{mL}$ final concentration). The 35 mm glass bottom dishes were incubated protected from light at RT for 20 minutes. Finally, the dye solution was removed and cells were washed twice with PBS.

Strategy II: Paclitaxel, MSC and combination treatment

Part II Mesenchymal stem cells

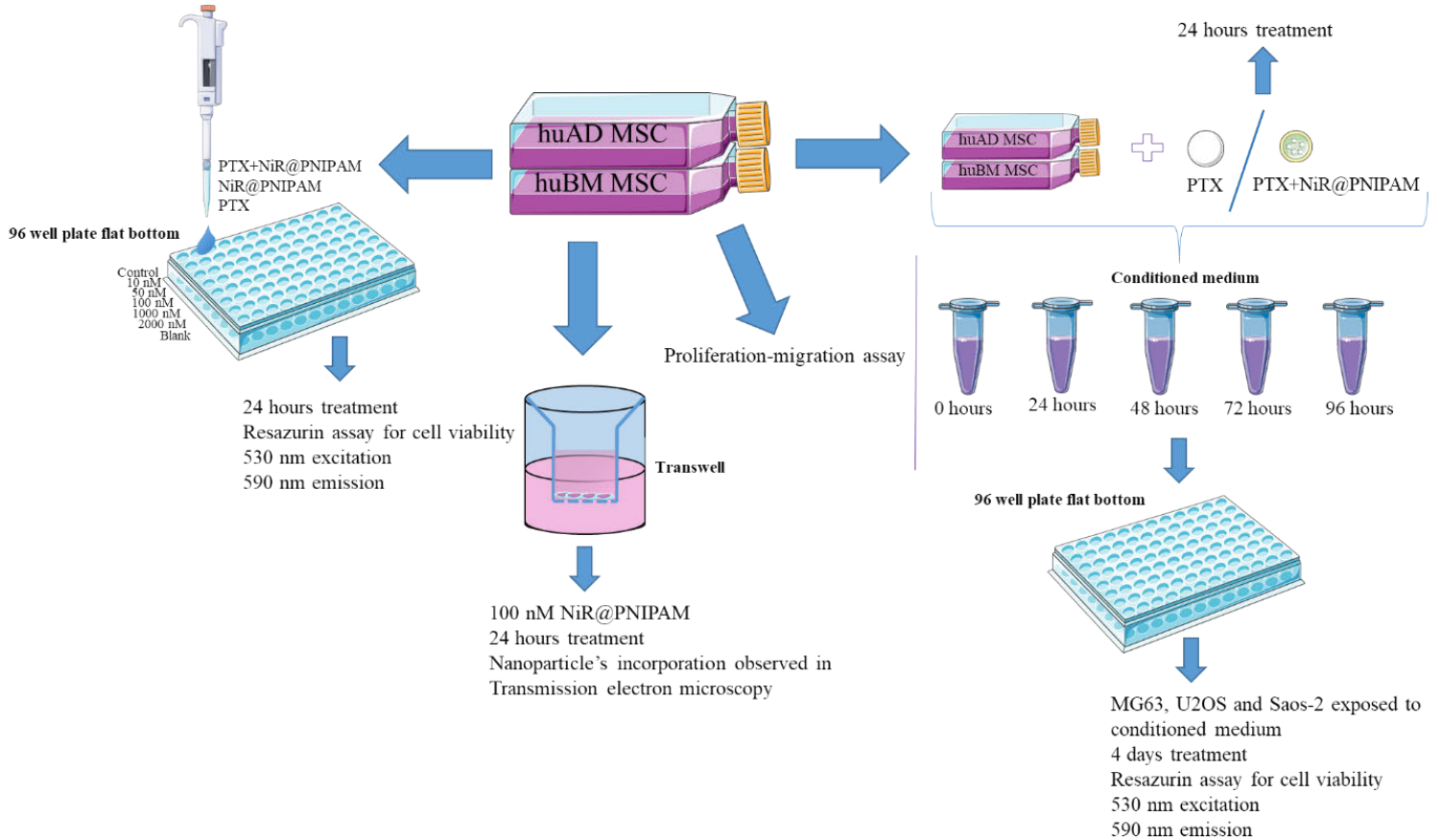


Figure 17. General overview of the materials and methods used in part II of strategy II.

1. Effects of PTX, PTX+NiR@PNIPAM and NiR@PNIPAM on cell viability

The effects of PTX, PTX+NiR@PNIPAM and NiR@PNIPAM on cell viability was assessed by resazurin assay. huAD-MSC and huBM-MSC were seeded in 96-well plates at a density of 5×10^3 cell/well, in 100 μ L of DMEM-hg, and incubated in standard culture conditions for 24 hours. After this time, cells were treated with different concentrations of PTX, PTX+NiR@PNIPAM and NiR@PNIPAM (10, 50, 100, 1,000 and 2000 nM) for 24 hours. Untreated cells and wells with medium were used as controls and blanks, respectively. Four wells were used for each condition. To assess viability, huAD-MSC and huBM-MSC were incubated for 3 hours in 90 μ M resazurin dissolved in culture medium. The fluorescence of the resazurin fluorescent dye was measured on a fluorometer plate reader at excitation 530 nm and emission 590 nm wavelength.

2. Cell uptake

2.1. Transmission electron microscopy of NiR@PNIPAM

To confirm huAD-MSC ability to internalize PNIPAM nanoparticles, 50,000 cells, in 200 μ L culture medium, were seeded on transwell filters (pore size=0.4 μ m) and placed in a 24-well plate (**Figure 18**). To let cell attachment and expansion, the plates were incubated in standard culture conditions for 48 hours. Then huAD-MSC were exposed to 100 nM of NiR@PNIPAM for 24 hours. Finally, nanoparticle incorporation was observed by TEM at BIONAND Electron Microscopy Service.

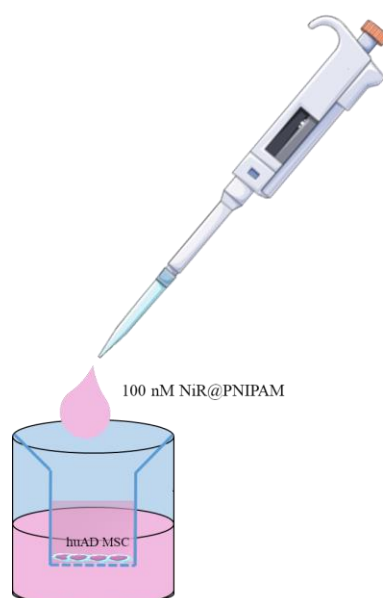


Figure 18. Schematic representation of huAD-MSC seeded in a transwell of a 24-well plate.

2.2. Confocal scanning laser microscopy of NiR@PNIPAM and PTX+NiR@PNIPAM within huAD-MSC

Nanoparticles internalized by huAD MSC were also observed by confocal microscopy, thanks to their red fluorescent tag (NiR). huAD-MSC were seeded in a total number of 100,000 cells in a 35 mm glass bottom dish and incubated in standard culture conditions for 24 hours. Then, cells were treated separately with 100 nM of NiR@PNIPAM and PTX+NiR@PNIPAM for 24 hours. huAD-MSC without any treatment was used as a control. After incubation, treatment medium was removed, cells were rinsed with 1 mL of PBS and fixed with 1 mL of 3.7% formaldehyde. Cell nuclei were stained with Hoechst 33342 (cyan fluorescence), and actin microfilaments with Phalloidin-Atto 488 (green fluorescence) as previously described for osteosarcoma cells (Part I, Section 3).

3. Proliferation-migration assay

Migration capacity of MSC carrying PTX-loaded nanoparticles was assayed by wound-healing assay, performed with two methods: scratch assay and 2-well insert assay. Procedures for both methods are described below.

3.1. Scratch assay

This assay is based on the creation of a gap on a confluent cell monolayer that will be closed by cells movement until new contacts between cells are formed (**Figure 19**). Images are acquired at different time points, and later analyzed. huBM-MSC were seeded in a 24-well plates at a rate of 50,000 cells/well, in 0,5 mL medium. To reach a monolayer confluence between 70 and 80%, the plate was incubated in standard culture conditions overnight. The next day huBM-MSC were exposed to 100 nM of PTX, PTX+NiR@PNIPAM and NiR@PNIPAM for 24 hours. Non-exposed cells were used as controls. Each condition was done in six wells. Afterwards, nanoparticle-containing media were removed and replaced with fresh DMEM-hg medium. The cell monolayer was scratched across the centre of the well with a 200- μ L pipette tip. To have a straight gap with similar width between wells the tip had to be perpendicular to the bottom of the well during the scratching. The medium was aspirated to remove both non-attached cells and cell debris. Then huBM-MSC were washed with PBS, and DMEM-hg was added to the well. On days 0 (immediately after scratching), 2 and 7 post-scratch, images of the cultures were taken in an inverted microscope. To make sure the same field was imaged in all acquisitions, marks had been made near the gap on the bottom of the wells, to serve as a reference point.

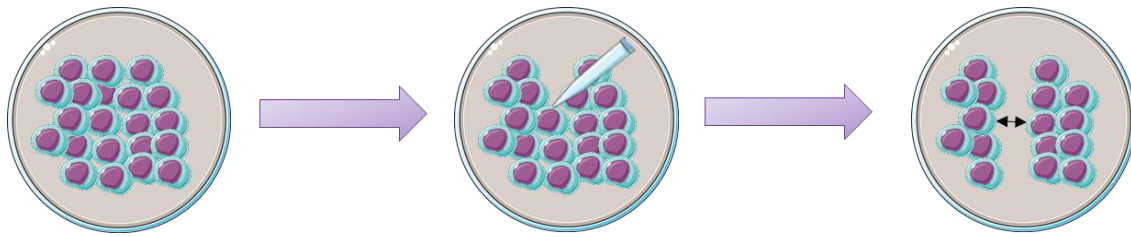


Figure 19. Schematic representation of scratch procedure in a well of a 24-well plate.

3.2. 2-well insert assay

2 well silicone inserts (Ibidi) are an alternative method to the scratch assay that guarantee a reproducible 500 μm cell free gap, thus avoiding the variability introduced by hand-made scratches. Silicone inserts contain two wells of the same area, separated by a 500 μm gap. They are adhered to the bottom of the plate, and cells are seeded on is wells and let grow to confluence. Then, the insert is removed, leaving two patches of confluent cells, separated by a 500 μm gap. To proceed with the 2-well insert assay, inserts were deposited with the help of sterile tweezers on the bottom of 24-well plates. Then, 70 μL of a 30,000 cell/mL MSC suspension were seeded in each well of the insert, and incubated in standard culture conditions until complete confluence. Afterwards, confluent MSC cultures were exposed to with 100 nM of PTX, PTX+NiR@PNIPAM and NiR@PNIPAM for 24 hours. Unexposed cells were used as controls. 2 wells of 24-well plate were used for each treatment condition. After removing the nanoparticle-containing medium, the cultures were washed with PBS and the gap was created by removing the inserts carefully with (Figure 20). MSC were washed again with PBS and covered with DMEM-hg. Pictures were taken at days 0, 2 and 7 post-gap formation.

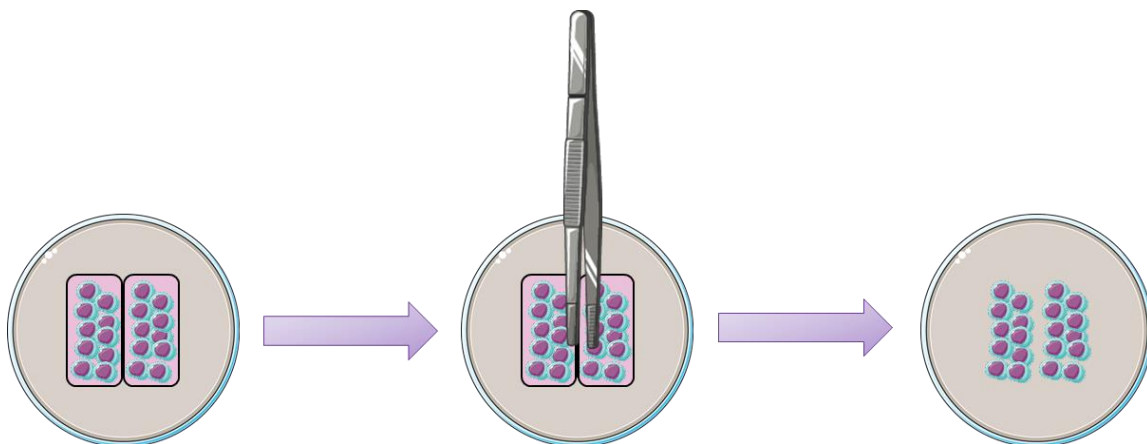


Figure 20. Schematic representation of 2 well culture-insert and its removal in a well of 24-well plate.

4. Conditioned medium

Conditioned medium (CM) by drug-carrying MSC was collected to verify the release of PTX, PTX+NiR@PNIPAM or its metabolites by mesenchymal stem cells, and also to evaluate if

any effect observed in osteosarcoma cells after interaction with drug-carrying MSC was due to the drug and not to factors released from the cell vehicle.

huAD and huBM-MSC were seeded at a density of 5,000 cells/cm² in T25 flasks and incubated in standard culture conditions overnight. The next day cells were treated with 100 nM of PTX+NiR@PNIPAM or 100 nM PTX for 24 hours. Controls consisted of untreated cells in DMEM-hg medium, while blank was an empty culture flask filled with DMEM-hg. After 24 hours, the CM with the treatment (time 0) was removed and stored at 4 °C. The medium was replaced with a fresh one without treatment. This procedure was repeated at 24, 48, 72 and 96 hours.

To test the cytotoxicity of the collected CMs, MG63 and U2OS were seeded at a density of 10⁴ cells/well in 100 µL of the corresponding medium, in 96-well plates. In case of Saos-2 seeding density of 20×10³ cells/mL. The plates were incubated in standard culture conditions for 24 hours, prior to addition of 100 µL/well of CM from each time point, and incubation for 4 days. At day 2 the CM medium was replaced for a new one. The viability of osteosarcoma cell lines was assessed by resazurin assay as previously described.

5. Time-lapse

Time-lapse is a real-time imaging tool that enable to monitor cellular processes, migration and interaction of living cells over a period of time. It was selected to demonstrate the ability of MSC to function as a proper cell vehicle where it would incorporate and release NiR@PNIPAM leading to observable osteosarcoma cells death *in vitro*. On day 1 huAD-MSC were seeded at a density of 100,000 cells in a 35 mm glass bottom dish and incubated in standard culture conditions for 24 hours. The next day, these cells were treated with 100 nM of NiR@PNIPAM for 24 hours. In parallel, 100,000 cells of Saos-2 were seeded in two 35 mm glass bottom dishes. One of the plates was used as a control, where the cancer cells received a complete DMEM-hg medium. On day 3, the treatment medium was removed, huAD-MSC were rinsed with 1 mL of PBS 1X, collected by trypsinization and seeded over osteosarcoma cells. To differentiate the two types of cells, huAD-MSC were stained with 2.5 mg/mL of Hoechst 33342 (cyan colour) before being detached and Saos-2 with 5 µM of CellTracker Green (green colour) 3 hours after the seeding. The nanoparticles were identified by NiR (red colour) tag. Finally, the time-lapse was done for 24 hours, where the images were captured every 20 minutes from 10 different positions inside the dish.

Strategy II: Paclitaxel, MSC and combination treatment

Part III

Paclitaxel/Paclitaxel+NiR@PNIPAM and oridonin combination

1. Effects of PTX+NiR@PNIPAM/PTX and ORI combination

The viability of a combined drug therapy was evaluated by resazurin assay. MG63, U2OS and Saos-2 were treated with different combinations of PTX or PTX+NiR@PNIPAM (CD_{50} , $CD_{50}/2$ and $CD_{50}/10$), and ORI (CD_{50} , $CD_{50}/2$ and $CD_{50}/10$).

The interaction between both drugs was quantified through the Chou-Talalay method, by calculating CI with *CompuSyn* software (Chou, 2010).

IV. Results and discussion

Strategy I: Doxorubicin and oridonin combination

“All substances are poisons; there is none that is not a poison. The right dose differentiates a poison from a remedy”.

Paracelsus

The history of osteosarcoma treatment has been full of complications. The implementation of chemotherapy to the surgery in 1970s substantially improved cancer therapy. Particularly, multidrug chemotherapy, as it is a multiagent approach, whose components have different target sites that make it difficult for cancer cells to mutate and adapt to novel conditions. Currently, the 5-year survival rate of patients treated with both surgery and chemotherapy is 65%. However, when osteosarcoma metastasizes to the lungs, this survival rate drops to 20%. A rate that has remained unchanged for the last 30 years (Chen, Yang, Wang, Zhang, & Lin, 2015; Kansara, Teng, Smyth, & Thomas, 2014; Wang, Yu, Xu, & Xu, 2015). Lack of validated and reliable biomarkers for diagnosis and prognosis are one of the determinants why there is no improvement in osteosarcoma patients' survival (Raimondi et al., 2017). Also, different mechanisms are responsible of the poor outcome, such as development of multidrug, autophagy-related resistance, cancer stem cell (CSC)-mediated drug resistance and deregulation of transduction pathways (Adamopoulos, Gargalionis, Basdra, & Papavassiliou, 2016; Cavalcanti et al., 2017; Gou et al., 2015; Yang et al., 2012).

In spite of the advances in chemotherapy and its relative success in the case of localized disease, osteosarcoma chemotherapy has not substantially changed for decades, being the MAP triad (high-dose methotrexate, doxorubicin and cisplatin) the standard treatment for children and young adults (Anderson, 2016; González-Fernández et al., 2017). The numerous unwanted side effects associated to chemotherapy represent the most important drawback of this multi-drug approach. Many side-effects are short-termed, and improve with time once chemotherapy administration stops. Among these are mucositis, alopecia, nausea and vomiting. But others can be permanent and life-threatening. Among these the most remarkable is doxorubicin-associated cardiotoxicity, which depends on its cumulative dosing, and can lead to irreversible heart failure (González-Fernández et al., 2017; Haghirsadat et al., 2017; Janeway & Grier, 2010; Thorn et al., 2011; Yang et al., 2012). Five years after being diagnosed with cancer, there is a high prevalence of cardiac conditions in survivors of childhood tumors, as compared to healthy siblings. It has been found that cancer survivors are 15 times more likely to have a heart failure, and 10 times more likely to have a coronary artery disease, as compared to the controls (Lipshultz, Patel, Franco, & Fisher, 2017). Myopathy is one of the leading causes of death in survivors of a pediatric cancer, after cancer recurrence and secondary tumors. Cardiac events are normally prevented by administering doxorubicin (DOX) in combination with a cardioprotective agent, usually dexrazoxane, whose chelating properties avoid the formation of intracellular iron-mediated free radicals (Lipshultz et al., 2014). Wexler *et al.*, in a long-term study, demonstrated that among 38 sarcoma patients who received dexrazoxane, only 22% presented a heart failure, compared to 67% of those that were administered with DOX alone (Wexler et al., 1996).

Coadministration with a cardioprotective agent proved to be safe without affecting the efficiency of cancer treatment with DOX (Lipshultz et al., 2014).

In this work, another approach was evaluated. Our goal was to reduce the needed dose of doxorubicin, and hence its undesired side-effects, by increasing its effectiveness. For this, a new combination treatment was evaluated, consisting on the coadministration of doxorubicin with a novel drug, oridonin.

Oridonin (ORI) is a natural product with proven cytostatic properties when given alone or in combination with another chemotherapeutic drugs. For example, ORI was able to overcome gemcitabine resistance in pancreatic cells (Wang et al., 2019). Synergy was observed when administered in combination with imatinib and cisplatin to treat leukemia and acute myeloid leukemia, respectively (Li, Lu, Xie, Wang, & Wang, 2018; Zhang et al., 2015). In a recent study of Li *et al.*, a synergistic effects against breast cancer was found when ORI and DOX were given together (Li et al., 2019). This suggest that the combination of both drugs could help to decrease the therapeutic doses of DOX, thus reducing its relevant side effects, like cardiotoxicity. To date, there are no studies of DOX and ORI combination in osteosarcoma. For this reason, the present strategy is aimed at studying the potential of simultaneous administration of DOX and ORI in osteosarcoma treatment.

Results

To test the efficiency of the combination treatment consisting from the administration of both DOX and ORI two different osteosarcoma cell lines, U2OS and Saos-2, were selected. The primordial difference between these lines consisted in their p53 status, a transcriptional factor involved in DNA repair. From the two cell lines Saos-2 carry a null mutation in p53 gene, while U2OS has a wild type presentation of the gene. In this way, it was though the response would mainly depend on the functionality of p53, as commonly mutations in this protein facilitate the proliferation of cancer cells (Hientz, Mohr, Bhakta-Guha, & Efferth, 2017; Hu et al., 2010).

1. Cell culture treatment

Osteosarcoma cell lines, Saos-2 and U2OS, were exposed to 7 different concentrations of DOX and ORI, in order to select the concentration that achieves 50% of cell death (CD₅₀) for each drug after 48 h of treatment. Cell viability was assessed with resazurin assay. For both drugs, a concentration-dependent decrease in cell viability was observed (**Figure 21**).

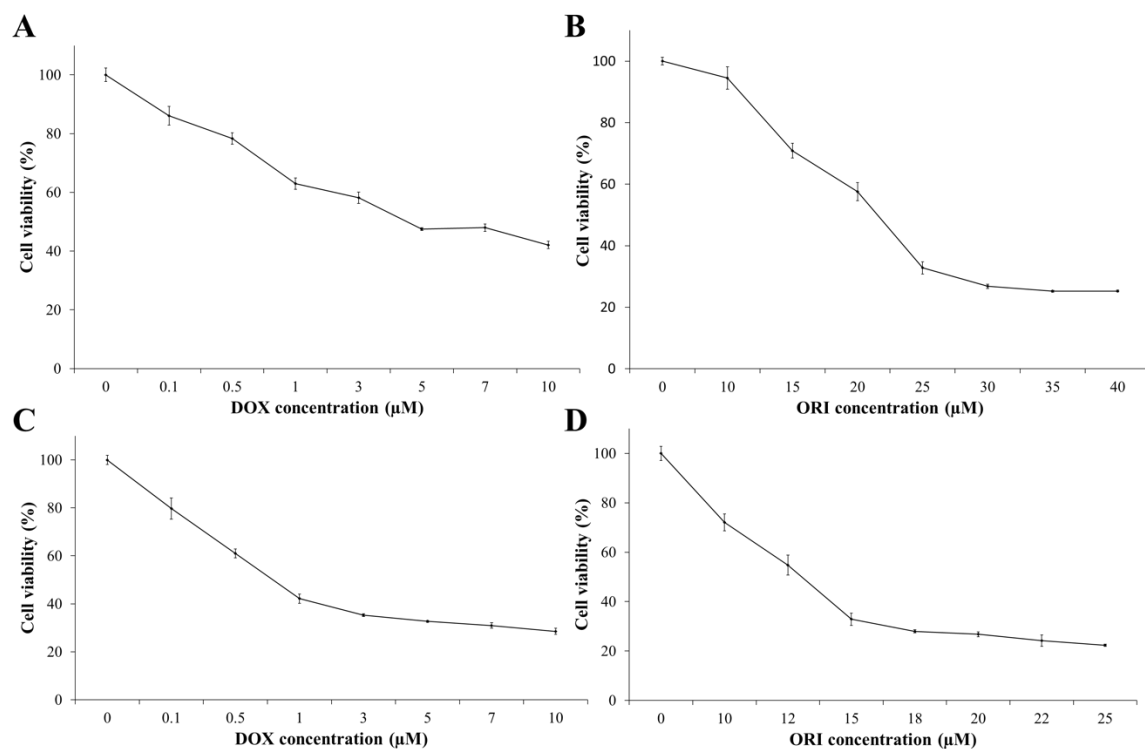


Figure 21. Toxicity evaluation of DOX and ORI. Saos-2 (A and B) and U2OS (C and D) viability was assessed after 48 h of exposure to different concentrations of DOX (A and C) and ORI (B and D) by resazurin assay. N=6 and data are represented as mean±SD.

Although both cell lines were sensitive to DOX and ORI, Saos-2 showed less sensitivity, as higher drug concentrations were needed to produce 50% of cell death. From these data, Saos-2

CD₅₀ was determined as 5 μ M for DOX and 20 μ M for ORI (**Figure 21A and B**), while U2OS CD₅₀ was determined as 1 μ M for DOX and 12 μ M for ORI (**Figure 21C and D**).

2. Combination treatment

Based on the cytotoxicity induced by the drugs alone, a combined effect of DOX plus ORI on osteosarcoma viability was evaluated. For this, different DOX doses (CD₅₀, CD₅₀/2 and CD₅₀/10) were given together with three different ORI concentrations (CD₅₀, CD₅₀/2 and CD₅₀/10). In total, osteosarcoma cell lines were exposed to 9 different drug combinations. In both cell lines the simultaneous treatment with DOX and ORI produced a higher cytotoxicity than the drugs alone (**Figure 22**), thus confirming ORI as a potential candidate for a combination therapy with DOX. The addition of ORI at its CD₅₀ to only a tenth of DOX CD₅₀ resulted in a lower Saos-2 viability than treatment with DOX CD₅₀. In different words, the addition of oridonin allowed reducing doxorubicin dose by ten-fold. More interesting, combining ORI and DOX at half their CD₅₀ (2,5 μ M DOX + 10 μ M ORI) yielded a similar effect. This dosing reduces doxorubicin dose to a half, but uses a dose of oridonin that causes very low cytotoxicity to Saos-2 (**Figure 22A and B**).

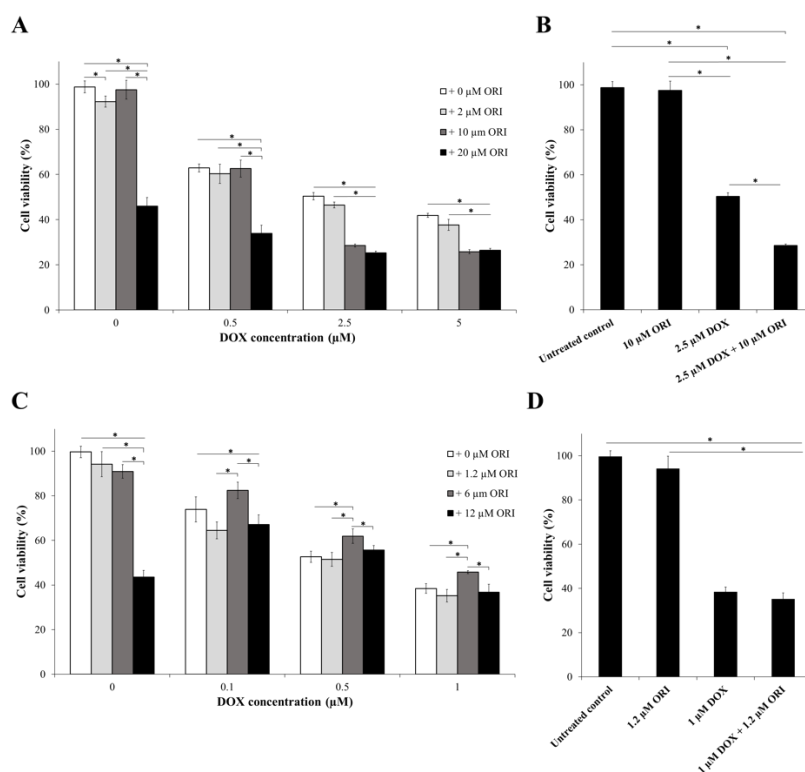


Figure 22. Toxicity evaluation of DOX and ORI combination. Saos-2 (A and B) and U2OS (C and D) cells were exposed for 48 h to concentrations of DOX (A and C) and ORI (B and D) corresponding to their CD₅₀, CD₅₀/2 and CD₅₀/10; as well as to combinations of both drugs. Cell viability was assessed by resazurin assay. Asterisk shows statistical significance (p < 0.05) according to a two-way ANOVA test followed by Tukey's multiple comparisons test. N=6 and data are represented as mean \pm SD.

In the case of U2OS, the combination of DOX and ORI caused only tiny effects in cytotoxicity as compared with DOX alone (**Figure 22C and D**). Only two DOX+ORI combinations showed a cytotoxic effect greater than that caused by DOX CD_{50} : one of them combined the CD_{50} dose of DOX (1 μM) and the CD_{50} dose of ORI (12 μM), and the other combined the CD_{50} dose of DOX with one tenth of ORI CD_{50} (1.2 μM).

The synergistic effect of DOX and ORI in Saos-2 was confirmed by calculating their combination index (CI) according to the Chou-Talalay method, which provides a quantitative definition of synergism, additive and antagonism (Chou, 2010). As shown in **Figure 23A**, a synergistic effect was observed for the simultaneous administration of DOX and ORI in Saos-2 cells.

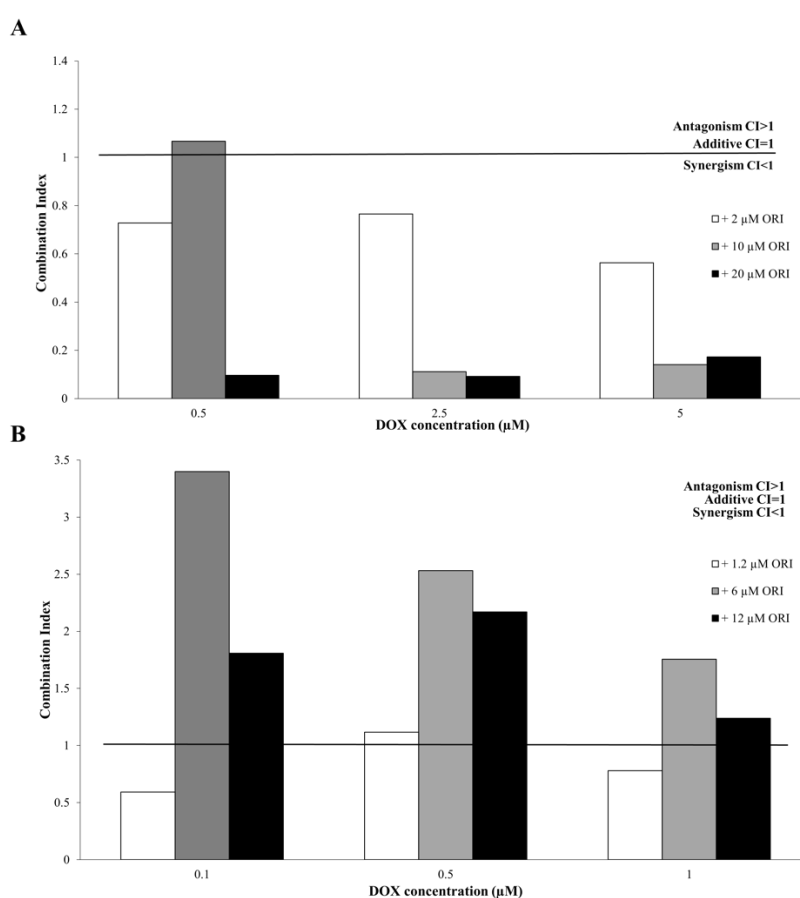


Figure 23. Combination index. Saos-2 (A) and U2OS (B) were treated with different combinations of DOX and ORI. The black line corresponds to CI of 1, representing an additive effect. Antagonism and synergism were considered when the values were over and under the line (CI=1), respectively.

In case of U2OS, a synergistic effect was observed only in two combinations (**Figure 23B**). One of this, 0.1 μM DOX and 1.2 μM ORI, does not represent an improved effect over doxorubicin CD_{50} on U2OS cells. Therefore, we focused on the combination of 1 μM DOX and 1.2 μM ORI for the following experiments.

Given that the goal was to reduce the dose of doxorubicin in chemotherapeutic treatments, combination therapy with oridonin was considered as promising in the case of U2OS cells, as it had been for Saos-2 cells. This striking difference in the behaviour of Saos-2 and U2OS cell lines, representative of two different osteosarcoma types, supports the application of personalized medicine principles to bone cancer treatment, and led us to further research on the mechanisms of action of the combined drugs. For this purpose, we chose, DOX and ORI dose combinations that had shown to enhance DOX CD_{50} cytotoxicity for each cell line. These were 2,5 μM DOX + 10 μM ORI for Saos-2 cells, and 1 μM DOX + 1.2 μM ORI for U2OS cells.

3. Effects of combination treatment on osteosarcoma cells morphology

Saos-2 were treated with 2.5 μM DOX, 10 μM ORI and the combination of both for 16 h, when a considerable cell death was detected for simultaneous administration of DOX and ORI. The produced effects on Saos-2 viability were observed and photographed. Untreated cells, used as control, were attached to the plate and displayed a polygonal-spindle morphology (**Figure 24A**). Dead cells were detached and looked round-shaped. Cultures treated with 10 μM ORI resembled control morphology, showing healthy and spindle-like shaped cells. However, some cells presented a round form and were detached. Saos-2 treated with 2.5 μM DOX showed less healthy cells than ORI-treated cultures, and cells exposed to DOX+ORI presented the highest mortality, with only a few cells still attached to the plate. These morphological data agree with viability data as measured with resazurin assay, obtained in the former experiment (**Figure 21A and B**).

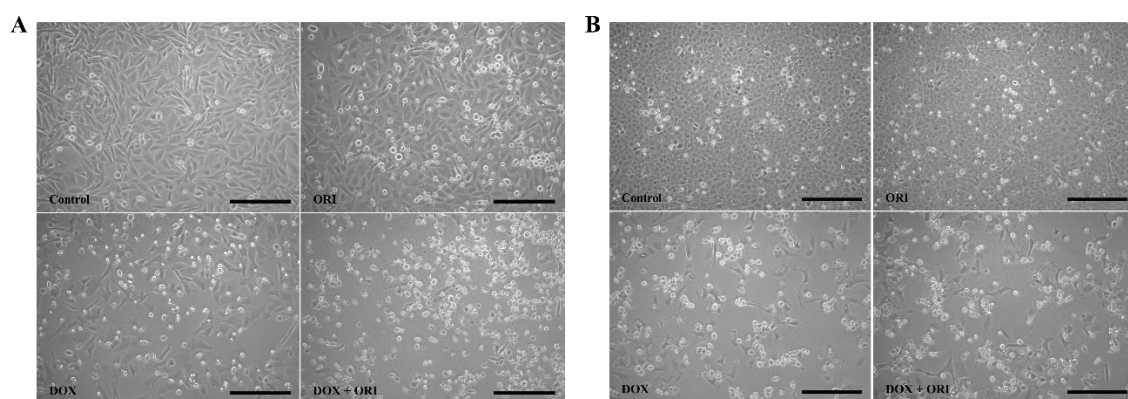


Figure 24. Effects of ORI, DOX and combination of both on osteosarcoma cells. Morphology of Saos-2 cultures after 16 h of treatment with 2.5 μM DOX, 10 μM ORI, and the combination of both (A). Morphology of U2OS cultures after 48 h of treatment with 1 μM DOX, 1.2 μM ORI, and the combination of both (B). Scale bar = 50 μm .

The effect of 1 μM DOX, 1.2 μM ORI and 1 μM DOX+1.2 μM ORI treatment on U2OS morphology was observed after being exposed for 48 h. Control cultures and cultures treated with 1.2 μM ORI presented similar polygonal morphology. The majority of cells were attached to the

plate and very few dead cells were present (**Figure 24B**). U2OS exposure to 1 μM DOX or the combination DOX + ORI showed considerably less healthy cells. These presented an elongated morphology, and were distanced from each other, due to the high mortality, that had erased many of the cells in the plate.

4. Cell uptake of DOX

In order to elucidate how oridonin increases doxorubicin cytotoxicity, DOX cell uptake was studied using flow cytometry, taking advantage of doxorubicin emission of red fluorescence (Duray, Cuono, & Madri, 1986). It was decided to evaluate the internalization of the chemotherapeutic agent at 2 h, based on literature review, where it was described that, after 1 h of exposure, it was possible to determine DOX fluorescence intensity within HeLa cells using flow cytometry (dos Reis et al., 2021). As expected, in the present work, the red self-fluorescence of DOX could be detected in DOX-treated cells, but no red fluorescence was detected in ORI-treated cells (**Figure 25**).

After 2 h of exposure to DOX+ORI (2.5 μM and 10 μM , respectively), Saos-2 cells presented a higher intracellular red fluorescence, as compared to cells treated with DOX alone, indicating that ORI is somehow increased the intracellular accumulation of DOX. This may be the reason for the enhanced toxicity induced by the drug combination.

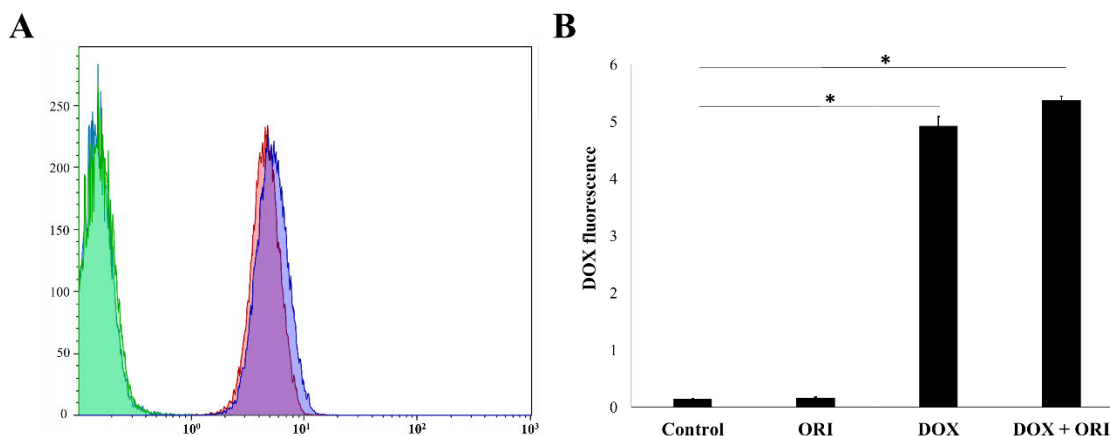


Figure 25. Cellular uptake of DOX in Saos-2. Fluorescence signals of control and drugs were detected by flow cytometry after 2 h of treatment (A). Quantification of DOX red fluorescence in control and drug-treated cells (B). One asterisk shows statistical significance ($p < 0.05$) between DOX+ORI/DOX and the rest of the treatment groups according to a two-way ANOVA test followed by a Tukey's multiple comparison test. $N=6$ and data are represented as mean \pm SD.

A completely different behaviour of DOX incorporation was observed in U2OS. No differences in red fluorescence intensity were detected, after 2 h of exposure, between U2OS cells treated with 1 μM DOX and cells treated with the combination 1 μM DOX + 1.2 μM ORI (**Figure 26A and B**). To have more clues that would unveil the slow uptake of DOX in presence of ORI,

this experiment was repeated, and U2OS cells were exposed to the drugs for 4 h. The results were the same. Actually, red fluorescence was now slightly higher in DOX-treated cells than in DOX+ORI-treated cells (**Figure 26C and D**). Therefore, unlike in Saos-2 cells, in U2OS ORI does not increase the intracellular accumulation of DOX. This difference between the two cell lines may account for the different cytotoxic effect of DOX+ORI combination therapy in each of them.

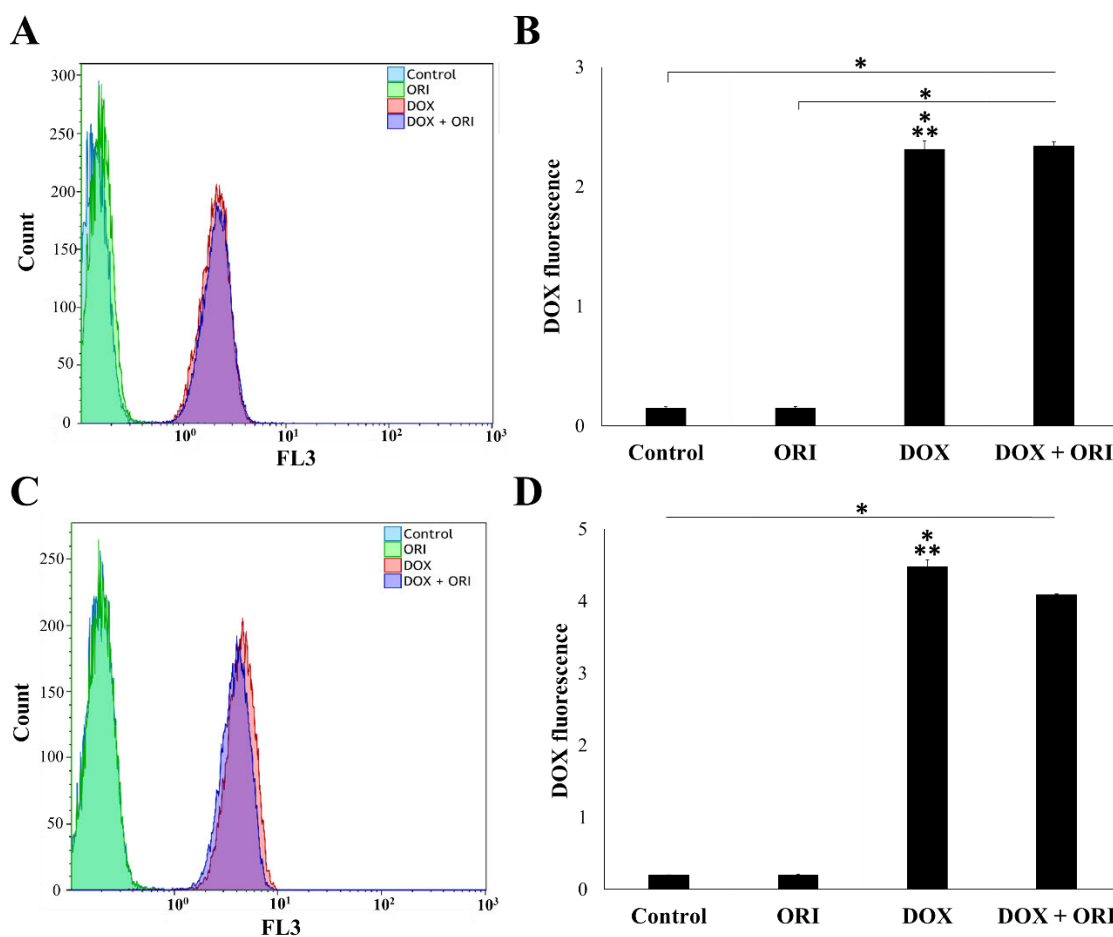


Figure 26. Cellular uptake of DOX in U2OS. Fluorescence signals of control and drugs were detected by flow cytometry after 2 h (A) and 4 h (C) of treatment. Quantification of DOX red fluorescence in control and drug-treated cells after 2 h (B) and 4 h (D) of exposure. One asterisk shows statistical significance ($p < 0.05$) between DOX+ORI and the rest of the treatment groups; in case of DOX one asterisk denotes significance with ORI, while two with the control according to a two-way ANOVA test followed by a Tukey's multiple comparison test. $N=6$ and data are represented as mean \pm SD.

5. Mitochondrial membrane potential

To understand the cytotoxic effects caused by DOX+ORI combined therapy in osteosarcoma cell lines, mitochondrial membrane potential was evaluated by measuring the fluorescence of JC-1 dye incorporated by the cells. The decrease in mitochondrial membrane potential is an indicator of early apoptotic events.

No significant changes in the mitochondrial membrane potential were observed in Saos-2 cells after 16 h of treatment with 2.5 μM DOX or with 10 μM ORI, as compared to controls (**Figure 27A and B**). However, the quantitative data showed a significant difference in cultures exposed to DOX+ORI, characterized by a marked shift from red to green fluorescence. This switch is an indicative feature of early events of cell death. Synergic drug combination treatment drastically affected cell viability in such way that, for measuring JC-1 fluorescence by flow cytometry, between 5,000 and 7,000 events were considered, as it was hard to reach 10,000 events in the DOX+ORI group.

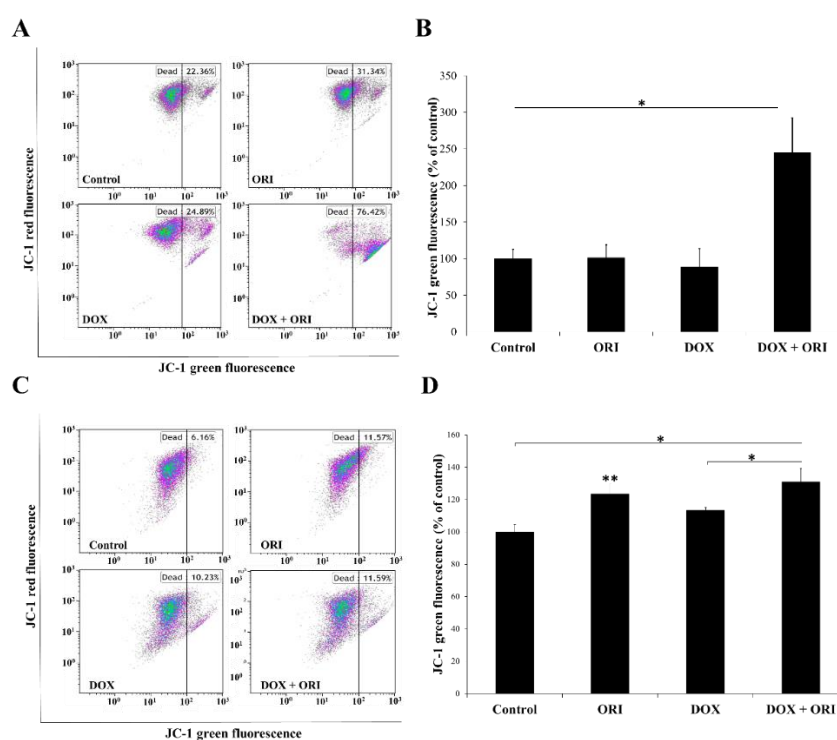


Figure 27. Effects of ORI, DOX and combination of both on osteosarcoma cells mitochondrial membrane potential. JC-1 red and green fluorescent signals in Saos-2 (A and B) and U2OS (C and D), as measured by flow cytometry. Red fluorescence is emitted by JC-1 aggregates, indicative of healthy mitochondria, while green is emitted by JC-1 monomers, indicative of altered mitochondria function (A and C). Quantification of JC-1 green fluorescence (B and D). The data of each treatment group was compared to the control, whose JC-1 green fluorescence was considered as 100%. Asterisk shows statistical significance ($p < 0.05$) between DOX+ORI and the rest of the treatment groups, while two denotes significance with the control according to a two-way ANOVA test followed by Tukey's multiple comparisons test. Data are represented as mean \pm SD.

In the case of U2OS cells, after 48 h exposure to 1 μM DOX the mitochondrial membrane potential was reduced, as JC-1 partially switched from red to green fluorescence, as compared to the controls (**Figure 27C and D**). Exposure to 1.2 μM ORI also produced an increase in green fluorescence higher than that observed in DOX-treated cells. The combined treatment with 1 μM

DOX + 1.2 μ M ORI caused a reduction of mitochondria membrane potential similar to that caused by ORI.

Of the two cell lines analysed, combination treatment was more drastic in Saos-2, as in a shorter time it produced a considerable induction of early apoptotic events. In U2OS, after a much longer exposure, DOX+ORI combined treatment yielded a similar outcome to that produced by one of the drugs.

6. Apoptosis induction

Changes in mitochondrial membrane potential, a hallmark of apoptosis initiation, were observed in the cell line sensitive to the combination treatment of DOX+ORI. Therefore, late cell death events were studied to further characterize the cellular mechanism underlying combination therapy cytotoxicity. For this purpose, treated cells were double-stained with Annexin V-FITC and Hoechst 33258.

In Saos-2 cultures, a higher percentage of apoptotic cells, or a higher apoptotic index, was observed in all drug-treated cultures, as compared with non-treated controls. Cells subject to the combination therapy presented a remarkably higher apoptotic index, being more than twice the one observed for DOX (**Figure 28A and B**).

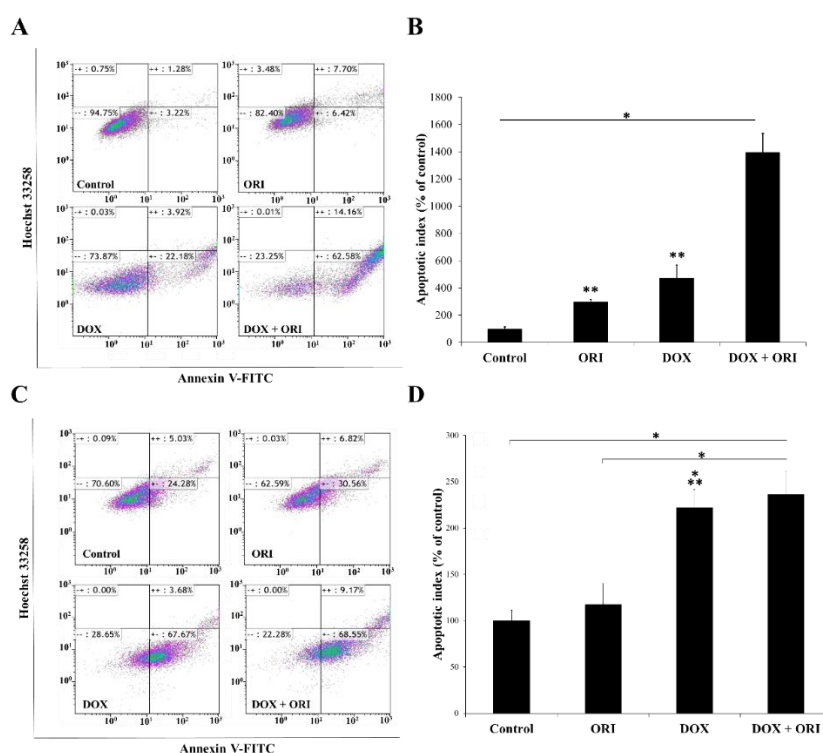


Figure 28. Effects of ORI, DOX and combination of both on osteosarcoma cells apoptosis. Percentage of apoptotic Saos-2 (A and B) and U2OS (C and D) cells determined by measuring Annexin V-FITC/Hoechst 33258 fluorescent signals in flow cytometer (A and C). Apoptotic index (B and D). The data

of early and late apoptosis of each treatment group was combined and compared to the control, whose percentage of apoptosis was considered as 100%. One asterisk shows statistical significance ($p < 0.05$) between DOX+ORI and the rest of the treatment groups, while two asterisks in DOX/ORI is compared to the control according to a two-way ANOVA test followed by Tukey's multiple comparison test. Data are represented as mean \pm SD.

In U2OS cells, only DOX-treated cultures presented an increased apoptotic index, but no significant differences were found between the cells treated with DOX alone and those simultaneously treated with DOX and ORI (**Figure 28C and D**).

In both cell lines studied, ORI treatment was not as potent as DOX or DOX+ORI to induce apoptosis, which is in agreement with the morphological observations. The results of apoptosis index correlated with those obtained for mitochondria membrane potential, where a significantly increased response to DOX+ORI was noted in Saos-2, but not for U2OS.

7. Induction of reactive oxygen species

The results from the above experiments suggested that DOX+ORI-induced cell death in sensitive osteosarcoma cells was mitochondrial-mediated. In many cases, the generation of ROS is linked to apoptosis. To determine its participation DOX+ORI mediated cytotoxicity, production of intracellular ROS was studied.

In Saos-2 cells, DOX and ORI were able to increase the levels of ROS after 16 h of exposure (**Figure 29A and B**). But an enhanced production was observed when both drugs were given together.

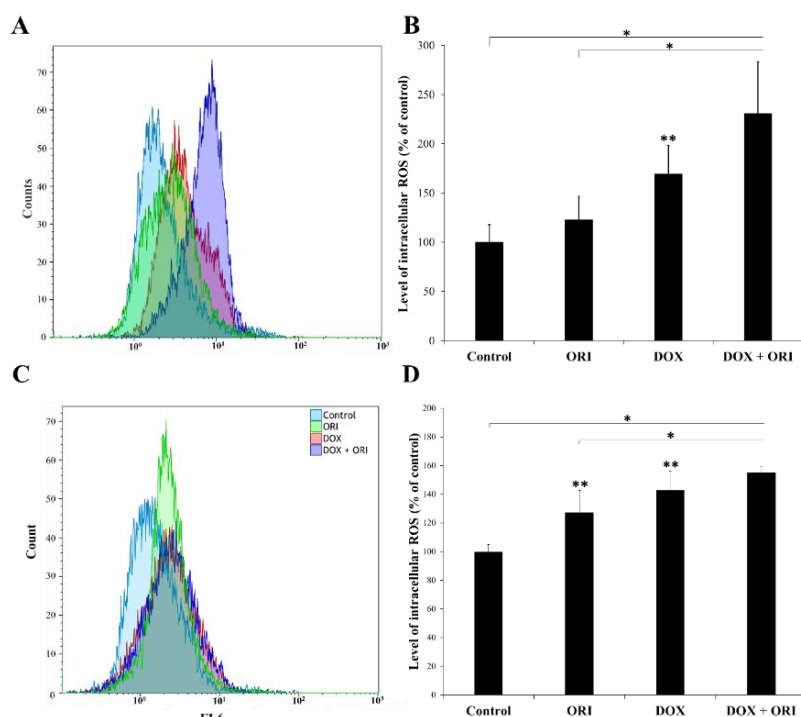


Figure 29. Intracellular levels of ROS caused by ORI, DOX and combination of both in osteosarcoma cells. Observation of ROS within Saos-2 (A and B) and U2OS (C and D) cells. Control and drugs ROS fluorescence signals were detected by flow cytometry (A and C). Quantification of the intracellular ROS levels (B and D). One asterisk shows statistical significance ($p < 0.05$) between DOX+ORI and the rest of the treatment groups, while two denotes significance with the control according to a two-way ANOVA test followed by Tukey's multiple comparisons test. Data are represented as mean \pm SD.

In U2OS cells, both ORI and DOX induced an elevation of intracellular ROS levels, but the combined therapy did not elevate intracellular ROS. No significant differences were found for this variable between DOX and DOX+ORI treated cells (**Figure 29C and D**).

Interestingly, the effects of ORI treatment on both osteosarcoma cell lines were similar, as from all the treatment groups it presented the lowest values of ROS production. This could relate to the reduced apoptosis observed in ORI-treated groups, as compared to groups treated with DOX or DOX+ORI. It is as well in accordance with the morphological observations.

8. Western blot

From the two cell lines, Saos-2 was the most susceptible to simultaneous administration of DOX and ORI compared to U2OS. For this reason, Saos-2 was selected to elucidate the effects of DOX, ORI and combination of both on the expression of Mcl-1, Bcl-2 and Bcl-XL, anti-apoptotic members of the Bcl-2 protein family, by Western Blot analysis. There was a tendency in Mcl-1 increase that was only detected in cells exposed to ORI alone (**Figure 30**). Bcl-2 and Bcl-XL were observed in both control and experimental conditions. Because of the variability in the obtained data, it is tempting to suggest their levels of expression to be slightly lower in DOX+ORI group than in cells exposed to DOX.

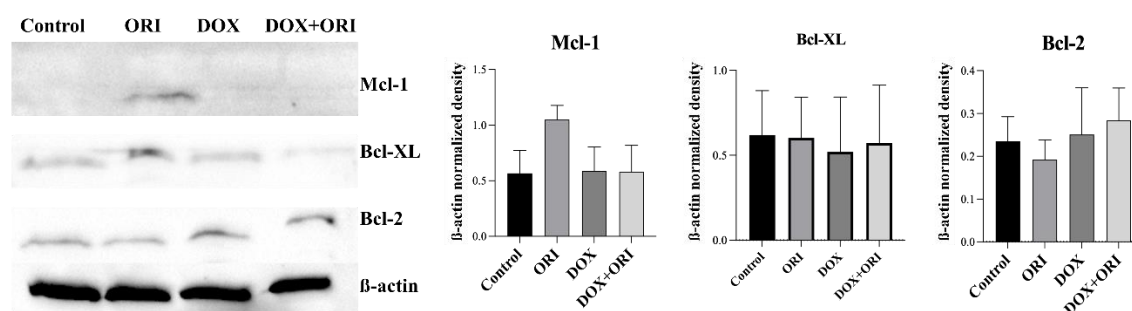


Figure 30. Effects of ORI, DOX and the combination of both on the expression of apoptosis-related proteins in Saos-2. The representative image blot showing the expression of Mcl-1, Bcl-2 and Bcl-XL after Saos-2 were exposed to DOX, ORI and DOX+ORI for 16 hours. β -actin was used as internal reference. Data were analysed by a Kruskal-Wallis and Dunn's multiple comparisons test. Results are represented as mean \pm SD.

9. Effects of ORI on human osteoblasts

ORI is a natural product whose efficiency in the treatment of different types of cancer is being studied. Its anti-tumour effects has been confirmed in the present work for one type of osteosarcoma. It is well established that the vast majority of the chemotherapeutic agents target both malignant and healthy cells. To evaluate the safety of ORI, different concentrations of the natural product were assessed in normal, human osteoblasts (NH Ost).

Untreated osteoblasts presented a fibroblastic morphology that was affected by the addition of increasing concentrations of ORI (**Figure 31**). As ORI concentration increased, cell density decreased, and more round-shaped cells, suggestive of cell death, were observed. 10 μM , the concentration used for combination therapy in Saos-2 sensitive cells, seemed to produce only mild effects on osteoblast morphology. In any case, further studies will be needed to evaluate the effect of oridonin in healthy cells, so as to assess the safety of oridonin therapy.

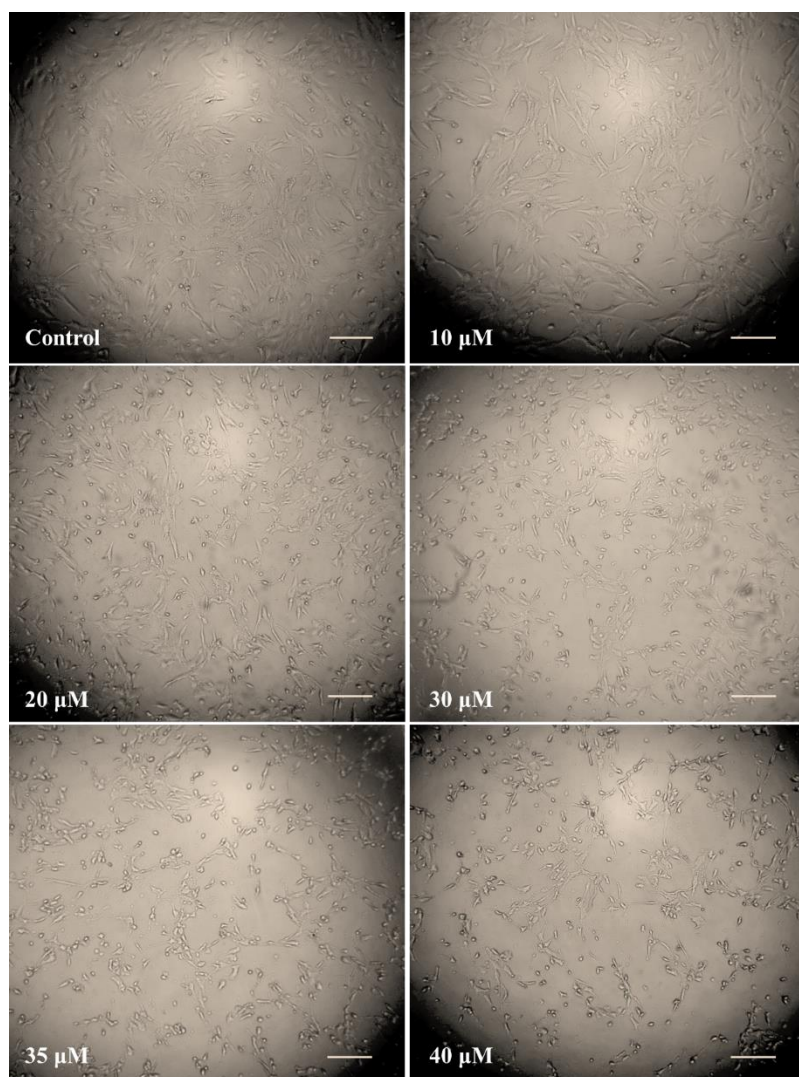


Figure 31. Effects of ORI on NH OST. Morphology of NH OST cultures after 7 h of treatment with different concentrations of ORI. Scale bar = 50 μm .

10. Pilot osteosarcoma xenograft model in nude mice

In order to confirm the anti-cancer effects of DOX, ORI and the combination of both it was necessary to establish a xenograft osteosarcoma model in immunodeficient nude mice. For this, previous *in vivo* experiments were necessary to carry out to establish proper inoculation conditions that would guarantee tumor formation. Different numbers of Saos-2 and U2OS cells were mixed with several concentrations of collagen type I. One month after subcutaneous injection of osteosarcoma cells no tumor formation was detected. For this reason, the experiment was repeated using Matrigel matrix that was diluted with a serum-free cell suspension 1:1. Neither development of the primary tumour nor distal metastasis were detected in mice injected with U2OS. However, Matrigel matrix mix facilitated Saos-2 engraftment as locally distributed tumours were observed. Metastasis was absent in this group of mice. Visual evaluation of extracted tumour tissues showed to be rigid and variable in size. Presence of calcified tissue in different degree was confirmed with a radiography (**Figure 32**).

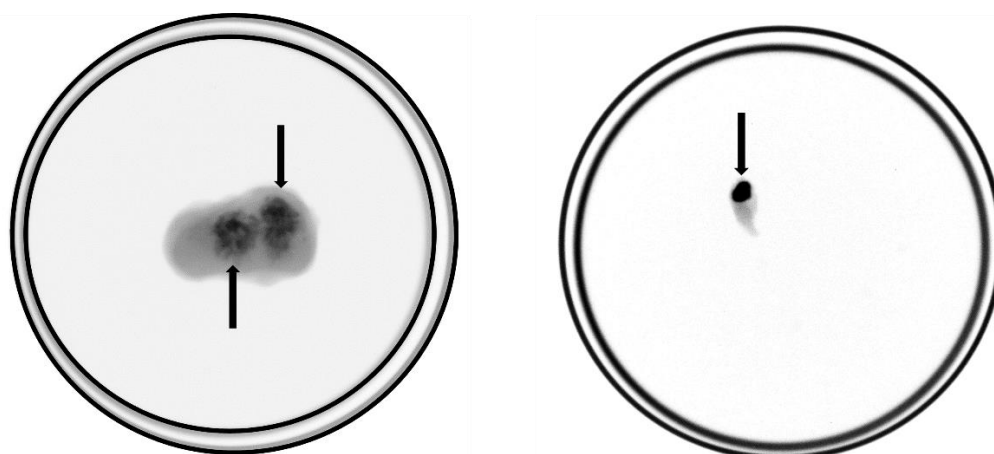


Figure 32. Radiographs of mice tumours. Representative radiograph images of Saos-2 tumours extracted from separate nude mice showing differences in size and calcification degree (black arrows). Scale bar = 1 cm.

This result indicates the tendency of Saos-2 cell line for calcium deposition that can be detected in one or several regions of the malignant tissue. Further histological examination revealed aberrant bone formation evident from cancer cells being surrounded with both mineralized and unmineralized matrix. Moreover, slight cartilage features were observed within the tumour (**Figure 33**).

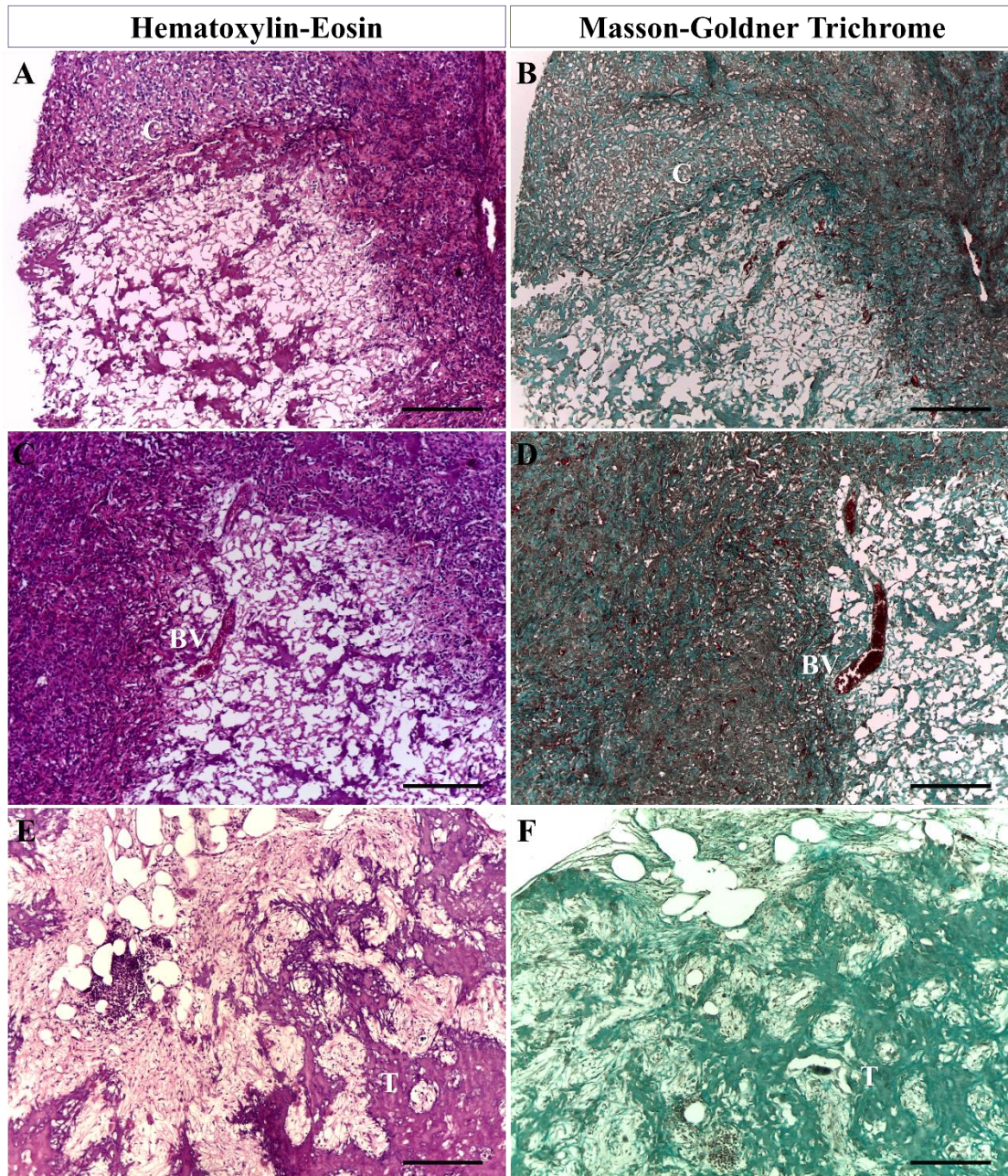


Figure 33. Histological characteristics of Saos-2 tumours in athymic nude mice. Representative histological images. Saos-2 tumours were fixed, decalcified, dehydrated, paraffin-embedded and sectioned. Left panel are images from Haematoxylin-Eosin staining, while right panel corresponds to Masson-Goldner Trichrome staining. C: cartilage feature. BV: blood vessel. T: trabeculae. Scale bar = 200 μ m.

The above results helped to get an insight into the tumour tissue architecture and decide the inoculation conditions for the osteosarcoma pilot study. Thus, to *in vivo* evaluate DOX+ORI combination therapy, female mice were subcutaneously inoculated with 2×10^6 Saos-2 cells in 100 μ L of serum-free McCoy's 5A medium containing 50% Matrigel. The weight of the animals and tumor growth was monitored. During the malignant tissue formation no apparent adverse effects were detected on the general mice's health state as no changes in food intake or pain signs were observed. Two months after Saos-2 injection presence of a subcutaneous solid osteosarcoma

cancer, characterized by a rounded or oval shape, was not detected in all of the studied mice. At this point of time DOX and ORI treatment was administered. The study of Li *et al.* in breast cancer was used as a guidance for this procedure, because at this moment it is the only work evaluating these drugs. The selected concentrations of DOX and ORI *in vitro* were extrapolated based on both *in vitro* and *in vivo* doses of two drugs used by Li *et al.* (Table 10).

Table 10. DOX+ORI treatment *in vitro* and *in vivo*.

| Treatment | Concentration <i>in vitro</i> | Dose <i>in vivo</i> |
|-----------|-------------------------------|---------------------|
| DOX | 2.5 μ M | 10 mg/kg |
| ORI | 10 μ M | 30 mg/kg |

The conversion of 2.5 μ M DOX resulted in a dose of 10 mg/kg that was considered to be high to be given together with ORI 30 mg/kg. The previous observations in human osteoblasts *in vitro* (Figure 30) may indicate there could be presence of some ORI-related adverse effects in addition to those corresponding to DOX *in vivo*. To minimize the suffering of mice it was decided to inject DOX 5 mg/kg instead of 10 mg/kg in combination with ORI 30 mg/kg. 5 groups of animals were established according to the treatment that was to be applied: saline (Control), ORI 30 mg/kg, DOX 5 mg/kg, DOX 10 mg/kg and DOX 5 mg/kg+ORI 30 mg/kg. The first administration of ORI 30 mg/kg alone and in combination with DOX produced visible pain signs with decreased mice activity followed by diarrhea. Even though the side effects were temporal, the administered dose was reduced and the following injections were carried on with ORI 20 mg/kg.

After 10 days of therapy, athymic nude mice were sacrificed by CO₂ inhalation. The calculated post mortem volume of each tumour in drug-treated groups showed to be significantly reduced as compared to the un-treated controls, while no changes were observed between the different treatments (Figure 34).

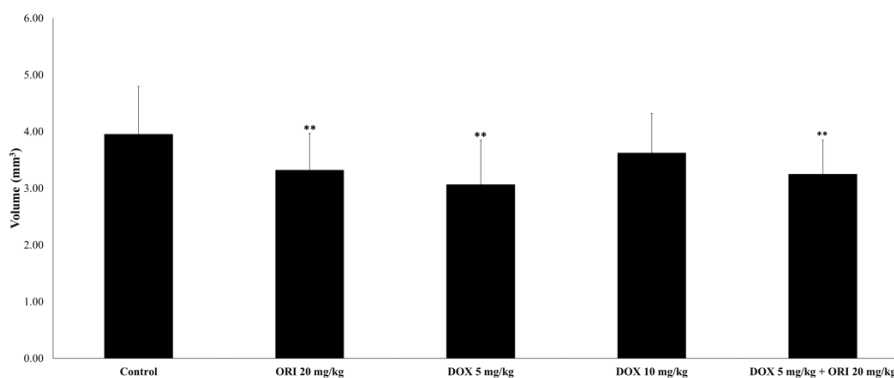


Figure 34. Effects of DOX and ORI treatment on osteosarcoma tumour growth. An osteosarcoma xenograft model was established by a subcutaneous injection of Saos-2 cells in athymic nude mice that later

were treated with saline (Control), ORI (20 mg/kg), DOX (5 mg/kg and 10 mg/kg) and DOX (5 mg/kg) + ORI (20 mg/kg) for 10 days. Two asterisk shows statistical significance ($p < 0.05$) compared to the Control according to a one-way ANOVA test followed by Tukey's multiple comparison test. Data are represented as mean \pm SD.

The resected malignant tissues were rigid and variable in size. From previous observations, Saos-2 showed to produce calcified tumours that were also detected in the present *in vivo* experiment by X-ray analysis (**Figure 35**).

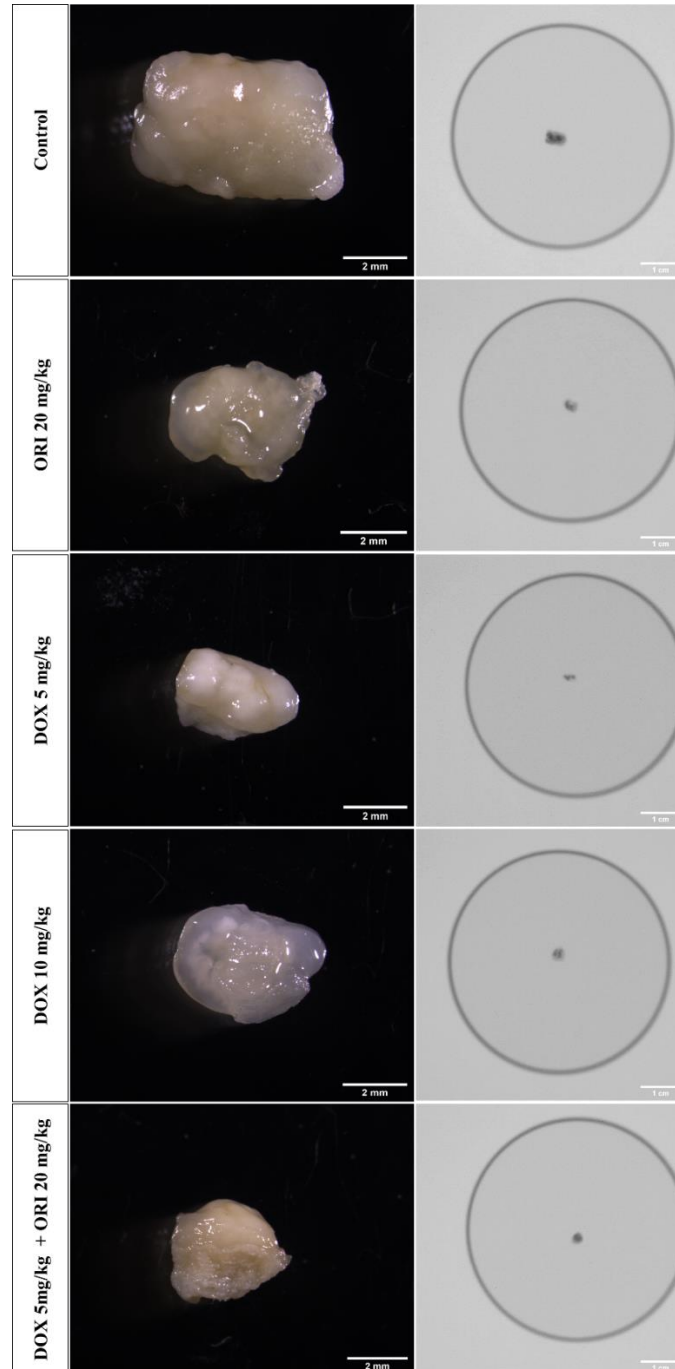


Figure 35. Saos-2 tumours. Representative images of Saos-2 tumours extracted from mice of different treatment groups: saline (Control), ORI 20 mg/kg, DOX 5 mg/kg, DOX 10 mg/kg and DOX 5 mg/kg +

ORI 20 mg/kg. Pictures from the left column were acquired with a stereomicroscope, while those in the right column correspond to radiograph images, where the dark dots represent calcified material.

Finally, to assess the toxicity as well as the protective effects of ORI against DOX induced damage, hearts and livers were analysed. The results showed lack of harm after ORI 20 mg/kg treatment, as liver size and morphology were no different from the controls (**Figure 36**).



Figure 36. Livers from control and treated mice. Liver photographs showing its size differences in athymic nude mice after being treated with saline (Control), ORI (20 mg/kg), DOX (5 mg/kg and 10 mg/kg) and DOX (5 mg/kg) + ORI (20 mg/kg) for 10 days.

Drastic changes in both morphology and weigh of the liver were detected after DOX administration in all the DOX-treated groups. However, the presence of ORI in the combination seems to be slightly protective against liver damage (**Figure 37**).

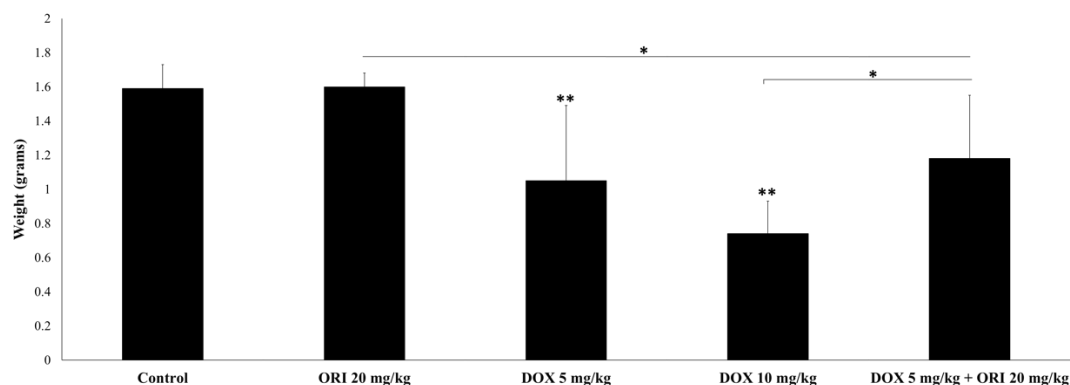


Figure 37. Liver weight from control and treated mice. Liver weight differences in athymic nude mice after being treated with saline (Control), ORI (20 mg/kg), DOX (5 mg/kg and 10 mg/kg) and DOX (5 mg/kg) + ORI (20 mg/kg) for 10 days. One asterisk shows statistical significance, while two compared to

the control according to a one-way ANOVA test followed by Tukey's multiple comparison test ($p < 0.05$). Data are represented as mean \pm SD.

In case of heart histology, minimal fibrosis was detected in all treated groups (**Figure 38**). This suggests ORI is not completely innocuous and presence of some side effects should be expected. Probably, a longer treatment duration could better elucidate the manifestation of adverse effects like cardiovascular fibrosis than the current work that consisted from a 10 day treatment.

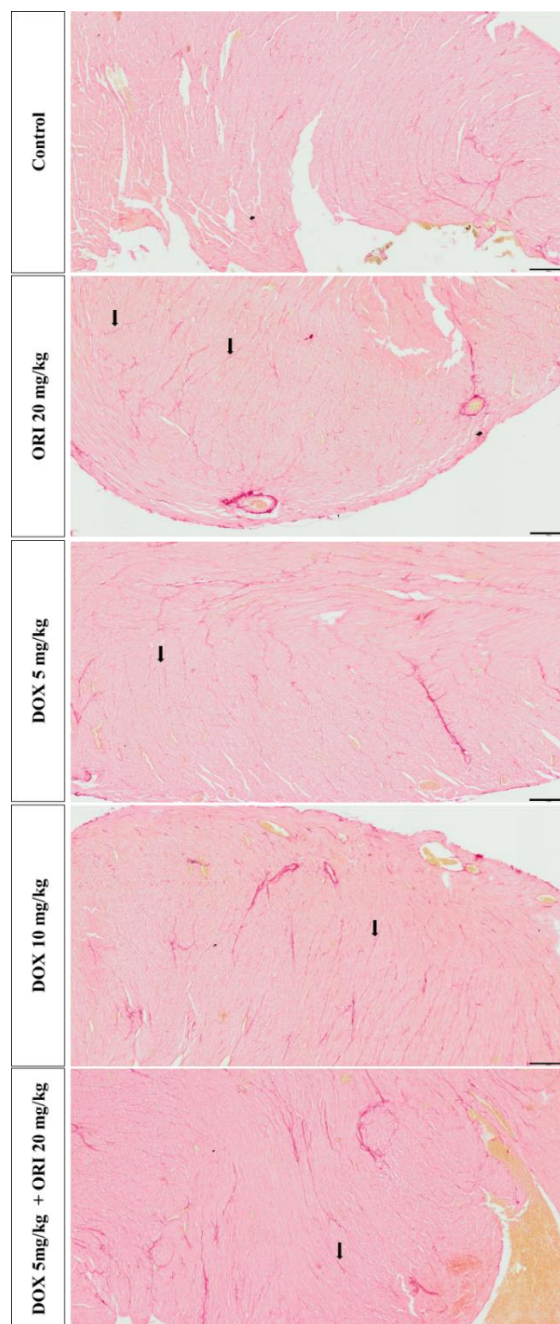


Figure 38. Collagen content in the hearts of athymic nude mice. Representative histological images of hearts that were fixed, dehydrated, paraffin-embedded, sectioned and stained with Picrosirius Red. Black arrows show a sign of a minimal fibrosis. Scale bar = 200 μ m.

Discussion

There are several types of paediatric cancers, including osteosarcoma, whose therapy options are limited and are full of challenges (Hewitt, Weiner, & Simone, 2003; ‘Workshop summery’, 2015). Presence of a tumour and posterior treatment is a stressful experience that both children and their relatives have to face. The current therapeutic option for osteosarcoma comprises a high-dose methotrexate, cisplatin and doxorubicin, a drug combination commonly known as MAP triad. It is a standard treatment that have been given bone cancer patients for the last 30 year accompanied by many adverse effects. The majority of them such as nausea, vomiting or alopecia are temporal and disappear with treatment cessation. But there are those that remain and represent an important health concern. Treatment with DOX alone or in combination with another drugs cause cardiotoxicity (Haghirsadat et al., 2017). In future many of the survivors of the childhood cancer will die from a myopathy. To avoid the unwanted side effects that can arise during and after therapy, doctors normally coadminister DOX with dexrazoxane, a cardioprotective agent (Lipshultz et al., 2014). In this work another drug combination was proposed as a strategy to minimize DOX-related cardiotoxicity where addition of dexrazoxane would no longer needed. To guarantee the effectiveness it had to fit the established criteria of a successful and safe treatment. The first, selected drug should act in synergy with DOX to produce a potent effect that is able to eliminate as much as possible malignant cells. This would reduce a potential recurrence. The second, the target of the selected drug should be different from DOX to make it difficult to the cancer cells to mutate and adapt to novel conditions. Again, this would diminish both resistance and recurrence of the malignant cells. The third, find a combination where the concentrations of the individual drugs are decreased, while the cytotoxicity is maintained or even enhanced. It is expected that in this way it would be possible to reduce the unwanted side effects. Already there are several studies evaluating the combination strategy to increase the therapeutic efficiency and safeness of DOX against different cancer types. Promising results were observed when the chemotherapeutic agent was given together with compounds of plant origin (curcumin), synthetic molecules (gamitrinib and edelfosine) and monoclonal antibodies (olamatunab) (González-Fernández et al., 2017; Higuchi et al., 2019; Park et al., 2014; Wen et al., 2019).

In the present work it was decided to combine the chemotherapeutic agent with a natural product ORI, isolated from a medicinal herb *R. rubescence*, for showing promising results in cancer therapy as it has anti-angiogenic properties, ability to inhibit growth and metastasis in different types of cancer, such as liver, colorectal, breast and ovarian (Chen et al., 2005; Li et al., 2019; Luo et al., 2019; Tan et al., 2011; Tian, Xie, Sheng, Wan, & Zhu, 2017; Wang & Zhu, 2019; Xia, Zhang, Li, & Guan, 2017; Yao et al., 2017). The anti-tumour effects of ORI were also demonstrated in osteosarcoma (Lu et al., 2018; Wang, Zhang, Bao, & Liu, 2017; Wang & Zhu,

2019). Lu *et al.* showed that cytotoxicity was achieved through mitochondria-mediated apoptosis due to activation of PPAR- γ and inhibition of Nrf2 pathway (Lu *et al.*, 2018). The established anti-tumour properties of ORI, made the researchers to combine it with different chemotherapeutic agents, such as gemcitabine, cisplatin and imatinib, to improve cancer treatment (Guo *et al.*, 2012; He *et al.*, 2017; Wang *et al.*, 2019). In a recent publication the influence of the natural product in combination with DOX was already evaluated against aggressive breast cancer. Li *et al.* suggested that the combined use of both drugs could decrease DOX dosage necessary for the reduction of the unwanted side effects, such as cardiotoxicity that is of especial concern. Also the therapeutic effects of DOX were enhanced in presence of ORI (Li *et al.*, 2019). The potent anti-tumour effect of ORI alone or in combination confirm the suitability of the natural product for the purposes that were established for this thesis. Moreover, the published data in several cancer types suggest there is no one specific mechanism by which ORI enhances the effects of different chemotherapeutic agents. Importantly, the target or targets of the natural product are independent from those of DOX. To date, there are no studies of DOX and ORI combination in osteosarcoma. For this two cell lines were selected based on their p53 status, which is a transcriptional factor involved in DNA repair, cell cycle and apoptosis. However, mutations in p53 facilitate angiogenesis, proliferation and invasion of the malignant cells. From the two selected cell lines Saos-2 carry a null mutation in p53 gene, while U2OS has a wild type presentation of the gene (Hientz *et al.*, 2017; Hu *et al.*, 2010).

According to our results, the individual administration of DOX and ORI reduced the viability of osteosarcoma cell lines, in a dose-dependent manner, after 48 h of exposure. DOX was more toxic compared to the natural product, as much lower concentrations were needed to reduce cell viability to 50%. Here it was confirmed Saos-2 and U2OS sensitivity to micromolar concentrations of ORI as observed in previous studies (Lu *et al.*, 2018; Wang *et al.*, 2017). Lu *et al.* showed U2OS to be more susceptible to the effects of the natural product after 48 h of treatment compared to Saos-2. It is in agreement with the findings of the present thesis. CD_{50} was determined as 1 μ M for DOX and 12 μ M for ORI in U2OS, while for Saos-2 it were 5 μ M and 20 μ M, respectively. These results are correlated with a p53 status. The functional protein will induce apoptosis in response to the damage produced by the chemotherapeutic agents. Mutated p53 is not as effective as the wild type and for this reason Saos-2 required more concentration of the individual drugs to achieve a reduction of 50% of cell viability. This supports the common idea that the efficiency of cancer therapy will partly depend on the p53 status, where those carrying mutations in the transcriptional factor are hard to treat leading to poor outcome (Somasundaram, 2000). In general, compared to the effects of DOX and ORI alone, combination treatment of both drugs resulted in enhanced death of osteosarcoma cells lines. However, not all combinations can produce synergism and improve cancer treatment. Some of them can even have

similar or worse outcome compared to the individual drugs. For this reason, it was necessary to evaluate several DOX and ORI combinations. Base on the calculated CI, synergism was found in the majority of combinations of both drugs in Saos-2. On the contrary, 7 out of 9 combinations produced either additive or antagonistic effects in U2OS. The combinations with synergy were observed to be composed from concentrations of DOX and ORI that were lower to their corresponding CD₅₀. In this way it is expected to reduce cardiotoxicity, that is the main goal of the present work, but also decrease possible influence of ORI in the manifestation of the unwanted side effects.

In order to understand the mechanism of DOX+ORI enhanced toxicity early and late apoptosis, intracellular accumulation of DOX and induction of ROS were studied in both cell lines. The outcome of the simultaneous treatment with DOX and ORI in U2OS was similar to one of the individual drugs. There was no difference in ROS induction and apoptosis between DOX and DOX+ORI, suggesting the anti-cancer effects to be caused mainly by chemotherapeutic agent and ORI had not contributed in DOX cytotoxicity. In Saos-2 the obtained results indicate ORI to increase the uptake of the chemotherapeutic agent, leading to more ROS production with posterior marked apoptosis that was not observed in cells receiving each drug alone. Given the elevated intracellular accumulation of DOX, it is reasonable to hypothesize that chemotherapeutic drug enhanced uptake induced by ORI may be responsible for combination therapy elevated cytotoxicity. It is known DOX to produce apoptosis through ROS induction even in cells with non-functional p53 (Tsang, Chau, Kong, Fung, & Kwok, 2003). Moreover, cancer cells are characterized by increased levels of oxidative stress (Snezhkina et al., 2019). Thus, chemotherapeutic agents that can further enhance ROS levels is another appealing strategy. Altogether, the data suggest that the observed synergistic effects between DOX and ORI may act through ORI inducing an increased accumulation of DOX within Saos-2 cells. Consequently, ROS induction could be possibly responsible of the mitochondrial damage (as supported by JC-1 data) and activation of the signalling cascade leading to eventual cellular apoptosis (data from Annexin V-FITC/Hoechst 33258 staining). Western Blot analysis revealed alteration in the expression of different anti-apoptotic members of Bcl-2 family. Bcl-2 and Bcl-XL were observed in both control and experimental conditions, being Bcl-XL level lower in both DOX and DOX+ORI treated cells. This could account for the higher level of apoptosis observed in those groups. However, Bcl-2 was increased in Saos-2 cells exposed to DOX alone and in combination with ORI. Probably, this could indicate a defensive mechanism of malignant cells as enhanced expression of Bcl-2 may block the pro-apoptotic signals and favour the survival of Saos-2 under stress condition. In case of Mcl-1, it was only detected in cells exposed to ORI alone. Demelash *et al.* found that Mcl-1 expression prevented ROS formation, through inhibition of NOX4, a NADPH oxidase, and its posterior translocation to the mitochondria (Demelash, Pfannenstiel,

Liu, & Gastman, 2017). The higher levels of Bcl-XL and Mcl-1 in ORI-treated cells are in agreement with reduced levels of ROS induction and less cell death. Thus, it corroborates the link between oxidative stress and apoptosis. The obtained data indicate that non-toxic low doses of the natural product favour the survival in Saos-2 with Mcl-1 expression, while it is tempting to speculate higher doses of ORI to inhibit Mcl-1 leading to cell death. However, further studies would be needed to confirm and understand the mechanism by which ROS is implicated in all treatment groups in Saos-2.

The main differential response of U2OS and Saos-2 to DOX+ORI combination consist in DOX intracellular accumulation. Saos-2, responsive to simultaneous administration of both drugs, presented an increased uptake of the chemotherapeutic agent that was not efficient in less responsive U2OS. According to this, the way the drugs are internalized could be the clue to the observed differences between cell lines. Normally, the chemotherapeutic drugs, DOX included, are internalised through passive diffusion (Speelmans, Staffhorst, de Kruijff, & de Wolf, 1994). The same should be true for ORI, even though there is no further information in this regard. If both doxorubicin and oridonin cross the membrane by diffusion, it can be speculated that lipid composition and packing of the cell membrane can be the determinant for intracellular drug incorporation. Actually, it has been observed that cancer cells present a distinct lipid profile on the membrane compared to healthy cells, and these differences may alter the signalling pathways leading to therapy resistance (Alves, Ribeiro, Nunes, & Reis, 2016). Taking into account this information and of Speelmans *et al.*, one can speculate that Saos-2 could exhibit higher membrane fluidity (Alves et al., 2016; Speelmans et al., 1994). Also, the passive diffusion of ORI could alter in a favourable way the structure of the membrane in such a manner it facilitated the entrance of DOX. On the contrary, U2OS membrane organization could be characterized by a more packed structure, with reduced fluidity. This might produce the entrapment of the natural product forming ORI-lipid complexes within the membrane. This would possibly lead to less available spaces for DOX to cross the membrane. The speculation is based on our observation of reduced amount of incorporated DOX in DOX+ORI treated U2OS cells, and in the effect observed after prolonging exposure time. The increased time of exposure might have led to more ORI trapped in U2OS membrane, reducing the passive diffusion of DOX.

These results confirm cancer heterogeneity a term that is referred to a population of cells that vary in their phenotype and mutation status. It will determine the sensitivity or resistance to a particular treatment. The same histopathological cancer type can be different between patients. Moreover, variations can be observed within the primary tumour tissue (Fisher, Pusztai, & Swanton, 2013). In the present work each cell line responded differently to DOX and ORI combination. Usually the outcome of the chemotherapy is explained in terms of variations in

cancer subpopulations. It is a simplistic way to understand tumour behaviour. However, cancer is dynamic and complex structure, where components of the extracellular matrix (ECM), cancer associated fibroblasts (CAFs), cancer stem cells (CSCs), amount of nutrients and oxygen will determine the identity of a tumour (Albini et al., 2015; Senthebane et al., 2017). All these factors make cancer unique. For this reason, it is suggested to switch from classical standard osteosarcoma treatment to a personalized medicine. In this way the therapy will be individualized as the adequate treatment option would depend on the genetic and morphological background patient's cancer is carrying. DOX and ORI combination explained in this work represents a promising approach for those tumours similar to Saos-2, while it is less efficient against cells such as U2OS. In general, the data showed the addition of ORI allow reducing DOX doses in osteosarcoma treatment, while enhancing the cytotoxic effects of the chemotherapeutic drug.

Given the successful results obtained for DOX+ORI combination therapy in Saos-2, a pilot *in vivo* osteosarcoma xenograft model was planned. Before, it was necessary to establish the proper inoculation conditions in athymic nude mice. For this different amounts of Saos-2 and U2OS (10^6 and 2×10^6 cells) were subcutaneously inoculated in two types of media, collagen type I and Matrigel. U2OS were not able to form any tumours *in vivo* that is in agreement with data from different studies (Jeong et al., 2017; Lauvrak et al., 2013). In case of Saos-2 a higher tumorigenic capacity was observed when 2×10^6 cells in serum-free McCoy's 5a medium were mixed with Matrigel in 1:1 final proportion. In a similar way, no Saos-2 tumors were detected when cells were inoculated in a suspension with collagen type I. The majority *in vivo* studies in cancer rely on Matrigel, as being rich in extracellular matrix proteins it favors the engraftment and increases the tumorigenic potential of tumor cells (Mullen, 2004). The results pointed Saos-2 cell suspension mixed with Matrigel to be optimal for pilot osteosarcoma study as it was the only cell line under this condition to produce tumors *in vivo*. After the animal study took place, mice were treated for 10 days with saline (Control), ORI, DOX and DOX+ORI. As it was a pilot study, the administrated concentrations were chosen on the basis of the available literature (Li et al., 2019). The initial ORI 30 mg/kg resulted in a visible pain followed by diarrhea. In order to improve the tolerability toward the natural product the ORI dose was reduced to 20 mg/kg. For the end of the experiment in DOX 10 mg/kg two mice died. Probably, animals from this treatment group would not survive in an experiment with more than 10 days of chemotherapeutic agent administration. These results suggest the studied doses to be high and adjustment for the next *in vivo* should include a wide range of DOX and ORI concentrations for a longer duration. The increase in the period of time would reveal the real efficiency and possible side effects of DOX+ORI. This could be the reason that explain little changes in the tumor volume detected after administration of the individual drugs alone and in combination. Also ORI cardioprotective effects were not observed during a short treatment time. If mice were not sacrificed after 10 day

of drug administration, it might be possible to detect some heart's changes. On the other hand, hepatoprotective effects were observed when the natural product was present. In the future experiments were the necessary adjustment of the conditions would be done, it is expected to confirm the efficiency of DOX+ORI, as it was found in breast cancer (Li et al., 2019). Additionally, corroborate cardio and hepatoprotective effects of the natural product in osteosarcoma xenograft model.

ORI is a promising natural product against a variety of cancer types. Still there are several gaps that should be filled in order to understand better its properties. For example, from pharmacokinetics studies 18 metabolites were identified after oral administration of the natural product in rats (Li, Zhang, Ma, Xie, & Huang, 2021). However, the role of these molecules is still to be elucidated. Although many studies claim ORI to be safe in non-tumorous tissues, observations made in this work in normal osteoblastic cells revealed that concentration over 20 μM to produce a dose-dependent toxicity. Based on previous osteosarcoma and osteoblast results explained in this study 10 μM of ORI was established as the maximal optimal concentration *in vitro*. The extrapolation of this value for *in vivo* produced a dose of 30 mg/kg that showed to be harmful for athymic nude mice. Neither swift nor damage in principal organs were found in old male BALB/c nude mice after 21 days of 30 mg/kg ORI administration in Lu *et al.* study (Lu et al., 2018). This clear discrepancy with the results of the present work could be attributed to a different mice stain and supplier of the natural product for the *in vivo*.

After reducing ORI dosage from 30 mg/kg to 20 mg/kg the animal general health condition was improved with posterior administration of the natural product. Analysis of the major organs showed the natural product to be relatively safe, as no apparent changes in liver's size were detected. On the contrary, an insight of a minimal cardiovascular fibrosis was observed. However, it is hard to conclude whether or not ORI is completely safe as the duration of the *in vivo* pilot study was short and it was not enough to reveal the potent side effects. Probably, administration of 20-30 days would give a better idea of the presentation of the unwanted side effects. In this regard the observed minimal cardiovascular fibrosis after a long treatment time could stay the same, indicating the relative safeness of ORI, or get worsen, meaning that there should pay attention to the safety issues (like heart functionality) when the natural product is given alone or in combination. There are very few studies reporting the risk of ORI administration. Xu *et al.* found certain degree of hepatic and myocardial toxicity in male BALB/c nude mice after 21 days of treatment with 10 mg/kg of ORI (Xu et al., 2020). It should be taken into account that chemotherapeutic drugs are normally toxic to both healthy and malignant cells, but the dose of the natural product and duration of the therapy are important determinants. Also the proper

identification of the risk and the ability to alleviate the presentation of the unwanted side effects can improve the tolerability of the treatment within a patient.

In summary, DOX and ORI combination represents a potential treatment option for osteosarcoma therapy.

Future perspectives

DOX and ORI combination represent a promising approach for osteosarcoma treatment and to complement the finding of this strategy the next experiments, briefly summarized, will be done as part of a postdoc study:

- Study PI3K/Akt signalling pathway *in vitro* to confirm the implication of the oxidative stress in ROS mediated apoptosis of osteosarcoma cell lines.

Strategy II: Paclitaxel, MSC and combination treatment

“To raise new questions, new possibilities, to regard old problems from a new angle, requires creative imagination and marks real advances in science”.

Albert Einstein

In the previous strategy I, a novel combination therapy was proposed to enhance doxorubicin efficiency and reduce its dosing and, hence, its life-threatening secondary effects. In this part, several approaches are evaluated, such as drug repositioning, drug encapsulation in nanoparticles and drug vectorization using mesenchymal stem cells.

Drug repositioning, or drug repurposing, is a strategy that seeks applying an already approved drug to diseases different to that for which the drug was originally approved. This strategy has several advantages over the developing of a totally new drug: first, since the repurposed drug is an approved one, its safety has already been assayed, and therefore the risks of failing safety trials is minimal. Related to this, because safety assessment and preclinical testing have already been completed, the time and cost of Phases I and II of clinical trials can be substantially reduced. Therefore, drug repositioning is a rapid and cost-efficient approach for the development of new therapies (Nowak-Sliwinska et al., 2019; Sleire et al., 2017). The four most commonly used chemotherapeutic agents for osteosarcoma treatment, high-dose methotrexate, cisplatin, doxorubicin and ifosfamide, in general, target the genetic material of the malignant cells (Chou & Gorlick, 2006). PTX, a drug typically given to patients with breast and lung cancer, acts through a different mechanism. It stabilizes the microtubules causing a G₂/M phase cell cycle arrest, with a subsequent induction of apoptosis (Farrar & Jacobs, 2020; Weaver, 2014; Zhang et al., 2014). To date there are few studies on PTX efficiency against osteosarcoma. For this reason, we aimed at studying the chances of repositioning paclitaxel for osteosarcoma treatment.

Chemotherapeutic drugs lack specificity toward cancer cells. Upon administration they get distributed all around the body and, as a result, they target healthy cells in non-tumorous tissue, while tumours may receive less dose than the necessary (Dadwal et al., 2018). A targeted delivery can be achieved by encapsulating the drug inside a nanoparticle. Nowadays, nanotechnology is getting attention in cancer treatment, as nanomaterials are biocompatible and, by acting as vehicle and vectors towards the target site, they may have the ability to reduce the toxicity and side-effects of the chemotherapeutic agents (Jalili et al., 2017). Different modifications of the nanoparticles can make them specific for targeting certain tumours and release the cargo under specific stimuli (Salimi et al., 2018; Yang et al., 2016). In the present strategy II PTX is going to be incorporated inside the thermo-responsive polymer PNIPAM, which is capable of releasing the drug when the temperature is higher than 32 °C (Jalili et al., 2017).

Because, to date, no specific markers of osteosarcoma cells have been found, we had no motif to vectorize PNIPAM nanoparticles towards osteosarcoma cells. To deliver PNIPAM-encapsulated PTX at the osteosarcoma site, MSC were evaluated as vehicles. There is a growing interest in MSC as cellular vehicles due to their hypoimmunogenicity and their tumour homing ability (Duchi et al., 2013), which make them able to engraft in tumours (Ghaedi et al., 2011).

Our goal was using the MSC with a double purpose, vectorization towards the bone sarcoma, thanks to MSC tumour-homing ability, and protection of the PNIPAM nanoparticles from vascular filtration or macrophage clearance (Gustafson, Holt-Casper, Grainger, & Ghandehari, 2015). It has been observed that the source of the MSC can have an important influence in its interaction with cancer cells. Some authors have observed this interaction can confer protection to the cancer cells against the effects of the chemotherapeutic drug, and others have described the opposite effect, *i.e.* sensibilisation to the drug (Houthuijzen, Daenen, Roodhart, & Voest, 2012; Pessina et al., 2011; Yao et al., 2017). In this strategy II, adult MSC from two different tissues were compared: adipose tissue-derived (AD-MSC) and bone marrow-derived (BM-MSC).

In brief, by combining nanotechnology and cell therapy, we aim to develop a “nano-engineered” MSC as a novel therapy for osteosarcoma treatment.

Results

Part I Osteosarcoma

1. Nanoparticles

1.1. Characterization of NiR@PNIPAM and PTX+NiR@PNIPAM

A reversible thermo-responsive “smart” polymer, PNIPAM, carrying paclitaxel (PTX), and Nile Red (NiR), was evaluated (PTX+NiR@PNIPAM). The same nanoparticle, without PTX drug cargo (NiR@PNIPAM), was used as control in all the experiments. Morphology and particle size were determined by TEM imaging. Both nanoparticles presented a good dispersion in aqueous medium, as no aggregations were observed (**Figure 39**).

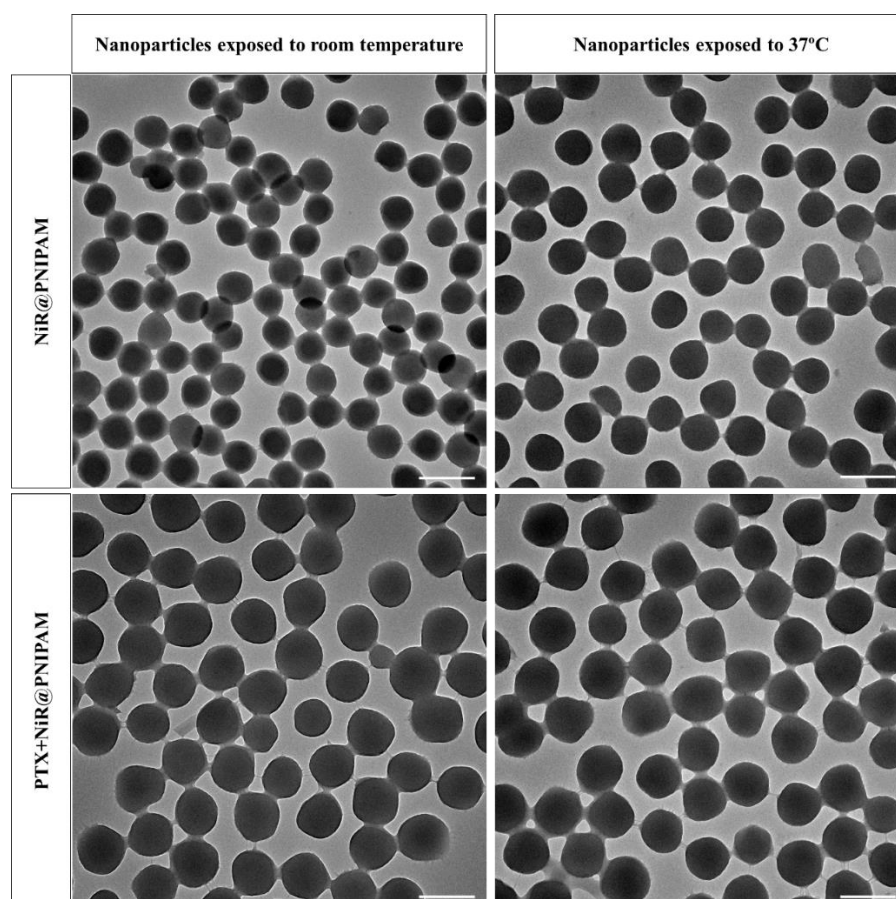


Figure 39. TEM images of the nanoparticles. NiR@PNIPAM and PTX+NiR@PNIPAM incubated at room temperature and 37 °C for 24 h. Scale bar = 500 nm.

The nanoparticles present a swollen hydrated state below their low critical solution temperature (LCST) of 32 °C, but they suffer a reversible shrinkage associated to drug release

when the temperature is above LCST. To confirm these size changes, the stock solution was diluted in MilliQ water and stored at room temperature (RT) as well as at 37 °C (body temperature and cell incubator temperature) for 24 h. Upon heating, both solutions of nanoparticles became turbid, as observed by naked eye. It was possible to detect nanoparticle size reduction using TEM (Table 11). However, the size of blank PNIPAM was reduced at RT compared to PNIPAM exposed to 37 °C. Possibly, heat generation caused by a prolonged exposure of this nanoparticle in TEM produced a transition to a shrinkage state, while the second sample cooled down to room temperature during their transference to the copper grid.

Table 11. Characterization of nanoparticles. Nanoparticle diameter after for 24 h incubation at different temperatures was analysed, in their dry form, from TEM images. Data are represented as mean±SD.

| | Room temperature | 37 °C |
|----------------|------------------|-----------------|
| NiR@PNIPAM | 307.69±19.88 nm | 336.18±20.96 nm |
| PTX+NiR@PNIPAM | 420.16±33.33 nm | 393.92±27.71 nm |

Finally, it is noticeable that PTX+NiR@PNIPAM nanoparticles were found bigger in diameter (420.16±33.33 nm) than NiR@PNIPAM (307.69±19.88 nm), suggesting that the size and/or diversity of the cargo may affect the size of the nanoparticle.

2. 2D cell culture

2.1. Effects of PTX, PTX+NiR@PNIPAM and NiR@PNIPAM on cell viability

MG63, Saos-2 and U2OS osteosarcoma cells were exposed to 6 different concentrations of PTX+NiR@PNIPAM, NiR@PNIPAM and cell viability was assessed by resazurin assay. NiR@PNIPAM caused a slight viability reduction at higher concentrations, but in all cases cell viability was at least 90% of untreated controls, and a concentration-dependent effect was not observed (Figure 40), so the nanoparticle can be considered as safe. In any case these data should be taken into account when *in vivo* experiments are planned.

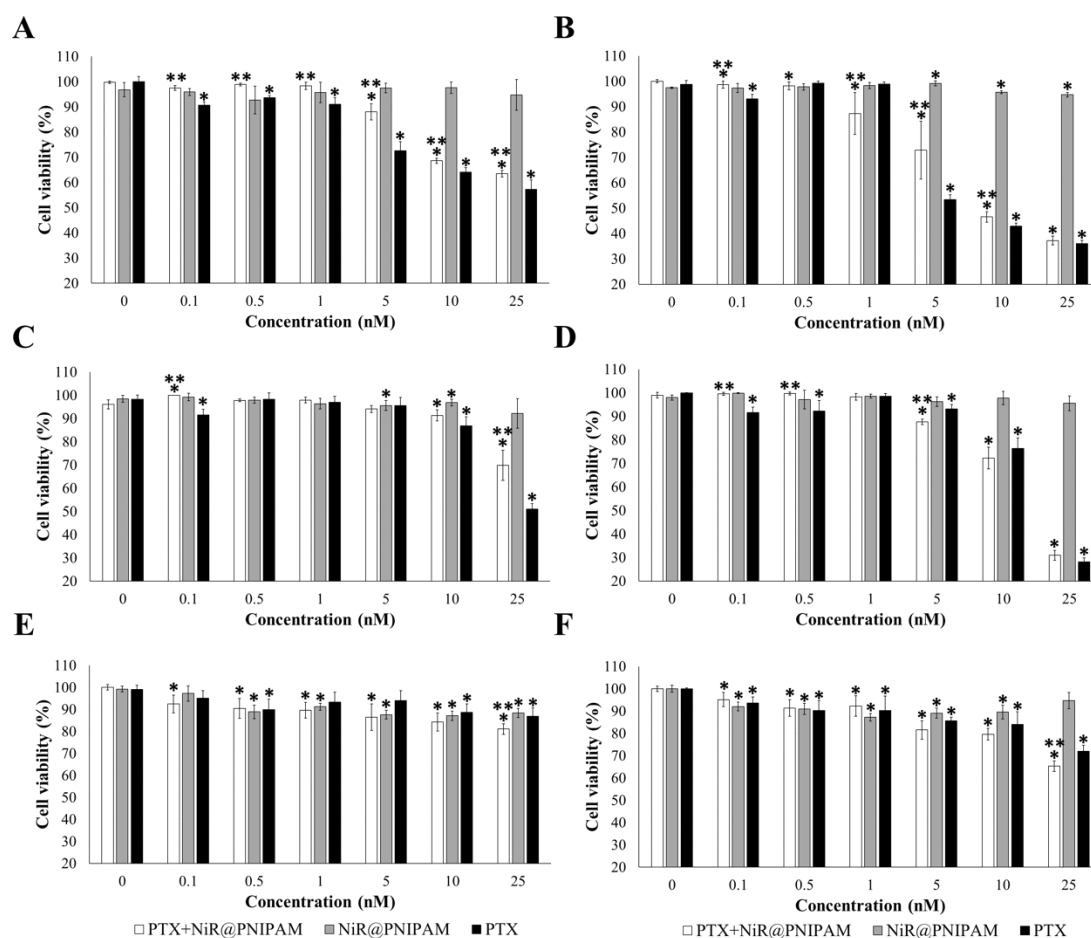


Figure 40. *In vitro* toxicity evaluation of PTX+NiR@PNIPAM, NiR@PNIPAM and PTX. MG63 (A and B), Saos-2 (C and D) and U2OS (E and F) were exposed to different concentrations of PTX+NiR@PNIPAM, NiR@PNIPAM and PTX for 4 days. The viability was assessed on days 2 (A, C, E) and 4 (B, D and F) by resazurin assay. One asterisk shows statistical significance compared to negative control, while two asterisks between PTX+NiR@PNIPAM and PTX of the same concentration tested in a t-Student test ($p < 0.05$). Data are represented as mean \pm SD.

In MG63 cells, concentrations above 5 nM of PTX, either nude or encapsulated in PNIPAM, produced a significant cytotoxic effect (**Figure 40A and B**). No cytotoxicity was observed at very low concentrations ranging from 0.1 to 1 nM. Interestingly, at day 2 and 4, almost in all the tested concentrations PTX alone presented better outcome compared to the encapsulated drug.

In Saos-2 cells, higher drug concentrations (10 and 25 nM) were needed, being the effects similar for the encapsulated and non-encapsulated PTX (**Figure 40C and D**).

U2OS cells showed some resistance to PTX, as none of the evaluated concentrations achieved a 50% decrease in cell viability (**Figure 40E and F**). Unlike MG63 and Saos-2, 25 nM of PTX+NiR@PNIPAM produced better outcome, as compared to PTX, at days 2 and 4. There were no differences in the rest of concentrations would it be drug alone or incorporated inside a nanoparticle.

Overall, these results show that PTX repositioning could be a feasible strategy for some types of osteosarcomas, as two of the tested cell lines were sensitive to the drug. They also show that PTX-sensitive cell lines were responsive to both the PNIPAM-encapsulated and the freely delivered drug.

2.2. Concentration that achieves 50% of cell death after 2 days of treatment

MG63, Saos-2 and U2OS were treated with 6 different concentrations of PTX+NiR@PNIPAM and PTX in order to select the concentration that achieved a 50% of cell death (CD_{50}) after 2 days of exposure, as this exposure time was decided to be used in the posterior experiments. Cell viability was assessed by resazurin assay.

In MG63, for the concentrations tested, no significant differences were observed between PTX+NiR@PNIPAM and PTX, with the exception of 50 and 250 nM, where the drug alone was more cytotoxic compared to the encapsulated one (**Figure 41A**). From these results, the concentration of both PTX+NiR@PNIPAM and PTX causing 50% cell death after 2 days of treatment was determined as $CD_{50} = 300$ nM.

In case of Saos-2, exposure to different concentrations of PTX alone and loaded in PNIPAM nanoparticle, a concentration of 75 nM was needed to produce 50% of viability at day 2. No differences were observed between PTX+NiR@PNIPAM and PTX (**Figure 41B**).

Finally, U2OS again showed resistance to PTX, as higher concentrations were needed to achieve 50% of cell viability (**Figure 40C**). Similar to the other cell lines, no differences were observed between the two presentations of PTX. From these data, the concentration of PTX+NiR@PNIPAM and PTX that was able to reduce U2OS cell viability to 50% was 2000 nM.

In general, the outcome of PTX+NiR@PNIPAM and PTX on osteosarcoma cell lines was similar. As mentioned before, the three cell lines presented different sensitivity to the drug, being U2OS the most resistant and Saos-2 the most sensitive.

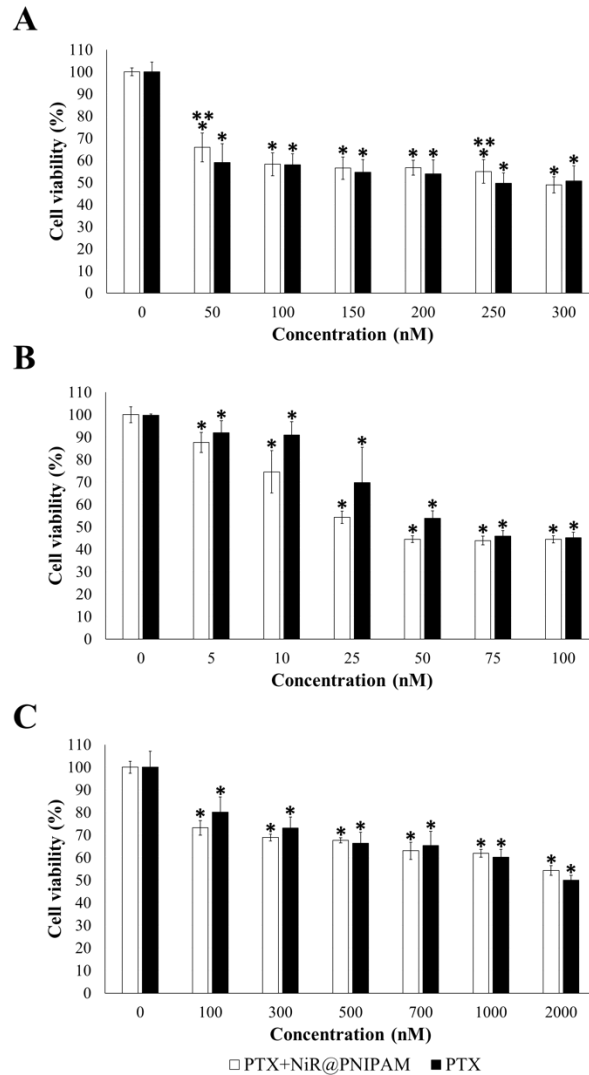


Figure 41. *In vitro* toxicity evaluation of PTX+NiR@PNIPAM and PTX after 2 days of treatment. MG63 (A), Saos-2 (B) and U2OS (C) were exposed to different concentrations of PTX+NiR@PNIPAM and PTX for 2 days. The viability was assessed by resazurin assay. One asterisk shows statistical significance compared to negative control, while two asterisks between PTX+NiR@PNIPAM and PTX of the same concentration tested in a t-Student test ($p < 0.05$). Data are represented as mean \pm SD.

3. 3D cell culture

Nowadays there are many concerns about the correlation between experimental results obtained with 2D-culture models and *in vivo* scenarios, as morphology, genetic expression and interaction with the extracellular matrix are all different. For this reason, 3D-culture models have gained much attention, as they are considered to be more representative of the *in vivo* situation. To compare and determine if there are differences in PTX drug treatment outcome between 2D and 3D cultures of osteosarcoma, the same concentrations of PTX+NiR@PNIPAM, NiR@PNIPAM and PTX previously used in flat cultures were tested in 3D-culture models.

To promote the formation of cellular spheroids osteosarcoma cells were seeded in ultra low attachment (ULA), conical-bottom, 96-well plates and centrifuged. Then, incubation in standard culture conditions took place.

The different cell lines showed a different ability to form spheroids. In the case of MG63 cells, compact and homogeneous spheroids could be observed after 3 days of incubation in standard culture conditions (**Figure 42A**). Saos-2 and U2OS cells, on the other hand, did not form compact spheroids. Instead, they formed several loose aggregates in each well (**Figure 42B** and **C**).

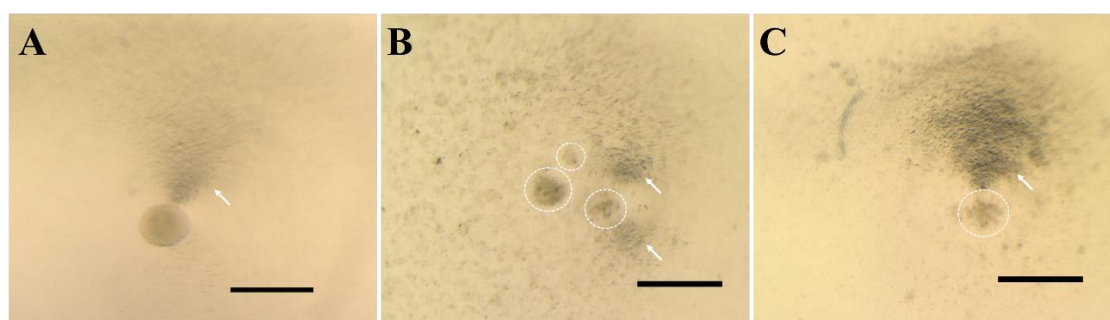


Figure 42. Spheroid formation. MG63 (A), Saos-2 (B) and U2OS (C) spheroids after 3 days of incubation in 96 ULA conical well plates. Pictures were acquired with a stereomicroscope. The white arrow points to the bottom of the conical plate. White dotted circles show the main and satellite cell aggregates. White arrows show the dark bottom of the conical plate, which sometimes can be mistaken for adhered tissue. Scale bar = 500 μ m.

For this reason, hanging drop was used as an alternative method to promote spheroid generation. This method also failed to promote Saos-2 and U2OS spheroid formation. As it was observed in centrifuged conical wells, loose aggregates, but no compact spheroids were formed after 48 h of incubation in suspension (**Figure 43**).

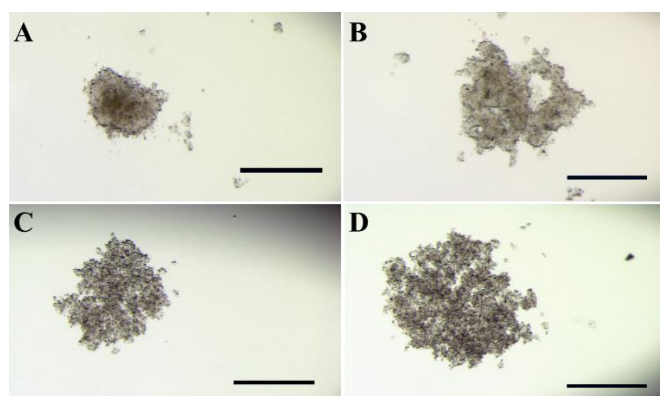


Figure 43. Hanging drop spheroid formation in Saos-2 and U2OS. 5,000 (A) and 10,000 (B) Saos-2 cells; 5,000 (C) and 10,000 (D) U2OS cells were seeded on the lid of a Petri dish that later was inverted. Loose aggregates were formed after 48 h of incubation. Pictures were acquired with a stereomicroscope. Scale bar = 500 μ m.

These observations indicate that osteosarcoma cell lines with epithelial morphology, like Saos-2 and U2OS, do not form spheroids as MG63 does with a spindle-like shape. At the same time the inability to form microtissues possibly can have influence on how both cell lines respond to the treatment.

Given that only MG63 cells formed spheroids, the effect of nude and encapsulated PTX treatment on osteosarcoma cell proceeded only with this cell line. After spheroid formation, cells were treated with different concentrations of PTX+NiR@PNIPAM, NiR@PNIPAM and PTX for 4 days. The volume of each spheroid was measured at the end of the experiment, and the results were expressed using a proliferation index, as percentages of the untreated controls. 3D cultures confirmed NiR@PNIPAM lacks cytotoxicity, as previously observed in 2D cultures (**Figure 44**). This proves the safety of the nanoparticle, and indicates that the observed cell death is caused by presence of PTX inside of NiR@PNIPAM and not by the components of the nanomaterial.

In case PTX-treated groups, a significant proliferation reduction occurred when spheroids were exposed to 5 and 10 nM of PTX+NiR@PNIPAM, as compared to those treated with PTX, suggesting an enhanced cellular uptake of the drug when loaded in nanoparticles (**Figure 44**). At the higher concentration tested (25 nM), the effect of both PTX+NiR@PNIPAM and PTX on MG63 spheroids was similar. Interestingly, in 3D cultures, 5 and 10 nM of encapsulated PTX, yielded the same effect as 25 nM PTX. This was unlike 2D cultures, where a concentration-dependent effect had been observed, and also unlike nude, non-encapsulated PTX, where also some concentration-dependent effect was observed in 3D cultures. This suggests that in 3D cultures, which more closely resemble the tumour conformation *in vivo*, the entry route of PTX into the cell might be more dependent on its presentation. Different mechanisms involved in particle uptake, as compared with the simple diffusion of nude PTX, may account for this result, which points at the possibility of drug dose reduction when presented in nanoparticles. PTX treatment effects achieved a higher cytotoxicity in flat cultures, which is not unexpected, as in this culture type all cells are exposed to the drug, a situation that does not occur *in vivo*. This experiment shows, in any case, that 3D conformation confers the cells a differential behaviour towards drugs. Data from both culture types should be taken into account for drug design, as flat cultures do not correctly resemble the *in vivo* situation as 3D systems do.

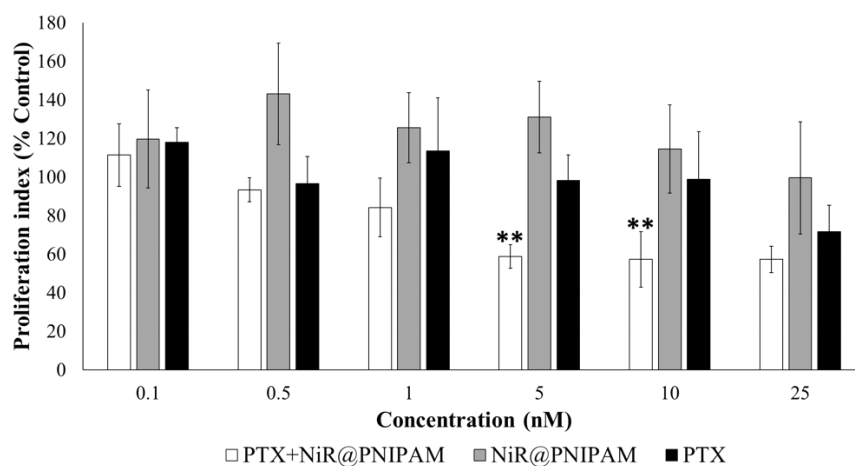


Figure 44. Proliferation index of MG63 spheroids. Microtissues were exposed to different concentrations of PTX+NiR@PNIPAM, NiR@PNIPAM and PTX for 4 days. Two asterisks show statistical significance between PTX+NiR@PNIPAM and PTX of the same concentration tested in a t-Student test ($p < 0.05$). Data are represented as mean \pm SD.

The information of the proliferation index was complemented with a qualitative LIVE/DEAD assay that is based on two fluorescent probes that differentially label live and dead cells. Typically, within a spheroid, there is a core of dead cells, as the medium does not reach the centre of the spheroid. Normally, proliferation of the viable cells closer to the surface compensates for lost cells at the core, and the spheroid maintains its size, at least for a while. This is what was observed in controls and in MG63 spheroids treated with NiR@PNIPAM. No significant changes were detected in spheroid size, as the majority of the cells were live viable (**Figure 45**). On the contrary, a gradual reduction of MG63 spheroid size could be observed with increasing concentrations of both PTX+NiR@PNIPAM and PTX (**Figure 45**). Visually, a higher PTX+NiR@PNIPAM inhibitory effect was evident, as compared to the nude drug. Interestingly, the necrotic core or dead cells (characterized by red colour) was more evident in spheroids treated with PTX, while in spheroids exposed to PTX+NiR@PNIPAM core cells presented red by mostly yellow fluorescence, indicative of dual labelling. These were possibly pre-apoptotic cells. This result suggests these cells have incorporated the drug-loaded nanoparticle, and the intracellularly released PTX was starting to alter microtubules, leading to a pre-apoptotic state.

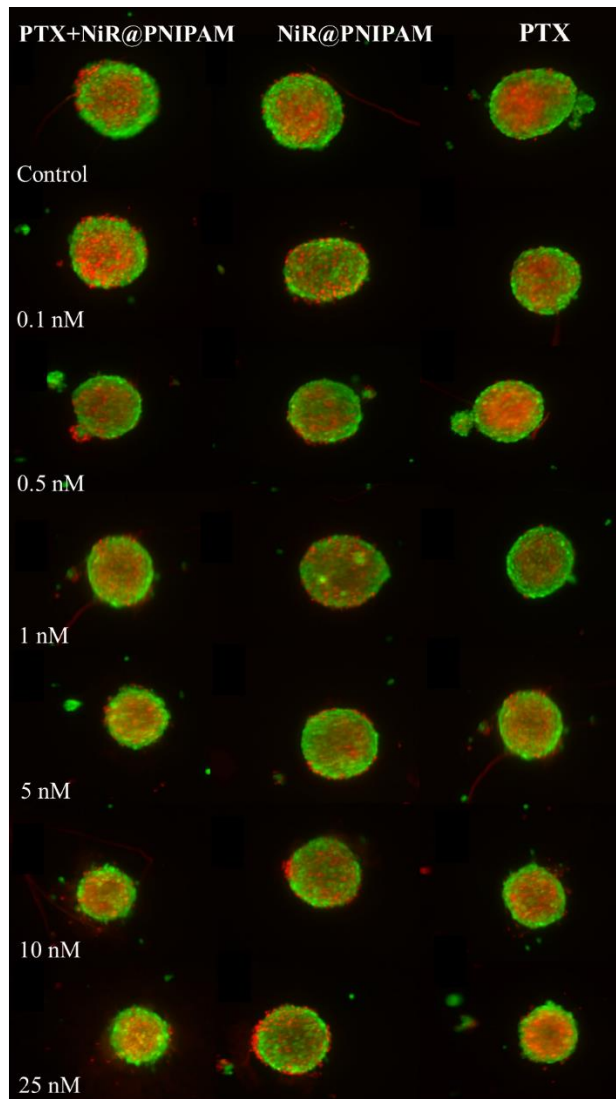


Figure 45. Two colour fluorescent staining of MG63 spheroids. Microtissues were exposed to different concentrations of PTX+NiR@PNIPAM, NiR@PNIPAM and PTX for 4 days. Morphological changes of the spheroids were assessed in LIVE/DEAD assay. Live cells are green (Calcein AM) and dead are red (EthD-1).

4. Collagen spheroids

The interaction of cancer cells with the extracellular matrix is essential for cancer development, as it has influence on cellular processes This is particularly relevant in the case of osteosarcoma, which is an osteoid matrix-producing tumour. To investigate cellular response to nude and nanoparticle-encapsulated PTX when cancer cells are surrounded by extracellular matrix, MG63, Saos-2 and U2OS were suspended in a collagen type I solution, to create collagen spheroids. These were treated for 4 days with the same concentrations of PTX+NiR@PNIPAM and PTX as flat cultures and cell spheroids, and their cell viability was assessed by resazurin assay. Interestingly, the presence of an extracellular matrix had a protective effect on MG63,

U2OS and Saos-2, as their sensitivity to both free and nanoparticle-encapsulated PTX was reduced, as compared to both flat and cell spheroid culture systems (**Figure 46**).

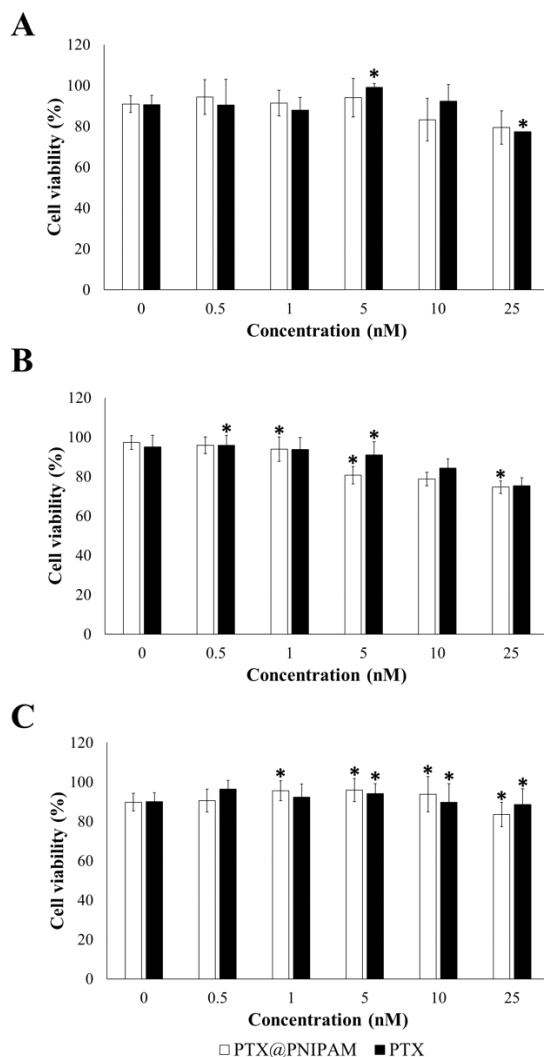


Figure 46. *In vitro* toxicity evaluation of osteosarcoma cells grown on collagen spheroids. MG63 (A), Saos-2 (B) and U2OS (C) on collagen spheroids were exposed to different concentrations of PTX+NiR@PNIPAM and PTX for 4 days. The viability was assessed by resazurin assay. One asterisk shows statistical significance compared to negative control tested in a t-Student test ($p < 0.05$). Data are represented as mean \pm SD.

In order for cancer cells to survive and invade surrounding tissues the extracellular matrix should be degraded that is achieved through proteases secretion. PTX can both stabilize microtubules and inhibit the synthesis of collagenase, affecting the proliferation of malignant cells (Stearns & Wang, 1992). The effects of the chemotherapeutic agent on the degradation of the matrix and migration was tested by seeding MG63 collagen spheroids on a Petri dish and 96 flat well plate. Control and the treatment group with 0.5 nM of PTX presented a contracted gel structure caused by cell migration as was confirmed in LIVE/DEAD assay and probably by

secretion of proteases (**Figure 47**). Collagen spheroids treated with 10 nM of chemotherapeutic drug were lost during the experiment. The increasing concentration of PTX affected the viability of MG63 cells within the collagen spheroid. In addition, it is reasonable to suppose the chemotherapeutic agent to affect proteases release, thus compromising the invasiveness of cancer cells. This was evident from less compacted collagen structures evident from both stereomicroscope and LIVE/DEAD images.

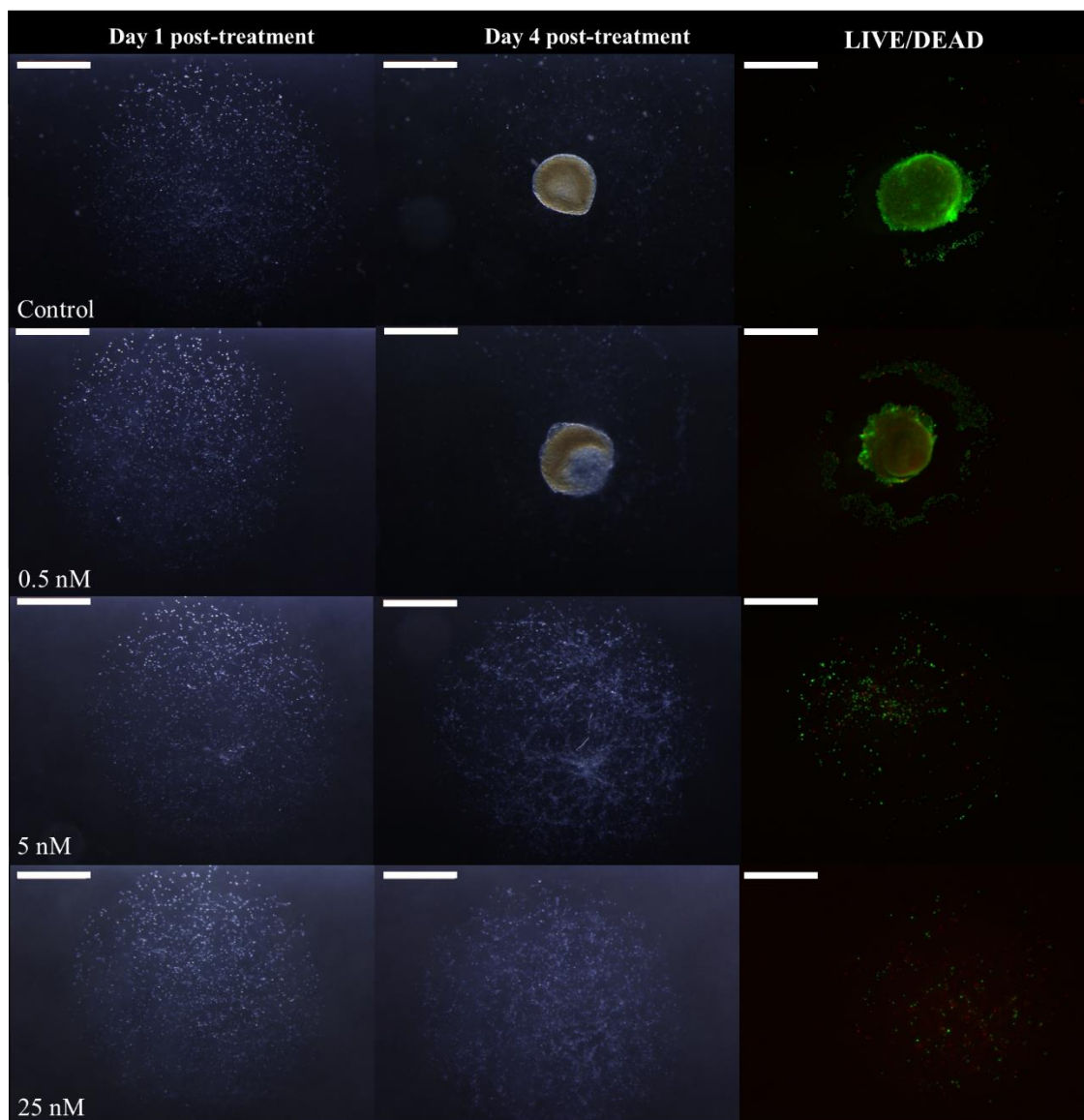


Figure 47. MG63 collagen spheroids treated with PTX. Morphological changes in MG63 collagen structure at days 1 and 4 post-treatment with different concentrations of PTX. The third column represents changes in LIVE/DEAD assay. Live cell are green (Calcein AM) and dead are red (EthD-1). Pictures were acquired with a stereomicroscope. Scale bar = 1 mm.

Similar effects were achieved when PTX was loaded inside a nanoparticle (**Figure 48**).

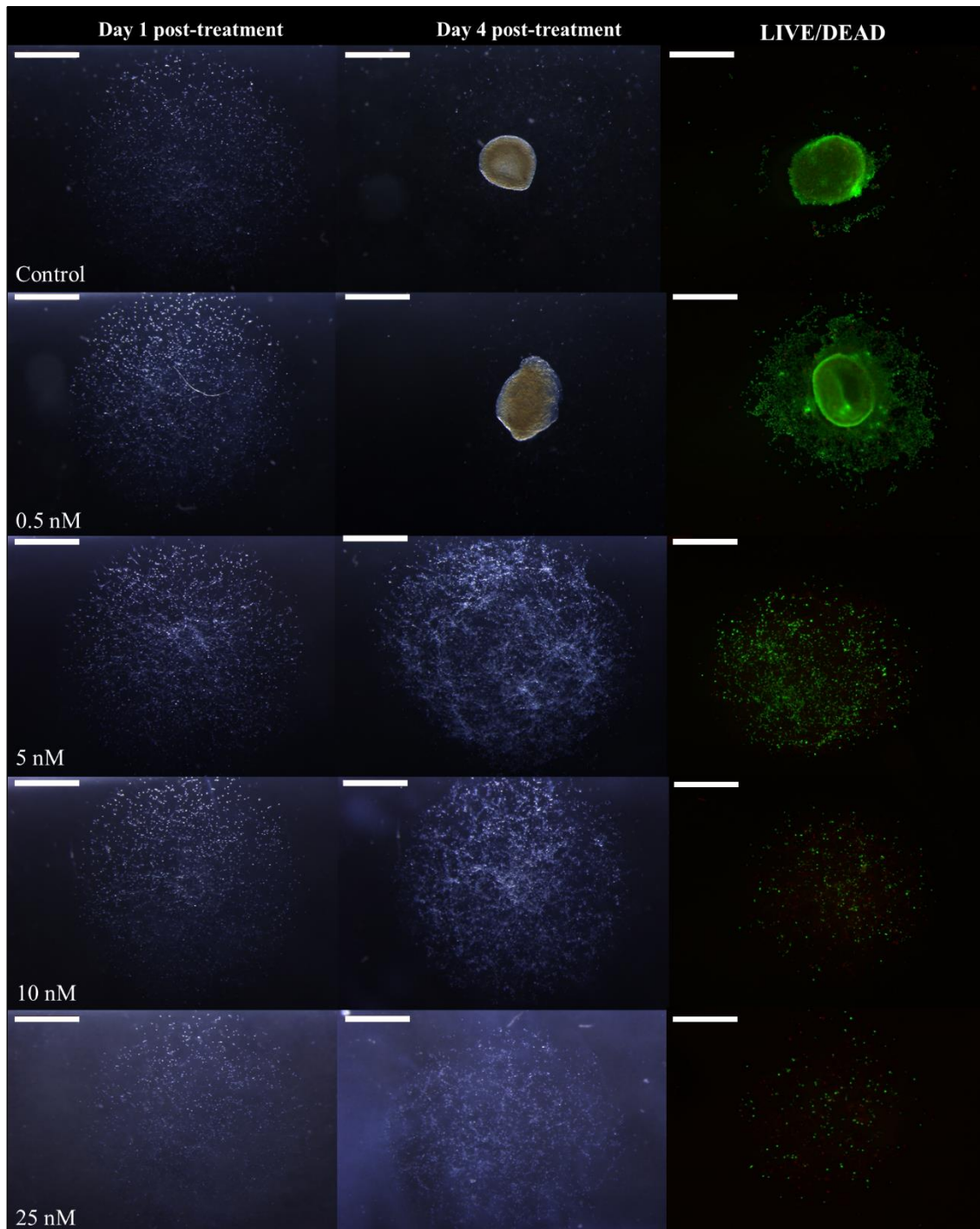


Figure 48. MG63 collagen spheroids treated with PTX+NiR@PNIPAM. Morphological changes in MG63 collagen structure at days 1 and 4 post-treatment with different concentrations of PTX+NiR@PNIPAM. The third column represents changes in LIVE/DEAD assay. Live cell are green (Calcein AM) and dead are red (EthD-1). Pictures were acquired with a stereomicroscope. Scale bar = 1 mm.

After confirming the ability of both presentations of PTX to inhibit the migration of osteosarcoma cells, the experiment was repeated in MG63 and U2OS in order to quantify the

migration distance from the collagen spheroid. However, it was not possible as cells completely covered the surface of the well (**Figure 49**).

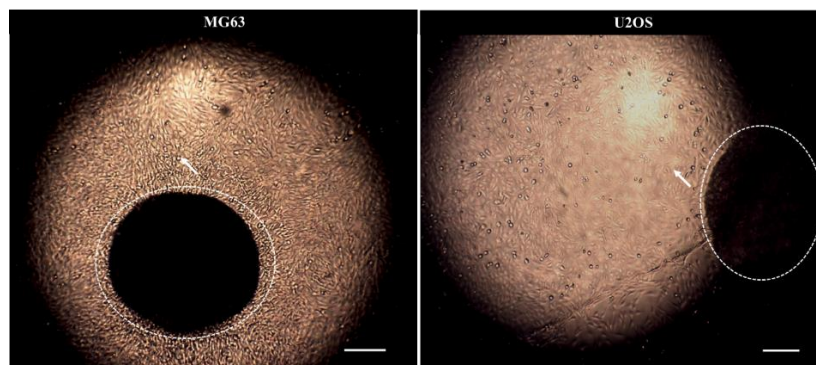


Figure 49. Control MG63 and U2OS collagen spheroids. MG63 and U2OS migration from a collagen spheroid (white dotted circle) to the surface of a 96 flat well plate at day 4 post-seeding. White arrows show cells that left the spheroid and covered the surface of the well. Scale bar = 50 μm .

As in the previous experiment, increasing concentrations of PTX and PTX+NiR@PNIPAM affected the ability of osteosarcoma cells to migrate out of the collagen spheroid. Moreover, it is possible to suggest a reduced amount of collagenase secreted due to a non-compacted structure (**Figure 50**). However, evaluation of the migration versus cell viability over time would enable to elucidate the relative significance of these effects caused by both free and encapsulated PTX.

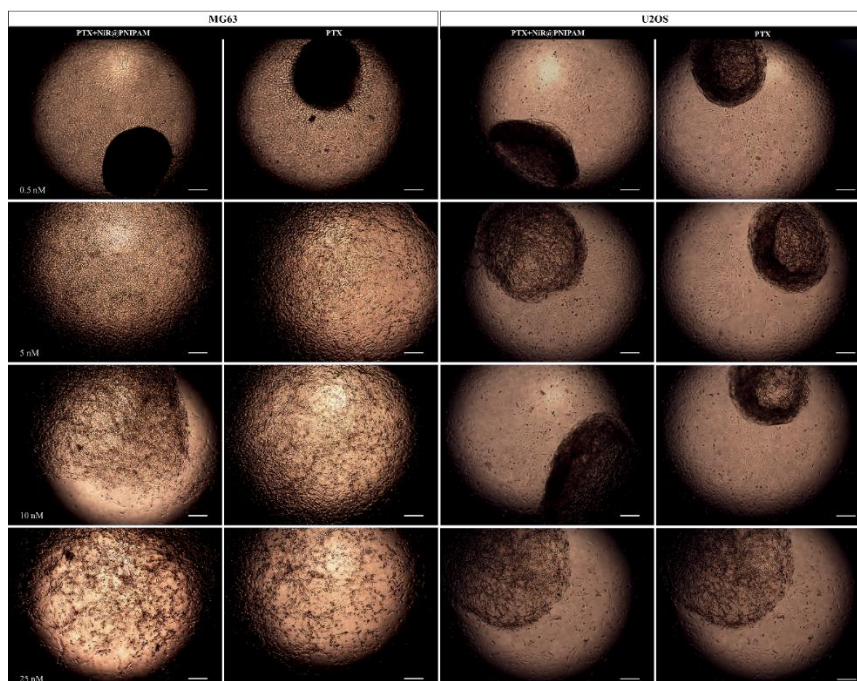


Figure 50. MG63 and U2OS collagen spheroids treated with PTX+NiR@PNIPAM and PTX. MG63 and U2OS migration from collagen spheroid to the surface of a 96 flat well plate after 4 days of treatment with different concentrations of PTX+NiR@PNIPAM and PTX. Scale bar = 50 μm .

5. Cell uptake of NiR@PNIPAM

The previous experiments in both 2D and 3D cell culture systems confirmed that osteosarcoma cell lines are, to a greater or lesser extent, sensitive to PTX, in both its free and encapsulated presentation. Inhibitory effects observed in three cell lines must have been possible due to cellular uptake of these different presentations of PTX. Free PTX enters the cells through passive diffusion, while the mechanisms of nanoparticle incorporation are completely different and depend on uptake via endocytosis. Given that mammalian cell culture temperature (37 °C) is above PNIPAM LCST of 32 °C, part of the nanoparticle drug cargo must have been released to the medium in cell culture conditions. However, the differential behaviour of 3D cultures confirms that drug delivery as nanoparticles must be taking place. To confirm this hypothesis, nanoparticle incorporation into the cells was assessed by confocal scanning microscopy. In order to not disrupt cell morphology, drug-free, NiR@PNIPAM was chosen to establish nanoparticle intracellular localization.

The rate of NiR@PNIPAM nanoparticle incorporation was different between cell lines. In U2OS, NiR@PNIPAM were observed inside the cell after 24 h of exposure, while in MG63 and Saos-2 they were detected after 12-15 h of treatment (**Figure 51** and **Figure 52**).

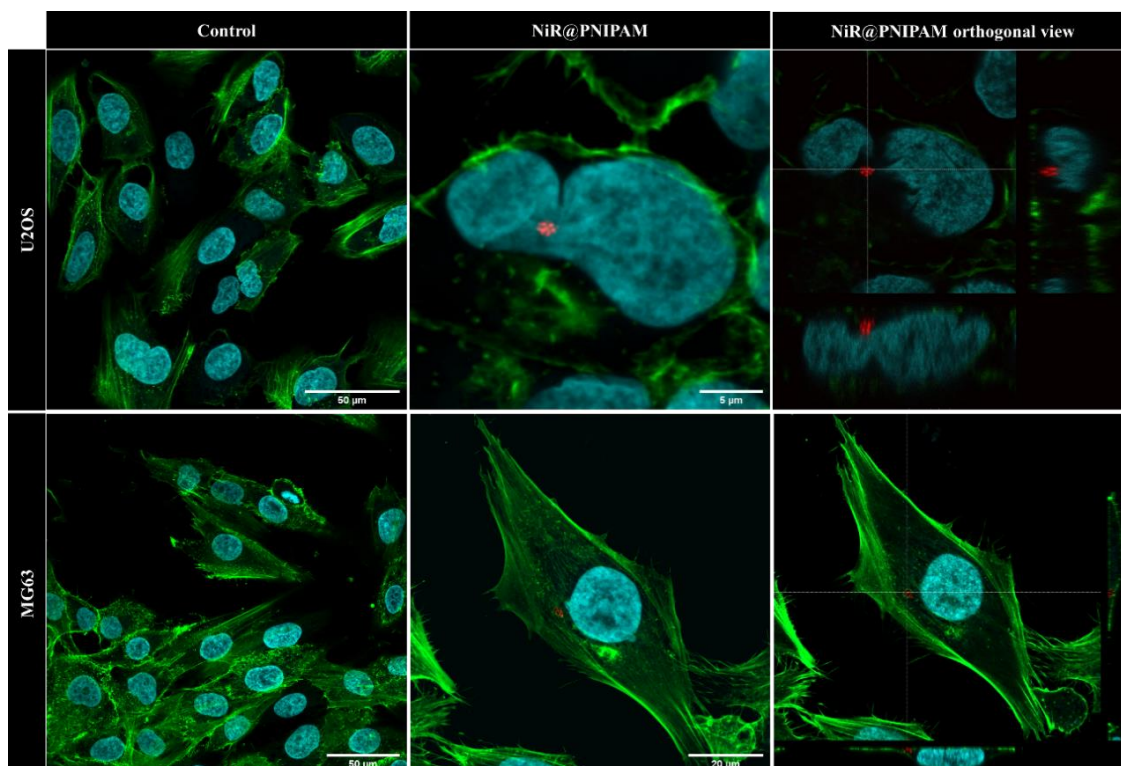


Figure 51. U2OS and MG63 uptake of NiR@PNIPAM. Intracellular accumulation of NiR@PNIPAM in U2OS was detected after 24 h of exposure, while in MG63 after 12-15 h of treatment. Osteosarcoma cells, double-stained with Hoechst 33342 (cyan nuclei), and Phalloidin-Atto 488 (green microfilaments). NiR@PNIPAM nanoparticles are visible as red dots thanks to NiR fluorescence. The third column show

orthogonal view from different planes (XY, XZ or YZ). Perinuclear localization of the nanoparticle within osteosarcoma cells can be observed.

The presence of the fluorescence tag, NiR, made it possible to localize the nanoparticles inside the cells. NiR@PNIPAM could be easily distinguished by its size and spherical shape. In all three cell lines studied, PNIPAM nanoparticles were observed in perinuclear locations (**Figure 51** and **Figure 52**). Interestingly, the internalized nanoparticles grouped together simulating a flower-like structure. Orthogonal slicing in MG63 showed NiR@PNIPAM as accumulated inside a large vesicle (**Figure 51**). Besides perinuclear localization, nanoparticles were observed close to the cell membrane (**Figure 52**), a location that might be related to uptake.

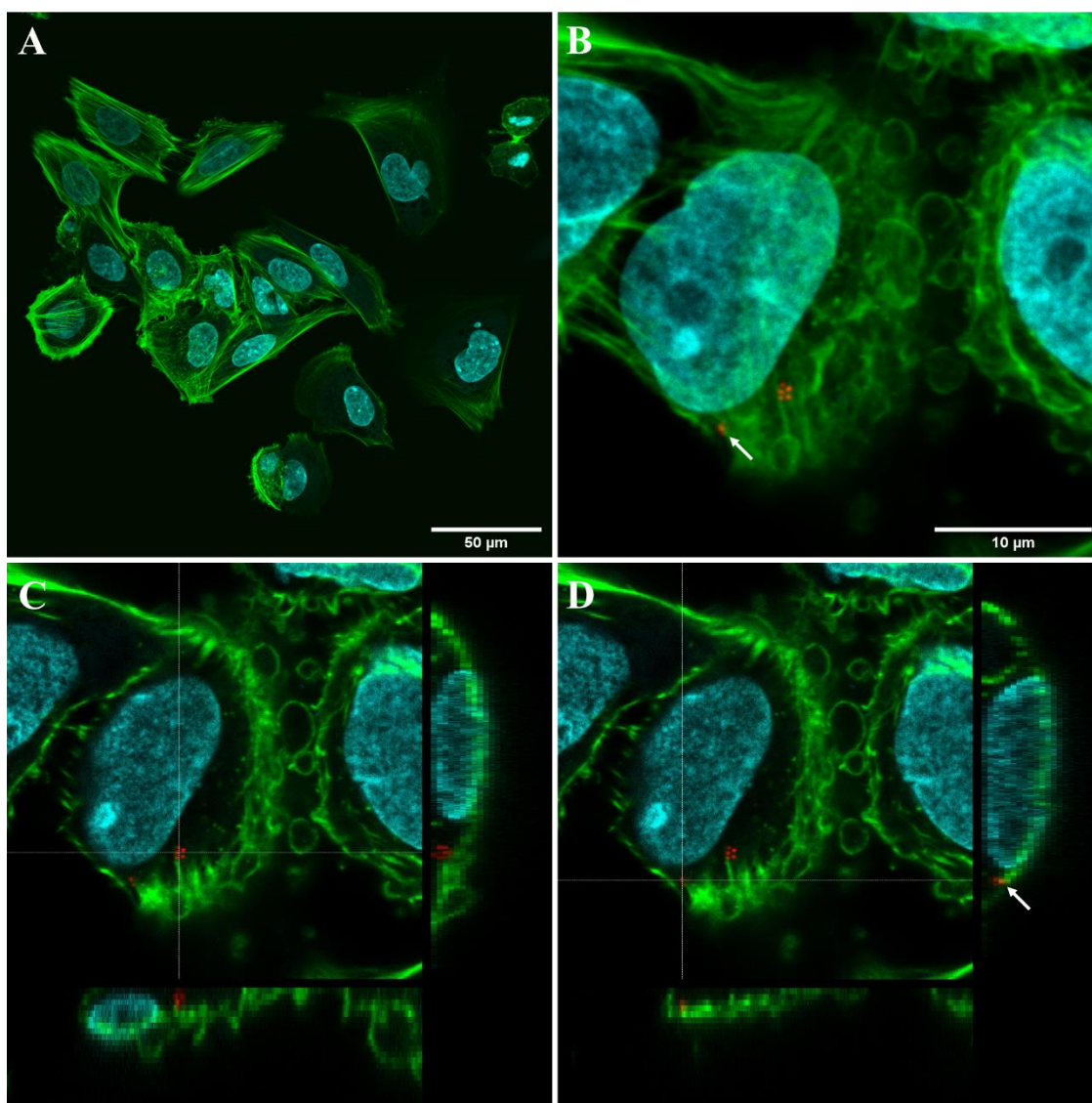


Figure 52. Saos-2 uptake of NiR@PNIPAM. The intracellular accumulation within Saos-2 was observed after being exposed for 12-15 h to NiR@PNIPAM. Cancer cells, as observed by confocal microscopy were double-stained with Hoechst 33342 (cyan nuclei), and Phalloidin-Atto 488 (green microfilaments). NiR@PNIPAM nanoparticles are visible as red dots thanks to NiR fluorescence. A: Control. B: PNIPAM-

exposed culture. C and D: Orthogonal view from different planes (XY, XZ or YZ). Nanoparticles are visible in perinuclear locations, and also close to the cell membrane (white arrows)

In general, NiR@PNIPAM nanoparticles could be observed inside the cells in all osteosarcoma lines tested. They were either grouped and enclosed in membrane vesicles, or free in the cytosol.

Part II

Mesenchymal stem cells

The homing of MSC towards tumour sites is well established (Lin et al., 2019). The need of vehicles with specific tumour-targeting capacity makes these cells an ideal candidate for the vectorization of drugs and drug-loaded nanoparticles. MSC of different origin were evaluated and compared, as there is some controversy about if cells from different sources can potentiate the cytotoxic effect of the chemotherapeutic drug or, on the contrary, give protection to cancer cells.

1. Effect of free and encapsulated PTX on MSC

In order to establish the ability of huAD-MSC and huBM-MSC to act as a carrier for PTX, either free or encapsulated, the effect of the drug in these cell was studied. Cell viability was assessed, by resazurin assay, after being exposed, for 24 h, to growing concentrations of PTX+NiR@PNIPAM, NiR@PNIPAM and PTX. As expected, a concentration-dependent effect of the drug was observed in both huAD-MSC and huBM-MSC. However, cell viability was above 75 % in all cases, showing a certain resistance of MSCs to PTX, in short-term exposures, which makes them suitable as carrier candidates. No significant differences were observed in cell response to different presentations of PTX (**Figure 53**). Microscopy observations showed that the higher tested concentrations of both nanoparticles (1 and 2 μ M), produced considerable precipitation, so that the culture surfaces appeared opaque after 1 h of exposure, making it impossible to observe the MSC. Besides, the precipitation of PTX+NiR@PNIPAM and NiR@PNIPAM could exert mechanical stress and damage cells, leading to overestimation of MSC death. For this reason, 100 nM was selected as an appropriate concentration for the following experiments.

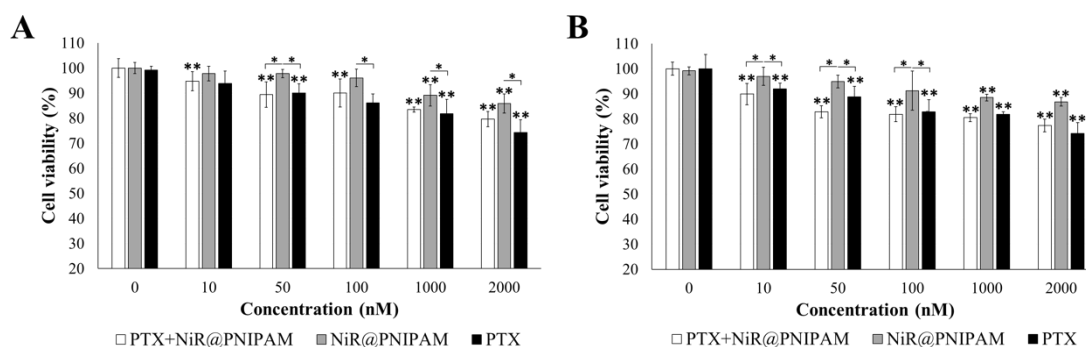


Figure 53. *In vitro* toxicity evaluation of PTX+NiR@PNIPAM, NiR@PNIPAM and PTX in MSC. huAD-MSC (A) and huBM-MSC (B) were exposed to different concentrations of PTX+NiR@PNIPAM, NiR@PNIPAM and PTX for 24 h. The viability was assessed by resazurin assay. One asterisk represent statistical significance within a treatment groups, while two asterisks show significance compared to the negative control according to a two-way ANOVA test followed by Tukey's multiple comparisons test ($p < 0.05$). Data are represented as mean \pm SD.

2. Cell uptake

To confirm the suitability of MSC as a cellular vehicle for drug-loaded nanoparticle delivery, the internalization of NiR@PNIPAM was evaluated by confocal microscopy and TEM.

Presence of a fluorescent tag, NiR, in both drug-loaded and unloaded nanoparticles enabled their visualization by a laser scanning confocal microscopy. Both types of nanoparticle were observed as clusters within the cell (**Figure 54**).

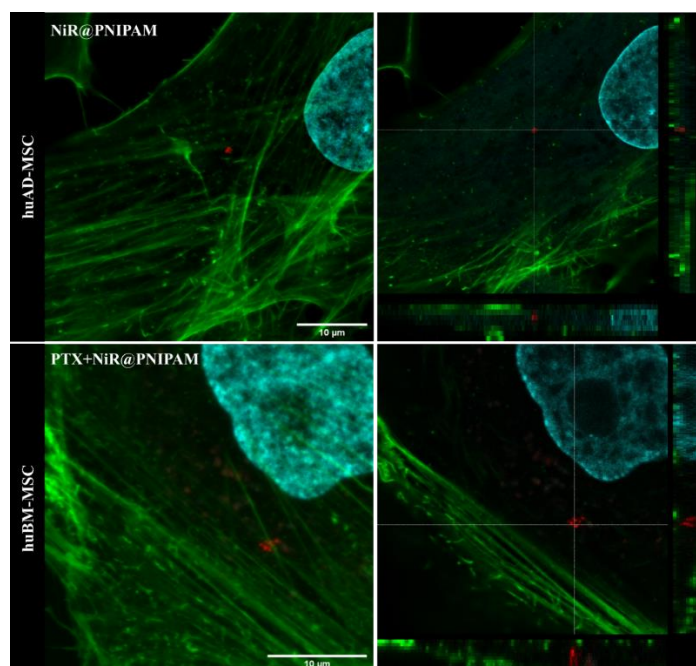


Figure 54. huAD-MSC and huBM-MSC uptake of nanoparticles. huAD-MSC and huBM-MSC were exposed to 100 nM of NiR@PNIPAM and PTX+NiR@PNIPAM for 24 h, fixed and double-stained with Hoechst 33342 (cyan), to label nuclei, and phalloidin-Atto 488 (green), to label actin microfilaments.

PNIPAM nanoparticles are visible in red due to their NiR tag. Pictures were acquired with confocal scanning laser microscope. Red dots represent the nanoparticles. The second column show orthogonal view from different planes (XY, XZ or YZ) of NiR@PNIPAM and PTX+NiR@PNIPAM uptake.

For TEM, NiR@PNIPAM was chosen, in order to not disturb cell morphology. TEM images showed cellular internalization of the nanoparticle, which was localized in vesicles (**Figure 55**).

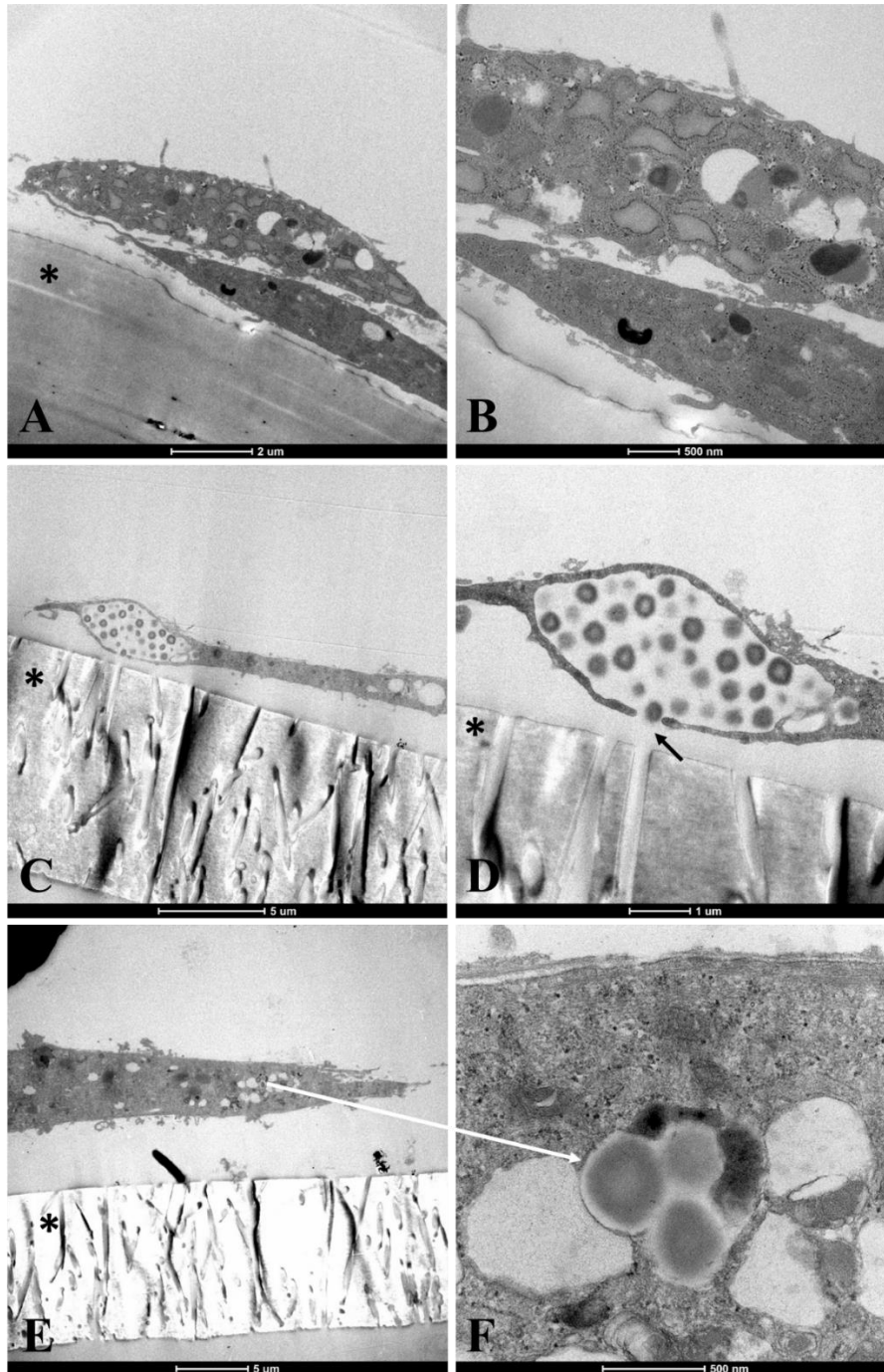


Figure 55. TEM images of huAD-MSC incorporation of NiR@PNIPAM. The first column (A, C and E) shows widefield images. The second column (B, D and F) shows higher magnifications of the images on the left. A – B: Control cultures, not exposed to the nanoparticle. C-F: huAD-MSC exposed to 100 nM

of NiR@PNIPAM for 24 h. (*) Transwell filter. Black arrow in D points to a membrane aperture, suggestive of nanoparticle internalization or release. White arrow shows the NiR@PNIPAM loaded vesicle.

TEM and confocal scanning laser microscope confirm the eligibility of huAD-MSC as a cellular vehicle to carry the nanomaterial for further *in vitro* and *in vivo* studies.

In case of PTX the internalization was not checked for two reasons. First, the drug lacked any tag, making its visualization difficult. Second, our goal was to load MSC with encapsulated drug in order to avoid damage to the cell vehicle and have a certain control over drug release. In the case of the thermosensitive PNIPAM, this control would be exerted by controlling the temperature at the target tissue.

3. Migration of MSC carrying drug-loaded nanoparticles

Once checked that huAD-MSC could incorporate PNIPAM nanoparticles, next step was to confirm that these cells would retain their tumour-homing capacity in spite of the nanoparticle load. To test this, wound healing assays were performed in huBM-MSC and huAD-MSC that had been previously loaded with PTX+NiR@PNIPAM, NiR@PNIPAM or PTX.

First wound healing assay performed was a scratch assay, based on the creation of a gap within a confluent cell monolayer by scratching it with a pipette tip. Control (not loaded) MSC and MSC carrying NiR@PNIPAM took 2 days to close the gap (**Figure 56**), once again confirming the safety of PNIPAM nanoparticles at the cellular level. However, exposure of MSC to either 100 nM of PTX+NiR@PNIPAM or 100 nM PTX slowed the closure of the gap, and these cultures took 7 days to fill the defect. The behaviour of MSC from two origins was the same. For this reason, result are shown for huBM-MSC (**Figure 56**). Since NiR@PNIPAM exposure did not affect cellular processes involved in gap closure, it is likely that the slower gap filling observed in PTX+NiR@PNIPAM is due to partial release of PTX from the nanoparticle.

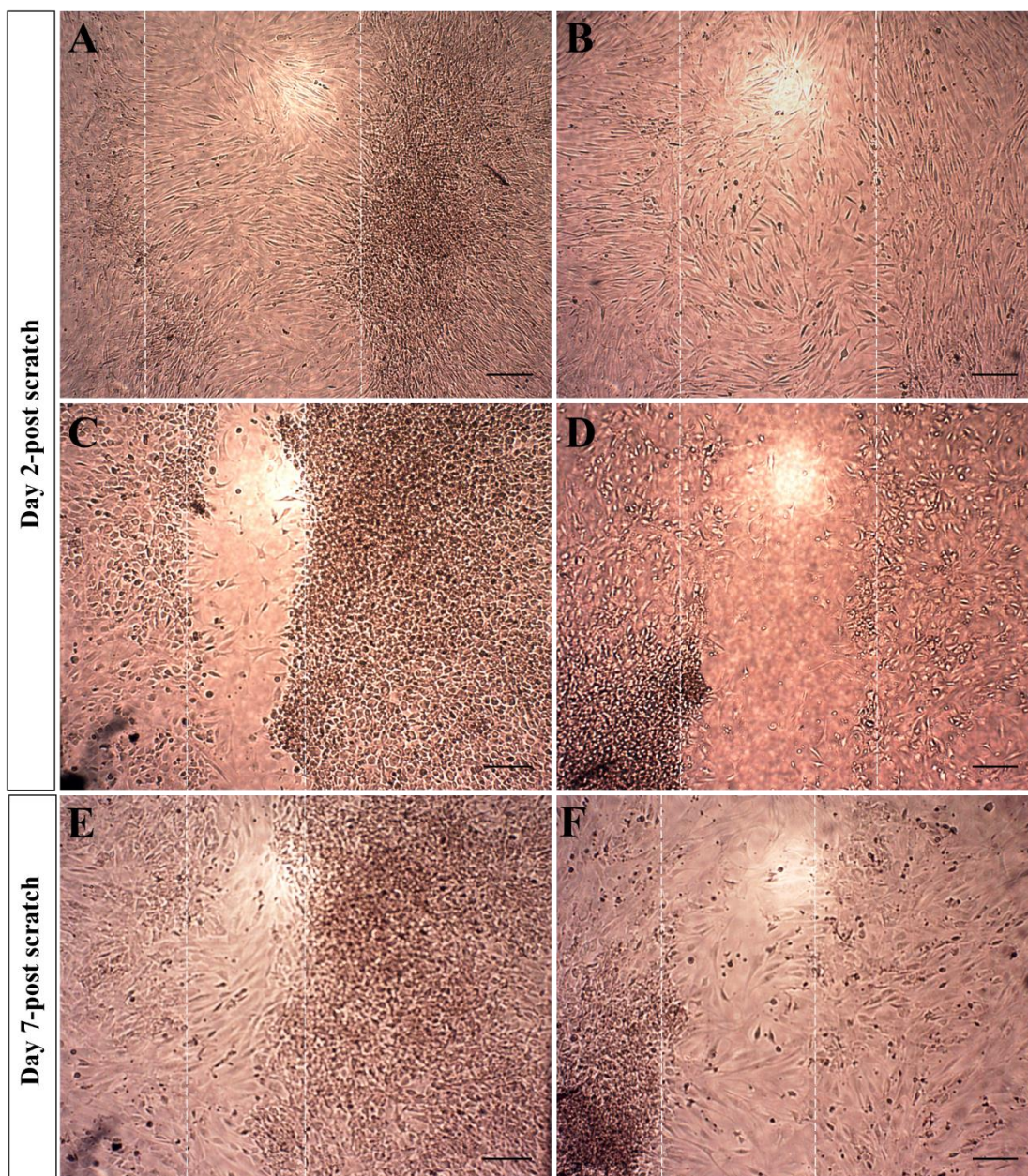


Figure 56. Scratch assay in huBM-MSC. A: Control. B: Cells carrying NiR@PNIPAM. C and E: Cells carrying PTX+NiR@PNIPAM. D and F: Cells exposed to PTX. White dotted lines mark the scratched area (i.e. the gap created in the cell monolayer). Scale bar = 50 μm . Similar results were found for huAD-MSC (data not shown).

Even though the scratch assay is an inexpensive and very simple method, it produces high variability and low reproducibility, as the gap formed by the pipet tip is not always a straight line or the gap has a varying area. During scratching some cells are partially detached that later reattach to the well plate, and contribute to the overestimation of the gap-filling rate. Additionally, scratch procedure can affect the results by damaging the cells. In order to get precise and uniform response a 2-well insert assay was performed. This alternative, more precise method, confirmed the results observed in the scratch assay (**Figure 57**).

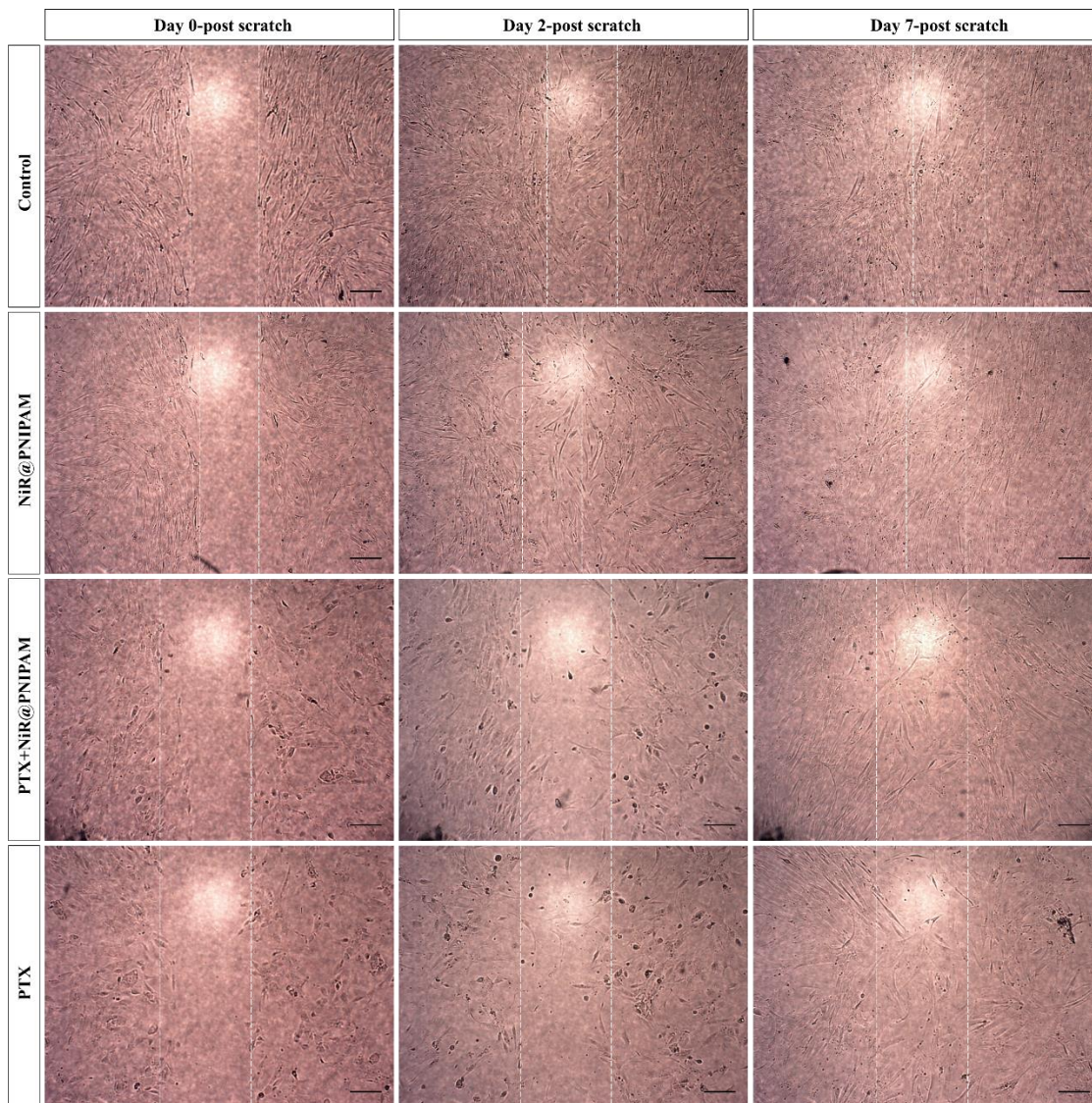


Figure 57. 2-well insert assay in huBM-MSC. huBM MSC were seeded in 2 well silicone inserts and exposed to 100 nM of PTX+NiR@PNIPAM, NiR@PNIPAM and PTX for 24 h. Then the inserts were removed and the treatment medium was changed for a fresh medium without treatment. Pictures were acquired at days 0, 2 and 7 post-insert removal. White dotted lines mark the gap area, which has a 500 μm width. Scale bar = 50 μm .

The results of huAD and huBM-MSC indicate that the exposure to both PTX presentations does not affect cellular mechanisms involved in gap-filling (proliferation and migration) in a permanent way after the treatment is stopped, as almost full recovery was achieved at day 7. However, it should be reasonable to take into account the fact that these cell properties were partly compromised. Possibly modifications in PNIPAM will be needed to guarantee it releases the chemotherapeutic agent after temperature rises over 37 °C.

4. Conditioned medium

MSC loading and release of a sufficient amount of the drug cargo is crucial to be able to target and kill malignant cells. A sustained drug (or its metabolite) release to the medium is expected. To verify the release of PTX from MSC carrying PTX+NiR@PNIPAM, as well as to confirm that the negative effects seen in osteosarcoma are caused by drug and not by factors released from cell vehicle, conditioned media was collected from huAD and huBM-MSC cultures exposed to 100 nM of the two presentations of PTX, and their effect evaluated by resazurin assay in osteosarcoma cell lines. Media from unexposed MSC cultures, and media that had not been in contact with cells, were used as controls. To differentiate both controls, conditioned media from MSC not exposed to PTX, in any presentation, will be hereafter called “CM Control”, while control media not in contact with cells will be called “CM Blank”.

To be sure the negative effects that can be observed in cancer cells are not influenced by factors released from MSC, the CM of both control and blank were first evaluated on cancer cells. After 4 days of exposure the viability of three osteosarcoma cell lines was slightly affected (Figure 58), but in no case there was a significant difference between media conditioned by untreated MSC and media not in contact with any cells (CM Control and CM Blank). Therefore, the decrease in viability could not be attributed to factors released by the cells, but rather to the characteristics of the medium itself. Possibly the high glucose concentration in DMEM-hg, the medium used to culture MSC, is responsible for the observed decrease in cell viability. Some authors have described that high glucose concentration can induce oxidative stress in cancer cell lines, including osteosarcoma, leading to apoptosis (Abbasi, Khosravi, Aidy, & Shafiei, 2016; Luo et al., 2018).

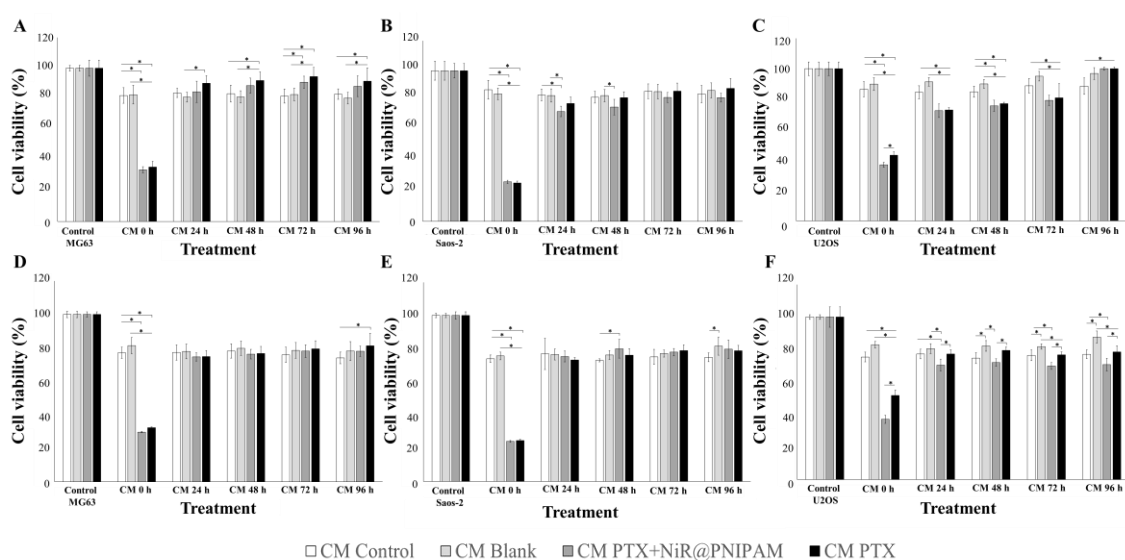


Figure 58. huAD and huBM-MSC anti-proliferative activity against osteosarcoma cell lines. CM was collected from huAD (A-C) and huBM (D-F) MSC at time 0, 24, 48, 72 and 96 h. CM Control corresponds

to MSC in DMEM-hg medium. CM Blank, DMEM-hg that was not in contact with cells. huAD and huBM-MSC were treated with 100 nM of PTX+NiR@PNIPAM and PTX for 24 h. CM was collected at time 0 (includes the treatment), 24, 48, 72 and 96 h post-treatment removal. MG63 (A and D), Saos-2 (B and E) and U2OS (D and F) were exposed to CM for 4 days. Osteosarcoma control consisted from cells in their corresponding medium. Cell viability was assessed by resazurin assay. Asterisk shows statistical significance ($p < 0.05$) according to a two-way ANOVA test followed by Tukey's multiple comparisons test. Data are represented as mean \pm SD.

In case of CM from huAB and huBM-MSC exposed to 100 nM PTX+NiR@PNIPAM or PTX, the anti-tumour effects were not observed (**Figure 58**). Possibly, these cells were not able to incorporate a considerable amount of different presentations of PTX, as the CM with the treatment (time 0) was potent enough to reduce the viability of three osteosarcoma cells lines after 4 days of exposure. Also, the amount of PTX+NiR@PNIPAM, PTX or its metabolite released was probably too low, so that it had no or little effect on the cancer cells. Another alternative to be explored in the future studies is the absence of drug, or drug-loaded nanoparticle, release from MSC when there is no direct cell-to-cell contact with osteosarcoma cells.

5. Time-lapse

In order to detect the release of NiR@PNIPAM from huAD-MSC, a time-lapse against Saos-2 cells was performed for 24 h. The nanoparticles within the cellular vehicle were not observed in the vast majority of huAD-MSC. Moreover, release of NiR@PNIPAM from cellular vehicle was not detected during the time-lapse. However, independently from the cargo huAD-MSC were able to migrate and induce apoptosis in Saos-2 cells (**Figure 59A and B**). The interaction between huAD-MSC and Saos-2 was observed (**Figure 59C**). From a previous preliminary study between MG63 and non-charged huAD-MSC with NiR@PNIPAM cell-cell interactions though filipodia extension were detected (**Figure 59D**). It suggests a physical contact with huAD-MSC to be responsible of the visible induction of cancer cell death. The time-lapse videos of the corresponding images can be observed in the following link:

<https://www.dropbox.com/sh/rzd32playkux1ye/AACkKJ8gQhw4kcWTvU9WzYTva?dl=0>

These results show that independently from NiR@PNIPAM mesenchymal stem cells from adipose tissue origin to induce apoptosis in two different osteosarcoma cell lines, Saos-2 and MG63.

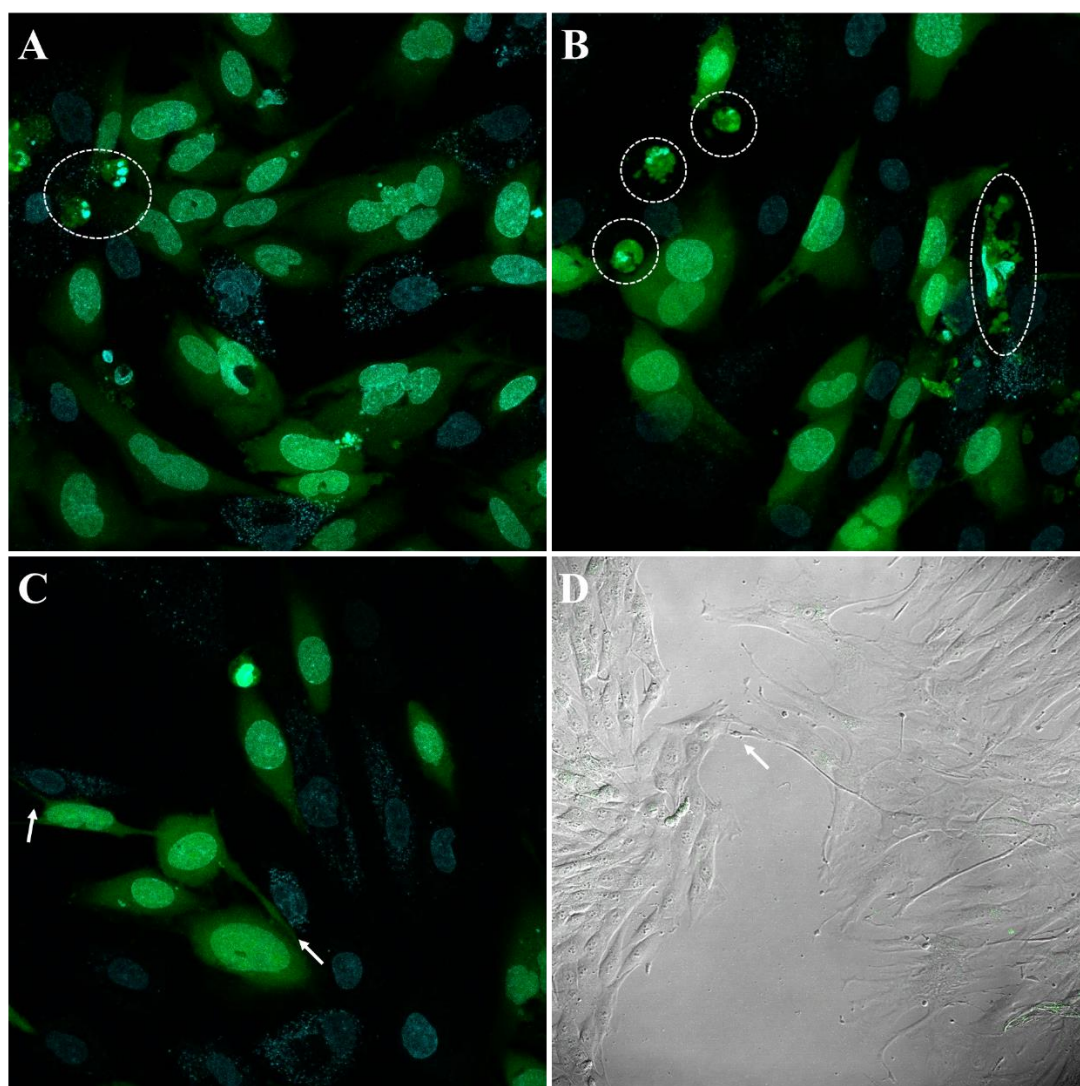


Figure 59. Representative images from time-lapse. huAD-MSC was previously exposed to 100 nM of NiR@PNIPAM for 24 h. Later the cells were collected by trypsinization and seeded over Saos-2 (A-C). For a preliminary time-lapse, represented in a black field, MG63 were seeded on the left side of a 2 well culture-insert, while huAD-MSC on the right side (D). Images were captured every 20 min using a confocal scanning laser microscope during 24 h. huAD-MSC were stained with Hoechst 33342 (cyan) and Saos-2 with CellTracker Green (green). White dotted circles represent apoptotic Saos-2 cells. White arrows show physical interaction of huAD-MSC with osteosarcoma cells.

Part III

Osteosarcoma: combination treatment

The main goal of the present part was to evaluate the possibility of PTX repositioning in osteosarcoma treatment and if its incorporation into a thermo-responsive nanoparticle would be feasible and modify, or not, the efficiency of the drug as an antitumoral agent. For a targeted delivery of the drug towards the sarcoma, MSC were evaluated, by virtue of their tumour-homing capacity.

In strategy I we showed the ability of ORI to improve the efficiency of DOX when both drugs were given together. Knowing the ability of the natural product to enhance the anti-tumour effects of DOX, and considering that the concentration of drug delivered by MSC is limited and might not be enough for an efficient tumour killing, we speculated ORI could be used to enhance PTX effect, so that small amounts of the drug were still enough to exert an effective anti-tumour action. For this reason, combination therapy of ORI and PTX were tested, in both formulations: PTX and PTX+NiR@PNIPAM.

To evaluate the combined effect of ORI and PTX+NiR@PNIPAM or PTX on Saos-2 viability, cells were simultaneously exposed to different concentrations of the drugs. Based on the cytotoxicity data obtained from previous experiments, different ORI doses (CD_{50} , $CD_{50}/2$ and $CD_{50}/10$) were combined with different PTX+NiR@PNIPAM and PTX doses (CD_{50} , $CD_{50}/2$ and $CD_{50}/10$).

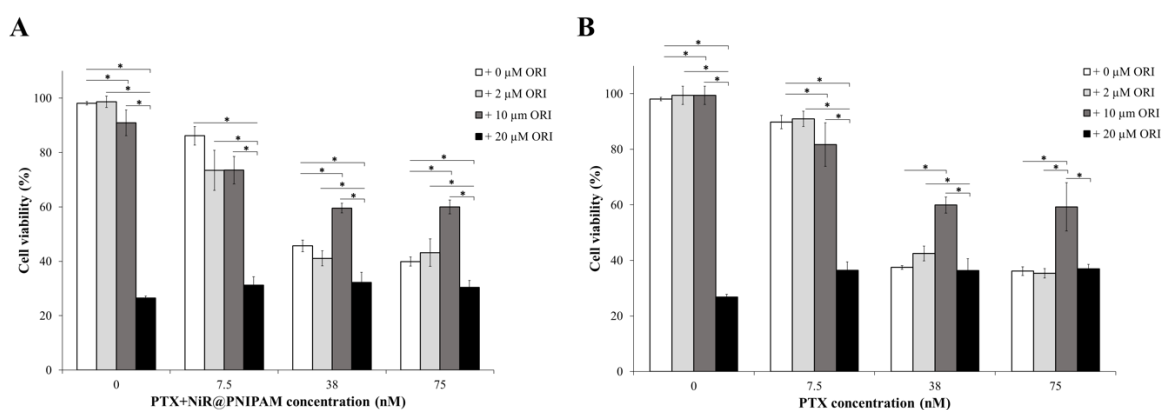


Figure 60. Toxicity evaluation of PTX+NiR@PNIPAM/PTX and ORI combination. Saos-2 cells were exposed for 48 h to concentrations of PTX+NiR@PNIPAM (A), PTX (B) and ORI corresponding to their CD_{50} , $CD_{50}/2$ and $CD_{50}/10$; as well as to combinations of drugs. Cell viability was assessed by resazurin assay. Asterisk shows statistical significance ($p < 0.05$) according to a two-way ANOVA test followed by Tukey's multiple comparisons test. Data are represented as mean \pm SD.

As observed in **figure 60**, in Saos-2 cells the combined treatment with PNIPAM-encapsulated PTX produced similar or only slightly better cytotoxic effects, as compared to the drugs administrated alone. The best outcome was observed when both presentations of PTX were combined with 20 μ M of ORI. Even though these combinations were able to reduce the viability of Saos-2 cell treated with PTX+NiR@PNIPAM or PTX (as compared to PTX alone), it didn't prove to be better than the individual administration of 20 μ M ORI. When the concentration of the natural product was reduced, no improvement was observed, as the cytotoxicity outcome was similar that produced by the individual drugs. Actually, CI calculation showed that most of the combinations tested presented antagonistic effects (**Figure 61**). Based on these data, a suitable combination for Saos-2 treatment would be 38 nM PTX+NiR@PNIPAM or PTX plus 2 μ M ORI.

This combination is synergistic for both the PNIPAM-encapsulated drug, and the free drug, although in the latter there is only a slight synergistic effect.

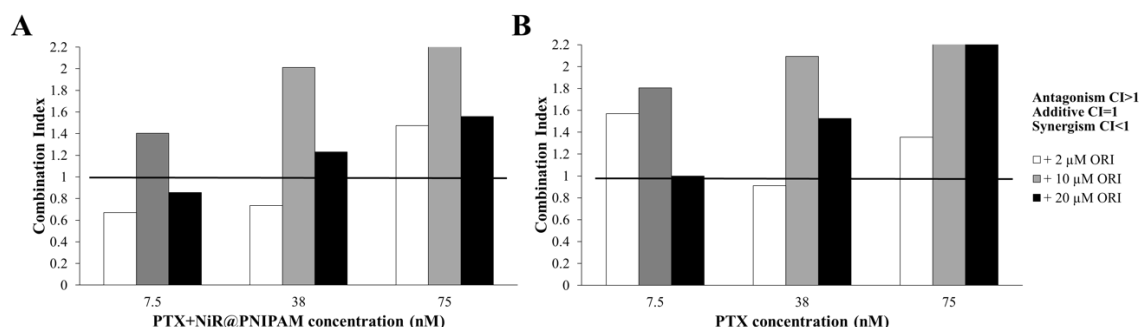


Figure 61. CI of Saos-2. Cells were treated with different combinations of PTX+NiR@PNIPAM, or PTX, and ORI. The black line corresponds to CI of 1, representing an additive effect. Antagonism and synergism were considered when the values were above and below the line (CI=1), respectively.

The exposure of U2OS to different combinations of ORI and the two presentations of PTX, showed better outcome when the chemotherapeutic drug was given together with the natural product, as compared to the drug-loaded nanoparticle (Figure 62). This might be attributed to the different mechanisms involved in cellular uptake of free and encapsulated PTX.

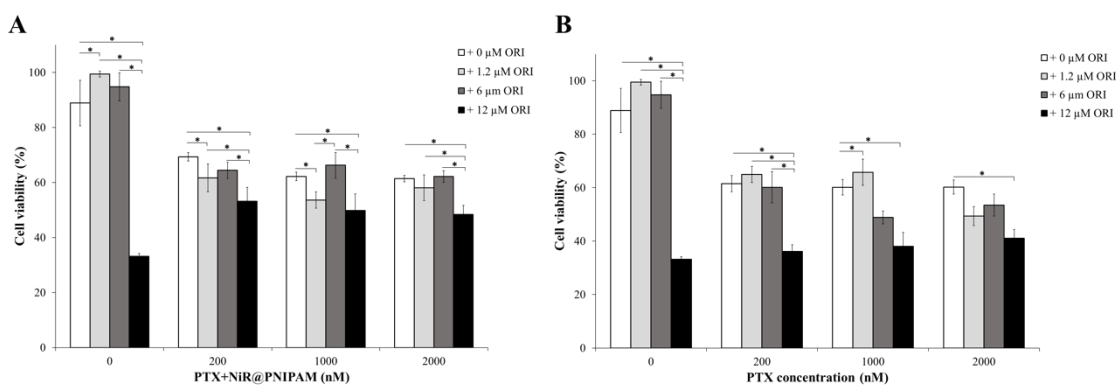


Figure 62. Toxicity evaluation of PTX+NiR@PNIPAM/PTX and ORI combination. U2OS cells were exposed for 48 h to concentrations of PTX+NiR@PNIPAM (A), PTX (B) and ORI corresponding to their CD_{50} , $CD_{50}/2$ and $CD_{50}/10$; as well as to combinations of drugs. Cell viability was assessed by resazurin assay. Asterisk shows statistical significance ($p < 0.05$) according to a two-way ANOVA test followed by Tukey's multiple comparisons test. Data are represented as mean \pm SD.

These discrepancies were confirmed by the CI (Figure 63). There were few candidates of PTX+NiR@PNIPAM and ORI combinations and those leading to synergistic effect based on CI values were only slightly more cytotoxic than PTX+NiR@PNIPAM alone. Taking into account both viability outcome and CI, the better drug combination among those tested would be 200 nM

PTX+NiR@PNIPAM/PTX and 12 μ M ORI. As observed for Saos-2, none of the combined treatments caused a higher cytotoxicity than oridonin when administered at its CD_{50} .

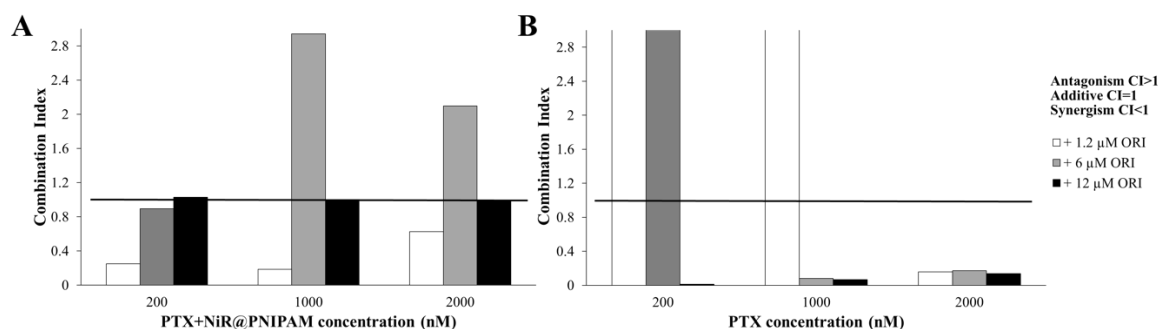


Figure 63. CI of U2OS. Cells were treated with different combinations of PTX+NiR@PNIPAM/PTX and ORI. The black line corresponds to CI of 1, representing an additive effect. Antagonism and synergism were considered when the values were over and under the line (CI=1), respectively.

Finally, the combination treatment yielded better results in MG63 cells, where the combined drugs caused a greater cytotoxicity than individual drugs (**Figure 64**).

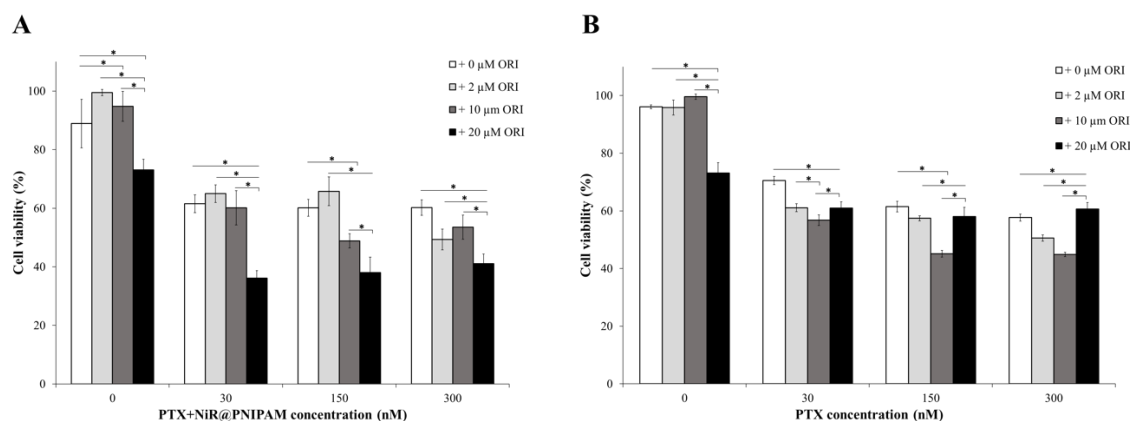


Figure 64. Toxicity evaluation of PTX+NiR@PNIPAM/PTX and ORI combination. MG63 cells were exposed for 48 h to concentrations of PTX+NiR@PNIPAM (A), PTX (B) and ORI corresponding to their CD_{50} , $CD_{50}/2$ and $CD_{50}/10$; as well as to combinations of drugs. Cell viability was assessed by resazurin assay. Asterisk shows statistical significance ($p < 0.05$) according to a two-way ANOVA test followed by Tukey's multiple comparisons test. Data are represented as mean \pm SD.

In contrast to Saos-2 and U2OS, in MG63 cells cell viability data and CI results paralleled each other, both for free and PNIPAM-encapsulated PTX, showing multiple combinations that had a synergistic effect and yielded a higher cytotoxicity than the individual drugs. The best synergistic combination was 150 nM PTX+NiR@PNIPAM or PTX and 10 μ M ORI (**Figure 65**).

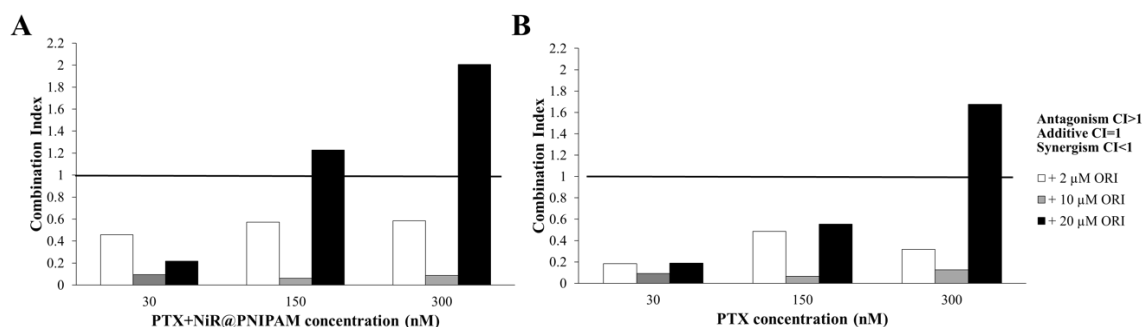


Figure 65. CI of MG63. Cells were treated with different combinations of PTX+NiR@PNIPAM/PTX and ORI. The black line corresponds to CI of 1, representing an additive effect. Antagonism and synergism were considered when the values were over and under the line (CI=1), respectively.

Discussion

Osteosarcoma is a bone cancer whose aggressiveness is determined by a rapid formation of metastasis, typically in lungs, at early stages. At this point, the malignant cells are typically chemoresistant (Gorlick & Khanna, 2010). This suggests innovative strategies are necessary in order to improve osteosarcoma therapy and patient's prognosis. Drug repositioning is an alternative to novel drug development, where all the biocompatibility and toxicity studies have been previously done, reducing time and cost. The original intention of drug repurposing was to give a second chance for those drugs that failed in their initial application. Right now this approach has become a breakthrough for rare and neglected diseases, such as conventional osteosarcoma, which represents 0.2% of all the malignant tumours (Nowak-Sliwinska et al., 2019; Osakwe & Rizvi, 2016; Picci, 2007). For this type of cancer the standard drug combination is the so-called MAP triad, composed of drugs that mainly target the genetic material, and cause severe and permanent aftermath (Chou & Gorlick, 2006). PTX is a chemotherapeutic agent approved by FDA for breast, lung and ovarian cancer treatment (Farrar & Jacobs, 2020). Instead of acting on a DNA level, this drug disrupt the microtubules, causing a cell cycle arrest in G₂/M phase with subsequent induction of apoptosis (Zhang et al., 2014). The efficiency against other types of tumours and a completely different mechanism of action made PTX to be a candidate in this work. Already the cytotoxic effects of the chemotherapeutic agent was evaluated and confirmed in several osteosarcoma cell lines (Guo, Zeng, Dong, & Lei, 2002; Liu, Song, Lin, & Liu, 2010). However, it was reported these cells to be less sensitive to PTX compared to other agents (Kim et al., 2013). Moreover, as any chemotherapeutic drug, PTX lacks specificity so it targets both healthy and malignant cells. In order to improve PTX efficiency and consequently osteosarcoma treatment, different strategies were evaluated, such as encapsulation within a thermo-responsive nanoparticle, MSC as a cell vehicle of the nanocarrier and combination therapy with ORI.

PNIPAM nanoparticles loaded with a fluorescent tag (Nile Red or NiR) have been used in the present work. Their characterization by TEM confirmed that both PTX-loaded and PTX-unloaded nanoparticles (PTX+NiR@PNIPAM and NiR@PNIPAM, respectively) were spherical in shape and presented a homogeneous dispersion with no signs of aggregation. Presence of PTX inside the nanoparticle was responsible for a higher average diameter of PTX+NiR@PNIPAM (420.16 ± 33.33 nm) as compared to NiR@PNIPAM (307.69 ± 19.88 nm), at room temperature. The capacity to respond and release the drug in response to temperature changes (temperature superior to 32 °C) is the principal property of PTX+NiR@PNIPAM, and will determine the success of the treatment. Size changes were confirmed with a transition from room temperature to 37 °C, a temperature cells are normally exposed. PTX+NiR@PNIPAM presented a size suitable for intravenous administration, as capillaries are 5 μ m in diameter (Singh & Lillard, 2009).

In order to assess if osteosarcoma is sensitive to PTX, and if this sensibility is affected by PNIPAM encapsulation, osteosarcoma cells were exposed to both PTX and PTX+NiR@PNIPAM, and their viability analysed. Different cell lines were used for this purpose because there are distinct types of osteosarcoma and, even within the same tumour, the malignant tissue is composed of a heterogeneous population with different morphologies and mutations status. As expected, the studied osteosarcoma cell lines showed distinct sensitivity to PTX drug. Of the three cell lines analysed, U2OS was the most resistant, while Saos-2 was the most sensitive. Similar results were described by Tsai *et al.*, who found U2OS cells to be more resistant to PTX, as compared to MG63 (Tsai, Huang, Su, & Tang, 2014). The differences were attributed to an increased level of connective tissue growth factor (CTGF), which promotes the expression of survivin, a molecule that inhibits apoptosis, leading to malignant cell survival. On the contrary, suppression of CTGF makes cells more sensitive to the effects of PTX (Tsai *et al.*, 2014). Another mechanism proposed for PTX resistance is autophagy, a process of self-degradation where damaged organelles or non-functional proteins are recycled. In cancerous cells, autophagy can promote cell survival or death depending on the cell type. In osteosarcoma, it has been proposed that autophagy helps malignant cells to withstand chemotherapy conditions by facilitating the maintenance of energy levels (Glick, Barth, & Macleod, 2010). The exact mechanism implicated in this process is still unclear, but there are some suggestions. Guo *et al.* showed that autophagy is activated in MG63 through hypoxia-inducible factor (HIF)-1 α (Gou *et al.*, 2015). In general, available studies agree that inhibition of autophagy sensitizes osteosarcoma cells to the effects of PTX (Gou *et al.*, 2015; Jakhar *et al.*, 2018; Kim *et al.*, 2013).

Be it autophagy or another “escape” mechanism, the present results agree with previous studies showing that osteosarcoma cells are not as sensitive to PTX as they are to other chemotherapeutic drugs. In a viability assay of the present work, osteosarcoma cell lines were not drastically affected after 2 days exposure to PTX, and 4 days-exposures were required for acute

effects. Similar viability values have been reported by Kim *et al.* for Saos-2 (Kim *et al.*, 2013). This type of studies, where reduced sensitivity of osteosarcoma cells to PTX were observed, were the reason behind the encapsulation of the chemotherapeutic drug within a nanoparticle and its posterior vectorization in MSC as cellular vehicle.

In an effort to evaluate the effectiveness of different PTX treatment strategies, the exposure time was selected based on the study of a pH-responsive PTX-loaded hollow-poly(4-vinylpyridine) (P4VP) nanoparticle performed in the group that synthesized the thermo-responsive nanomaterial for the present work (Contreras-Cáceres *et al.*, 2017). Additionally, there are many reports exposing osteosarcoma cells to the effects of PTX for 4 days (Kim *et al.*, 2013; Liu *et al.*, 2010). In general, it was possible to observe a time-dependent decrease in the viability of three osteosarcoma cell lines treated with a nanomolar range of the chemotherapeutic agent. In general, at the last day of exposure with the maximum concentration tested (25 nM) almost no differences were observed between PTX and PTX+NiR@PNIPAM in MG63 and Saos-2. This is attributed to the fact that the amount of the chemotherapeutic agent alone was adjusted to be the same as in the nanoparticle during the treatment. On the other hand, significant differences were observed between PTX and PTX+NiR@PNIPAM in U2OS. In this case, the encapsulated drug was more cytotoxic compared to the chemotherapeutic agent alone. However, no differences were observed in the concentration below 25 nM, suggesting that the pipetting could be the reason behind. In any case, these results indicate PTX+NiR@PNIPAM to be suitable for osteosarcoma treatment as its cytotoxicity outcome was similar to PTX alone.

The toxicity of drug-free NiR@PNIPAM was assessed in both malignant (osteosarcoma) and healthy (huAD-MSC and huBM-MSC) cells. The nanoparticle showed to be safe, meaning that the observed anti-cancer effects were caused by PTX instead of impurities that could remain after the synthesis of NiR@PNIPAM. It is in agreement with several studies that demonstrated the safety of this type of nanoparticle (Capella *et al.*, 2019; Salimi *et al.*, 2018). All this confirms NiR@PNIPAM to be a proper drug carrier that can be securely administered in future animal models or clinical trials.

Although monolayer cell cultures have traditionally been the standard method for *in vitro* drug efficiency assessment, there are nowadays many doubts related to the correlation between results obtained from 2D culture systems and the *in vivo* scenario (Sitarski, Fairfield, Falank, & Reagan, 2018). Cells grown in a monolayer are flat and elongated, and only one part of the cell is in contact with the environment. Besides morphology, cells in 2D and 3D display different gene expression profiles, and different cell-cell and cell-extracellular matrix (ECM) interactions. 3D culture systems are considered much more representative of the *in vivo* situation. The spheroid architecture simulates an avascular tumour and it is a valid technique to study the effects in a

small fraction of aggregated cancer cells. *In vivo*, tumour microtissues are composed of three regions, according to the availability of oxygen and nutrients: proliferative region, located in the periphery; hypoxic region, beneath the proliferative one; and necrotic region, at the centre of the spheroid (Breslin & O'Driscoll, 2013; De Luca et al., 2018; Sitarski et al., 2018). Previous 3D studies in osteosarcoma cells have revealed an agreement between results obtained through this method and those obtained *in vivo* (Breslin & O'Driscoll, 2013). Some bone cancer microtissues have shown a higher drug resistance as compared to cells grown in a monolayer (De Luca et al., 2018). For this reason, it was important to confirm the effects of PTX+NiR@PNIPAM and PTX in a 3D cell culture system.

Three different methods were used to produce osteosarcoma spheroids or microtissues, centrifugation, hanging-drop and extracellular matrix encapsulation. The first two rely exclusively on cell-to-cell contacts for forming and maintaining the spheroid architecture, while the third creates a microenvironment based on extracellular matrix proteins, typically collagen type I. Of the three osteosarcoma cell lines tested, only the non-epithelioid MG63 could form cellular spheroids, while the epithelioid U2OS and Saos-2 needed an extracellular matrix to form microtissues. In a similar way Martella *et al.* used the same three osteosarcoma cell lines, but the effects of the treatment were evaluated only in MG63 microtissues (Martella et al., 2018). However there are studies that produced Saos-2 and U2OS spheroids (Rimann et al., 2014; Tan, Chia, Toh, Goh, & Nathan, 2013). Actually, it is reported that not all tumour cell lines are able to form tight microtissues, but instead generate 3D irregular aggregates with different size and morphology (Sant & Johnston, 2017).

According to the results of the present work, MG63 spheroids are sensitive to PTX drug either in its free form and encapsulated in PNIPAM nanoparticles. Interestingly, the outcome of the drug-loaded nanoparticle was much better compared to the drug alone. LIVE/DEAD assay showed that spheroids exposed to increasing concentrations of PTX were not as much reduced in size as microtissues exposed to the same concentrations of PTX+NiR@PNIPAM. This may be an indication of the ability of the nanoparticle to elude tissular mechanisms of drug resistance. The presence of increased necrotic region is indicative of the effects on cell spheroids and to avoid much more of this the negative impact cells have to decrease its permeability. Monteiro *et al.* described that the formation of the central necrotic region in osteosarcoma spheroids promotes drug resistance and tumorigenesis (Monteiro, Gaspar, Ferreira, & Mano, 2020), a resistance that is possibly mediated by a reduction of tissue permeability, according to different studies (Baek, Seo, Kim, Hulme, & An, 2016; Monteiro et al., 2020). In the present study, spheroids treated with free PTX, particularly with high doses (*e.g.* 25 nM), showed a much more conspicuous necrotic region than those treated with PNIPAM-encapsulated PTX. According to Monteiro *et al.* and other authors, the presence and densification of the MG63 spheroids core could be a protective

mechanism against the adverse effects of PTX, because in this way the permeability to the drug will drop. In the case of PTX+NiR@PNIPAM the drug is not “visible” to malignant cells as it is localized in a non-toxic nanocarrier.

Another possible explanation for the better outcome of the nanoparticle-encapsulated drug lies on the different routes for cellular incorporation followed by PTX and PTX+NiR@PNIPAM. The cellular uptake of nanocarrier occurs commonly through endocytosis, which is a slower process compared to the passive diffusion of the PTX (Kou, Sun, Zhai, & He, 2013). The gradual escape of the nanoparticles from lysosomal vesicles and posterior release of the chemotherapeutic agent within the cytoplasm could explain the presence of what seems to be pre-apoptotic cells observed as yellow spots in LIVE/DEAD images after being MG63 spheroids exposed to PTX+NiR@PNIPAM. Martella *et al.* treated MG63 microtissues with free and encapsulated PTX in keratin nanoparticles, found a higher spheroid size reduction in the second case. TEM images showed the presence of a central necrotic region and apoptotic nuclei that made the authors suggest to be caused by prolong effects of PTX on MG63 spheroids (Martella *et al.*, 2018).

The tumour tissue is well represented in a 3D cell culture, but this model is simplistic as it doesn't include ECM, which normally represents 60% of the tumour mass. Its composition and density within cancer tissue usually affects drug transport, as well as nutrients and oxygen supply. Therefore, ECM has a huge influence on cancer cell proliferation, migration and invasion (Henke, Nandigama, & Ergün, 2020; Li & Kumacheva, 2018; Monteiro *et al.*, 2020). Collagen type I was employed in this work as it is widely used to recreate the ECM (Li & Kumacheva, 2018). For this reason, it was necessary to evaluate the apoptosis induction by PTX+NiR@PNIPAM and PTX in 3D collagen spheroids. MG63, Saos-2 and U2OS matrix mix was grown in suspension in a 96 ULA well plate, where no differences in cell viability were detected. This means presence of ECM confers protection to the cancer cells by acting as a barrier for PTX+NiR@PNIPAM and PTX to diffuse in the structure. Consequently, the amount of the chemotherapeutic drugs that is able to reach cancer cells is very low. These results were opposite to those obtained from 2D system. Similarly it was reported MSC grown in the collagen hydrogel were resistant to the effects of the treatment in comparison to the cells in the monolayer and the same explanation was proposed (Li & Kumacheva, 2018). Even though the collagen I spheroids generate an optimal microenvironment as observed from non-treated cell viability of three osteosarcoma cell lines, the matrix doesn't permit to establish an architecture similar to a 3D microtissues that in general is composed from three main regions. However, it is proposed collagen spheroids to be useful to study the early events of cancer initiation, while cell microtissues can be used to evaluate the later stages of the disease (Monteiro *et al.*, 2020).

The degradation of ECM by protease release is fundamental for cancer cells to migrate and invade surrounding tissues. The increasing concentrations of both free and encapsulated PTX decreased the proliferation and migration in MG63 and U2OS. Apart from stabilizing microtubules, it is known the chemotherapeutic agent to inhibit the synthesis of collagenase (Stearns & Wang, 1992). Osteosarcoma cells in collagen spheroids receiving higher concentrations presented a less compacted structure suggesting apoptosis induction followed by a reduced amount of secreted proteases.

To assess the cellular uptake of the nanoparticles, the intracellular distribution of NiR@PNIPAM was evaluated in the three osteosarcoma cell lines. In this case, NiR@PNIPAM were preferred over PTX+NiR@PNIPAM because the presence of PTX could affect cellular morphology. All three osteosarcoma cell lines studied incorporated NiR@PNIPAM, but each of them presented different uptake rates, being U2OS the slower at internalizing PNIPAM nanoparticles. This points to the uptake rate as being unique for each cell line. The internalization of PNIPAM nanoparticles of different sizes has been studied in several cell lines (Guo et al., 2017; Naha et al., 2010). It is really hard to say if NiR@PNIPAM is accumulated in cytoplasm or in vesicles. Different studies suggest that the nanoparticle is retained in the lysosomes and remain there for more than 24 h (Guo et al., 2017; Naha et al., 2010; Salvati et al., 2011). In case of the present work, accumulation of NiR@PNIPAM inside a large vesicle was observed from orthogonal slices in MG63. However, there is no further evidence to confirm if these were lysosomes.

The nanoparticles used in this work were not vectorized, as they were not designed to target a specific tissue. Although the surface of nanoparticles can be modified, there are, to date, no specific markers of osteosarcoma. Consequently, no target molecule is available for vehicle vectorization. An alternative strategy is to take advantage of the tumour-homing ability of MSC (Duchi et al., 2013; Pessina et al., 2011; Yao et al., 2017). These cells can be easily obtained and expanded *in vitro*, they are hypoimmunogenic and can home to both the primary tumours and the metastatic ones (Porada & Almeida-Porada, 2010). At first, both adipose and bone marrow-derived MSC were used in this study, because MSC from different tissues may have different homing capacity and different ability to incorporate and release the cargo (Porada & Almeida-Porada, 2010; Strioga, Viswanathan, Darinskas, Slaby, & Michalek, 2012). However, huAD-MSC were finally selected as vectorization vehicle, for practical reasons: large amounts can be obtained in a much simpler way, as compared to huBM-MSC.

The ability of huAD-MSC to incorporate NiR@PNIPAM and PTX+NiR@PNIPAM was studied by confocal microscopy and TEM in huAD-MSC. Both methods demonstrated nanoparticles to be accumulated within the cell. TEM images showed NiR@PNIPAM to be either

in free form or in membrane-enclosed clusters. The latter could be lysosomes or late-endosomes. The lack of additional surface modifications in PNIPAM nanoparticle make it release the cargo when the temperature is above its LCST of 32 °C. It is reasonable to speculate part of the encapsulated PTX to be released when cells are incubated with PTX+NiR@PNIPAM in standard culture conditions, where the temperature is 37 °C. For this reason, it was necessary to find a proper concentration of the cargo-loaded nanoparticle that would incorporate a considerable amount of encapsulated drug and compensate PTX loss due to PNIPAM characteristics. huAD-MSC and huBM-MSC showed to tolerate concentrations up to 2 μM of PTX and PTX+NiR@PNIPAM with slight reduction in cell viability after 24 h of exposure. As no drastic changes were observed it was decided to carry on with 100 nM of both presentations of the chemotherapeutic agent. Reduction in proliferation and migration capacities of MSC from two different sources was detected after being in contact with the selected concentration of both PTX and PTX+NiR@PNIPAM. However, the cells were able to recover, evident from the gap filling in both scratch and insert assays, at day 7 post-treatment cessation. On the contrary, control and treated cells with 100 nM of NiR@PNIPAM were able to close the aperture at day 2 post-treatment removal. Similar finding were reported by Harris *et al.* where a decrease in the proliferation of human adipose-derived MSC was observed after PTX exposure. Although the growth capacities were recovered after day 5 post-treatment cessation (Harris et al., 2017). From the results of the present work and based on the equal outcomes of both free and encapsulated PTX, it is possible to conclude the chemotherapeutic drug was partly released to the cell culture medium before the nanoparticle reached the cells during the incubation in standard culture conditions for 24 h. In order to improve the delivery and release of the cargo it would be necessary to increase PNIPAM's LCST from 32 °C to 37.5 or 38 °C. In this way it is expected the loss of PTX to be avoided improving the outcome of the therapy. The temperature that induce structural changes of the nanocarrier can be modified to a desired one by performing a copolymerization synthesis with different monomers (Hoare & Pelton, 2007). Interestingly, independently from the cargo, physical interaction between huAD-MSC and osteosarcoma cells was observed during the time-lapse. Moreover, the physical interaction between these two different cell lines induced apoptosis in Saos-2. This suggests the soluble factors possibly released by cancer cells to be a potent driving force for huAD-MSC. Even though the amount of incorporated and released cargo-loaded nanoparticle was impossible to detect, it was possible to confirm the anti-cancer activity of these cells. Currently, there are several discrepancies of MSC role in cancer therapy as both pro and antitumorigenic effects were observed (Babajani, Soltani, Jamshidi, Farjoo, & Niknejad, 2020; Xuan, Tian, Zhao, Sun, & Huang, 2021). In case of osteosarcoma the majority of reports agree these cells to facilitate malignant cell growth. On the contrary, very few studies showed MSC inhibition of bone cancer cells growth and migration. One of such includes the exposure of MG63 to the conditional medium from Wharton's jelly-derived MSC from the umbilical cord

(Zheng, Wang, Chen, Hua, & Cai, 2018). Also in the present work it was possible to observe the anti-tumour effects of huAD-MSC against Saos-2 where a clear apoptosis induction was detected during a time-lapse study. In general, it is believed the outcome to depend on the cancer type, tissue of origin of MSC and interaction between malignant cells, MSC and tumour microenvironment (Kaur Sarhadi et al., 2021).

The next step was to evaluate the capacity to incorporate and release both presentations of PTX from huAD and huBM-MSC. For this CM was collected at different time points and given to three different osteosarcoma cell lines. The viability of cancer cells was not affected and these results suggests that MSC should be exposed to concentrations much higher than 100 nM of PTX and PTX+NiR@PNIPAM to guarantee a sufficient release of cargo to have observable effects on osteosarcoma. The first study to demonstrate PTX uptake and release from MSC without genetic manipulation was Pessina *et al.* The authors had to expose the cellular vehicle with 2,000 ng/mL of PTX for 24 h and from this initial amount only 8% was incorporated after 24 h. However the released amount in CM was enough to inhibit the proliferation of cells from glioblastoma and prostate carcinoma *in vitro* (Pessina et al., 2011).

Concerned by the low toxicity induced by PTX in osteosarcoma, which has been also described by other authors (Hattinger et al., 2016; Nallani, Goodwin, Buckley, Buckley, & Desai, 2004; Wagner, Yin, Eaves, Currier, & Cripe, 2014), the effects of PTX and PTX+NiR@PNIPAM in combination with oridonin was evaluated. The rationale for choosing these drugs were the results about oridonin effect in osteosarcoma cell lines, obtained in a previous work (strategy I), and the different mechanism of action of ORI and PTX, which could be advantageous in cancer treatment, as they will simultaneously act on different targets, reducing the possibility of malignant cells survival. Up to date, this is the first study evaluating the combination of ORI and PTX, alone or encapsulated in osteosarcoma.

Importantly, the selected combinations were composed from drugs doses lower CD_{50} of those individually administered. In this way the PTX and ORI associated adverse side effects can be reduced by decreasing the concentration of the drugs, while maintaining the efficiency. However, in case of U2OS some side effects of the combination could be attributed to 12 μ M of ORI, as doses over 10 μ M showed to affect the morphology of NH OST. Moreover, in Saos-2 the majority of concentrations tested of both presentations of PTX and ORI lead to antagonistic effects. This means that the studied doses were not the appropriate one and a wide range of concentrations should tested in order to find those pairs of drugs that work in synergy.

Finally, better cytotoxicity and CI values were obtained when the natural product was combined with a non-encapsulated chemotherapeutic drug compared to PTX+NiR@PNIPAM. The mechanism of uptake could be responsible of the observed effects. As it was previously

mentioned the nanoparticles are normally incorporated through endocytosis, while the chemotherapeutic drug enters through passive diffusion. It is tentative to speculate that the anti-cancer effect of PTX+NiR@PNIPAM plus ORI could be similar to the combination of PTX and natural product when the exposure is more than 48 h. In this way it would be possible to achieve prolonged results, as ORI will be the first one to reach its target due to passive diffusion and later there is a PTX related outcome after being released from the nanoparticles. This idea should be proved in future studies. Even though there is no direct study evaluating the effects of ORI and PTX, Wang *et al.* demonstrated synergistic effects between geridonin, an ORI derivative, and PTX through apoptosis induction (Wang et al., 2016). Based on all these findings the combination treatment for osteosarcoma should consist from PTX plus ORI and the simultaneous administration of both drugs can be proposed as another MSC independent approach to be evaluated in posterior *in vitro* and *in vivo* studies for bone cancer treatment. On the other hand, the uptake and mechanistic characteristic of PTX+NiR@PNIPAM+ORI should be taken into account as it may guarantee a prolong effect, where the nanocarrier could be locally administrated within the tumour tissue and the natural product given through intravenous injection.

Future perspectives

Many questions and curiosities arose during the realization of the experimental part of the present thesis. Also there are several aspects that had to be left unattended. One of such included the *in vivo* part that was impossible to perform due to lack of time. For this reason to be able to answer to the proposed questions and complement the findings of the present thesis the following experiments, briefly summarized, will be done as a part of a postdoc study:

- Evaluate the effects on tumour reduction of established PTX+NiR@PNIPAM dose administered through intravenous injection in a xenograft model.
- Expose huAD-MSC to a varying concentrations of PTX+NiR@PNIPAM for 24 h and collect CM at different time points *in vitro*. Test the anti-tumour effect of the obtained CM in three osteosarcoma cell lines.
- Evaluate the intravenous administration of PTX+NiR@PNIPAM loaded huAD-MSC in a xenograft model.
- Study the pathway involved in the uptake and posterior intracellular distribution of both NiR@PNIPAM and PTX+NiR@PNIPAM in osteosarcoma cells.
- Evaluate the cytotoxicity-related cellular events of PTX/PTX+NiR@PNIPAM and ORI combination in osteosarcoma cells. Based on this results focus on a specific pathway that can be implicated. Finally, evaluate the effects of a selected combination in a xenograft model.

V. General discussion

“It is said that if you know your enemies and know yourself, you will not be imperilled in a hundred battles; if you do not know your enemies but do know yourself, you will win one and loose one; if you do not know your enemies nor yourself, you will be imperilled in every single battle”.

Sun Tzu

In spite of the many advances in the discovery of novel drugs and administration methods, the treatment options for osteosarcoma have not changed substantially in the last 30 years, and the chemotherapeutic regime applied for this cancer remains the same as in the last century. Consequently, the survival rates of the patients have not changed for decades (Anderson, 2016; González-Fernández et al., 2017). This fact points to the need of developing novel strategies that would improve the patient's quality of life. For this reason, three different approaches were evaluated in the present work. Combination treatment is a methodology already known and used in chemotherapy. Doxorubicin is one of the most efficient drugs for osteosarcoma and other cancer types. However, its applicability is limited by the occurrence of a life-threatening side effect in form of cardiotoxicity, which can drive to heart failure later in life (Janeway & Grier, 2010; Thorn et al., 2011). To eliminate or minimize this drawback, the possibility of combining doxorubicin with oridonin was evaluated. It was found that both drugs work in synergy, so that ORI coadministration could maintain the anti-cancer efficiency of DOX even when used at low doses. The response observed for different cell lines to the combination treatment should be taken into account for future development of this combination therapy. It would be interesting to observe the outcome of this two-drug regime as part of a neoadjuvant chemotherapy. There is chance for it to be better tolerated than the current three-or-more drug regimen used to treat osteosarcoma. However, before, it is necessary to study ORI in more detail. For example, it is known that the natural product generates 17 different metabolites whose implication in the observed outcome, and potential effects *in vivo*, are not yet understood (Xiang Li et al., 2021). As any chemotherapeutic agent given at high doses, it is expected the natural product will produce some side effects that should previously be identified, in order to control them during a possible future therapy. In the present work, it was found that ORI produces toxicity in osteoblasts *in vitro*, and organ damage *in vivo*. These results are in agreement with a few studies reporting concerns about ORI's safety (Xiang Li et al., 2021).

It is common that chemotherapeutic drugs do not to work against cancer cells because they have acquired resistance over time. The introduction of a novel agent to the list of drugs commonly used to treat bone cancer represents a feasible solution. For this purpose, an FDA approved chemotherapeutic drug can be repositioned from one type of cancer to another with no need for additional biodistribution or safety studies. One of such drugs could be PTX, which has been herein evaluated, and corroborated its effectiveness against osteosarcoma cells, with some degree of variation as to its effectiveness, depending of the osteosarcoma type studied. This chemotherapeutic agent could be administered in a two-drug or multi-drug regime instead of DOX. Never besides DOX, as administration of both drugs together would enhance cardiotoxicity (Minotti et al., 2001). Also, the combination of PTX and ORI represents another reasonable

alternative for osteosarcoma treatment. However, further studies are still needed to determine the right doses of both drugs that would act in synergy against cancer cells.

The proposed treatment strategies showed in the present work produced a variable response between different osteosarcoma cell lines. These results are in a line with heterogeneity of cancer cells that are known to be composed from malignant cells carrying a variety of mutations. Different patients diagnosed with the same tumour type would respond in a distinct way to the standard chemotherapy. Moreover, variations in the mutation status can be observed within the primary cancer (Fisher et al., 2013). Thus, it is reasonable to suggest chemotherapy not to be universally effective against all types of osteosarcoma. However, the viable solution is to switch from standard treatment option to a personalized medicine. In this way, patients will receive a specific drug combination that could be administered in several manners according to genetic and morphological background of the tumour. At this moment, there are not specific molecular markers that would diagnose osteosarcoma and predict its response to the available treatment options. Hence, this research line is essential and should be taken into account in order to improve the survival of paediatric patients, where an early diagnosis before metastasis manifestation would be possible. Already there studies reporting several molecular markers but their implication in osteosarcoma still need further investigation (Raimondi et al., 2017).

The outcome of the chemotherapeutic agents can be enhanced by encapsulating them inside a nanoparticle. In this way, the nanocarrier would target specifically the malignant cells and release the cargo under specific stimuli. This approach would facilitate the reduction drug doses, thus minimising adverse effects. However, the presence of different physiological barriers within the body make it difficult for nanocarriers to reach its target (Du, Yu, & Zheng, 2018). Most importantly, there is still an absence of cell surface markers that characterizes osteosarcoma cells, making them distinguishable from healthy cells. Therefore, there is not target available to vectorize nanoparticles towards osteosarcoma cells. A possible solution is the use of MSC as cellular vehicle of drug-loaded nanoparticle. One of the important characteristics of these cells is their ability to migrate and home to tissues where there is damage, inflammation or hypoxia (Ghaedi et al., 2011). Therefore, MSC loaded with a nanocarrier can infiltrate deeply inside the tumour tissue, where hypoxia predominates and release the drug-loaded nanoparticle. On the contrary, nanocarriers administered alone would only target the cancer cells located in the periphery of the tumour, without the possibility to reach the inner zone, thus affecting the outcome of the treatment. The cell and nanoparticle based approach would be a feasible solution for osteosarcoma patients with relapsed cancer or for those who failed the first-line treatment.

The strategies explored in the present work are promising for bone cancer treatment. Further improvements in the combination of MSC and nanoparticles are still needed before this system is

applied to patients. Each of the evaluated approaches is believed to eliminate cancer cells, improve drug tolerability and reduce adverse effects. Thus, facilitating paediatric patients a better quality of life.

VI. Conclusions

“It is time, it is time for me too to depart. Like an old man who has outlived his contemporaries and feels a sad inner emptiness, Kostolglotov felt that evening that the ward was no longer his home, even though ... there were the same old patients asking the same old questions again and again as though they had never been asked before: ... Will they cure me or won't they? What other remedies are there that might help?”

Aleksandr Solzhenitsyn, Cancer Ward

Strategy I: Doxorubicin and oridonin combination

- Osteosarcoma cell viability is reduced after exposure to doxorubicin or oridonin, administered alone or in combination.
- Osteosarcoma cell lines present different sensitivity to the individual drugs being U2OS the most sensitive and Saos-2 the most resistant to both doxorubicin and oridonin exposure.
- Oridonin enhances the cytotoxic effects of doxorubicin in Saos-2 cell line, but not in U2OS.
- An increased cell uptake of doxorubicin occurs in Saos-2 cells exposed simultaneously to doxorubicin and oridonin. This effect is not observed in U2OS cells.
- Doxorubicin and oridonin combination induces apoptosis in osteosarcoma through mitochondrial toxicity, possibly mediated by ROS.
- Increasing concentrations of oridonin elicit morphological changes in human osteoblasts *in vitro*, suggesting lower doses to be optimal for safe administration, with few unwanted side effects in combination treatment.
- Saos-2 cells form tumours when xenotransplanted into athymic nude mice. These tumours produce osteoid extracellular matrix, with calcified extracellular matrix nodules.
- The combination treatment of doxorubicin and oridonin *in vivo* reduces tumour volume compared to the untreated athymic nude mice but, at the tested doses, the effects of the combination are similar to those of the drugs being administered alone.
- Administration of oridonin *in vivo* produces minimal fibrosis.
- Presence of oridonin in the combination treatment seems to have slightly protective effects against liver damage.
- In Saos-2-like osteosarcomas, the co-administration of oridonin in doxorubicin-based chemotherapeutic regimes could allow reducing the dosage of doxorubicin, thus reducing the unwanted secondary-effects of this drug.

Strategy II: Paclitaxel, MSC and combination treatment

- Both nanoparticles, NiR@PNIPAM and PTX+NiR@PNIPAM, are spherical in shape with the ability to respond to variations in the temperature.
- NiR@PNIPAM are biocompatible nanoparticles, not showing any cytotoxicity in the tested osteosarcoma cell lines, nor in mesenchymal stem cells derived from bone marrow or adipose tissue.
- Osteosarcoma cell lines are sensitive to paclitaxel, both alone or encapsulated in NiR@PNIPAM, making the drug a feasible candidate for the treatment of this type of cancer.
- Osteosarcoma cell lines possess different sensitivity to paclitaxel, and this differential sensitivity is not affected by PNIPAM encapsulation. Saos-2 is the most susceptible and U2OS is the most resistant to both PTX and PTX+NiR@PNIPAM.
- MG63 cell line is able to form spheroids, while U2OS and Saos-2, with epithelial morphology, are not.
- PTX and PTX+NiR@PNIPAM have similar cytotoxicity in 2D cultures, but a greater sensitivity to the drug-loaded nanoparticle is observed in 3D cultures.
- When grown in 3D cultures within a supportive extracellular matrix (collagen), all the osteosarcoma cell lines present less sensitivity to PTX, either free or encapsulated.
- The migration capacities of MG63 and U2OS are affected with increasing concentrations of both free and encapsulated PTX.
- NiR@PNIPAM accumulates in a perinuclear region within osteosarcoma cells. The nanoparticle is either enclosed in membrane vesicle or free in cytosol.
- Human adipose and bone marrow-derived MSC are resistant to a wide range of both PTX and PTX+NiR@PNIPAM concentrations during short-term exposure.
- NiR@PNIPAM are incorporated, accumulated within the vesicles and possibly released by huAD-MSC, supporting the eligibility of these cells as cellular vehicle for cancer treatment.
- Human adipose and bone marrow-derived MSC recover its proliferation and migration capacities after paclitaxel treatment removal.
- The concentration of paclitaxel, either alone or encapsulated in PNIPAM, given to human adipose and bone marrow-derived MSC is not enough to have observable cytotoxicity in osteosarcoma cells exposed to their conditioned medium.

- A physical contact between paclitaxel-loaded human adipose tissue-derived MSC and osteosarcoma cells (Saos-2 and MG63) could be the trigger for the malignant cells apoptosis.
- The cytotoxicity outcome of free paclitaxel combined with oridonin is better than the simultaneous administration of PNIPAM-encapsulated paclitaxel with oridonin.

VII. Bibliography

Abbasi, N., Khosravi, A., Aidy, A., & Shafiei, M. (2016). Biphasic Response to Luteolin in MG-63 Osteoblast-Like Cells under High Glucose-Induced Oxidative Stress. *Iranian Journal of Medical Sciences*, 41(2), 118-125.

Adamopoulos, C., Gargalionis, A. N., Basdra, E. K., & Papavassiliou, A. G. (2016). Deciphering signaling networks in osteosarcoma pathobiology. *Experimental Biology and Medicine*, 241(12), 1296-1305.

Ai, J. W., Liu, B., & Liu, W. D. (2017). Folic acid-tagged titanium dioxide nanoparticles for enhanced anticancer effect in osteosarcoma cells. *Materials science & engineering. C, Materials for biological applications*, 76, 1181–1187.

Albini, A., Bruno, A., Gallo, C., Pajardi, G., Noonan, D. M., & Dallaglio, K. (2015). Cancer stem cells and the tumor microenvironment: interplay in tumor heterogeneity. *Connective Tissue Research*, 56(5), 414.

Alexandre, J., Hu, Y., Lu, W., Pelicano, H., & Huang, P. (2007). Novel action of paclitaxel against cancer cells: Bystander effect mediated by reactive oxygen species. *Cancer Research*, 67(8), 3512-3517.

Alexis, F., Pridgen, E., Molnar, L. K., & Farokhzad, O. C. (2008). Factors affecting the clearance and biodistribution of polymeric nanoparticles. *Molecular pharmaceutics*, 5(4), 505-515.

Alqahtani, D., AlSheddi, M., & Al-Sadhan, R. (2015). Epithelioid Osteosarcoma of the Maxilla: A Case Report and Review of the Literature. *International journal of surgical pathology*, 23(6), 495-499.

Alves, A. C., Ribeiro, D., Nunes, C., & Reis, S. (2016). Biophysics in cancer: The relevance of drug-membrane interaction studies. *Biochimica et biophysica acta*, 1858(9), 2231-2244.

Amara, I., Touati, W., Beaune, P., & de Waziers, I. (2014). Mesenchymal stem cells as cellular vehicles for prodrug gene therapy against tumors. *Biochimie*, 105, 4-11.

Anderson M. E. (2016). Update on Survival in Osteosarcoma. *The Orthopedic clinics of North America*, 47(1), 283/292.

Anninga, J. K., Gelderblom, H., Fiocco, M., Kroep, J. R., Taminiau, A. H., Hogendoorn, P. C., & Egeler, R. M. (2011). Chemotherapeutic adjuvant treatment for osteosarcoma: where do we stand?. *European journal of cancer (Oxford, England : 1990)*, 47(16), 2431-2445.

Babajani, A., Soltani, P., Jamshidi, E., Farjoo, M. H., & Niknejad, H. (2020). Recent Advances on Drug-Loaded Mesenchymal Stem Cells With Anti-neoplastic Agents for Targeted Treatment of Cancer. *Frontiers in bioengineering and biotechnology*, 8, 748.

Bacci, G., Ferrari, S., Sangiorgi, L., Picci, P., Casadei, R., Orlandi, M., Iantorno, D., Battistini, A., & Zanone, A. (1994). Prognostic significance of serum lactate dehydrogenase in patients with osteosarcoma of the extremities. *Journal of chemotherapy*, 6(3), 204-210.

Bacci, G., Ferrari, S., Longhi, A., Forni, C., Zavatta, M., Versari, M., & Smith, K. (2002). High-grade osteosarcoma of the extremity: differences between localized and metastatic tumors at presentation. *Journal of pediatric hematology/oncology*, 24(1), 27-30.

Baek, N., Seo, O. W., Kim, M., Hulme, J., & An, S. S. (2016). Monitoring the effects of doxorubicin on 3D-spheroid tumor cells in real-time. *OncoTargets and therapy*, 9, 7207-7218.

Baumann, S., & Hennes, T. (2016). Collagen Accumulation in Osteosarcoma Cells lacking GLT25D1 Collagen Galactosyltransferase. *The Journal of biological chemistry*, 291(35), 18514-18524.

Berendsen, A. D., & Olsen, B. R. (2015). Bone development. *Bone*, 80, 14-18.

Berger A. (2002). Magnetic resonance imaging. *BMJ (Clinical research ed.)*, 324(7328), 35.

Bernardo, M. E., Emons, J. A. M., Karperien, M., Nauta, A. J., Willemze, R., Roelofs, H., ... Fibbe, W. E. (2007). Human mesenchymal stem cells derived from bone marrow display a better chondrogenic differentiation compared with other sources. *Connective Tissue Research*, 48(3), 132-140.

Biga, L. M., Dawson, S., Harwell, A., Hopkins, R., Kaufmann, J., LeMaster, M., ... Runyeon, J. Bone Tissue and the Skeletal System. In *Anatomy & Physiology*. Oregon State University. <https://doi.org/10.1177/089686080802801S03>

Bone Formation and Development - Anatomy and Physiology - OpenStax. (n.d.). Retrieved 3 February 2020, from <https://openstax.org/books/anatomy-and-physiology/pages/6-4-bone-formation-and-development>

Boskey, A. L., & Coleman, R. (2010, December). Critical reviews in oral biology & medicine: Aging and bone. *Journal of Dental Research*.

Boskey, Adele L., & Robey, P. G. (2013). The Composition of Bone. In J. Clifford & M. Rosen (Eds.), *Primer on the Metabolic Bone Diseases and Disorders of Mineral Metabolism* (pp. 49-58). Ames: John Wiley & Sons Inc. <https://doi.org/10.1002/9781118453926.ch6>

Brenner, W., Bohuslavizki, K. H., & Eary, J. F. (2003). PET imaging of osteosarcoma. *Journal of nuclear medicine : official publication, Society of Nuclear Medicine*, 44(6), 930-942.

Breslin, S., & O'Driscoll, L. (2013). Three-dimensional cell culture: the missing link in drug discovery. *Drug discovery today*, 18(5-6), 240-249.

Brigman, B. E., Kumagai, S. G., & McGuire, M. H. (2003). Rotationplasty after failed limb-sparing tumor surgery: a report of two cases. *Clinical orthopaedics and related research*, (415), 254-260.

Bullens, P. H., Minderhoud, N. M., de Waal Malefijt, M. C., Veth, R. P., Buma, P., & Schreuder, H. W. (2009). Survival of massive allografts in segmental oncological bone defect reconstructions. *International orthopaedics*, 33(3), 757-760.

Cahyadi, S. D., Antoro, A., & Swandika, B. (2019). A giant cell rich osteosarcoma of the proximal ulnar bone treated by elbow arthroplasty: A case report. *International journal of surgery case reports*, 58, 157-161.

Calvert, G. T., Randall, R. L., Jones, K. B., Cannon-Albright, L., Lessnick, S., & Schiffman, J. D. (2012). At-risk populations for osteosarcoma: the syndromes and beyond. *Sarcoma*, 2012, 152382.

Capella, V., Rivero, R. E., Liaudat, A. C., Ibarra, L. E., Roma, D. A., Alustiza, F., Mañas, F., Barbero, C. A., Bosch, P., Rivarola, C. R., & Rodriguez, N. (2019). Cytotoxicity and bioadhesive properties of poly-*N*-isopropylacrylamide hydrogel. *Heliyon*, 5(4), e01474.

Cappetta, D., De Angelis, A., Sapio, L., Prezioso, L., Illiano, M., Quaini, F., ... Urbanek, K. (2017). Oxidative Stress and Cellular Response to Doxorubicin: A Common Factor in the Complex Milieu of Anthracycline Cardiotoxicity. *Oxidative Medicine and Cellular Longevity*, 2017, 1521020.

Carrle, D., & Bielack, S. S. (2006). Current strategies of chemotherapy in osteosarcoma. *International orthopaedics*, 30(6), 445-451.

Cavalcanti, S., Meohas, W., Ribeiro, G. D. O., Gholamin, S., Razavi, M., Sa, C. De, ... Kahn, S. A. (2017). Patient-derived osteosarcoma cells are resistant to methotrexate. *PloS one*, 12(9), e0184891.

Chan, E. S. L., & Cronstein, B. N. (2013). Mechanisms of action of methotrexate. *Bulletin of the Hospital for Joint Diseases (Vol. 71)*.

Chan, J. K. C. (2014). The Wonderful Colors of the Hematoxylin–Eosin Stain in Diagnostic Surgical Pathology. *International Journal of Surgical Pathology*, 22(1), 12-32.

Chen, B., Yang, J. Z., Wang, L. F., Zhang, Y. J., & Lin, X. J. (2015). Ifosfamide-loaded poly (lactic-co-glycolic acid) PLGA-dextran polymeric nanoparticles to improve the antitumor efficacy in Osteosarcoma. *BMC cancer*, 15, 752.

Chen, J., Lee, S. K., Abd-Elgaliel, W. R., Liang, L., Galende, E. Y., Hajjar, R. J., & Tung, C. H. (2011). Assessment of Cardiovascular Fibrosis Using Novel Fluorescent Probes. *PLoS ONE*, 6(4), e19097.

Chen, S., Gao, J., Halicka, H. D., Huang, X., Traganos, F., & Darzynkiewicz, Z. (2005). The cytostatic and cytotoxic effects of oridonin (Rubescenin), a diterpenoid from *Rabdosia rubescens*, on tumor cells of different lineage. *International journal of oncology*, 26(3), 579-588.

Chen, Y., Xu, S. F., Xu, M., & Yu, X. C. (2017). Intentional marginal resection of periosteal osteosarcoma in combination with neoadjuvant chemotherapy: A report of two cases and a review of the literature. *Oncology letters*, 13(3), 1343-1347.

Chou, A. J., & Gorlick, R. (2006). Chemotherapy resistance in osteosarcoma: current challenges and future directions. *Expert review of anticancer therapy*, 6(7), 1075-1085.

Chou T. C. (2010). Drug combination studies and their synergy quantification using the Chou-Talalay method. *Cancer research*, 70(2), 440-446.

Chow L. T. (2016). Giant cell rich osteosarcoma revisited-diagnostic criteria and histopathologic patterns, Ki67, CDK4, and MDM2 expression, changes in response to bisphosphonate and denosumab treatment. *Virchows Archiv : an international journal of pathology*, 468(6), 741-755.

Chung, L. H., Wu, P. K., Chen, C. F., Weng, H. K., Chen, T. H., & Chen, W. M. (2016). Pathological fractures in predicting clinical outcomes for patients with osteosarcoma. *BMC musculoskeletal disorders*, 17(1), 503.

Contreras-Cáceres, R., Leiva, M. C., Ortiz, R., Díaz, A., Perazzoli, G., Casado-Rodríguez, M. A., Melguizo, C., Baeyens, J.M., López-Romero, J.M., & Prados, J. (2017). Paclitaxel-loaded hollow-poly(4-vinylpyridine) nanoparticles enhance drug chemotherapeutic efficacy in lung and breast cancer cell lines. *Nano Research*, 10, 856-875.

Cooper, G. M. (2000). *The Cell: A Molecular Approach*. Sunderland: Sinauer Associates.

Correa H. (2016). Li-Fraumeni Syndrome. *Journal of pediatric genetics*, 5(2), 84-88.

Cowan, P. T., & Kahai, P. (2021). Anatomy, Bones. In *StatPearls*. StatPearls Publishing.

Czerniak, B. (1998). *Dorfman and Czerniak's Bone Tumors*. Philadelphia: Elsevier Inc.

Dadwal, A., Baldi, A., & Kumar Narang, R. (2018). Nanoparticles as carriers for drug delivery in cancer. *Artificial cells, nanomedicine, and biotechnology*, 46, 295-305.

Dasari, S., & Tchounwou, P. B. (2014). Cisplatin in cancer therapy: molecular mechanisms of action. *European journal of pharmacology*, 740, 364-378.

De Jong, W. H., & Borm, P. J. (2008). Drug delivery and nanoparticles: applications and hazards. *International journal of nanomedicine*, 3(2), 133-149.

De Luca, A., Raimondi, L., Salamanna, F., Carina, V., Costa, V., Bellavia, D., Alessandro, R., Fini, M., & Giavaresi, G. (2018). Relevance of 3d culture systems to study osteosarcoma environment. *Journal of experimental & clinical cancer research: CR*, 37(1), 2.

Deeb, D. A., Dick, E., Sergot, A. A., Sundblom, L., & Gedroyc, W. (2011). Magnetic resonance imaging of the small bowel. *Radiography*, 17(1), 67-71.

Demelash, A., Pfannenstiel, L. W., Liu, L., & Gastman, B. R. (2017). Mcl-1 regulates reactive oxygen species via NOX4 during chemotherapy-induced senescence. *Oncotarget*, 8(17), 28154-28168.

Dessypris, E. N., Brenner, D. E., Baer, M. R., & Hande, K. R. (1988). Uptake and Intracellular Distribution of Doxorubicin Metabolites in B-Lymphocytes of Chronic Lymphocytic Leukemia. *Cancer Research*, 48(3), 503-506.

Deyrup, A. T., Montag, A. G., Inwards, C. Y., Xu, Z., Swee, R. G., & Krishnan Unni, K. (2007). Sarcomas arising in Paget disease of bone: a clinicopathologic analysis of 70 cases. *Archives of pathology & laboratory medicine*, 131(6), 942-946.

Ding, Y., Ding, C., Ye, N., Liu, Z., Wold, E. A., Chen, H., ... Zhou, J. (2016). Discovery and development of natural product oridonin-inspired anticancer agents. *European journal of medicinal chemistry*, 122, 102-117.

Dos Reis, S.B., de Oliveira Silva, J., Garcia-Fossa, F., Leite, E. A., Malachias, A., Pound-Lana, G., Mosqueira, V. C. F., Oliveira, M. C., de Barros, A. L. B., de Jesus, M. B. (2021). Mechanistic insights into the intracellular release of doxorubicin from pH-sensitive liposomes. *Biomedicine and Pharmacotherapy*, 134:110952.

Douglas, J. (2011). Pathogenesis of Osteochondrosis. In *Diagnosis and Management of Lameness in the Horse* (pp. 617-625). Elsevier.

Du, B., Yu, M., & Zheng, J. (2018). Transport and interactions of nanoparticles in the kidneys. *Nature Reviews Materials*, 3(10), 358-374.

Duchi, S., Sotgiu, G., Lucarelli, E., Ballestri, M., Dozza, B., Santi, S., Guerrini, A., Dambruoso, P., Giannini, S., Donati, D., Ferroni, C., & Varchi, G. (2013). Mesenchymal stem cells as delivery vehicle of porphyrin loaded nanoparticles: effective photoinduced in vitro killing of osteosarcoma. *Journal of controlled release : official journal of the Controlled Release Society*, *168*(2), 225-237.

Duray, P. H., Cuono, C. B., & Madri, J. A. (1986). Demonstration of cutaneous doxorubicin extravasation by rhodamine-filtered fluorescence microscopy. *Journal of surgical oncology*, *31*(1), 21-25.

Durfee, R. A., Mohammed, M., & Luu, H. H. (2016). Review of Osteosarcoma and Current Management. *Rheumatology and therapy*, *3*(2), 221-243.

Eftekhari F. (2009). Imaging assessment of osteosarcoma in childhood and adolescence: diagnosis, staging, and evaluating response to chemotherapy. *Cancer treatment and research*, *152*, 33-62.

Enneking, W. F., & Kagan, A. (1975). "Skip" metastases in osteosarcoma. *Cancer*, *36*(6), 2192-2205.

Fan, X. L., Cai, G. P., Zhu, L. L., & Ding, G. M. (2015). Efficacy and safety of ifosfamide-based chemotherapy for osteosarcoma: a meta-analysis. *Drug design, development and therapy*, *9*, 5925-5932.

Fang, C., Shi, B., Pei, Y. Y., Hong, M. H., Wu, J., & Chen, H. Z. (2006). In vivo tumor targeting of tumor necrosis factor-alpha-loaded stealth nanoparticles: effect of MePEG molecular weight and particle size. *European journal of pharmaceutical sciences : official journal of the European Federation for Pharmaceutical Sciences*, *27*(1), 27-36.

Farrar, M. C., & Jacobs, T. F. (2021). Paclitaxel. In *StatPearls*. StatPearls Publishing.

Ferlay, J., Colombet, M., Soerjomataram, I., Dyba, T., Randi, G., Bettio, M., ... Bray, F. (2018). Cancer incidence and mortality patterns in Europe: Estimates for 40 countries and 25 major cancers in 2018. *European journal of cancer*, *103*, 356-387.

Fernandes, R. J., Harkey, M. A., Weis, M., Askew, J. W., & Eyre, D. R. (2007). The post-translational phenotype of collagen synthesized by SAOS-2 osteosarcoma cells. *Bone*, *40*(5), 1343-1351.

Ferrís I Tortajada, J., Berbel Tornero, O., Ortega García, J. A., Claudio-Morales, L., García I Castell, J., Martí Perales, V., & Miranda Casas, L. (2005). Factores de riesgo para los tumores óseos malignos pediátricos. *Anales de Pediatría*, *63*(6), 537-547.

Fisher, R., Pusztai, L., & Swanton, C. (2013). Cancer heterogeneity: implications for targeted therapeutics. *British journal of cancer*, *108*(3), 479-485.

Fletcher, C., Unni, K., & Mertens, F. (2002). *Pathology and Genetics of Tumours of Soft Tissue and Bone*. France: IARC Press.

Florencio-Silva, R., Sasso, G. R., Sasso-Cerri, E., Simões, M. J., & Cerri, P. S. (2015). Biology of Bone Tissue: Structure, Function, and Factors That Influence Bone Cells. *BioMed research international*, *2015*, 421746.

Fox, M. G., & Trotta, B. M. (2013). Osteosarcoma: review of the various types with emphasis on recent advancements in imaging. *Seminars in musculoskeletal radiology*, *17*(2), 123-136.

Friedman, B., & Cronstein, B. (2019). Methotrexate mechanism in treatment of rheumatoid arthritis. *Joint bone spine*, *86*(3), 301-307.

Fu, Y., Lan, T., Cai, H., Lu, A., & Yu, W. (2018). Meta-analysis of serum lactate dehydrogenase and prognosis for osteosarcoma. *Medicine*, *97*(19), e0741.

Furlanut, M., & Franceschi, L. (2003). Pharmacology of ifosfamide. *Oncology*, *65 Suppl 2*, 2-6.

Gangireddy, M., & Nookala, V. (2021). Ifosfamide. In *StatPearls*. StatPearls Publishing.

Gerson, S. L., Caimi, P. F., William, B. M., & Creger, R. J. (2018). Pharmacology and Molecular Mechanisms of Antineoplastic Agents for Hematologic Malignancies. In *Hematology: Basic Principles and Practice* (pp. 849-912). Elsevier Inc. <https://doi.org/10.1016/B978-0-323-35762-3.00057-3>

Ghaedi, M., Soleimani, M., Taghvaie, N. M., Sheikhatollahi, M., Azadmanesh, K., Lotfi, A. S., & Wu, J. (2011). Mesenchymal stem cells as vehicles for targeted delivery of anti-angiogenic protein to solid tumors. *The journal of gene medicine*, *13*(3), 171-180.

Gilbert, S. (2000). Osteogenesis: The Development of Bones. In *Developmental Biology*. Sunderland: Sinauer Associates.

Glick, D., Barth, S., & Macleod, K. F. (2010). Autophagy: cellular and molecular mechanisms. *The Journal of pathology*, *221*(1), 3-12.

Gold, J. M., & Raja, A. (2021). Cisplatin. In *StatPearls*. StatPearls Publishing.

González-Fernández, Y., Imbuluzqueta, E., Zalacain, M., Mollinedo, F., Patiño-García, A., & Blanco-Prieto, M. J. (2017). Doxorubicin and edelfosine lipid nanoparticles are effective acting synergistically against drug-resistant osteosarcoma cancer cells. *Cancer letters*, *388*, 262-268.

Gorini, S., De Angelis, A., Berrino, L., Malara, N., Rosano, G., & Ferraro, E. (2018). Chemotherapeutic Drugs and Mitochondrial Dysfunction: Focus on Doxorubicin, Trastuzumab, and Sunitinib. *Oxidative medicine and cellular longevity*, 2018, 7582730.

Gorlick, R., & Khanna, C. (2010). Osteosarcoma. *Journal of bone and mineral research: the official journal of the American Society for Bone and Mineral Research*, 25(4), 683-691.

Guo, Y., Huang, C., Li, G., Chen, T., Li, J., & Huang, Z. (2015). Paxlitaxel induces apoptosis accompanied by protective autophagy in osteosarcoma cells through hypoxia-inducible factor-1 α pathway. *Molecular medicine reports*, 12(3), 3681-3687.

Gradl, G., Postl, L. K., Lenze, U., Stolberg-Stolberg, J., Pohlig, F., Rechl, H., ... Kirchhoff, C. (2015). Long-term functional outcome and quality of life following rotationplasty for treatment of malignant tumors. *BMC Musculoskeletal Disorders*, 16.

Greish K. (2007). Enhanced permeability and retention of macromolecular drugs in solid tumors: a royal gate for targeted anticancer nanomedicines. *Journal of drug targeting*, 15(7-8), 457-464.

Grimer, R. J., Bielack, S., Flege, S., Cannon, S. R., Foleas, G., Andreeff, I., ... Gosheger, G. (2005). Periosteal osteosarcoma - a European review of outcome. *European journal of cancer (Oxford, England : 1990)*, 41(18), 2806-2811.

Gulia, A., Puri, A., Pruthi, M., & Desai, S. (2014). Oncological and functional outcome of periosteal osteosarcoma. *Indian journal of orthopaedics*, 48(3), 279-284.

Guo, W., Zeng, C., Dong, F., & Lei, W. (2002). Paclitaxel-induced apoptosis in osteosarcoma cell line U-2 OS. *Chinese medical journal*, 115(12), 1796-1801.

Guo, Y., Shan, Q., Gong, Y., Lin, J., Yang, X., & Zhou, R. (2012). Oridonin in combination with imatinib exerts synergetic anti-leukemia effect in Ph⁺ acute lymphoblastic leukemia cells in vitro by inhibiting activation of LYN/mTOR signaling pathway. *Cancer biology & therapy*, 13(13), 1244-1254.

Guo, Z., Li, S., Wang, C., Xu, J., Kirk, B., Wu, J., Liu, Z., & Xue, W. (2017). Biocompatibility and cellular uptake mechanisms of poly(N-isopropylacrylamide) in different cells. *Journal of Bioactive and Compatible Polymers*, 32(1), 17-31.

Gustafson, H. H., Holt-Casper, D., Grainger, D. W., & Ghandehari, H. (2015). Nanoparticle Uptake: The Phagocyte Problem. *Nano today*, 10(4), 487-510.

Haghirsadat, F., Amoabediny, G., Sheikha, M. H., Forouzanfar, T., Helder, M. N., & Zandieh-Doulabi, B. (2017). A Novel Approach on Drug Delivery: Investigation of A New Nano-

Formulation of Liposomal Doxorubicin and Biological Evaluation of Entrapped Doxorubicin on Various Osteosarcoma Cell Lines. *Cell journal*, 19, 55-65.

Hameed, M., & Mandelker, D. (2018). Tumor Syndromes Predisposing to Osteosarcoma. *Advances in Anatomic Pathology*, (pp. 217-222). Lippincott Williams and Wilkins. <https://doi.org/10.1097/PAP.0000000000000190>

Hanna, H., Mir, L. M., & Andre, F. M. (2018). In vitro osteoblastic differentiation of mesenchymal stem cells generates cell layers with distinct properties. *Stem cell research & therapy*, 9(1), 203.

Hansen, M. F., Seton, M., & Merchant, A. (2007). Osteosarcoma in Paget's disease of bone. *Journal of bone and mineral research: the official journal of the American Society for Bone and Mineral Research*, 21, 58-63.

Harris, W. M., Zhang, P., Plastini, M., Ortiz, T., Kappy, N., Benites, J., Alexeev, E., Chang, S., Brockunier, R., Carpenter, J. P., & Brown, S. A. (2017). Evaluation of function and recovery of adipose-derived stem cells after exposure to paclitaxel. *Cytotherapy*, 19(2), 211-221.

Hattinger, C. M., Vella, S., Tavanti, E., Fanelli, M., Picci, P., & Serra, M. (2016). Pharmacogenomics of second-line drugs used for treatment of unresponsive or relapsed osteosarcoma patients. *Pharmacogenomics*, 17(18), 2097-2114.

He, Z., Xiao, X., Li, S., Guo, Y., Huang, Q., Shi, X., Wang, X., & Liu, Y. (2017). Oridonin induces apoptosis and reverses drug resistance in cisplatin resistant human gastric cancer cells. *Oncology letters*, 14(2), 2499-2504.

Hegyí, M., Semsei, A. F., Jakab, Z., Antal, I., Kiss, J., Szendroi, M., ... Kovacs, G. (2011). Good prognosis of localized osteosarcoma in young patients treated with limb-salvage surgery and chemotherapy. *Pediatric blood & cancer*, 57(3), 415-422.

Henke, E., Nandigama, R., & Ergün, S. (2020). Extracellular Matrix in the Tumor Microenvironment and Its Impact on Cancer Therapy. *Frontiers in molecular biosciences*, 6, 160.

Hewitt, M., Weiner, S., & Simone, J. (Eds.). (2003). The Epidemiology of Childhood Cancer. In *Childhood Cancer Survivorship: Improving care and quality of life*. Washington: National Academies Press.

Hickman, E. S., Moroni, M. C., & Helin, K. (2002). The role of p53 and pRB in apoptosis and cancer. *Current opinion in genetics & development*, 12(1), 60-66.

Hientz, K., Mohr, A., Bhakta-Guha, D., & Efferth, T. (2017). The role of p53 in cancer drug resistance and targeted chemotherapy. *Oncotarget*, 8(5), 8921-8946.

Higuchi, T., Sugisawa, N., Miyake, K., Oshiro, H., Yamamoto, N., Hayashi, K., ... Hoffman, R. M. (2019). The Combination of Olaratumab with Doxorubicin and Cisplatin Regresses a Chemotherapy-Resistant Osteosarcoma in a Patient-Derived Orthotopic Xenograft Mouse Model. *Translational oncology*, *12*(9), 1257-1263.

Hoare, T., & Pelton, R. (2007). Functionalized Microgel Swelling: Comparing Theory and Experiment. *The Journal of Physical Chemistry B*, *111*(41), 11895-11906.

Holmboe, L., Andersen, A. M., Mørkrid, L., Slørdal, L., & Hall, K. S. (2012). High dose methotrexate chemotherapy: pharmacokinetics, folate and toxicity in osteosarcoma patients. *British journal of clinical pharmacology*, *73*(1), 106-114.

Houthuijzen, J. M., Daenen, L. G., Roodhart, J. M., & Voest, E. E. (2012). The role of mesenchymal stem cells in anti-cancer drug resistance and tumour progression. *British journal of cancer*, *106*(12), 1901-1906.

Howard, S. C., McCormick, J., Pui, C. H., Buddington, R. K., & Harvey, R. D. (2016). Preventing and Managing Toxicities of High-Dose Methotrexate. *The oncologist*, *21*(12), 1471-1482.

Hu, X., Yu, A. X., Qi, B. W., Fu, T., Wu, G., Zhou, M., ... Xu, J. H. (2010). The expression and significance of IDH1 and p53 in osteosarcoma. *Journal of experimental & clinical cancer research : CR*, *29*(1), 43.

Huang, Y., Johnson, K. R., Norris, J. S., & Fan, W. (2000). Nuclear factor-kappaB/IkappaB signaling pathway may contribute to the mediation of paclitaxel-induced apoptosis in solid tumor cells. *Cancer research*, *60*(16), 4426-4432.

Ibrahim, M. A., Hazhirkarzar, B., & Dublin, A. B. (2021). Gadolinium Magnetic Resonance Imaging. In *StatPearls*. StatPearls Publishing.

Ichikawa, Y., Ghanefar, M., Bayeva, M., Wu, R., Khechaduri, A., Naga Prasad, S. V., ... Ardehali, H. (2014). Cardiotoxicity of doxorubicin is mediated through mitochondrial iron accumulation. *The Journal of clinical investigation*, *124*(2), 617-630.

Jakhar, R., Luijten, M., Wong, A., Cheng, B., Guo, K., Neo, S. P., Au, B., Kulkarni, M., Lim, K. J., Maimaiti, J., Chong, H. C., Lim, E. H., Tan, T., Ong, K. W., Sim, Y., Wong, J., Khoo, J., Ho, J., Chua, B. T., Sinha, I., ... Crasta, K. C. (2018). Autophagy Governs Protumorigenic Effects of Mitotic Slippage-induced Senescence. *Molecular cancer research : MCR*, *16*(11), 1625-1640.

Jalili, N. A., Jaiswal, M. K., Peak, C. W., Cross, L. M., & Gaharwar, A. K. (2017). Injectable nanoengineered stimuli-responsive hydrogels for on-demand and localized therapeutic delivery. *Nanoscale*, *9*(40), 15379-15389.

Janeway, K. A., & Grier, H. E. (2010). Sequelae of osteosarcoma medical therapy: a review of rare acute toxicities and late effects. *The Lancet. Oncology*, *11*(7), 670-678.

Jarvis, M., Krishnan, V., & Mitragotri, S. (2019). Nanocrystals: A perspective on translational research and clinical studies. *Bioengineering & translational medicine*, *4*(1), 5-16.

Jauregui, J. J., Nadarajah, V., Munn, J., Pivec, R., Kapadia, B. H., Lerman, D. M., & Maheshwari, A. V. (2018). Limb Salvage Versus Amputation in Conventional Appendicular Osteosarcoma: a Systematic Review. *Indian journal of surgical oncology*, *9*(2), 232-240.

Jawad, M. U., & Scully, S. P. (2010). In brief: classifications in brief: enneking classification: benign and malignant tumors of the musculoskeletal system. *Clinical orthopaedics and related research*, *468*(7), 2000-2002.

Jeong, Y.-J., Cho, H.-J., Chung, F.-L., Wang, X., Hoe, H.-S., Park, K.-K., ... Chang, Y.-C. (2017). Isothiocyanates suppress the invasion and metastasis of tumors by targeting FAK/MMP-9 activity. *Oncotarget*, *8*(38), 63949-63962.

Jeys, L. M., Kulkarni, A., Grimer, R. J., Carter, S. R., Tillman, R. M., & Abudu, A. (2008). Endoprosthetic reconstruction for the treatment of musculoskeletal tumors of the appendicular skeleton and pelvis. *The Journal of bone and joint surgery. American volume*, *90*(6), 1265-1271.

Johnson-Arbor, K., & Dubey, R. (2021). Doxorubicin. In *StatPearls*. StatPearls Publishing.

Kansara, M., Teng, M. W., Smyth, M. J., & Thomas, D. M. (2014). Translational biology of osteosarcoma. *Nature reviews. Cancer*, *14*(11), 722-735.

Karimi, M., Sahandi Zangabad, P., Ghasemi, A., Amiri, M., Bahrami, M., Malekzad, H., ... Hamblin, M. R. (2016). Temperature-Responsive Smart Nanocarriers for Delivery Of Therapeutic Agents: Applications and Recent Advances. *ACS applied materials & interfaces*, *8*(33), 21107-21133.

Kaur, B., Faktorová, D., Peña-Díaz, P., & Lukeš, J. (n.d.). Cell Counting using a haemocytometer (Neubauer cell chamber) with fixer.
<https://doi.org/10.17504/protocols.io.hfxb3pn>

Kaur Sarhadi, V., Daddali, R., Seppänen-Kajansinkko, R., Pathogenesis, O., Klimczak, A., Kaltschmidt, C., & Mertzluft, F. (2021). Mesenchymal Stem Cells and Extracellular Vesicles in Osteosarcoma Pathogenesis and Therapy. *International Journal of Molecular Sciences*, *22*(20):11035.

Kim, H. J., Lee, S. G., Kim, Y. J., Park, J. E., Lee, K. Y., Yoo, Y. H., & Kim, J. M. (2013). Cytoprotective role of autophagy during paclitaxel-induced apoptosis in Saos-2 osteosarcoma cells. *International journal of oncology*, *42*(6), 1985-1992.

Kimura, Y., Tomihara, K., Tachinami, H., Imaue, S., Nakamori, K., Fujiwara, K., ... Noguchi, M. (2017). Conventional osteosarcoma of the mandible successfully treated with radical surgery and adjuvant chemotherapy after responding poorly to neoadjuvant chemotherapy: a case report. *Journal of medical case reports*, 11(1), 210.

Kingston D. G. (2007). The shape of things to come: structural and synthetic studies of taxol and related compounds. *Phytochemistry*, 68(14), 1844-1854.

Kleinerman, R. A., Schonfeld, S. J., & Tucker, M. A. (2012). Sarcomas in hereditary retinoblastoma. *Clinical sarcoma research*, 2(1), 15.

Kohler, D. R., & Goldspiel, B. R. (1994). Paclitaxel (taxol). *Pharmacotherapy*, 14(1), 3-34.

Kou, L., Sun, J., Zhai, Y., & He, Z. (2013). The endocytosis and intracellular fate of nanomedicines: Implication for rational design. *Asian Journal of Pharmaceutical Sciences*, 8(1), 1-10.

Krampera, M., Franchini, M., Pizzolo, G., & Aprili, G. (2007). Mesenchymal stem cells: from biology to clinical use. *Blood transfusion = Trasfusione del sangue*, 5(3), 120-129.

Kularatne, S. A., & Low, P. S. (2010). Targeting of nanoparticles: folate receptor. *Methods in molecular biology (Clifton, N.J.)*, 624, 249-265.

Kundu Z. S. (2014). Classification, imaging, biopsy and staging of osteosarcoma. *Indian journal of orthopaedics*, 48(3), 238-246.

Lavogina, D., Lust, H., Tahk, M. J., Laasfeld, T., Vellama, H., Nasirova, N., Vardja, M., Eskla, K. L., Salumets, A., Rincken, A., Jaal, J. (2022) Revisiting the resazurin-based sensing of cellular viability: widening the application horizon. *Biosensors (Basel)*, 12(4):196.

Lauvrak, S. U., Munthe, E., Kresse, S. H., Stratford, E. W., Namløs, H. M., Meza-Zepeda, L. A., & Myklebost, O. (2013). Functional characterisation of osteosarcoma cell lines and identification of mRNAs and miRNAs associated with aggressive cancer phenotypes. *British journal of cancer*, 109(8), 2228-2236.

Le, B. Q., Nurcombe, V., Cool, S. M., van Blitterswijk, C. A., de Boer, J., & LaPointe, V. (2017). The Components of Bone and What They Can Teach Us about Regeneration. *Materials (Basel, Switzerland)*, 11(1), 14.

Leavey, P. J., Day, M. D., Booth, T., & Maale, G. (2003). Skip metastasis in osteosarcoma. *Journal of pediatric hematology/oncology*, 25(10), 806-808.

Lee, L. F., Li, G., Templeton, D. J., & Ting, J. P. (1998). Paclitaxel (Taxol)-induced gene expression and cell death are both mediated by the activation of c-Jun NH2-terminal kinase (JNK/SAPK). *The Journal of biological chemistry*, 273(43), 28253-28260.

Li, J., Wu, Y., Wang, D., Zou, L., Fu, C., Zhang, J., & Leung, G. P. (2019). Oridonin synergistically enhances the anti-tumor efficacy of doxorubicin against aggressive breast cancer via pro-apoptotic and anti-angiogenic effects. *Pharmacological research*, 146, 104313.

Li, X., Zhang, C. T., Ma, W., Xie, X., & Huang, Q. (2021). Oridonin: A Review of Its Pharmacology, Pharmacokinetics and Toxicity. *Frontiers in pharmacology*, 12, 645824.

Li, X., Yan, M. L., & Yu, Q. (2017). Identification of candidate drugs for the treatment of metastatic osteosarcoma through a subpathway analysis method. *Oncology letters*, 13(6), 4378-4384.

Li, X., Lu, Q., Xie, W., Wang, Y., & Wang, G. (2018). Anti-tumor effects of triptolide on angiogenesis and cell apoptosis in osteosarcoma cells by inducing autophagy via repressing Wnt/ β -Catenin signaling. *Biochemical and biophysical research communications*, 496(2), 443-449.

Li, Y., & Kumacheva, E. (2018). Hydrogel microenvironments for cancer spheroid growth and drug screening. *Science advances*, 4(4), eaas8998.

Limaïem, F., Davis, D. D., & Sticco, K. L. (2021). Chondrosarcoma. In *StatPearls*. StatPearls Publishing.

Lin, P. P., & Patel, S. (2013). Osteosarcoma. In P. P. Lin & S. Patel (Eds.), *Bone Sarcoma*. Boston: Springer US. <https://doi.org/10.1007/978-1-4614-5194-5>

Lin, W., Huang, L., Li, Y., Fang, B., Li, G., Chen, L., & Xu, L. (2019). Mesenchymal Stem Cells and Cancer: Clinical Challenges and Opportunities. *BioMed research international*, 2019, 2820853.

Lindsey, B. A., Markel, J. E., & Kleinerman, E. S. (2017). Osteosarcoma Overview. *Rheumatology and therapy*, 4(1), 25-43.

Lipshultz, S. E., Patel, N., Franco, V. I., & Fisher, S. (2017). Late Cardiac Effects in Childhood Cancer Survivors. In *Cardio-Oncology: Principles, Prevention and Management* (pp. 173–186). Elsevier Inc. <https://doi.org/10.1016/B978-0-12-803547-4.00011-2>

Lipshultz, Steven E., Diamond, M. B., Franco, V. I., Aggarwal, S., Leger, K., Santos, M. V., ... Chow, E. J. (2014). Managing chemotherapy-related cardiotoxicity in survivors of childhood cancers. *Paediatric drugs*, 16(5), 373-389.

Liu, S.-Y., Song, S.-X., Lin, L., & Liu, X. (2010). Molecular Mechanism of Cell Apoptosis by Paclitaxel and Pirarubicin in a Human Osteosarcoma Cell Line. *Chemotherapy*, 56(2), 101-107.

Liu, T., Ling, L., Zhang, Q., Liu, Y., & Guo, X. (2019). Evaluation of the Efficacy of Pasteurized Autograft and Intramedullary Vascularized Fibular Transfer for Osteosarcoma of the Femoral Diaphysis. *Orthopaedic surgery*, 11(5), 826-834.

Lu, Y., Li, Y., & Wu, W. (2016). Injected nanocrystals for targeted drug delivery. *Acta pharmaceutica Sinica. B*, 6(2), 106-113.

Lu, Y., Sun, Y., Zhu, J., Yu, L., Jiang, X., Zhang, J., Dong, X., ... Zhang, Q. (2018). Oridonin exerts anticancer effect on osteosarcoma by activating PPAR- γ and inhibiting Nrf2 pathway. *Cell death & disease*, 9(1), 15.

Luo, D., Yi, Y., Peng, K., Liu, T., Yang, J., Liu, S., ... Wan, S. (2019). Oridonin derivatives as potential anticancer drug candidates triggering apoptosis through mitochondrial pathway in the liver cancer cells. *European journal of medicinal chemistry*, 178, 365-379.

Luo, J., Xiang, Y., Xu, X., Fang, D., Li, D., Ni, F., Zhu, X., Chen, B., & Zhou, M. (2018). High Glucose-Induced ROS Production Stimulates Proliferation of Pancreatic Cancer via Inactivating the JNK Pathway. *Oxidative medicine and cellular longevity*, 2018, 6917206.

Mahajan, A., Woo, S. Y., Kornguth, D. G., Hughes, D., Huh, W., Chang, E. L., ... Anderson, P. (2008). Multimodality treatment of osteosarcoma: radiation in a high-risk cohort. *Pediatric blood & cancer*, 50(5), 976-982.

Malhas, A. M., Sumathi, V. P., James, S. L., Menna, C., Carter, S. R., Tillman, R. M., ... Grimer, R. J. (2012). Low-grade central osteosarcoma: a difficult condition to diagnose. *Sarcoma*, 2012, 764796.

Marie, P. J., & Cohen-Solal, M. (2018). The Expanding Life and Functions of Osteogenic Cells: From Simple Bone-Making Cells to Multifunctional Cells and Beyond. *Journal of bone and mineral research: the official journal of the American Society for Bone and Mineral Research*, 33(2), 199-210.

Marina, N. M., Smeland, S., Bielack, S. S., Bernstein, M., Jovic, G., Krailo, M. D., ... Whelan, J. S. (2016). Comparison of MAPIE versus MAP in patients with a poor response to preoperative chemotherapy for newly diagnosed high-grade osteosarcoma (EURAMOS-1): an open-label, international, randomised controlled trial. *The Lancet Oncology*, 17(10), 1396-1408.

Martella, E., Ferroni, C., Guerrini, A., Ballestri, M., Columbaro, M., Santi, S., Sotgiu, G., Serra, M., Donati, D. M., Lucarelli, E., Varchi, G., & Duchi, S. (2018). Functionalized Keratin as

Nanotechnology-Based Drug Delivery System for the Pharmacological Treatment of Osteosarcoma. *International journal of molecular sciences*, 19(11), 3670.

Martin, J. W., Squire, J. A., & Zielenska, M. (2012). The genetics of osteosarcoma. *Sarcoma*, 2012, 627254.

Marupudi, N. I., Han, J. E., Li, K. W., Renard, V. M., Tyler, B. M., & Brem, H. (2007). Paclitaxel: a review of adverse toxicities and novel delivery strategies. *Expert opinion on drug safety*, 6(5), 609-621.

Minotti, G., Saponiero, A., Licata, S., Menna, P., Calafiore, A. M., Teodori, G., & Gianni, L. (2001). Paclitaxel and docetaxel enhance the metabolism of doxorubicin to toxic species in human myocardium. *Clinical cancer research: an official journal of the American Association for Cancer Research*, 7(6), 1511-1515.

Mirabello, L., Troisi, R. J., & Savage, S. A. (2009). International osteosarcoma incidence patterns in children and adolescents, middle ages and elderly persons. *International journal of cancer*, 125(1), 229-234.

Mirabello, L., Yeager, M., Mai, P. L., Gastier-foster, J. M., Gorlick, R., Khanna, C., ... Savage, S. A. (2015). Germline TP53 variants and susceptibility to osteosarcoma. *Journal of the National Cancer Institute*, 107(7), djv101.

Misaghi, A., Goldin, A., Awad, M., & Kulidjian, A. A. (2018). Osteosarcoma: a comprehensive review. *SICOT-J*, 4, 12.

Monteiro, M. V., Gaspar, V. M., Ferreira, L. P., & Mano, J. F. (2020). Hydrogel 3D in vitro tumor models for screening cell aggregation mediated drug response. *Biomaterials Science*, 8(7), 1855-1864.

Mullen P. (2004). The use of Matrigel to facilitate the establishment of human cancer cell lines as xenografts. *Methods in molecular medicine*, 88, 287-292.

Naha, P. C., Bhattacharya, K., Tenuta, T., Dawson, K. A., Lynch, I., Gracia, A., Lyng, F. M., & Byrne, H. J. (2010). Intracellular localisation, geno- and cytotoxic response of polyN-isopropylacrylamide (PNIPAM) nanoparticles to human keratinocyte (HaCaT) and colon cells (SW 480). *Toxicology letters*, 198(2), 134-143.

Nallani, S. C., Goodwin, B., Buckley, A. R., Buckley, D. J., & Desai, P. B. (2004). Differences in the induction of cytochrome P450 3A4 by taxane anticancer drugs, docetaxel and paclitaxel, assessed employing primary human hepatocytes. *Cancer chemotherapy and pharmacology*, 54(3), 219-229.

Nowak-Sliwinska, P., Scapozza, L., & Ruiz i Altaba, A. (2019). Drug repurposing in oncology: Compounds, pathways, phenotypes and computational approaches for colorectal cancer. *Biochimica et biophysica acta. Reviews on cancer*, 1871(2), 434-454.

Odes, E. J., Randolph-Quinney, P. S., Steyn, M., Throckmorton, Z., Smilg, J. S., Zipfel, B., ... Berger, L. R. (2016). Earliest hominin cancer: 1.7-million-yearold osteosarcoma from Swartkrans cave, South Africa. *South African Journal of Science*, 112(7-8), 7-11.

Okada, K., Frassica, F. J., Sim, F. H., Beabout, J. W., Bond, J. R., & Unni, K. K. (1994). Parosteal osteosarcoma. A clinicopathological study. *The Journal of bone and joint surgery. American volume*, 76(3), 366-378.

Okada, K., Hasegawa, T., & Yokoyama, R. (2001). Rosette-forming epithelioid osteosarcoma: a histologic subtype with highly aggressive clinical behavior. *Human pathology*, 32(7), 726-733.

Osakwe, O., & Rizvi, S. A. A. (2016). Introduction. In *Social Aspects of Drug Discovery, Development and Commercialization* (pp. xvii–xxx). Elsevier.

Paioli, A., Rocca, M., Cevolani, L., Rimondi, E., Vanel, D., Palmerini, E., ... Ferrari, S. (2017). Osteosarcoma follow-up: chest X-ray or computed tomography?. *Clinical sarcoma research*, 7, 3.

Park, H. K., Lee, J. E., Lim, J., Jo, D. E., Park, S. A., Suh, P. G., & Kang, B. H. (2014). Combination treatment with doxorubicin and gamitrinib synergistically augments anticancer activity through enhanced activation of Bim. *BMC cancer*, 14, 431.

Pessina, A., Bonomi, A., Coccè, V., Invernici, G., Navone, S., Cavicchini, L., Sisto, F., Ferrari, M., Viganò, L., Locatelli, A., Ciusani, E., Cappelletti, G., Cartelli, D., Arnaldo, C., Parati, E., Marfia, G., Pallini, R., Falchetti, M. L., & Alessandri, G. (2011). Mesenchymal stromal cells primed with paclitaxel provide a new approach for cancer therapy. *PloS one*, 6(12), e28321.

Picci P. (2007). Osteosarcoma (osteogenic sarcoma). *Orphanet journal of rare diseases*, 2, 6.

Porada, C. D., & Almeida-Porada, G. (2010). Mesenchymal stem cells as therapeutics and vehicles for gene and drug delivery. *Advanced drug delivery reviews*, 62(12), 1156-1166.

Prater, S., & McKeon, B. (2021). Osteosarcoma. In *StatPearls*. StatPearls Publishing.

Raimondi, L., De Luca, A., Costa, V., Amodio, N., Carina, V., Bellavia, D., ... Giavaresi, G. (2017). Circulating biomarkers in osteosarcoma: new translational tools for diagnosis and treatment. *Oncotarget*, 8(59), 100831-100851.

Rauch F. (2005). Bone growth in length and width: the Yin and Yang of bone stability. *Journal of musculoskeletal & neuronal interactions*, 5(3), 194-201.

Rentsch, C., Schneiders, W., Manthey, S., Rentsch, B., & Rammelt, S. (2014). Comprehensive histological evaluation of bone implants. *Biomatter*, 4, e27993.

Rimann, M., Laternser, S., Gvozdenovic, A., Muff, R., Fuchs, B., Kelm, J. M., & Graf-Hausner, U. (2014). An in vitro osteosarcoma 3D microtissue model for drug development. *Journal of biotechnology*, 189, 129-135.

Rizvi, S., & Saleh, A. M. (2018). Applications of nanoparticle systems in drug delivery technology. *Saudi pharmaceutical journal: SPJ:the official publication of the Saudi Pharmaceutical Society*, 26(1), 64-70.

Roth, V. (2006). Doubling Time Calculator. Retrieved from https://doubling-time.com/compute_more.php

Sadat Tabatabaei Mirakabad, F., Nejati-Koshki, K., Akbarzadeh, A., Yamchi, M. R., Milani, M., Zarghami, N., ... Joo, S. W. (2014). PLGA-based nanoparticles as cancer drug delivery systems. *Asian Pacific journal of cancer prevention : APJCP*, 15(2), 517-535.

Salimi, F., Dilmaghani, K. A., Alizadeh, E., Akbarzadeh, A., & Davaran, S. (2018). Enhancing cisplatin delivery to hepatocellular carcinoma HepG2 cells using dual sensitive smart nanocomposite. *Artificial cells, nanomedicine, and biotechnology*, 46(5), 949-958.

Salvati, A., Aberg, C., dos Santos, T., Varela, J., Pinto, P., Lynch, I., & Dawson, K. A. (2011). Experimental and theoretical comparison of intracellular import of polymeric nanoparticles and small molecules: toward models of uptake kinetics. *Nanomedicine: nanotechnology, biology, and medicine*, 7(6), 818-826.

Kumar, V. S., Barwar, N., & Khan, S. A. (2014). Surface osteosarcomas: Diagnosis, treatment and outcome. *Indian journal of orthopaedics*, 48(3), 255-261.

Sant, S., & Johnston, P. A. (2017). The production of 3D tumor spheroids for cancer drug discovery. *Drug discovery today. Technologies*, 23, 27-36.

Šašić, S. (2007). *Pharmaceutical Applications of Raman Spectroscopy*. Hoboken: John Wiley & Sons, Inc.

Schwarz, R., Bruland, O., Cassoni, A., Schomberg, P., & Bielack, S. (2009). The Role of Radiotherapy in osteosarcoma. In *Cancer Treatment and Research* (pp. 147–164).

Senthebane, D. A., Rowe, A., Thomford, N. E., Shipanga, H., Munro, D., Al Mazeedi, M. A. M., ... Dzobo, K. (2017). The Role of Tumor Microenvironment in Chemoresistance: To Survive, Keep Your Enemies Closer. *International journal of molecular sciences*, 18(7), 1586.

Shapiro, F. D., & Eyre, D. R. (1982). Collagen polymorphism in extracellular matrix of human osteosarcoma. *Journal of the National Cancer Institute*, 69(5), 1009-1016.

Shehadeh, A., Noveau, J., Malawer, M., & Henshaw, R. (2010). Late complications and survival of endoprosthetic reconstruction after resection of bone tumors. *Clinical orthopaedics and related research*, 468(11), 2885-2895.

Singh, R., & Lillard, J. W., Jr (2009). Nanoparticle-based targeted drug delivery. *Experimental and molecular pathology*, 86(3), 215-223.

Sitarski, A. M., Fairfield, H., Falank, C., & Reagan, M. R. (2018). 3d Tissue Engineered In Vitro Models Of Cancer In Bone. *ACS biomaterials science & engineering*, 4(2), 324-336.

Sleire, L., Førde, H. E., Netland, I. A., Leiss, L., Skeie, B. S., & Enger, P. Ø. (2017). Drug repurposing in cancer. *Pharmacological research*, 124, 74-91.

Snezhkina, A. V., Kudryavtseva, A. V., Kardymon, O. L., Savvateeva, M. V., Melnikova, N. V., Krasnov, G. S., & Dmitriev, A. A. (2019). ROS Generation and Antioxidant Defense Systems in Normal and Malignant Cells. *Oxidative Medicine and Cellular Longevity*, 2019, 1-17.

Somasundaram K. (2000). Tumor suppressor p53: regulation and function. *Frontiers in bioscience : a journal and virtual library*, 5, D424-D437.

Speelmans, G., Staffhorst, R. W. H. M., de Kruijff, B., & de Wolf, F. A. (1994). Transport Studies of Doxorubicin in Model Membranes Indicate a Difference in Passive Diffusion across and Binding at the Outer and Inner Leaflet of the Plasma Membrane. *Biochemistry*, 33(46), 13761-13768.

Staals, E. L., Bacchini, P., & Bertoni, F. (2008). High-grade surface osteosarcoma: A Review of 25 cases from the Rizzoli Institute. *Cancer*, 112(7), 1592-1599.

Stearns, M. E., & Wang, M. (1992). Taxol blocks processes essential for prostate tumor cell (PC-3 ML) invasion and metastases. *Cancer research*, 52(13), 3776-3781.

Stiller, C. A., Bielack, S. S., Jundt, G., & Steliarova-Foucher, E. (2006). Bone tumours in European children and adolescents, 1978–1997. Report from the Automated Childhood Cancer Information System project. *European Journal of Cancer*, 42(13), 2124-2135.

Strioga, M., Viswanathan, S., Darinskas, A., Slaby, O., & Michalek, J. (2012). Same or not the same? Comparison of adipose tissue-derived versus bone marrow-derived mesenchymal stem and stromal cells. *Stem cells and development*, 21(14), 2724-2752.

Sun, Y., Jiang, X., Lu, Y., Zhu, J., Yu, L., Ma, B., & Zhang, Q. (2018). Oridonin prevents epithelial-mesenchymal transition and TGF- β 1-induced epithelial-mesenchymal transition by inhibiting TGF- β 1/Smad2/3 in osteosarcoma. *Chemico-biological interactions*, 296, 57-64.

Tan, P. H., Chia, S. S., Toh, S. L., Goh, J. C., & Nathan, S. S. (2016). Three-dimensional spatial configuration of tumour cells confers resistance to chemotherapy independent of drug delivery. *Journal of tissue engineering and regenerative medicine*, 10(8), 637-646.

Tan, W., Lu, J., Huang, M., Li, Y., Chen, M., Wu, G., ... Wang, Y. (2011). Anti-cancer natural products isolated from chinese medicinal herbs. *Chinese medicine*, 6(1), 27.

Taupin, T., Decouvelaere, A. V., Vaz, G., & Thiesse, P. (2016). Accuracy of core needle biopsy for the diagnosis of osteosarcoma: A retrospective analysis of 73 patients. *Diagnostic and interventional imaging*, 97(3), 327-331.

Thorn, C. F., Oshiro, C., Marsh, S., Hernandez-Boussard, T., McLeod, H., Klein, T. E., & Altman, R. B. (2011). Doxorubicin pathways: pharmacodynamics and adverse effects. *Pharmacogenetics and genomics*, 21(7), 440-446.

Tian, L., Xie, K., Sheng, D., Wan, X., & Zhu, G. (2017). Antiangiogenic effects of oridonin. *BMC complementary and alternative medicine*, 17(1), 192.

Tiwari, A., Jain, S., Mehta, S., Kumar, R., Kapoor, G., & Kumar, K. (2014). Limb salvage surgery for osteosarcoma: Early results in Indian patients. *Indian journal of orthopaedics*, 48(3), 266-272.

Toki, S., Kobayashi, E., Yoshida, A., Ogura, K., Wakai, S., Yoshimoto, S., ... Kawai, A. (2019). A clinical comparison between dedifferentiated low-grade osteosarcoma and conventional osteosarcoma. *The bone & joint journal*, 101-B(6), 745-752.

Tsai, H. C., Huang, C. Y., Su, H. L., & Tang, C. H. (2014). CTGF increases drug resistance to paclitaxel by upregulating survivin expression in human osteosarcoma cells. *Biochimica et biophysica acta*, 1843(5), 846-854.

Tsang, W. P., Chau, S. P. Y., Kong, S. K., Fung, K. P., & Kwok, T. T. (2003). Reactive oxygen species mediate doxorubicin induced p53-independent apoptosis. *Life Sciences*, 73(16), 2047-2058.

Turanli, B., Grötli, M., Boren, J., Nielsen, J., Uhlen, M., Arga, K. Y., & Mardinoglu, A. (2018). Drug Repositioning for Effective Prostate Cancer Treatment. *Frontiers in physiology*, *9*, 500.

Umscheid, C. A., Margolis, D. J., & Grossman, C. E. (2011). Key concepts of clinical trials: a narrative review. *Postgraduate medicine*, *123*(5), 194-204.

Ventola C. L. (2012). The nanomedicine revolution: part 1: emerging concepts. *P & T : a peer-reviewed journal for formulary management*, *37*(9), 512–525.

Ventola C. L. (2017). Progress in Nanomedicine: Approved and Investigational Nanodrugs. *P & T: a peer-reviewed journal for formulary management*, *42*(12), 742-755.

Virgone-Carlotta, A., Lemasson, M., Mertani, H. C., Diaz, J. J., Monnier, S., Dehoux, T., ... Rieu, J. P. (2017). In-depth phenotypic characterization of multicellular tumor spheroids: Effects of 5-Fluorouracil. *PLoS ONE*, *12*(11), 1-18.

Wagner, L. M., Yin, H., Eaves, D., Currier, M., & Cripe, T. P. (2014). Preclinical evaluation of nanoparticle albumin-bound paclitaxel for treatment of pediatric bone sarcoma. *Pediatric blood & cancer*, *61*(11), 2096-2098.

Wang, B., Shen, C., Li, Y., Zhang, T., Huang, H., Ren, J., ... Xu, B. (2019). Oridonin overcomes the gemcitabine resistant PANC-1/Gem cells by regulating GST pi and LRP/1 ERK/JNK signalling. *OncoTargets and therapy*, *12*, 5751-5765.

Wang, B., Yu, X. C., Xu, S. F., & Xu, M. (2015). Paclitaxel and etoposide co-loaded polymeric nanoparticles for the effective combination therapy against human osteosarcoma. *Journal of nanobiotechnology*, *13*, 22.

Wang, L. L., Gannavarapu, A., Kozinetz, C. A., Levy, M. L., Lewis, R. A., Chintagumpala, M. M., ... Plon, S. E. (2003). Association between osteosarcoma and deleterious mutations in the RECQL4 gene in Rothmund-Thomson syndrome. *Journal of the National Cancer Institute*, *95*(9), 669–674.

Wang, L. L., Levy, M. L., Lewis, R. A., Chintagumpala, M. M., Lev, D., Rogers, M., & Plon, S. E. (2001). Clinical manifestations in a cohort of 41 Rothmund-Thomson syndrome patients. *American journal of medical genetics*, *102*(1), 11-17.

Wang, S. Q., Wang, C., Chang, L. M., Zhou, K. R., Wang, J. W., Ke, Y., Yang, D. X., Shi, H. G., Wang, R., Shi, X. L., Ma, L. Y., & Liu, H. M. (2016). Geridonin and paclitaxel act synergistically to inhibit the proliferation of gastric cancer cells through ROS-mediated regulation of the PTEN/PI3K/Akt pathway. *Oncotarget*, *7*(45), 72990-73002.

Wang, X. H., Zhang, S. F., Bao, J. T., & Liu, F. Y. (2017). Oridonin synergizes with Nutlin-3 in osteosarcoma cells by modulating the levels of multiple Bcl-2 family proteins. *Tumour biology: the journal of the International Society for Oncodevelopmental Biology and Medicine*, 39(6), 1010428317701638.

Wang, X., Hui, R., Chen, Y., Wang, W., Chen, Y., Gong, X., & Jin, J. (2019). Discovery of Novel Doxorubicin Metabolites in MCF7 Doxorubicin-Resistant Cells. *Frontiers in pharmacology*, 10, 1434.

Wang, Y., & Zhu, Z. (2019). Oridonin inhibits metastasis of human ovarian cancer cells by suppressing the mTOR pathway. *Archives of Medical Science*, 15(4), 1017-1027.

Weaver B. A. (2014). How Taxol/paclitaxel kills cancer cells. *Molecular biology of the cell*, 25(18), 2677-2681.

Wei, X., Yang, X., Han, Z. P., Qu, F. F., Shao, L., & Shi, Y. F. (2013). Mesenchymal stem cells: a new trend for cell therapy. *Acta pharmacologica Sinica*, 34(6), 747-754.

Wells, C. M., Harris, M., Choi, L., Murali, V. P., Guerra, F. D., & Jennings, J. A. (2019). Stimuli-Responsive Drug Release from Smart Polymers. *Journal of functional biomaterials*, 10(3), 34.

Wen, C., Fu, L., Huang, J., Dai, Y., Wang, B., Xu, G., ... Zhou, H. (2019). Curcumin reverses doxorubicin resistance via inhibition the efflux function of ABCB4 in doxorubicin-resistant breast cancer cells. *Molecular medicine reports*, 19(6), 5162-5168.

Wexler, L. H., Andrich, M. P., Venzon, D., Berg, S. L., Weaver-McClure, L., Chen, C. C., ... Horowitz, M. E. (1996). Randomized trial of the cardioprotective agent ICRF-187 in pediatric sarcoma patients treated with doxorubicin. *Journal of Clinical Oncology*, 14(2), 362-372.

Widhe, B., & Widhe, T. (2000). Initial Symptoms and Clinical Features in Osteosarcoma and Ewing Sarcoma*. *The Journal of Bone and Joint Surgery-American Volume*, 82(5), 667-674.

Wilczewska, A. Z., Niemirowicz, K., Markiewicz, K. H., & Car, H. (2012). Nanoparticles as drug delivery systems. *Pharmacological reports : PR*, 64(5), 1020-1037.

Wold, L. E., Unni, K. K., Beabout, J. W., Sim, F. H., & Dahlin, D. C. (1984). Dedifferentiated parosteal osteosarcoma. *The Journal of bone and joint surgery. American volume*, 66(1), 53-59.

Wong, F., Boice, J. J., Abramson, D., Tarone, R., Kleinerman, R., Stovall, M., ... Li, F. (1997). Cancer incidence after retinoblastoma. Radiation dose and sarcoma risk. *JAMA*, 278(15), 1262-1267.

Workshop summary. (2015). Washington: National Academies Press. Retrieved from <https://www.ncbi.nlm.nih.gov/books/NBK316376/>

Xia, S., Zhang, X., Li, C., & Guan, H. (2017). Oridonin inhibits breast cancer growth and metastasis through blocking the Notch signaling. *Saudi pharmaceutical journal : SPJ : the official publication of the Saudi Pharmaceutical Society*, 25(4), 638-643.

Xie, L., Zhao, T., Cai, J., Su, Y., Wang, Z., & Dong, W. (2016). Methotrexate induces DNA damage and inhibits homologous recombination repair in choriocarcinoma cells. *Oncotargets and therapy*, 9, 7115-7122.

Xu, J., Wold, E. A., Ding, Y., Shen, Q., & Zhou, J. (2018). Therapeutic Potential of Oridonin and Its Analogs: From Anticancer and Antiinflammation to Neuroprotection. *Molecules (Basel, Switzerland)*, 23(2), 474.

Xu, L., Bi, Y., Xu, Y., Zhang, Z., Xu, W., Zhang, S., & Chen, J. (2020). Oridonin inhibits the migration and epithelial-to-mesenchymal transition of small cell lung cancer cells by suppressing FAK-ERK1/2 signalling pathway. *Journal of cellular and molecular medicine*, 24(8), 4480-4493.

Xuan, X., Tian, C., Zhao, M., Sun, Y., & Huang, C. (2021). Mesenchymal stem cells in cancer progression and anticancer therapeutic resistance. *Cancer cell international*, 21(1), 595.

Yang, F., Teves, S. S., Kemp, C. J., & Henikoff, S. (2014). Doxorubicin, DNA torsion, and chromatin dynamics. *Biochimica et biophysica acta*, 1845(1), 84-89.

Yang, H., Wang, Q., Huang, S., Xiao, A., Li, F., Gan, L., & Yang, X. (2016). Smart pH/Redox Dual-Responsive Nanogels for On-Demand Intracellular Anticancer Drug Release. *ACS applied materials & interfaces*, 8(12), 7729-7738.

Yang, Y., Niu, X., Zhang, Q., Hao, L., Ding, Y., & Xu, H. (2012). The Efficacy of Abraxane on Osteosarcoma Xenografts in Nude Mice and Expression of Secreted Protein, Acidic and Rich in Cysteine. *The American Journal of the Medical Sciences*, 344(3), 199-205.

Yao, S., Li, X., Liu, J., Sun, Y., Wang, Z., & Jiang, Y. (2017). Maximized nanodrug-loaded mesenchymal stem cells by a dual drug-loaded mode for the systemic treatment of metastatic lung cancer. *Drug delivery*, 24(1), 1372-1383.

Yao, Z., Xie, F., Li, M., Liang, Z., Xu, W., Yang, J., ... Qu, L. H. (2017). Oridonin induces autophagy via inhibition of glucose metabolism in p53-mutated colorectal cancer cells. *Cell Death and Disease*, 8(2), e2633.

Yoshida, G. J., Fuchimoto, Y., Osumi, T., Shimada, H., Hosaka, S., Morioka, H., ... Kuroda, T. (2012). Li-Fraumeni syndrome with simultaneous osteosarcoma and liver cancer: increased expression of a CD44 variant isoform after chemotherapy. *BMC cancer*, *12*, 444.

Yu, X., Trase, I., Ren, M., Duval, K., Guo, X., & Chen, Z. (2016). Design of Nanoparticle-Based Carriers for Targeted Drug Delivery. *Journal of nanomaterials*, *2016*, 1087250.

Zhang, D., Yang, R., Wang, S., & Dong, Z. (2014). Paclitaxel: new uses for an old drug. *Drug design, development and therapy*, *8*, 279-284.

Zhang, L., Lyer, A., Yang, X., Kobayashi, E., Guo, Y., Mankin, H., ... Mansoor Amiji, M. (2015). Polymeric nanoparticle-based delivery of microRNA-199a-3p inhibits proliferation and growth of osteosarcoma cells. *International journal of nanomedicine*, *10*, 2913-2924.

Zhang, X., & Guan, Z. (2018). PET/CT in the diagnosis and prognosis of osteosarcoma. *Frontiers in bioscience (Landmark edition)*, *23*, 2157-2165.

Zheng, Y., Wang, G., Chen, R., Hua, Y., & Cai, Z. (2018). Mesenchymal stem cells in the osteosarcoma microenvironment: their biological properties, influence on tumor growth, and therapeutic implications. *Stem cell research & therapy*, *9*(1), 22.

Zhou, G. B., Kang, H., Wang, L., Gao, L., Liu, P., Xie, J., ... Zhu, C. (2007). Oridonin, a diterpenoid extracted from medicinal herbs, targets AML1-ETO fusion protein and shows potent antitumor activity with low adverse effects on t(8;21) leukemia in vitro and in vivo. *Blood*, *109*(8), 3441-3450.

Zreiqat, H., Dunstan, C., & Rosen, V. (2015). *A Tissue Regeneration Approach to Bone and Cartilage Repair*. (Hala Zreiqat, C. R. Dunstan, & V. Rosen, Eds.), Springer. Cham: Springer International Publishing. <https://doi.org/10.1007/978-3-319-13266-2>.

VIII. Appendix: Supplementary material

6. Morphologies of cell lines

6.1. Osteosarcoma

MG63 osteosarcoma cell line presented a fibroblast morphology, characterized by spindle-like shape, while Saos-2 and U2OS had epithelial morphology with polygonal-spindle forms (Figure A1).

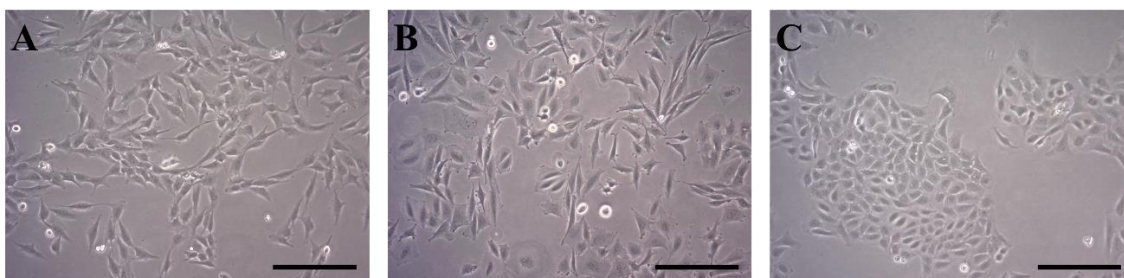


Figure A1. Morphology of osteosarcoma cell lines. Images of MG63 (A) Saos-2 (B) and U2OS (C) were acquired by using a 10X objective of phase-contrast microscope. Scale bar = 50 μ m.

6.2. Human MSC

huAD and huBM-MSC showed similar morphology with a characteristic fibroblastic spindle shape (Figure A2).

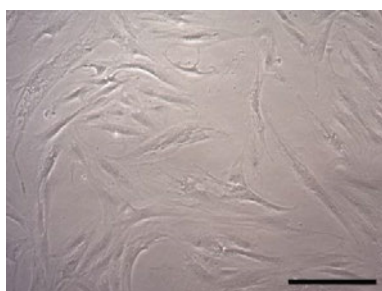


Figure A2. Morphology of huAD-MSC. Images of huAD-MSC were acquired by using a 10X objective of phase-contrast microscope. Scale bar = 50 μ m.

7. Calibration curve

7.1. Osteosarcoma

The calibration curve facilitates the conversion of fluorescent measurements into cell number. For this cell proliferation and viability was determined using resazurin assay (Figure A3).

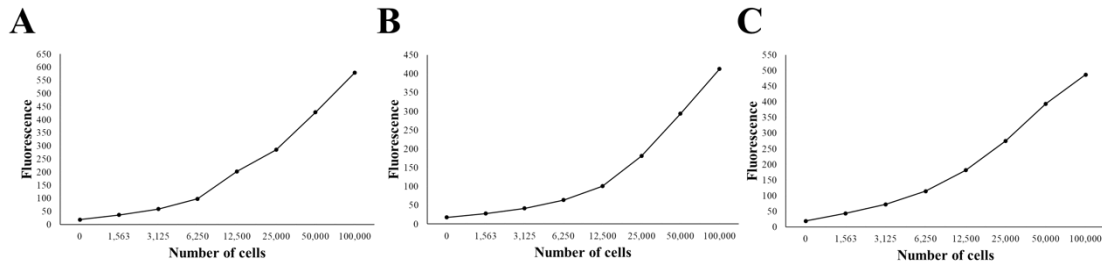


Figure A3. Calibration curve of osteosarcoma cell lines. Different number of MG63 (A), Saos-2 (B) and U2OS (C) cells were obtained by making a serial dilution in a 96-well flat bottom plate. 8 wells were used, where the last one was a blank (well without cells in a complete medium). The plates were incubated for 2 h to let cell attachment. Later, MG63 and U2OS were incubated with resazurin fluorescent dye for 3 hours, while Saos-2 was incubated for 4 hours. The fluorescence was read at excitation 530 nm and emission 590 nm wavelengths.

7.2. Human MSC

Similarly to osteosarcoma cell lines, the proliferation and viability of huAD and huBM-MSC was evaluated in resazurin assay (**Figure A4**).

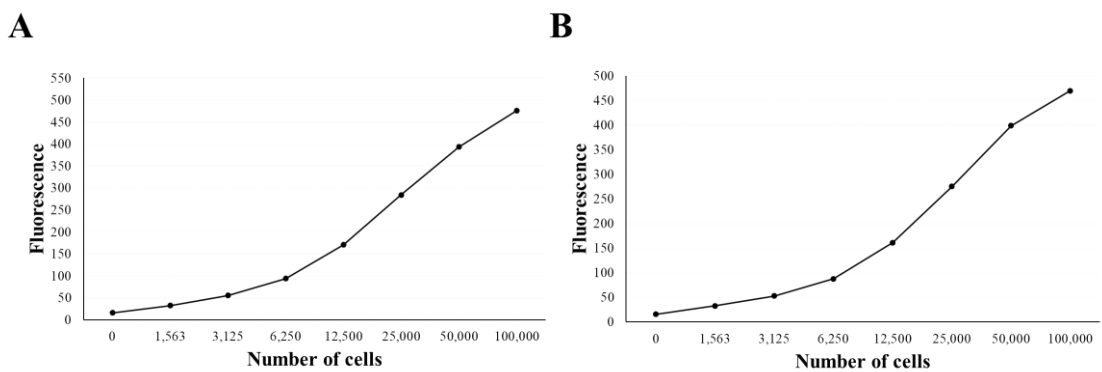


Figure A4. Calibration curve of MSC. Different number of huAD MSC (A) and huBM-MSC (B) were obtained by making a serial dilution in a 96-well flat bottom plate. 8 wells were used, where the last one was a blank. The plate was incubated for 2 h to let cell attachment. huAD and huBM-MSC were incubated with resazurin fluorescent dye for 3 hours. The fluorescent was read at excitation 530 nm and emission 590 nm wavelengths.

8. Growth curve and doubling time of osteosarcoma cells

The doubling time is the time that is required for cells to double in number and it is an intrinsic property of each cell line. It was calculated to know the appropriate time and seeding number of MG63, Saos-2 and U2OS that should be used in the experiments. The doubling time was determined using two different approaches. The first was based on resazurin fluorescent dye. For this, 5,000 and 10,000 MG63 cells were seeded in 100 μ L of a complete α MEM medium and the number of cells was inferred from fluorescence measurements done at days 0, 2, 3, 6 and 9

(Figure A5). The doubling time of MG63 was approximately 2 days and an initial seeding concentration of 10,000 cells in a 96-well plate was selected for the posterior experiments.

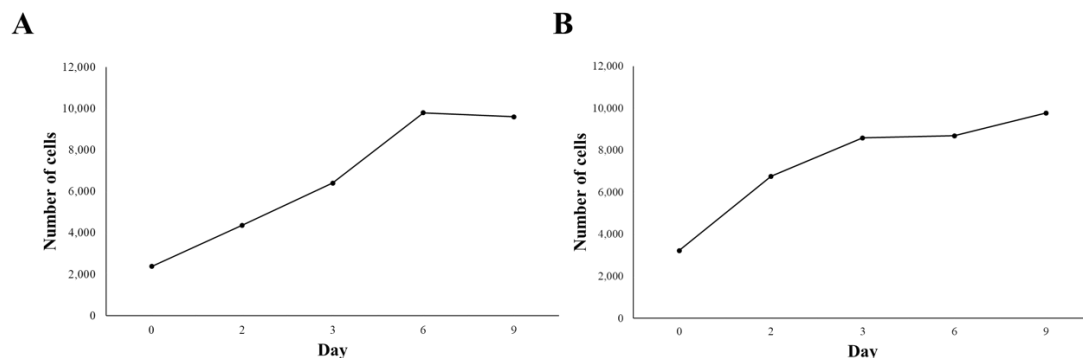


Figure A5. Growth curve of MG63. 5,000 (A) and 10,000 (B) cells were seeded in 96-well plate. The proliferation was assessed on days 0, 2, 3, 6 and 9 in resazurin assay. The number of cells was determined using the formula: $y = 79.315x - 143.56$.

Next, 5,000, 10,000 and 20,000 Saos-2 cells were seeded in 100 μ L of complete McCoy's 5A medium and the number of cells was inferred from fluorescence measurements done at days 1, 3, 4, 7, 10, 14 and 17 (Figure A6). The doubling time of Saos-2 was more than 4 days and it was influenced by seeding number. Apparently, this cell line required more than 24 h for proper attachment to the bottom of the 96-well plate that was evident from cell number reduction after resazurin assay and washing steps were performed. It was evident in wells seeded with 5,000 cell, where with each measurements there were less cells, leading to a considerable reduction in cell growth. This was especially obvious when there was no big interval between the days, such as days 1, 3 and 4 that would enable cell recovery. Also wells with 10,000 Saos-2 cells were affected with time, but it was not as drastic as in previous case. On the contrary, in wells seeded with 20,000 cells, probably, there was some decrease in cell number that was not notorious, due to higher seeding number. From the three different seeding concentrations, the appropriate number of cells to be used in the posterior experiments in a 96-well plate was 20,000.

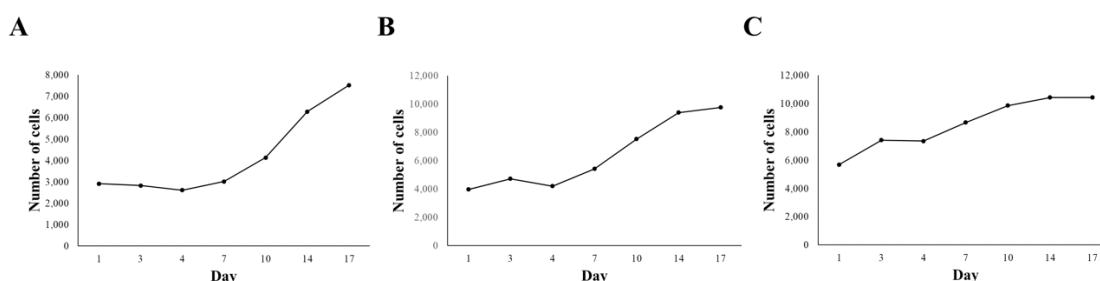


Figure A6. Growth curve of Saos-2. 5,000 (A), 10,000 (B) and 20,000 (C) cells were seeded in 96-well plate. The proliferation was assessed on days 1, 3, 4, 7, 10, 14 and 17 in resazurin assay. The number of cells was determined using the next formula: $y = 54.156x - 101.2$.

Finally, 5,000, 10,000 and 20,000 U2OS cells were seeded in 100 μ L of complete McCoy's 5A medium and the number of cells was inferred from fluorescence measurements done at days 1, 3, 5, 7, 9, 14 and 16 (**Figure A7**). The doubling time of U2OS was more than 7 days and it was influenced by seeding number. This cell line presented a similar behaviour to Saos-2, where for proper cell attachment, apparently, more than 24 h were needed. This probably was influenced identical epithelial morphology between both cell lines. However, 10,000 U2OS cells were selected for posterior experiments, as at this seeding density there was no considerable decrease in cell number compared to Saos-2.

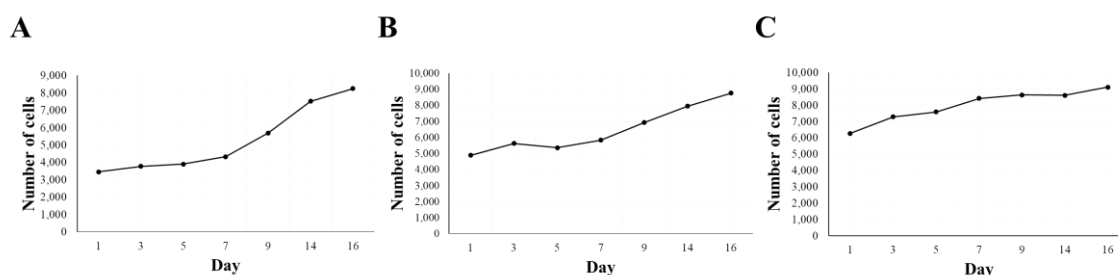


Figure A7. Growth curve of U2OS. 5,000 (A), 10,000 (B) and 20,000 (C) cells were seeded in 96-well plate. The proliferation was assessed on days 1, 3, 5, 7, 9, 14 and 16 in resazurin assay. The number of cells was determined using the next formula: $y = 67.893x - 107.34$.

The second approach to determine the doubling time of each cell line was cell counting using a Neubauer chamber. In this case each day cell number was determined by Trypan Blue extrusion assay in each well by counting cells in a Neubauer chamber. The initial amount of MG63, Saos-2 and U2OS cells seeded at time 0 was 100,000. The cell number was counted at 24, 48, 72 and 96 hours and an online program was used to determine the doubling time of each cell line. The time that MG63 took to double in number was 33 hours. This value was in accordance with the result from resazurin assay.

In case of Saos-2 and U2OS the doubling time was 60 and 34 hours, respectively. This results were contrary to those based on resazurin fluorescent dye. It showed that a manual counting was a reliable method for doubling time estimation as cells were not exposed to resazurin fluorescent dye, which is known to be slightly cytotoxic, or to several washing steps, where aspiration was hypothesized to be responsible of some cell loss, during different time points.

9. Growth rate of human MSC

5,000, 10,000 and 20,000 huAD and huBM-MSC cells were seeded in a complete DMEM-hg medium to establish the appropriate seeding number that should be used in the posterior experiments in a 96-well plate. The fluorescence measurements resazurin assay were performed at 24 and 48 h. The results showed a gradual growth of both huAD and huBM-MSC (**Figure A8**). 5,000 cells of two cell lines were used as a good seeding number for producing 70% of confluence

in a single well from 96-well flat bottom plate. In case of 10,000 and 20,000 cells there was between 90 and 100% of confluence that could lead to contact inhibition resulting in slow proliferation and favour the transition from undifferentiated to differentiated state.

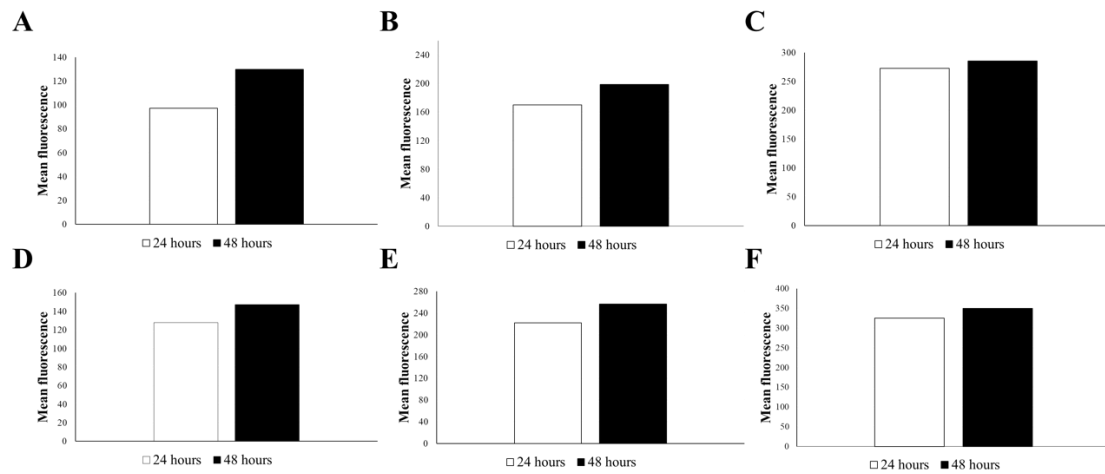


Figure A8. Growth rate of MSC. huAD-MSC (A-C) and huBM-MSC (D-F) were evaluated. 5,000 (A and D), 10,000 (B and E) and 20,000 (C and F) cells were seeded in 96-well plate. The proliferation was assessed at 24 and 48 h in resazurin assay. The results are expressed as mean fluorescence of 8 measurements.

IX. Publications



Oridonin enhances antitumor effects of doxorubicin in human osteosarcoma cells

Liliya Kazantseva^{1,2,3} · José Becerra^{1,2,3,4} · Leonor Santos-Ruiz^{1,2,3,4}

Received: 8 May 2021 / Revised: 13 August 2021 / Accepted: 17 August 2021 / Published online: 24 August 2021
© The Author(s) 2021

Abstract

Background Doxorubicin is the chemotherapeutic drug of choice in osteosarcoma treatment, but its cumulative administration causes dilated cardiomyopathy. Combination therapy represents a potential strategy to reduce the therapeutic dosage of the chemotherapeutic agent and minimize its side effects. The aim of this study was to evaluate the potential of oridonin, a natural product from the medicinal herb *Rabdosia rubescens*, to act in combination with doxorubicin for osteosarcoma treatment. To date, there are no reports of the simultaneous administration of both drugs in osteosarcoma therapy.

Methods The combined administration of different doses of oridonin and doxorubicin, as compared with the drugs alone, were tested in an *in vitro* model of osteosarcoma. The synergistic effect of the drugs on cell death was assessed by *Alamar-Blue*[™] and by *CompuSyn* software. Early and late apoptosis markers (JC-1 fluorescence and Annexin V immunofluorescence), as well as the production of reactive oxygen species, were evaluated by flow cytometry. Western blot was used to assess the expression of anti-apoptotic proteins.

Results Oridonin and doxorubicin presented a synergistic cytotoxic effect in osteosarcoma cells. In the presence of sub-cytotoxic concentrations of the natural product, there was an increased accumulation of intracellular doxorubicin, increased levels of reactive oxygen species (ROS), alteration of mitochondria membrane potential and a higher rate of apoptosis.

Conclusion The combined use of oridonin and doxorubicin could help to reduce the clinical dosage of doxorubicin and its dangerous side effects.

Keywords Osteosarcoma · Doxorubicin · Oridonin · Synergism · Combination therapy · Cardioprotection

Abbreviations

DOX Doxorubicin

ORI Oridonin

ROS Reactive Oxygen Species

CI Combination Index

CD₅₀ 50% Cell Death

Introduction

Osteosarcoma is a bone tumor characterized by the presence of differentiated osteoblasts producing immature osteoid matrix. It is one of the most common cancers affecting children and adolescents, and has a second peak of incidence after the age of 50 [1, 2].

Doxorubicin (DOX) is possibly the most commonly used drug alone or in combination with high-dose methotrexate and cisplatin for osteosarcoma treatment [2, 3]. It is an anthracycline that achieves its therapeutic activity through DNA intercalation, leading to inhibition of topoisomerase-II function. Its efficiency, however, is limited by presence of a life-threatening side effect in the form of cardiotoxicity, which depends on cumulative dosing and can drive to congestive heart failure later in life [2, 4–6].

✉ Leonor Santos-Ruiz
lsantos@uma.es

¹ Andalusian Centre for Nanomedicine and Biotechnology-BIONAND, Universidad de Málaga, Parque Tecnológico de Andalucía, C/ Severo Ochoa, 35, 29590 Campanillas Málaga, Spain

² Centro de Investigación Biomédica en Red, Biotecnología, Biomateriales y Nanomedicina (CIBER-BBN), Madrid, Spain



³ Instituto de Investigación Biomédica de Málaga-IBIMA, Málaga, Spain

⁴ Departamento de Biología Celular, Genética y Fisiología Facultad de Ciencias, Universidad de Málaga, Campus de Teatinos, 29071 Málaga, Spain



Review

Traditional Medicinal Plants as a Source of Inspiration for Osteosarcoma Therapy

Liliya Kazantseva ¹, José Becerra ^{1,2,3}  and Leonor Santos-Ruiz ^{1,2,3,*} 

¹ Instituto de Investigación Biomédica de Málaga y Plataforma en Nanomedicina-IBIMA Plataforma BIONAND, 29590 Málaga, Spain

² Centro de Investigación Biomédica en Red de Bioingeniería, Biomateriales y Nanomedicina (CIBER-BBN), Instituto de Salud Carlos III, 28029 Madrid, Spain

³ Department of Cell Biology, Genetics and Physiology, Universidad de Málaga, 29071 Málaga, Spain

* Correspondence: lsantos@uma.es

Abstract: Osteosarcoma is one of the most common types of bone cancers among paediatric patients. Despite the advances made in surgery, chemo-, and radiotherapy, the mortality rate of metastatic osteosarcoma remains unchangeably high. The standard drug combination used to treat this bone cancer has remained the same for the last 20 years, and it produces many dangerous side effects. Through history, from ancient to modern times, nature has been a remarkable source of chemical diversity, used to alleviate human disease. The application of modern scientific technology to the study of natural products has identified many specific molecules with anti-cancer properties. This review describes the latest discovered anti-cancer compounds extracted from traditional medicinal plants, with a focus on osteosarcoma research, and on their cellular and molecular mechanisms of action. The presented compounds have proven to kill osteosarcoma cells by interfering with different pathways: apoptosis induction, stimulation of autophagy, generation of reactive oxygen species, etc. This wide variety of cellular targets confer natural products the potential to be used as chemotherapeutic drugs, and also the ability to act as sensitizers in drug combination treatments. The major hindrance for these molecules is low bioavailability. A problem that may be solved by chemical modification or nano-encapsulation.

Keywords: osteosarcoma; natural products; traditional medicinal plants; drug discovery; signaling pathway; combination therapy



Citation: Kazantseva, L.; Becerra, J.; Santos-Ruiz, L. Traditional Medicinal Plants as a Source of Inspiration for Osteosarcoma Therapy. *Molecules* **2022**, *27*, 5008. <https://doi.org/10.3390/molecules27155008>

Academic Editor: Jih-Jung Chen

Received: 5 July 2022

Accepted: 29 July 2022

Published: 6 August 2022

Publisher's Note: MDPI stays neutral with regard to jurisdictional claims in published maps and institutional affiliations.



Copyright: © 2022 by the authors. Licensee MDPI, Basel, Switzerland. This article is an open access article distributed under the terms and conditions of the Creative Commons Attribution (CC BY) license (<https://creativecommons.org/licenses/by/4.0/>).

1. Introduction

Osteosarcoma, a bone cancer mainly arising in children and adolescents between the ages of 10 and 14, represents 3–5% of childhood cancer [1,2]. The annual incidence of this disease is 5.6 cases per million of paediatric patients [3]. Osteosarcoma occurs in the metaphysis of the wide portion of the long bones, which is characterized by an accelerated cell division, necessary for bone elongation [2]. During this process, cells can suffer different changes, such as loss of the tumour suppressor gene functionality, which will make them develop into a cancer. Moreover, some conditions are well known to predispose paediatric patients to osteosarcoma. These include retinoblastoma, Li–Fraumeni, and Rothmund–Thomson syndromes [4].

Even though this type of bone cancer is predominant in the young population, adults over the age of 50 are the second-highest risk group for suffering osteosarcoma [5]. In this case it is a secondary tumour caused by irradiation exposure to treat another type of cancer, which occurred previously in life [2]. Also, osteosarcoma can result from a sarcomatous transformation, a rare complication observed in elderly patients with Paget's disease of the bone. In this group of patients, long bones are no longer the principal site affected by the tumour. Instead, jaw and pelvis are the most affected [6,7].

